Applications of the functional renormalization group to quantum liquids

Dissertation
zur Erlangung des Doktorgrades
der Naturwissenschaften

vorgelegt beim Fachbereich Physik
der Johann Wolfgang Goethe - Universität
in Frankfurt am Main

von
Sascha Ledowski
aus Langenhagen

Frankfurt (2007)

(D 30)

vom Fachbereich Physik der

Johann Wolfgang Goethe - Universität

als Dissertation angenommen.

Dekan: Prof. Dr. W. Aßmus

Gutachter : Prof. Dr. P. Kopietz
Prof. Dr. C. Gros
Prof. Dr. H. Frahm

Datum der Disputation: 19.08.2008

Abstract

Non-perturbative effects and strong interactions still challenge the theoretical treatment of condensed matter physics. One of the most promising tools to study these effects is the renormalization group. This thesis is dedicated to the investigation of approximation schemes and applications of the functional renormalization group for one-particle irreducible vertices.

Part of this work deals with weakly interacting bosons at the critical point of Bose-Einstein condensation. Performing an expansion in relevance for physical vertices a method is presented to calculate the full momentum dependence of the self-energy. Application of this result in turn enables the calculation of the interaction induced shift of the critical temperature.

The second part of this thesis investigates systems of interacting fermions in low dimensions. Within the renormalization group framework a generally valid exact self-consistency equation for the shape of the true Fermi surface is derived. After the study of a toy model of two coupled metallic chains the two dimensional system of an infinite array of metallic chains is considered. Bosonizing the interaction by means of a Hubbard-Stratonovich transformation facilitates the successful extrapolation of the weak coupling analysis to strong coupling. Here these systems undergo a *confinement transition* as the renormalized interchain hopping amplitude $t_\perp$ vanishes.

Contents

Chapter 1

Introduction

Strong correlations and non-perturbative effects lead to a variety of interesting physical phenomena and still challenge the theoretical description. Whereas in one dimension some quantum systems are exactly treatable for example by bosonization or the Bethe-Ansatz, these schemes rely on stringent restrictions and generally are not successful in higher dimensions. Concepts like the Luttinger liquid likewise do not carry forward. On the other hand Landau's Fermi liquid theory which describes elementary excitations of normal fermionic systems in terms of so called quasiparticles and mean field theory are often only applicable in three or more dimensions. Perturbation theory which tries to express physical quantities in a power-series of a small coupling parameter fails by definition and even in areas where it might be applicable it is often plagued by divergences.

Many prominent recent discoveries in condensed matter physics deal with strongly interacting two-dimensional systems where neither of the approaches above is adequate. In the second half of the last century a powerful tool termed renormalization group emerged. It is manifestly non-perturbative and, apart from numerical methods, one of the most promising methods to treat strong interactions. Meanwhile it has been successfully applied to a variety of physical systems and it is hoped for that it might help to understand such challenging problems as high-T_c superconductivity.

1.1 The renormalization group

The early developments of the renormalization group (RG) came from the area of elementary particle physics. It started with the observation of Thomson in 1881 that naively evaluated the energy of a point like charged particle (electron) must be infinite. Similar ultraviolet divergences appeared in perturbative treatments of quantum field theories. However these infinities could be absorbed by suitable redefinitions of bare couplings in terms of measurable quantities and divergent diagrams [1, 2]. At that time renormalization was somehow merely regarded as

a trick to cure these kind of divergences.

Renormalization entered condensed matter physics and its understanding took a leap when Kadanoff [3, 4] introduced his real-space RG technique where degrees of freedom are successively reduced by a discrete blocking transformation. Wilson then extended [5–7] this approach to consider infinitesimal renormalization steps by the notion of a continuous flow of an infinite set of parameters. In the context of critical phenomena the RG helped to explain the appearance of universality classes with identical critical exponents for systems that fall into the same class. Further on the emergence of mean field behaviour at or above an upper critical dimension as well as various relations between critical exponents could be understood.

To explain the basic idea of the renormalization group we write a general Hamiltonian as

$$H = \mathbf{V} \cdot \mathbf{\Phi} \tag{1.1}$$

where $\mathbf{V}$ is a vector of coupling parameters and $\mathbf{\Phi}$ a vector of suitable products of operators. The RG procedure can then be subdivided into three steps as follows

1. Reduce the degrees of freedom by integrating out high momentum modes over an infinitesimal momentum shell. This leads to an infinitesimal change of parameters as $\mathbf{V} \to \mathbf{V}'$.

2. Rescale momenta by a factor s such that the system size stays constant. $\mathbf{K} \to \mathbf{K}' = \mathbf{K}s$.

3. Rescale operators and parameters such that the Hamiltonian stays form-invariant and the rescaled parameters approach a fixed point $\mathbf{V}^*$.

A scheme how to employ these infinitesimal renormalization steps was first implemented by Wegner and Houghton [8] using a sharp cutoff procedure, which however necessitated the use of discrete momenta. Later on Polchinski [9] considered a continuous renormalization group flow with a smooth cutoff and laid the basis for a proof of perturbative renormalizability. However this approach inconveniently turned out to be quite sensitive on the form of the cutoff. Nevertheless Polchinskis contribution triggered an increased research and since then the renormalization group has evolved into a variety of different schemes, see e.g. [10] for a review. For numerical computations the powerful method of density matrix renormalization developed by White [11, 12] emerged. Building on earlier work [13–15] it soon was realized by Wetterich and Morris [16, 17] that it is advantageous to consider the renormalization group for the Legendre effective action, with one-particle irreducible vertices as building blocks. This scheme even allowed for an unambiguous use of a sharp cutoff, which considerably simplifies explicit calculations.

As the focus of early developments of the renormalization group for condensed matter physics lay on the understanding of classical critical phenomena, initially only bosonic fields describing fluctuations of the order parameter were considered. Consequently it took some time until the usefulness of this method to study the quantum theory of interacting fermions was noted. Here the definition of high and low energy modes for normal metals has to be made with reference to the true Fermi surface of the full interacting system [18–21]. One of the most frequently investigated systems is the two-dimensional Hubbard model [22–26] because of its possible relevance toward an understanding of high-T_c superconductors. As it has been noted by [25, 27–32] a Fermi surface with nearly flat sectors can become truncated such that the quasiparticle weight vanishes. This non Fermi liquid behaviour might explain some anomalous properties of high-T_c superconductors as has been speculated by [33–36].

There are a variety of different implementations of the functional RG. Most authors however neglect the rescaling of fields and vertices as it has originally been advocated for by Wilson [6], see [37] as well. Especially when performing calculations beyond one loop this rescaling step might be crucial to obtain the correct fixed point. A formulation which explicitly takes it into account has been developed by [20, 21, 38] for interacting fermions and in a more general form by [39–41]. In the following we adopt these formulations and investigate a variety of physical systems.

1.2 Outline of thesis

We briefly describe the outline of this thesis. In a first introductory chapter we lay out our notation and the basic formulation of the functional renormalization group. This chapter merely recapitulates results obtained by other authors [20, 21, 38–41] which however we deem fundamental to understand the following chapters.

Thereafter we add a short discussion of approximation schemes and propose an expansion in the relevance (determined by the scaling dimensions) of vertices. We present what we term the *adiabatic approximation* which allows us to express vertex functions whose flow is exclusively governed by irrelevant vertices solely in terms of relevant and marginal ones.

The main part of this thesis falls into the examination of two different physical systems. At first we investigate weakly interacting bosons at the critical point of Bose-Einstein condensation. Applying the approximations discussed before we are able to derive an explicit expression for the full momentum dependent one-particle self-energy. Using this result we obtain the interaction induced shift of the critical temperature. Finally we investigate the convergence of our approximation scheme by including higher orders.

The second main topic is the determination of the Fermi surface of interacting fermions. We are able to derive an exact self-consistency equation which relates the shape of the Fermi surface to the effective interaction along the complete trajectory of the RG. As next step we apply this equation to study the true Fermi surface of a system of two coupled metallic chains. Of special interest here is the occurrence/absence of a *confinement transition* which denotes the case of an interaction induced vanishing of the interchain hopping amplitude. We identify the relevant interaction promoting confinement and bosonize it by means of a Hubbard-Stratonovich transformation. Using the adiabatic approximation for the boson Greensfunction then allows a successful treatment even of the strong interacting case. Thereafter we move to the physically more relevant case of a quasi two-dimensional system of infinitely many coupled metallic chains. Here the Fermi surface consists of two disconnected weakly curved sheets. We are able to show that this system indeed undergoes a confinement transition which is characterized by a vanishing curvature of these sheets at finite interaction strength.

Finally this thesis is concluded by a short recapitulation and discussion of the relevant results.

Chapter 2

The functional renormalization group

The aim of this chapter is to lay out the basic formalism of the functional renormalization group. We start with an introduction to the notation and proceed introducing various generating functionals. This is followed by a derivation of the flow equations for the one-particle irreducible Greensfunctions. We discuss different cutoffs and finally complete the Wilsonian RG procedure by rescaling momenta and vertices. The results presented in this chapter have to a great extent been derived elsewhere [18, 38, 39, 41] and we closely follow the notation laid out within.

2.1 Notation

To allow for a greater number of applications we consider theories with fermionic $\bar{\psi}_\alpha, \psi_\alpha$ and complex $\phi_\alpha^*, \phi_\alpha$ or real valued φ bosonic fields. We collect these fields into a vector $\mathbf{\Phi}$. For convenience we use such an order that the fermionic fields appear first followed by the complex bosonic ones and the real valued bosonic fields as last

$$\mathbf{\Phi}(\{\mathbf{K}\}) = \left(\bar{\psi}_{\mathbf{1}}(\mathbf{K}_{\bar{\psi}_{\mathbf{1}}}), \psi_{\mathbf{1}}(\mathbf{K}_{\psi_{\mathbf{1}}}), \dots ; \phi_{\mathbf{1}}^*(\mathbf{K}_{\phi_{\mathbf{1}}^*}), \phi_{\mathbf{1}}(\mathbf{K}_{\phi_{\mathbf{1}}}), \dots ; \varphi_{\mathbf{1}}(\mathbf{K}_{\varphi_{\mathbf{1}}}), \dots \right) \ . \quad (2.1)$$

Here we have defined the composite momentum vector $\mathbf{K}$ which contains the fermionic or bosonic Matsubara frequencies $i\omega_n$ and the D-dimensional momentum $\mathbf{k}$

$$\mathbf{K} = (i\omega_n, \mathbf{k}) \ . \quad (2.2)$$

As a shorthand we shall use

$$\int_{\mathbf{K}} = \frac{1}{\beta V} \sum_{\omega_n, \mathbf{k}} \xrightarrow{\beta, V \to \infty} \int \frac{d\omega}{2\pi} \frac{d^d k}{(2\pi)^D} \ . \quad (2.3)$$

Decomposing the action into a free and an interacting part

$$S = S_0 + S_I \ , \tag{2.4}$$

the first is written as

$$S_0 = -\frac{1}{2} \boldsymbol{\Phi} \cdot \mathbf{G}_0^{-1} \cdot \boldsymbol{\Phi} \ . \tag{2.5}$$

Here we have introduced the scalar product

$$\mathbf{A} \cdot \mathbf{B} = \sum_\alpha \int_{\mathbf{X}} A_\alpha(\mathbf{X}) B_\alpha(\mathbf{X}) \ , \tag{2.6}$$

where X refers to the space spanned by Matsubara time and real space. For convenience we will always work in momentum space. In this representation the scalar product is easily obtained as an integral over the Matsubara frequency and momenta. We just have to be careful to use the correct momentum dependence of the fields to ensure momentum conservation in the integral. Additionally we define for later use the tensor product

$$[\mathbf{A} \otimes \mathbf{B}]_{\alpha\beta} = \mathbf{A}_\alpha \mathbf{B}_\beta \ . \tag{2.7}$$

The inverse bare Greensfunction (here for one fermionic and one real bosonic field) is given as matrix in the space spanned by the particle species index and momentum by

$$\mathbf{G}_0^{-1}(\mathbf{K}, \mathbf{K}') = \begin{pmatrix} 0 & -G_0^{-1}(\mathbf{K}) & 0 \\ G_0^{-1}(\mathbf{K}) & 0 & 0 \\ 0 & 0 & -F_0^{-1}(\mathbf{K}) \end{pmatrix} \delta_{\mathbf{K},\mathbf{K}'} \ , \tag{2.8}$$

where the components are the usual one particle bare Greensfunctions. Inversion of (2.8) is simple and reads

$$\mathbf{G}_0(\mathbf{K}, \mathbf{K}') = \begin{pmatrix} 0 & G_0(\mathbf{K}) & 0 \\ -G_0(\mathbf{K}) & 0 & 0 \\ 0 & 0 & -F_0(\mathbf{K}) \end{pmatrix} \delta_{\mathbf{K},\mathbf{K}'} \ . \tag{2.9}$$

It is convenient to define a matrix $\mathbf{Z}$ as

$$Z_{\alpha\beta} = \delta_{\alpha\beta}\zeta_\alpha \ , \tag{2.10}$$

where $\zeta = -1$ for a fermionic field and $\zeta = 1$ for a bosonic field. With the help of this matrix we can write the transposed Greensfunction as

$$\mathbf{G}_0^T = \mathbf{Z} \cdot \mathbf{G}_0 = \mathbf{G}_0 \cdot \mathbf{Z} \ . \tag{2.11}$$

2.2   Generating functionals

We now investigate the generating functionals for different Greensfunction. We consider their basic definition and properties as well as the relations between them. Details of the derivation and additional information about their properties can for example be found in [42]. Our goal is to arrive at a formulation for the one-particle irreducible (1-PI) vertices. It is these vertices that we will study the exact renormalization group equations for later on.

2.2.1   Disconnected Greensfunctions

The disconnected Greensfunctions are defined as the expectation value of the corresponding product of fields as

$$\mathcal{G}_{\alpha_1 \ldots \alpha_n} = \frac{1}{\mathcal{Z}_0} \int \mathcal{D}\mathbf{\Phi} \; \Phi_{\alpha_1} \cdot \ldots \cdot \Phi_{\alpha_n} e^{-S_0[\mathbf{\Phi}] - S_I[\mathbf{\Phi}]} \; , \tag{2.12}$$

with the free partition function

$$\mathcal{Z}_0 = \int \mathcal{D}\mathbf{\Phi} \; e^{-S_0[\mathbf{\Phi}]} \; . \tag{2.13}$$

Another way of expressing these Greensfunctions is to write them as derivatives of a generating functional with respect to sources. We introduce these source fields J_α with the same gradation as the corresponding fields (i.e. fermionic or bosonic). The generating functional can then be written as

$$\mathcal{G}[\mathbf{J}] = \frac{1}{\mathcal{Z}_0} \int \mathcal{D}\mathbf{\Phi} \; e^{-S_0[\mathbf{\Phi}] - S_I[\mathbf{\Phi}] + \mathbf{J} \cdot \mathbf{\Phi}} \; , \tag{2.14}$$

and the Greensfunctions as

$$\mathcal{G}^{(n)}_{\alpha_1 \ldots \alpha_n} = \left. \frac{\partial^n \mathcal{G}[\mathbf{J}]}{\partial J_{\alpha_1} \ldots \partial J_{\alpha_n}} \right|_{\mathbf{J}=\mathbf{0}} \; . \tag{2.15}$$

2.2.2   Connected Greensfunctions

It is simple to show that the generating functional $\mathcal{G}_c$ for connected Greensfunctions can be expressed as

$$e^{\mathcal{G}_c[\mathbf{J}]} = \mathcal{G}[\mathbf{J}] \; . \tag{2.16}$$

Differentiating with respect to the sources n-times lets us obtain the connected n-point functions as

$$\mathcal{G}^{(n)}_{c,\alpha_1 \ldots \alpha_n} = \left. \frac{\partial^n \mathcal{G}_c[\mathbf{J}]}{\partial J_{\alpha_1} \ldots \partial J_{\alpha_n}} \right|_{\mathbf{J}=\mathbf{0}} \; , \tag{2.17}$$

and as a special case the full propagator

$$\mathbf{G}_{\alpha\beta} = -\mathcal{G}_{c,\alpha\beta}^{(2)} \ . \tag{2.18}$$

Formally we can replace in the interaction part of the action the field dependence by the derivative with respect to the corresponding source. The path integral in (2.14) can then be carried out and we receive

$$\mathcal{G}[\mathbf{J}] = e^{-S_I[\partial_{\mathbf{J}}]} e^{-\frac{1}{2}\mathbf{J}\cdot\mathbf{G}_0^T\cdot\mathbf{J}} \ . \tag{2.19}$$

In principle we can use this expression to derive a perturbative expansion for the Greensfunctions.

2.2.3   One-particle irreducible vertices

Taking a look at the expansion (2.19) we observe that the resulting diagrams still can be decomposed in more fundamental building blocks. These blocks consist of diagrams that can not be separated by cutting a single propagator line - this property is called one-particle irreducible (1-PI).

To derive the generating functional for these 1-PI vertices we have to perform a Legendre transformation. Therefore we define

$$\tilde{\mathbf{\Phi}} = \partial_{\mathbf{J}}\mathcal{G}_c[\mathbf{J}] \ , \tag{2.20}$$

which is basically the expectation value of the field $\mathbf{\Phi}$ in the presence of the sources $\mathbf{J}$. The Legendre transformation then yields the effective action

$$\mathcal{L}[\tilde{\mathbf{\Phi}}] = \mathbf{J}\cdot\tilde{\mathbf{\Phi}} - \mathcal{G}_c[\mathbf{J}[\tilde{\mathbf{\Phi}}]] \ . \tag{2.21}$$

We can now then express the sources as derivatives of this effective action as

$$\mathbf{J} = \mathbf{Z}\cdot\partial_{\tilde{\mathbf{\Phi}}}\mathcal{L} \ . \tag{2.22}$$

Using the chain rule

$$\partial_{\tilde{\mathbf{\Phi}}} = (\partial_{\tilde{\mathbf{\Phi}}}\otimes\partial_{\tilde{\mathbf{\Phi}}})\mathcal{L}\cdot\mathbf{Z}\cdot\partial_{\mathbf{J}} \ , \tag{2.23}$$

we derive the identity

$$\mathbf{1} = (\partial_{\tilde{\mathbf{\Phi}}}\otimes\partial_{\tilde{\mathbf{\Phi}}})\mathcal{L}\cdot\mathbf{Z}\cdot(\partial_{\mathbf{J}}\otimes\partial_{\mathbf{J}})\mathcal{G}_c \ , \tag{2.24}$$

which we shall apply in a moment.

Now for $n \geq 3$ the effective action $\mathcal{L}$ clearly is the generator for 1-PI n-point functions. However for $n = 2$ (which is the self-energy) we observe that we have to subtract the free action to arrive at the desired functional

$$\Gamma[\tilde{\mathbf{\Phi}}] = \mathcal{L}[\tilde{\mathbf{\Phi}}] - \mathbf{S_0}[\tilde{\mathbf{\Phi}}] \ . \tag{2.25}$$

The 1-PI n-point vertices $\Gamma^{(n)}$ are now defined as the coefficient of the series

$$\Gamma[\tilde{\mathbf{\Phi}}] = \sum_{n=0}^{\infty} \frac{1}{n!} \Gamma^{(n)}_{\alpha_1 \ldots \alpha_n} \tilde{\Phi}_{\alpha_1} \ldots \tilde{\Phi}_{\alpha_n} \ . \tag{2.26}$$

For simplicity of notation we will from now on use Φ instead of $\tilde{\Phi}$ keeping in mind the difference between the two.

Before we proceed to the derivation of the renormalization group equations we like to derive a relation between the connected 2-point function $\mathcal{G}_c^{(2)}$ and the 1-PI vertices. We start with defining the functional

$$\mathbf{U} = [(\partial_{\mathbf{\Phi}} \otimes \partial_{\mathbf{\Phi}})\Gamma - (\partial_{\mathbf{\Phi}} \otimes \partial_{\mathbf{\Phi}})\Gamma|_{\mathbf{\Phi}=0}]^T =: [(\partial_{\mathbf{\Phi}} \otimes \partial_{\mathbf{\Phi}})\Gamma]^T - \mathbf{\Sigma} \ . \tag{2.27}$$

This translates into

$$(\partial_{\mathbf{\Phi}} \otimes \partial_{\mathbf{\Phi}})\mathcal{L} = \mathbf{U} - [\mathbf{G}^{-1}]^T \ , \tag{2.28}$$

with the full propagator

$$\mathbf{G}^{-1} = \mathbf{G}_0^{-1} - \mathbf{\Sigma} \ . \tag{2.29}$$

Together with (2.24) we finally obtain

$$(\partial_{\mathbf{J}} \otimes \partial_{\mathbf{J}})\mathcal{G}_c = \mathbf{Z} \cdot [(\partial_{\mathbf{\Phi}} \otimes \partial_{\mathbf{\Phi}})\mathcal{L}]^{-1} = -\mathbf{Z} \cdot \mathbf{G}^T \cdot \left[\mathbf{1} - \mathbf{U}^T \cdot \mathbf{G}^T\right]^{-1} \ , \tag{2.30}$$

which is the relation we where looking for.

2.3   Exact renormalization group equations

The basic idea of the renormalization group is to successively integrate out high energy modes of our theory. This procedure leaves us with an infinite set of differential equations for the vertices - which to solve is our ultimate goal. To set up the renormalization group procedure we have to somehow separate the high energy modes from the low energy modes. We start by introducing the scales Λ_α (which might be different for different fields α). Here Λ_α acts as an infrared cut-off whereas the initial value $\Lambda_\alpha^{(0)}$ as an ultraviolet cutoff. In contrast to field theories for elementary particles in condensed matter physics these ultraviolet cutoffs possess a physical significance and are for example determined by the inverse lattice spacing.

To associate with a particle of type α and momentum $\mathbf{K}$ a certain scale for comparison with Λ_α we introduce the functions $\Omega_\alpha(\mathbf{K}) > 0$. The implementation of the cutoff is via the help of cutoff functions

$$\tilde{\Theta}_\alpha(\Lambda_\alpha, \Omega_\alpha(\mathbf{K}), \Lambda_\alpha^{(0)}) \in [0, 1] \ . \tag{2.31}$$

Without the need to become more specific at this point these cutoff functions are chosen to suppress the low energy and too high energy modes ($\tilde{\Theta} \to 0$ for $\Omega < \Lambda$ or $\Omega > \Lambda^{(0)}$) whereas to allow propagation of the modes in between these energy scales ($\tilde{\Theta} \to 1$ for $\Lambda < \Omega < \Lambda^{(0)}$). For systems with a Fermi surface the distinction between high energy and low energy modes has to be made with respect to this Fermi surface which a-priori is not known [18]. We will later on develop a scheme to obtain the true Fermi surface in a self consistent way. Collecting the cutoff functions into a diagonal matrix $\tilde{\Theta}$ we modify the bare Greensfunction as

$$\mathbf{G}_0 \to \mathbf{G}_0 \cdot \tilde{\Theta} \ . \tag{2.32}$$

However it is generally not necessary to make all Greensfunctions cutoff dependent. In most cases it is sufficient to perform the RG just with one restricted field. Additionally note that apart from the multiplicative scheme as introduced above there are other possibilities to implement the cutoff, e.g. the Litim cutoff [43].

The renormalization group is now implemented by reducing the scales Λ_α toward zero. We differentiate the generating functional for disconnected Greensfunction with respect to one of the cutoffs

$$\partial_{\Lambda_\alpha} \mathcal{G}[\mathbf{J}] = \left(\frac{1}{2} \partial_{\mathbf{J}} \cdot \partial_{\Lambda_\alpha} \mathbf{G}_0^{-1} \cdot \partial_{\mathbf{J}} - \partial_{\Lambda_\alpha} \ln(\mathcal{Z}_0) \right) \mathcal{G}[\mathbf{J}] \ , \tag{2.33}$$

to obtain the renormalization group equations for the disconnected Greensfunctions. Moving on to connected Greensfunctions results in

$$\partial_{\Lambda_\alpha} \mathcal{G}_c[\mathbf{J}] = \frac{1}{2}(\partial_{\mathbf{J}}\mathcal{G}_c) \cdot \partial_{\Lambda_\alpha} \mathbf{G}_0^{-1} \cdot (\partial_{\mathbf{J}}\mathcal{G}_c) + \frac{1}{2} tr \left(\partial_{\Lambda_\alpha} \mathbf{G}_0^{-1} [(\partial_{\mathbf{J}} \otimes \partial_{\mathbf{J}})\mathcal{G}_c]^T \right) - \partial_{\Lambda_\alpha} \ln(\mathcal{Z}_0). \tag{2.34}$$

Before proceeding to the flow equations for 1-PI vertices we have to note that

$$\partial_{\Lambda_\alpha} \mathcal{L}[\mathbf{\Phi}] = -\partial_{\Lambda_\alpha} \ \mathcal{G}_c[\mathbf{J}]\big|_{\mathbf{J}=\mathbf{J}[\mathbf{\Phi}]} \ , \tag{2.35}$$

as in $\mathcal{L}$ the fields $\mathbf{\Phi}$ are held constant rather than the sources $\mathbf{J}$. Therefore we obtain

$$\partial_{\Lambda_\alpha} \Gamma[\mathbf{\Phi}] = -\frac{1}{2} tr \left(\partial_{\Lambda_\alpha} \mathbf{G}_0^{-1} [(\partial_{\mathbf{J}} \otimes \partial_{\mathbf{J}})\mathcal{G}_c]^T \right) + \partial_{\Lambda_\alpha} \ln(\mathcal{Z}_0) \ . \tag{2.36}$$

Remembering (2.30) and performing some rearrangements we finally get [39, 41]

$$\begin{aligned} \partial_{\Lambda_\alpha} \Gamma[\mathbf{\Phi}] \ &= \ -\frac{1}{2} tr \left(\mathbf{Z} \cdot [\dot{\mathbf{G}}^{(\alpha)}]^T \cdot \mathbf{U}^T \left[\mathbf{1} - \mathbf{G}^T \cdot \mathbf{U}^T \right]^{-1} \right) \\ &\quad -\frac{1}{2} tr \left(\mathbf{Z} \cdot [\dot{\mathbf{G}}_0^{(\alpha)}]^T \cdot \mathbf{\Sigma}^T \left[\mathbf{1} - \mathbf{G}_0^T \cdot \mathbf{\Sigma}^T \right]^{-1} \right) \ . \end{aligned} \tag{2.37}$$

Here we have introduced

$$\begin{aligned} \dot{\mathbf{G}}^{(\alpha)} \ &= \ -\mathbf{G} \cdot \partial_{\Lambda_\alpha} \mathbf{G}_0^{-1} \cdot \mathbf{G} \ , \\ \dot{\mathbf{G}}_0^{(\alpha)} \ &= \ \partial_{\Lambda_\alpha} \mathbf{G}_0 \ . \end{aligned} \tag{2.38}$$

We note that the first line in (2.37) vanishes for vanishing fields $\mathbf{\Phi}$ whereas the second line is field independent. Therefore the latter describes the interaction induced flow of the grand canonical potential.

To obtain the flow equations for the vertices $\Gamma^{(n)}$ we expand both sides of (2.37) in powers of the fields and identify coefficients with the same field dependence. Explicitly this yields for $n \geq 1$

$$\partial_{\Lambda_\alpha} \Gamma^{(n)}_{\alpha_1 \dots \alpha_n} = -\frac{1}{2} \sum_{l=1}^{\infty} \sum_{m1_1, \dots, m_l=1}^{\infty} \delta_{n, m_1 + \dots + m_l} S_{\beta_1 \dots \beta_{m_1}; \dots; \beta_{1+m_1+\dots+m_{l-1}} \dots \beta_n} \cdot \qquad (2.39)$$

$$\cdot tr \left(\mathbf{Z} \cdot [\dot{\mathbf{G}}^\alpha]^T \cdot \mathbf{\Gamma}^{(m_1+2)T}_{\beta_1 \dots \beta_{m_1}} \cdot \mathbf{G}^T \mathbf{\Gamma}^{(m_1+2)T}_{\beta_{m_1+1} \dots \beta_{m_1+m_2}} \cdot \mathbf{G}^T \cdot \dots \cdot \mathbf{\Gamma}^{(m_1+2)T}_{\beta_{1+m_1+\dots+m_{l-1}} \dots \beta_n} \right) ,$$

with the matrices

$$[\mathbf{\Gamma}^{(m_1+2)}_{\beta_1 \dots \beta_{m_1}}]_{\alpha \alpha'} = \Gamma^{(m_1+2)}_{\alpha \alpha' \beta_1 \dots \beta_{m_1}} . \qquad (2.40)$$

This result is due to [39, 41]. The symmetrization operator is defined as

$$S_{\beta_1 \dots \beta_{m_1}; \dots; \beta_{1+m_1+\dots+m_{l-1}} \dots \beta_n} A_{\beta_1 \dots \beta_n} = \frac{1}{\prod_i m_i!} \sum_P sg_\zeta(P) A_{\beta_{P(1)} \dots \beta_{P(n)}} , \qquad (2.41)$$

where P is a permutation of $1 \dots n$ and $sg_\zeta(P)$ keeps track of the sign generated when permuting fermionic and bosonic fields according to P.

Actually we are interested only in the physical vertices $\Gamma^{(n,m,\dots)}$ where the superscript denotes how many fields of each species are coupled by this vertex (e.g. n fermions, m complex bosons etc.). For example we write the vertex describing the scattering of a fermion by absorption of a boson as $\Gamma^{(2,1)}$, i.e. there are two fermionic lines and one bosonic. We obtain these by (anti-)symmetrizing (dependent on if we consider fermions or bosons) the external legs of the vertices $\Gamma^{(n+m+\dots)}_{\alpha_1 \dots \alpha_{(n+m+\dots)}}$.

Ever since Feynman invented his technique of diagrammatic representations physicists made wide use of them. So do we and introduce a set of diagrams to describe the flow equations, see figure 2.3. For simplicity we shall graphically not distinguish between rescaled or un-rescaled vertices.
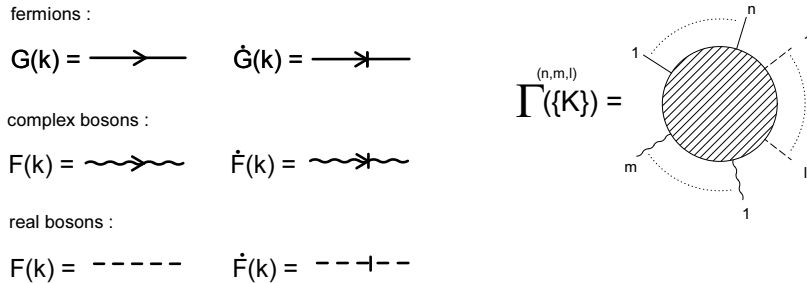

Figure 2.1: Graphical representation for Greensfunctions and vertices.

Within this work we shall only consider theories without spontaneous symmetry breaking. A generalization to theories with finite expectation values of the fields may be found in [40].

2.4   The cutoff function

We now turn toward the discussion of the cutoff functions $\tilde{\Theta}$. Actually the final results (i.e. at $\Lambda = 0$) of an exact renormalization group treatment should not depend on the cutoff chosen. However as we shall employ a couple of approximations and truncation of the infinite hierarchy of flow equations this scheme independence may be violated. Therefore we like to now how different cutoffs behave under these approximations. We also have to take into account whether the cutoffs preserve certain symmetries of our original theory at intermediate scales. And last but not least the ability to actually perform computations with these cutoffs has to be considered.

The cutoff function

We assume that the cutoff functions can be written (suppressing the index α for the time) as products of an infrared and an ultraviolet cutoff

$$\tilde{\Theta}(\Lambda, \Omega, \Lambda^{(0)}) = \tilde{\Theta}_{IR}(\Lambda, \Omega)\tilde{\Theta}_{UV}(\Lambda^{(0)}, \Omega) \, , \qquad (2.42)$$

with

$$\tilde{\Theta}_{IR}(\Lambda, \Omega) = 1 - \tilde{\Theta}_{UV}(\Lambda, \Omega) \, . \qquad (2.43)$$

Now some (of many) possible choices for the ultraviolet cutoff function $\tilde{\Theta}_{UV}$ are

- sharp cutoff $\tilde{\Theta}_{UV}(\Lambda, \Omega) = \Theta(\Lambda - \Omega)$

- exponential cutoff $\tilde{\Theta}_{UV}(\Lambda, \Omega) = e^{-\Omega^2/\Lambda^2}$

- power law cutoff $\tilde{\Theta}_{UV}(\Lambda, \Omega) = (1 + (\Omega/\Lambda)^{2+2\kappa})^{-1}$ with $\kappa > 0$

The convergence of the momentum-scale expansion (we shall comment on this expansion in section 3.1) for the 2-loop β-function with these cutoffs has been investigated by [44]. Here the authors found the exponential cutoff to produce fast converging results whereas the series obtained by using the power law cutoff actually diverged. The sharp cutoff lies somewhere in between with very slowly converging results. However as long as we are interested in the first terms of this expansion only the results of the sharp cutoff coincide with those of an exponential cutoff.

On the other hand only the sharp cutoff and power law cutoff are known to conserve reparametrization invariance, that is the invariance of the flow equations

under an arbitrary rescaling of fields, when used within a momentum-scale expansion [45, 46]. Most prominently a broken reparametrization invariance would result in an ambiguous determination of the anomalous dimensions. Note that within this work we use a different approximation scheme, namely the expansion in relevance (see section 3.1). However there seem to be similarities between these two methods and we assume results regarding the cutoff function derived within the momentum-scale expansion to be approximately valid for our scheme.

There are more exotic choices possible for the cutoffs as well, notably the (IR) Litim cutoff [43]. This cutoff is obtained by adding to the denominator of the bare Greensfunction the term $R(\Lambda, \Omega) = (\Lambda^2 - \Omega^2)\Theta(\Lambda - \Omega)$. Application to ϕ^4 theory with finite expectation values yields quite useful results with good convergence properties [47].

As a compromise between convergence properties and computational simplicity in this work we shall exclusively make use of the sharp cutoff. We write it as

$$\tilde{\Theta}(\Lambda, \Omega, \Lambda^{(0)}) = \Theta(\Omega - \Lambda)\Theta(\Lambda^{(0)} - \Omega) =: \Theta(\Lambda < \Omega < \Lambda^{(0)}) \, . \qquad (2.44)$$

Note however that this cutoff is not precisely defined at $\Omega = \Lambda$ or $\Omega = \Lambda^{(0)}$. Additionally the inverse bare propagator is ill defined for $\Omega \notin [\Lambda, \Lambda^{(0)}]$. To cure these problems we understand the function $\Theta(x)$ to represent an approximate step-function only which varies smoothly at $x = 0$ and is strictly positive. Only after we have performed all relevant calculations we employ some kind of limiting procedure under which $\Theta(x)$ approaches a real step-function. For all practical computations it is sufficient to have a scheme available to calculate products of this quasi-stepfunction at $x = 0$. As it has been pointed out by [17] the rigorous way to perform these calculations is to use

$$F\left(\Lambda, \Theta(\Lambda < \Omega < \Lambda^{(0)})\right) \partial_\Lambda \Theta(\Lambda < \Omega < \Lambda^{(0)}) = -\delta(\Omega - \Lambda)\int_0^1 dx \quad F(\Lambda, x), \qquad (2.45)$$

for arbitrary (analytical) functions F. We can now apply this equation to explore the meaning of (2.38) by noting that it indeed results into

$$\dot{G} = -\frac{\delta(\Omega - \Lambda)}{G_0^{-1} - \Sigma} \, , \qquad (2.46)$$

where we have assumed that the most singular contribution stems from the derivative of the Θ-function. Here G_0^{-1} has to be understood not to be multiplied with the cutoff function.

The scale functions Ω

As already mentioned the functions $\Omega(\mathbf{K})$ shall map a particle of momentum $\mathbf{K}$ to some scale to compare it to Λ. For bosons the most obvious choice is just to

use the modulus of the momentum vector

$$\Omega_B(\mathbf{K}) = |\mathbf{k}| \ . \tag{2.47}$$

Considering fermions we have to use as reference manifold the true (full interacting) Fermi surface [20, 38, 48]. The Fermi surface is conveniently defined by the bare dispersion $\epsilon_{\mathbf{k}}$ as the set of momenta obeying

$$\epsilon_{\mathbf{k}} = \mu - \Sigma(i0, \mathbf{k}) \ , \tag{2.48}$$

with the chemical potential μ and the full self energy Σ. We use the (D-1)-dimensional momentum $(\mathbf{k}_\perp)$ to denote a point on the Fermi surface as $\mathbf{k}_F(\mathbf{k}_\perp)$. To define a local normal component $k_\parallel$ we expand the bare dispersion around the true Fermi surface as

$$\begin{aligned}
\epsilon_{\mathbf{k}} - \epsilon_F &= (\mathbf{k} - \mathbf{k}_F(\mathbf{k}_\perp)) \cdot \partial_{\mathbf{k}} \epsilon_{\mathbf{k}}|_{\mathbf{k}=\mathbf{k}_F} + O\left((\mathbf{k} - \mathbf{k}_F(\mathbf{k}_\perp))^2\right) \\
&= (\mathbf{k} - \mathbf{k}_F(\mathbf{k}_\perp)) \cdot \mathbf{v}_F(\mathbf{k}_\perp) + O\left((\mathbf{k} - \mathbf{k}_F(\mathbf{k}_\perp))^2\right) \\
&= k_\parallel |\mathbf{v}_F(\mathbf{k}_\perp)| + O(k_\parallel^2) \ .
\end{aligned} \tag{2.49}$$

Note that the Fermi velocity vector as defined above is not necessarily perpendicular to the true Fermi surface. General momenta are then decomposed as
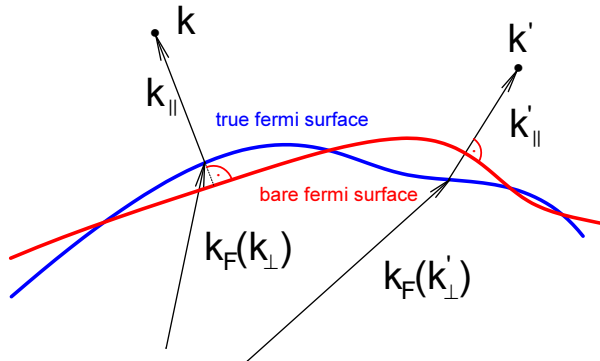
Figure 2.2: Example of a local coordinate system defined by the true Fermi surface and the bare dispersion.

depicted in figure 2.2 as

$$\mathbf{k} = \mathbf{k}_F(\mathbf{k}_\perp) + \mathbf{k}_\parallel \ , \tag{2.50}$$

with

$$\mathbf{k}_\parallel = k_\parallel \frac{\mathbf{v}_F(\mathbf{k}_\perp)}{|\mathbf{v}_F(\mathbf{k}_\perp)|} \ . \tag{2.51}$$

For the scale Ω we simply use

$$\Omega_F(\mathbf{k}) = |k_\parallel| \ . \tag{2.52}$$

For an one-dimensional system with just two symmetric Fermi points this is easily accomplished by

$$\Omega_F(\mathbf{k}) = ||k| - |k_F|| \ . \tag{2.53}$$

In higher dimensions the use of a curved coordinate system usually makes our equations cumbersome. Here it often is advantageous to divide the Fermi surface into patches with approximate flat sectors within these patches. We then decompose momenta into components perpendicular ($\mathbf{k}_\perp$) and parallel ($\mathbf{k}_\parallel$) to the normal vector of the base surface of these patches in the same manner as in (2.50) and use (2.52) with the now differently defined $\mathbf{k}_\parallel$, see figure 2.3.
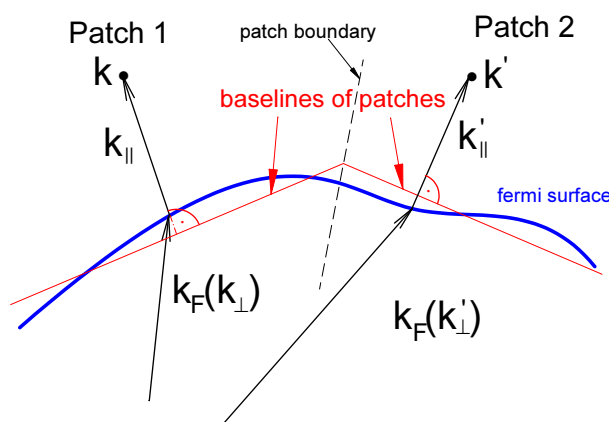
Figure 2.3: Example of a local coordinate system defined by patches

Generally when performing the coordinate transformation $\mathbf{k} \rightarrow (\mathbf{k}_\perp, k_\parallel)$ we have to evaluate the Jacobian determinant to determine the integration measure as

$$\int_{\mathbf{k}} = \int_{\mathbf{k}_\perp, k_\perp} = \int \frac{d\mathbf{k}_\perp}{(2\pi)^{D-1}} \int \frac{dk_\parallel}{2\pi} J(\mathbf{k}_\perp, k_\parallel) \ , \tag{2.54}$$

with

$$J(\mathbf{k}_\perp, k_\parallel) = \left| \frac{\partial(\mathbf{k})}{\partial(\mathbf{k}_\perp, k_\parallel)} \right| \ . \tag{2.55}$$

2.5 Bosonization of the interaction

2.5.1 Hubbard-Stratonovich transformation

It turns out to be rather helpful in some cases to bosonize the interaction part S_I of the action by means of a Hubbard-Stratonovich (HS) transformation [41, 49–52]. Writing the interaction in a bilinear form

$$S_I = \bar{\boldsymbol{\rho}} \cdot \mathbf{V} \cdot \boldsymbol{\rho} \ , \tag{2.56}$$

and using multiple Gaussian integrals we observe the identity

$$e^{-S_I} = e^{-\bar{\boldsymbol{\rho}} \cdot \mathbf{V} \cdot \boldsymbol{\rho}} = \int \mathcal{D}(\bar{\mathbf{z}}\mathbf{z}) \det(\mathbf{V}) e^{-\bar{\mathbf{z}} \cdot \mathbf{V}^{-1} \cdot \mathbf{z} - i\bar{\boldsymbol{\rho}} \cdot \mathbf{z} - i\bar{\mathbf{z}} \cdot \boldsymbol{\rho}} . \tag{2.57}$$

Therefore by introducing the bosonic fields $\bar{z}, z$ we can write the action as

$$\begin{aligned} S_0 &\rightarrow S_0 + \bar{\mathbf{z}} \cdot \mathbf{V}^{-1} \cdot \mathbf{z} , \\ S_I &\rightarrow i\bar{\boldsymbol{\rho}} \cdot \mathbf{z} + i\bar{\mathbf{z}} \cdot \boldsymbol{\rho} , \end{aligned} \tag{2.58}$$

for complex ρ or

$$\begin{aligned} S_0 &\rightarrow S_0 + \frac{1}{2}\mathbf{z} \cdot \mathbf{V}^{-1} \cdot \mathbf{z} , \\ S_I &\rightarrow i\boldsymbol{\rho} \cdot \mathbf{z} , \end{aligned} \tag{2.59}$$

for real valued $\boldsymbol{\rho}$ (and z). The factor $\det(\mathbf{V})$ just adds a field independent term to the action which contributes to the free energy. As we do not investigate the free energy in this work we have omitted this contribution in (2.58) and (2.59).

2.5.2   Interaction cutoff

If we now use such a bosonized interaction we can multiply the corresponding propagator with a cutoff function as we have done with "true" bosonic fields. This amounts to using an interaction cutoff, i.e. the momentum transfer of the interaction is restricted by $\Lambda, \Lambda^{(0)}$. If for example our original theory just contains a single component fermionic field and a cutoff Λ_F - to which we refer as bandwidth cutoff - , after the HS-transformation there are actually two different cutoffs Λ_F and Λ_B and therefore two infinite sets of flow equations. This scheme has extensively been discussed by [50] who considered more general frequency dependent cutoffs as well. For one-dimensional electronic systems these different cutoffs have been investigated by [53].

The equations for Λ_F at $\Lambda_B = \Lambda_B^{(0)}$ are simply solvable and generate an infinite number of purely bosonic vertices $\Gamma^{(0,m)}$. The initial values [39, 41] of these vertices are defined by closed fermionic loops with the corresponding number (i.e. m) of bosonic legs

$$\Gamma_{\Lambda_B^{(0)}}^{(0,m)}(\mathbf{K}_1, \ldots, \mathbf{K}_m) = i^m \mathcal{S} \int_{\mathbf{K}} G(\mathbf{K})G(\mathbf{K}+\mathbf{K}_1) \cdot \ldots \cdot G(\mathbf{K}+\mathbf{K}_1+\ldots+\mathbf{K}_m). \tag{2.60}$$

Note that the propagator G is free of any infrared cutoff. The operator $\mathcal{S}$ symmetrizes the integral with respect to the external momenta. In most cases we do not need to regularize the fermions and may drop the UV-cutoff from the fermionic propagators in (2.60).

The bosonic vertex $\Gamma^{(0,2)}$ contributes to the bosonic self energy - we call this term the polarization Π. Therefore the full bosonic propagator can be written as

$$F^{-1} = F_0^{-1} + \Pi \ . \tag{2.61}$$

However keep in mind that the polarization generally will be renormalized as well as we lower the cutoff Λ_B.

2.6 Rescaling

As the infinite hierarchy of flow equations is only exactly treatable in exceptional circumstances we have to perform some kind of truncation. This is conveniently done by classifying the vertices according to their relevance. The term "relevance" here has a precise physical meaning and is determined by the scaling dimension of the corresponding vertex - we will come back to this in a moment.

To perform a renormalization group treatment in Wilsonian fashion (and to find out about the scaling dimensions) we have to rescale frequencies, momenta and vertices such as to flow into a fixed point. The details of the rescaling are not unique but depend on the details of this fixed point. Following [50] we introduce dynamical exponents z_α to describe how frequencies and momenta for each kind of particle are rescaled relative to each other. Note that in this work Λ_α always has the dimension of momentum.

2.6.1 Reparametrization

We introduce the flow parameters τ_α to write the scales as

$$\Lambda_\alpha(\tau_\alpha) = \Lambda_\alpha^{(0)} e^{-\tau_\alpha} \ . \tag{2.62}$$

The renormalization group flow is now generated by successively moving from $\tau = 0$ to $\tau \to \infty$. We rewrite the flow equations with respect to the change of the parameters τ_α.

It is convenient to work with one scale only $\Lambda_\alpha = \Lambda$ so we only have one infinite set of flow equations. We therefore only use one flow parameter τ. If for example we make use of the partial bosonization of the interaction Λ then refers to the bosonic interaction-scale Λ_B if we work with an interaction cutoff (where the fermionic cutoff has vanished from the theory).

2.6.2 Rescaling of momenta

Bosonic momenta

We rescale bosonic momenta toward zero as (α referring to a bosonic field)

$$\mathbf{q}_\alpha \ = \ \frac{\mathbf{k}_\alpha}{\Lambda_\alpha} \ , \tag{2.63}$$

$$\epsilon_\alpha \;\; = \;\; \frac{\omega_\alpha}{\Lambda_\alpha^{z_\alpha}} \; . \tag{2.64}$$

Note that the rescaled frequencies ϵ_α as defined above are not necessarily dimensionless. However if desired we can always include some normalization factor to achieve this property. The scheme above generally works well in all dimensions. The measure of integration is then simply

$$\int_{\mathbf{K}} = \Lambda^{D+z_\phi} \int_{\mathbf{Q}} \; , \tag{2.65}$$

with

$$\int_{\mathbf{Q}} = \int \frac{d\mathbf{q}}{(2\pi)^D} \int \frac{d\epsilon}{2\pi} \; . \tag{2.66}$$

It might be more convenient in some cases to use a different normalization and to pull out a factor which will be absorbed again by a redefinition of the vertices.

Fermionic momenta

If we consider fermions it is much less obvious how to rescale correctly. We have to use the true (full interacting) Fermi surface as a reference [19, 38]. The most obvious choice is to use the coordinate system defined by the shape of the Fermi surface or a patch around the Fermi surface as explained in section 2.4 to define

$$q_{\alpha\parallel} \;\; = \;\; \frac{|\mathbf{v}_F(\mathbf{k}_\perp)| \, k_{\alpha\parallel}}{\Lambda_\alpha} \; , \tag{2.67}$$

$$\epsilon_\alpha \;\; = \;\; \frac{\omega_\alpha}{\Lambda_\alpha^{z_\alpha}} \; . \tag{2.68}$$

We have some freedom of choice to rescale directions parallel to the Fermi surface. In many cases the energy dispersion does not depend on $\mathbf{k}_\perp$ if we stay close enough to the Fermi surface. In this case we can formally treat the parallel directions as mere parameters and use a rescaling like

$$\mathbf{q}_{\alpha\perp} = \frac{\mathbf{k}_{\alpha\perp}}{\Lambda_\alpha^{(0)}} \; . \tag{2.69}$$

just to make them dimensionless. We could use any other typical scale instead of $\Lambda_\alpha^{(0)}$ as well. The integration over the rescaled momenta for fermions is defined as

$$\int_{\mathbf{K}} = \nu_0 \Lambda^{1+z_\psi} \int_{\mathbf{Q}} \; , \tag{2.70}$$

with

$$\int_{\mathbf{Q}} = \int \frac{d\mathbf{q}_\perp}{\int d\mathbf{q}_\perp \tilde{J}(\mathbf{q}_\perp, 0)} \int dq_\parallel \tilde{J}(\mathbf{q}_\perp, q_\parallel) \int \frac{d\epsilon}{2\pi} \; . \tag{2.71}$$

Here we have introduced the density of states of the non-interacting system at the true Fermi surface

$$\nu_0 = \int_{\mathbf{k}} \delta(\epsilon_{\mathbf{k}} - \epsilon_F(\mathbf{k}_\perp)) \ , \tag{2.72}$$

and the rescaled Jacobian

$$\tilde{J}(\mathbf{q}_\perp, q_\parallel) = \frac{J(\mathbf{k}_\perp, k_\parallel)}{|\mathbf{v}_F(\mathbf{k}_\perp)|} \ . \tag{2.73}$$

Mixed theories

If the problem contains both bosons and fermions that interact it is convenient to use the same rescaling to simplify the constraints of momentum conservation. Which of the rescaling schemes (2.63), (2.67) we use depends on the details of the problem and there is no standard way.

2.6.3   Rescaling of vertices and fields

To complete our preparation for a Wilsonian RG treatment we finally rescale vertices and fields.

Field-rescaling

The usual approach is to fix the field rescaling by requiring invariance of the Gaussian part of the action under the rescaling. The details depend on the form of the propagator and we give a few examples.

For fermions (adding the true Fermi energy and subtracting it by a redefinition of the 2-point vertex) we write the Gaussian part as

$$S^{(2)} = - \int_{\mathbf{K}} \bar{\psi}(\mathbf{K}) \left(i\omega_n - \xi_{\mathbf{k}} - \Gamma^{(2)}(\mathbf{K}) \right) \psi(\mathbf{K}) \ . \tag{2.74}$$

Allowing for an anomalous scaling dimension Z_ψ of the fields and writing rescaled quantities with a tilde "~" and using (2.71) this has to the same as

$$S^{(2)} = - \int_{\mathbf{Q}} \bar{\tilde{\psi}}(\mathbf{Q}) \left(i\epsilon Z_\psi - \tilde{\xi}_{\mathbf{q}} Z_\psi - \tilde{\Gamma}^{(2)}(\mathbf{K}) \right) \tilde{\psi}(\mathbf{Q}) \ . \tag{2.75}$$

To satisfy this condition we have to rescale the fields according to

$$\psi(\mathbf{K}) = \sqrt{\frac{Z_\psi}{\Lambda^{1+2z_\psi}}} \tilde{\psi}(\mathbf{Q}) \ . \tag{2.76}$$

In most cases the energy dispersion will be linear when expanded around the Fermi surface so that $z_\psi = 1$.

Considering a complex bosonic field we write the Gaussian part as

$$S^{(2)} = -\int_{\mathbf{K}} \phi^*(\mathbf{K}) \left(i\omega_n - \epsilon_{\mathbf{k}} - \Pi(\mathbf{K}) \right) \phi(\mathbf{K}) \ . \tag{2.77}$$

Invariance of this Gaussian part using (2.66) requires to rescale

$$\phi(\mathbf{K}) = \sqrt{\frac{Z_\phi}{\Lambda^{D+2z_\psi}}} \tilde{\phi}(\mathbf{Q}) \ . \tag{2.78}$$

The bosonic dispersion is in most cases quadratic so that $z_\phi = 2$. The generalization to other cases is straightforward.

Vertex-rescaling

As we have determined how to rescale the fields finding the correct rescaling of the vertices follows from the requirement that the expansion of the functional $\Gamma[\boldsymbol{\Phi}]$ is invariant to all orders. As an example considering a purely fermionic theory the vertex $\Gamma^{(2n)}(\{\mathbf{K}\})$ describing the scattering of $2n$ fermions for $z_\psi = 1$ has to be rescaled as

$$\tilde{\Gamma}^{(2n)}(\{\mathbf{Q}\}) = \mathcal{R}^{(2n)} \, \Gamma^{(n,m)}(\{\mathbf{K}\}) \ , \tag{2.79}$$

with

$$\mathcal{R}^{(2n)} = \Lambda^{n-2} \left[Z_\tau(\mathbf{q}_{\perp 1}) \ldots Z_\tau(\mathbf{q}_{\perp 2n}) \right]^{\frac{1}{2}} \ . \tag{2.80}$$

We are free to pull out additional factors in the definition of the rescaled vertices if we do it in a consistent way. For example we might wish to factor out the density of states at the Fermi surface ν_0. Rescaled Greensfunctions $\tilde{G}$ are defined in the same way as

$$G_\alpha(\mathbf{K}) = \mathcal{R}^{(2)} \tilde{G}_\alpha(\mathbf{Q}) \ , \tag{2.81}$$

$$\Lambda \dot{G}_\alpha(\mathbf{K}) = -\mathcal{R}^{(2)} \dot{\tilde{G}}_\alpha(\mathbf{Q}) \ . \tag{2.82}$$

The anomalous dimensions η_α of the fields are introduced as derivatives of the anomalous scaling factors

$$\eta_\alpha = -\partial_\tau \ln \left(Z_{\tau,\alpha} \right) \ . \tag{2.83}$$

The full scaling-dimension of the vertices (again for fermions) under the RG is then obtained as

$$\left[\tilde{\Gamma}^{(2n)}(\{\mathbf{K}\}) \right] = 2 - n - \frac{\eta_1 + \ldots + \eta_{2n}}{2} \ , \tag{2.84}$$

where the word "full" indicates that we include the anomalous scaling due to interactions. Depending on the sign of this full scaling-dimension we term the vertices to be relevant, marginal and irrelevant:

$$
\begin{aligned}
[\Gamma] > 0 : &\quad \text{relevant} \\
[\Gamma] = 0 : &\quad \text{marginal} \\
[\Gamma] < 0 : &\quad \text{irrelevant}
\end{aligned}
$$

This terminology expresses how important a specific vertex is in the vicinity of a fixed point. Irrelevant vertices generally do not alter the fixed point structure but merely lead to quantitative changes which can be absorbed into a redefinition of the bare coupling constants [9, 18]. As we know the values for the anomalous dimensions usually only a-posteriori we sometimes neglect them in (2.84) and term the vertices to be *superficially* relevant, marginal or irrelevant.

We note that we can expand the vertices in powers of frequencies and momenta (see section 3.1). The coefficients of this expansion define vertices with increasingly smaller scaling-dimensions. For each additional power of momentum the scaling dimension is reduced by 1 and for each power of frequency by z_α. Therefore if we chose to consider relevant and marginal vertices only we often suffice with just the momentum-independent part and maybe the first one or two momentum-dependent terms of this expansion.

Rescaled flow equations

By application of the chain rule we get

$$
\partial_\tau = -\Lambda_\tau \partial_\Lambda \; . \tag{2.85}
$$

Now writing the flow of unrescaled vertices as

$$
\partial_\Lambda \Gamma^{(n)}(\{\mathbf{K}\}) = \dot{\Gamma}^{(n)}(\{\mathbf{K}\}) \; , \tag{2.86}
$$

we define using (2.80)

$$
\tilde{\dot{\Gamma}}^{(n)}(\{\mathbf{Q}\}) = -\Lambda \mathcal{R}^{(n)} \dot{\tilde{\Gamma}}^{(n)}(\{\mathbf{K}\}) \; . \tag{2.87}
$$

We can simply substitute in (2.39) unrescaled vertices and Greensfunction by their rescaled counterparts to obtain $\tilde{\dot{\Gamma}}$ - the minus sign in (2.87) gets compensated by the minus sign in the rescaled Greensfunction (2.82). The flow equations for the rescaled vertices can then be written as

$$
\partial_\tau \tilde{\Gamma}^{(n)}(\{\mathbf{Q}\}) = \left(\tilde{\mathcal{R}}^n - \sum_i \mathbf{Q}_i \cdot \partial_{\mathbf{Q}_i} \right) \tilde{\Gamma}^{(n)}(\{\mathbf{Q}\}) + \tilde{\dot{\Gamma}}^{(n)}(\{\mathbf{Q}\}) \; , \tag{2.88}
$$

with

$$
\tilde{\mathcal{R}}^n = [\tilde{\Gamma}^{(n)}] \; , \tag{2.89}
$$

and the shorthand

$$
\mathbf{Q}_i \cdot \partial_{\mathbf{Q}_i} = \mathbf{q}_i \cdot \partial_{\mathbf{q}_i} + z_i \epsilon_i \partial_{\epsilon_i} \; . \tag{2.90}
$$

We clearly observe the meaning of the scaling dimension and how it is successively reduced by higher powers of frequencies/momenta.

Chapter 3

Approximation methods

It is one thing to obtain the infinite hierarchy of flow equations for the exact renormalization group and another to actually derive any useful results. Except a few exceptional cases [39, 41] we have to rely on a couple of approximation methods. Our equations then generally loose their exactness and we try to apply only such approximations as to describe the system at hand at least qualitatively correct. In this chapter we discuss a few possible schemes for simplification.

3.1 Expanding in relevance

We shall use a truncation based on the relevance (in the spirit of scaling dimension) of the vertices in this work. The idea behind this approach is that irrelevant vertices do not alter the critical behaviour of a system but merely lead to a quantitative renormalization which can be absorbed by a redefinition of bare coupling parameters - actually these irrelevant vertices can be expressed in terms of the relevant and marginal ones [9, 18].

We expand all vertices in integer powers of frequencies and momenta. According to (2.88) the coefficients of this expansion become increasingly irrelevant with increasing powers of frequency/momentum. On the other hand even the scaling dimension of the momentum independent part of the vertices decreases with an increasing number of external legs. Retaining now only those vertices with a certain minimum scaling dimension (e.g. retaining only relevant and marginal vertices) therefore effectively truncates the infinite set of flow equations. In practical applications we then only have to consider a handful of vertices.

This approach has some similarities to the momentum-scale expansion carried forward by Morris [17, 44–46, 54, 55]. In the latter *all* vertices are considered up to a certain power of momentum - including just the constant parts leads to the *local potential approximation* [56]. However going beyond this leading order is in most cases impractical [17].

Unfortunately using a sharp cutoff (2.44) our approach suffers from similar

problems as the momentum-scale expansion [55] with the same sharp cut-off when going beyond the leading approximation. Here too we observe only a very weak convergence for physical quantities when including increasingly irrelevant couplings [57], see chapter 4.

3.1.1 Hybrid approach

To improve our results we use some kind of two-step hybrid approach. In the first step we just consider all relevant and marginal vertices and solve the corresponding flow equations. As second step we use these solutions as an input to the flow equations to obtain the full momentum dependence of the vertices without performing any further expansion in the momentum. By applying this procedure we approximately take the flow of infinitely many irrelevant vertices into account without the need to perform any further expansion. Hereby we (partially) avoid the weak convergence properties of the sharp cutoff procedure.

We apply this hybrid approach to investigate interacting bosons in three dimensions and it enables us to obtain the full momentum dependence of the self-energy in this case, see chapter 4. We also apply this approximation to the problem of confinement in a system of two coupled Luttinger chains, chapter 6, and a two-dimensional system of interacting fermions, chapter 7. In all cases the results are quite satisfactory keeping in mind the simplicity of the approach.

3.1.2 Bosonized interaction with interaction cutoff

We obtain the most reliable results when bosonizing the interaction by means of a Hubbard-Stratonovich transformation as laid out in section 2.5. Retaining only relevant and marginal vertices but keeping the full momentum dependence of the bosonic propagator even lets us successfully consider strong interacting particles, see chapters 6 and 7.

3.1.3 Example

We consider as an example a system of spinless interacting fermions in one dimension with a linear dispersion

$$\epsilon_k - \epsilon_F = v(|k| - |k_F|) \, . \tag{3.1}$$

This system of course is well known and exactly solvable [58–60]. We define the vertices $\tilde{r}, \tilde{v}, Z$ and $\tilde{g}$ as

$$\tilde{\Gamma}^{(2)}(Q) = \tilde{r} + i\epsilon(Z - 1) + q(Z - \tilde{v}) + O(\epsilon^2, q^2, i\epsilon q) \tag{3.2}$$

$$\tilde{\Gamma}^{(4)}(0) = \tilde{g} \tag{3.3}$$

and observe using (2.88) that $\tilde{r}$ is relevant with scaling dimension 1 whereas $\tilde{v}, Z$ and $\tilde{g}$ are (superficially) marginal. All other vertices are irrelevant. Using the expansion as above we can express the anomalous wavefunction rescaling as

$$Z_\tau = 1 + \partial_{i\epsilon} \tilde{\Gamma}_\tau^{(2)}(\mathbf{Q})|_{\mathbf{Q}=0} . \tag{3.4}$$

Noting the relation to the anomalous dimension (2.83) we can write the latter as

$$\eta_\tau = -\partial_{i\epsilon} \dot{\tilde{\Gamma}}_\tau^{(2)}(\mathbf{Q})|_{\mathbf{Q}=0} . \tag{3.5}$$

The flow for the renormalized fermi velocity is obtained as

$$\partial_\tau \tilde{v}_\tau = -\eta_\tau \tilde{v}_\tau - \partial_q \tilde{\Gamma}^{(2)}(\mathbf{Q})|_{\mathbf{Q}=0} . \tag{3.6}$$

Inserting the expansion (3.2) into the definition of the Greensfunction yields

$$\tilde{G}(\mathbf{Q}) = \frac{\Theta(1 < |q| < e^\tau)}{i\epsilon - \tilde{v}q - \tilde{r}} , \tag{3.7}$$

$$\dot{\tilde{G}}(\mathbf{Q}) = \frac{\delta(1 - |q|)}{i\epsilon - \tilde{v}q - \tilde{r}} . \tag{3.8}$$

We will use this approximation for the Greensfunction quite often. The set of flow equations forms a closed system which is easy to solve. However within this approximation we obtain the (wrong) result that the fixed point anomalous dimension vanishes $\eta^* = 0$ [20]. Using the hybrid approach as defined above greatly improves our estimate for η^* [20]. Bosonizing the interaction by means of a Hubbard-Stratonovich transformation and retaining only the relevant and marginal vertices (but the full momentum dependence of the bosonic propagator) actually yields the correct value for η^* [39].

3.2   Adiabatic approximation

In this section we shall justify what we term the adiabatic approximation for the bosonic Greensfunction. It builds on top of the expansion in relevance (see section 3.1) to approximately calculate the flow of vertices whose flow equation exclusively depends on irrelevant vertices (that we have chosen to neglect).

We will only consider its derivation for the bosonic polarization in the context of a bosonized interaction when working with an interaction cutoff. However we believe that this kind of approximation might be useful for other problems as well. We will apply it when investigating the problem of confinement of fermions in one or two dimensions, chapters 6 and 7.

3.2.1 Definition

We start by remembering the definition of the (rescaled) bosonic propagator

$$\tilde{F}^{-1}_{\sigma\sigma'}(\mathbf{Q}) = V^{-1}_{\sigma\sigma'} + \tilde{\Pi}_{\sigma\sigma'}(\mathbf{Q}). \tag{3.9}$$

with $\Pi(\mathbf{Q})$ given by (2.60). The flow of the polarization is generated by irrelevant vertices [41] that we have chosen not to consider, i.e. within the present approximation it is zero. Instead we define the adiabatic approximation for fermions with spin $\sigma = \pm 1$ as

$$\tilde{\Pi}_{\sigma\sigma';\tau}(\mathbf{Q}) = \int_{Q'} \tilde{\gamma}^2_{\sigma\sigma';\tau} \tilde{G}'_{\sigma;\tau}(\mathbf{Q} + \mathbf{Q}' - \sigma\delta_{\sigma\bar{\sigma}'}\tilde{\Delta}_\tau(\tau))\tilde{G}'_{\sigma';\tau}(\mathbf{Q}') . \tag{3.10}$$

Here $\tilde{\gamma}_{\sigma\sigma'}$ is the constant (marginal) part of the vertex $\tilde{\Gamma}^{(2,1)}_{\sigma\sigma';\tau}(\mathbf{Q_1}, \mathbf{Q_2})$ which scatters a fermion with spin σ and incoming momentum $\mathbf{Q_2}$ into a fermion with spin σ' by emission/absorption of a boson with incoming momentum $\mathbf{Q_1}$. Note that for an attractive interaction this vertex is real valued with the initial value $\tilde{\gamma}_{\sigma\sigma',0} = 1$ whereas for repulsive interactions it is complex with the initial value $\tilde{\gamma}_{\sigma\sigma',0} = i$. We have allowed for different fermi momenta which are separated by the τ-dependent rescaled magnetization $\tilde{\Delta}_\tau(\tau) = \frac{k_{\uparrow,\tau} - k_{\downarrow,\tau}}{\Lambda_\tau}$ with the fermi momenta at scale τ. Additionally we have defined $\bar{\sigma} = -\sigma$. The Greensfunctions $\tilde{G}'$ are modified in that way that we have dropped in the denominator the relevant frequency/momentum-independent part of the fermionic 2-point vertex.

3.2.2 Derivation

We give a derivation of the adiabatic approximation for an one-dimensional system (it is also valid if we can treat additional momentum dimensions as parameters). We are working with an interaction cutoff Λ_B. This can be viewed as using both an interaction and bandwidth cutoff Λ_F but integrating out the latter first. Now the result at any scale Λ^B should be independent of the trajectory in the two dimensional cutoff space spanned by $\left(\Lambda^F, \Lambda^B\right)$. Therefore we can reach the same point $\left(\Lambda^F = 0, \Lambda^B\right)$ by first scaling $\Lambda^B_0 \to \Lambda^B$ and then $\Lambda^F_0 \to 0$. As we work with rescaled variables we use the flow parameters

$$\Lambda^F = \Lambda^F_0 e^{-l} , \tag{3.11}$$

$$\Lambda^B = \Lambda^B_0 e^{-\tau} . \tag{3.12}$$

In principle all vertices now depend on both of the parameters l, τ. However we shall always use only one of the flow parameters as subscript to make clear how a specific vertex is rescaled. So we write all vertices either as functions of l (with an implicit dependence on τ) and then rescale according to the fermion cutoff picture

or we write them as functions of τ (and assume $l \to \infty$) and rescale according to the interaction cutoff. The calculations are a bit tedious and we have to be careful when switching between both pictures.

We start with the flow equation for the polarization with respect to l (at any fixed τ) which reads

$$\partial_l \tilde{\Pi}_{\sigma\sigma';l}(\mathbf{Q}_l) = -\mathbf{Q}_l \cdot \partial_{\mathbf{Q}_l} \tilde{\Pi}_{\sigma\sigma';l}(\mathbf{Q}_l) + \dot{\tilde{\Pi}}_{\sigma\sigma';l} , \tag{3.13}$$

with

$$
\begin{aligned}
\dot{\tilde{\Pi}}_{\sigma\sigma';l}(\mathbf{Q}_l; \tilde{\Delta}_l^*) &= \tilde{\gamma}_{\sigma\sigma';l}^2 \int_{\mathbf{Q}'_l} \Big(\dot{\tilde{G}}_{\sigma;l}(\mathbf{Q}'_l + \mathbf{Q}_l - \sigma\delta_{\sigma\bar{\sigma}'}\tilde{\Delta}_l^*)\tilde{G}_{\sigma';l}(\mathbf{Q}'_l) \\
&\qquad\qquad + \tilde{G}_{\sigma;l}(\mathbf{Q}'_l + \mathbf{Q}_l - \sigma\delta_{\sigma\bar{\sigma}'}\tilde{\Delta}_l^*)\dot{\tilde{G}}_{\sigma';l}(\mathbf{Q}'_l) \Big) \\
&=: \tilde{\gamma}_{\sigma\sigma';l}^2 \dot{\tilde{\Pi}}_{\sigma\sigma';l}'(\mathbf{Q}_l; \tilde{\Delta}_l^*) .
\end{aligned}
\tag{3.14}
$$

Additionally we have depicted this flow equation in figure 3.1.
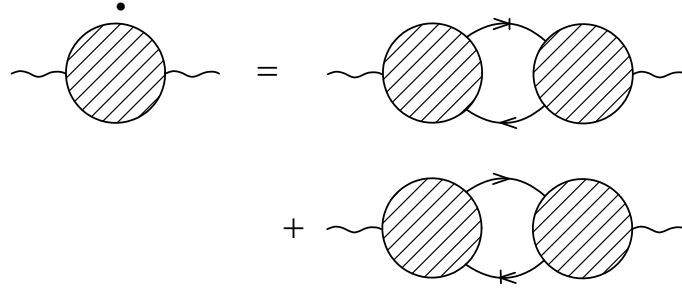
Figure 3.1: Flow of polarization as described in (3.14).

Note that here we have to expand momenta around the fermi surface at scale set by τ. The magnetization $\tilde{\Delta}_l^*$ is then defined as

$$\tilde{\Delta}_l^* = \frac{k_{\uparrow,\tau} - k_{\downarrow,\tau}}{\Lambda_l^F} . \tag{3.15}$$

On the other hand the flowing magnetization at scale τ is given by

$$\tilde{\Delta}_\tau(\tau) = \frac{k_{\uparrow,\tau} - k_{\downarrow,\tau}}{\Lambda_\tau^B} = e^{\tilde{l}-l}\tilde{\Delta}_l^* \tag{3.16}$$

with

$$\tilde{l} = \tau + \ln(\Lambda_0^F/\Lambda_0^B) . \tag{3.17}$$

We shall generally assume that $\Lambda_0^F > \Lambda_0^B$ such that always $\tilde{l} > 0$.

The important observation is now that at any fixed τ the momentum transfer of the interaction, i.e. the bosonic Greensfunction is restricted by the cutoffs Λ_τ^B and Λ_0^B. This restriction in turn imposes an upper and lower cutoff of momentum flowing through internal loops involving bosonic propagators. As l grows, i.e. Λ_l^F gets smaller, the momenta of the fermionic Greensfunctions get closer to the Fermi momenta. The momentum transfer through the loop gets smaller in turn until it reaches the lower cutoff Λ_τ^B where the corresponding diagrams vanish. As a consequence we obtain the following form of flow equation for the fermionic 2-point vertex

$$\partial_l \tilde{r}_{\sigma;l} = \tilde{r}_{\sigma;l} + B_{\sigma;l,\tau}\Theta(l < \tilde{l}(\tau)) \tag{3.18}$$

where the theta function is due to the non-trivial interaction cutoff parametrized by τ as explained above. We also have absorbed the flow due to the anomalous dimension (which vanishes for $l > \tilde{l}$) into B. So we can write

$$\tilde{r}_{\sigma;l>\tilde{l}} = e^{l-\tilde{l}}\tilde{r}_{\sigma;\tilde{l}} \,, \tag{3.19}$$

and there are similar expressions for the higher frequencies/momenta coefficients of the 2-point function (which is why $\eta_{l>\tilde{l}} = 0$). As we shall learn later on in chapter 5 the vertices $\tilde{r}$ have to be fine tuned to reach a fixed point. Looking at (3.19) this only can achieved if

$$\tilde{r}_{\sigma;l>\tilde{l}} = 0 \,. \tag{3.20}$$

Therefore we use in the definition (3.10) the modified Greensfunctions $\tilde{G}'$ - actually viewed from another angle the relevant part of the fermionic 2-point vertex is contained in the flowing magnetization $\tilde{\Delta}_\tau(\tau)$. By the same arguments as above the 3-point vertex obeys

$$\partial_l \tilde{\gamma}_l = A_{l,\tau}\Theta(l < \tilde{l}(\tau)) \tag{3.21}$$

and we define

$$\tilde{\gamma}_{l>\tilde{l}} = \tilde{\gamma}_{\tilde{l}} =: \tilde{\gamma}_\tau \,. \tag{3.22}$$

The important observation is that the vertices depend for $l > \tilde{l}$ only trivially on l by the rescaling of momenta.

Equation (3.13) is simply solvable as

$$\begin{aligned}
\Pi_{\sigma\sigma';l}(Q_l) &= \int_0^l dl' \, \dot{\tilde{\Pi}}_{\sigma\sigma';l'}(Q_{l'}; \tilde{\Delta}_{l'}^*) \\
&= \int_0^l dl' \, \dot{\tilde{\Pi}}_{\sigma\sigma';l'}(Q_{l'}e^{l'-l}; \tilde{\Delta}_{l'}^*) \,.
\end{aligned} \tag{3.23}$$

Transforming into the interaction cutoff picture it reads

$$\tilde{\Pi}_{\sigma\sigma';\tau}(Q_\tau) = \lim_{l\to\infty} \tilde{\Pi}_{\sigma\sigma';l}(Q_\tau e^{l-\tilde{l}})$$

$$
\begin{aligned}
&= \int_0^\infty dl \, \dot{\tilde{\Pi}}_{\sigma\sigma';l}(Q_\tau e^{l-\tilde{l}}; \tilde{\Delta}_{l'}^*) \\
&= \int_0^{\tilde{l}} dl \, \tilde{\gamma}_{\sigma\sigma';l}^2 \dot{\tilde{\Pi}}'_{\sigma\sigma';l}(Q_\tau e^{l-\tilde{l}}; \tilde{\Delta}_\tau(\tau) e^{l-\tilde{l}}) \\
&\quad + \tilde{\gamma}_{\sigma\sigma';\tau}^2 \int_{\tilde{l}}^\infty dl \, \dot{\tilde{\Pi}}'_{\sigma\sigma';l}(Q_\tau e^{l-\tilde{l}}; \tilde{\Delta}_\tau(\tau) e^{l-\tilde{l}}) \\
&=: \tilde{\Pi}_{\sigma\sigma';\tau}^{\text{gen}}(Q_\tau) + \tilde{\Pi}_{\sigma\sigma';\tau}^{\text{adiabat}}(Q_\tau) \, .
\end{aligned}
\tag{3.24}
$$

We note that the second part $\tilde{\Pi}^{\text{adiabat}}$ only trivially depends on l via the transformation of momenta - all the vertices here are evaluated at $l \to \infty$, i.e. they just depend on τ. The transformation for the fermionic Greensfunction between the two pictures is for $l > \tilde{l}$

$$
\begin{aligned}
\tilde{G}_{\sigma;l}(Q_l) &= e^{\tilde{l}-l} \tilde{G}_{\sigma;\tau}(Q_l e^{\tilde{l}-l}) \, \Theta(|q_l| - 1) \\
\dot{\tilde{G}}_{\sigma;l}(Q_l) &= \tilde{G}_{\sigma;\tau}(Q_l e^{\tilde{l}-l}) \, \delta(|q_l| - 1) \, .
\end{aligned}
\tag{3.25}
\tag{3.26}
$$

Note that we have not included any UV cutoff as we do not need it to regularize the polarization. The Greensfunction in the interaction cutoff picture $\tilde{G}_{\sigma;\tau}$ is free of any cutoff. We can now express for $l > \tilde{l}$

$$
\dot{\tilde{\Pi}}'_{\sigma\sigma';l}(Q_\tau e^{l-\tilde{l}}; \tilde{\Delta}_\tau(\tau) e^{l-\tilde{l}}) = \int_{Q'_\tau} \tilde{G}'_{\sigma;\tau}(\tilde{Q}_\tau + Q'_\tau) \tilde{G}'_{\sigma';\tau}(Q'_\tau) e^{l-\tilde{l}}
\tag{3.27}
$$
$$
\times \left\{ \delta(|\tilde{q}_\tau + q'_\tau| e^{l-\tilde{l}} - 1) \Theta(|q'_\tau| e^{l-\tilde{l}} - 1) + \Theta(1 < |\tilde{q}_\tau + q'_\tau| e^{l-\tilde{l}}) \delta(1 - |q'_\tau| e^{l-\tilde{l}}) \right\}
$$

with $\tilde{q} = q - \sigma \delta_{\sigma\bar{\sigma}'} \tilde{\Delta}_\tau(\tau)$. For $l < \tilde{l}$ we can not easily switch to the interaction cutoff picture. However we assume that we can define an effective $\tilde{G}_\tau$ which somehow depends on $\tilde{G}_l$ with $l \in [0, \tilde{l}]$. The important part that distinguishes between the adiabatic and the more general regime stems from the product $\{\delta\Theta + \Theta\delta\}$ in (3.27). To show how this works and without becoming too specific we note that the integration over q' in (3.27) will be regulated by the product of Greensfunction approximately such that only $q' \in [-\tilde{q}, 0]$ contribute. This actually holds exactly if we approximate $\tilde{G}'_\tau = \frac{1}{i\epsilon - vq}$. We then can write

$$
\dot{\tilde{\Pi}}_{\sigma\sigma';l}(Q_\tau e^{l-\tilde{l}}; \tilde{\Delta}_\tau^* e^{l-\tilde{l}}) = \int_{-\tilde{q}}^0 dq'_\tau \, X_{\sigma\sigma';l}(\tilde{Q}, q') e^{l-\tilde{l}}
\tag{3.28}
$$
$$
\times \left\{ \delta(|\tilde{q} + q'| e^{l-\tilde{l}} - 1) \Theta(|q'| e^{l-\tilde{l}} > 1) + \Theta(1 < |\tilde{q} + q'| e^{l-\tilde{l}}) \delta(1 - |q'| e^{l-\tilde{l}}) \right\}
$$

with some function X. Assuming we can somehow define an effective X^{eff} to calculate Π^{gen} we arrive at

$$
\tilde{\Pi}_{\sigma\sigma';\tau}^{\text{gen}}(Q_\tau) = \int_{-\tilde{q}}^0 dq'_\tau \, X_{\sigma\sigma';\tilde{l}}^{\text{eff}}(\tilde{Q}, q')
\tag{3.29}
$$
$$
\times \left\{ \theta(1 < |\tilde{q} + q'| < \min\{e^{\tilde{l}}, |q'|\}) + \theta(|q'| < \min\{e^{\tilde{l}}, |\tilde{q} + q'|\}) \right\}
$$

$$
\begin{aligned}
\tilde{\Pi}^{\text{adiabat}}_{\sigma\sigma';\tau}(Q_\tau) \;=\; & \int_{-\tilde{q}}^{0} dq'_\tau \, X_{\sigma\sigma';\tilde{l}}(\tilde{Q}, q') \\
& \times \{\theta(|\tilde{q} + q'| < \min\{1, |q'|\}) + \theta(|q'| < \min\{1, |\tilde{q} + q'|\})\} \; .
\end{aligned}
\tag{3.30}
$$

Taking a look at these expression we observe that as long as $|\tilde{q}| < 2$ just the adiabatic part contributes and therefore the adiabatic approximation is exactly valid. As the momentum gets larger the general part grows and there is a smooth crossover to the more general regime as $\tilde{q} \to \infty$.

Actually in most cases we only need the bosonic propagator to calculate the flow of other couplings. In this case it is sufficient to evaluate it at $q' = \pm 1$. Let's for the time look at the spinless Tomonaga-Luttinger model with $g_2 = g_4$. Here we can conclude that if we use $\tilde{G}'_\tau = \frac{1}{i\epsilon - q}$ for simplicity we get

$$
\Pi^{\text{gen}}_\tau(i\epsilon, \pm 1) = 0
\tag{3.31}
$$

and

$$
\Pi^{\text{adiabat}}_\tau(i\epsilon, \pm 1) = -\frac{\tilde{\gamma}^2_\tau}{\pi} \frac{1}{\epsilon^2 + 1}
\tag{3.32}
$$

and we observe that for these momenta the adiabatic approximation is valid along the complete trajectory τ. Note that we can not expect that the approximation for the Greensfunction we have performed above is valid for all τ. However we assume that at least at momentum $q = \pm 1$ it is close to the exact expression.

Turning back to a system with finite magnetization we distinguish the cases $|\tilde{\Delta}_\tau(\tau)| < 1$ and $|\tilde{\Delta}_\tau(\tau)| > 1$. Only in the former $|q| = 1$ implies $|\tilde{q}| < 2$ and we receive the result that $\Pi^{\text{gen}}_\tau(\pm 1) = 0$ - the adiabatic approximation is valid for all τ. In the latter there is some mixing between general and adiabatic contributions and there is no simple approximation. However later on when we investigate the flow of the fermionic 2-point vertex we observe that this flow is dominated by the region $|\tilde{\Delta}_\tau(\tau)| < 1$. Therefore the error induced by using the adiabatic approximation (3.10) instead of the full expression is in most cases negligible.

Considering the full flow equation for the polarization [41] which involves higher order vertices we note that the adiabatic approximation is self-consistent if we assume a similar adiabatic approximation to hold for these higher order vertices in turn.

Chapter 4

Weakly interacting bosons at the critical point of BEC

In this chapter we apply the functional renormalization group to study weakly interacting bosons at the critical point of Bose-Einstein condensation (BEC). As the phase-transition occurs at finite temperatures the physics can adequately be described by an effective classical field theory. We consider the flow of the relevant and marginal vertices of the theory and solve the corresponding flow equations. In a next step we are able to calculate the momentum dependence of the self-energy and to obtain the interaction induced shift of the critical temperature. Finally we improve the approximations by extending our approach to include even some irrelevant vertices. The work described below has been published in [57, 61]

4.1 Introduction

The physics of Bose-Einstein condensation (BEC) has a long history. Inspired by a 1924 paper of Bose [62] Einstein extended this work and developed the idea of a gas of non-interacting bosons condensing into the same quantum-state at low enough temperatures [63, 64]. The basic idea is that as the temperature is lowered the de-Broglie wavelength of the atoms grows until it becomes of the order of the inter-atomic distance. At this point the quantum-statistical nature of the atoms becomes important and if they are bosons they tend to occupy the same quantum-state - a Bose-Einstein condensate forms. Although superfluidity was discovered in ^{4}He a decade later [65, 66] and interpreted as a manifestation of BEC in a strongly interacting gas [67], BEC in (quasi) non-interacting gases remained unobserved until recently. Only after the development of sophisticated means of trapping and cooling atoms to sufficiently low temperatures (a few 100 nK) progress was made. Finally in 1995 two groups almost simultaneously reported the first experimental observation of BEC in dilute atomic gases [68, 69] and were rewarded with the Nobel Price later on. Triggered by these experiments

the field of BEC has attracted an increasing amount of research in the last years, see [70, 71] for a review.
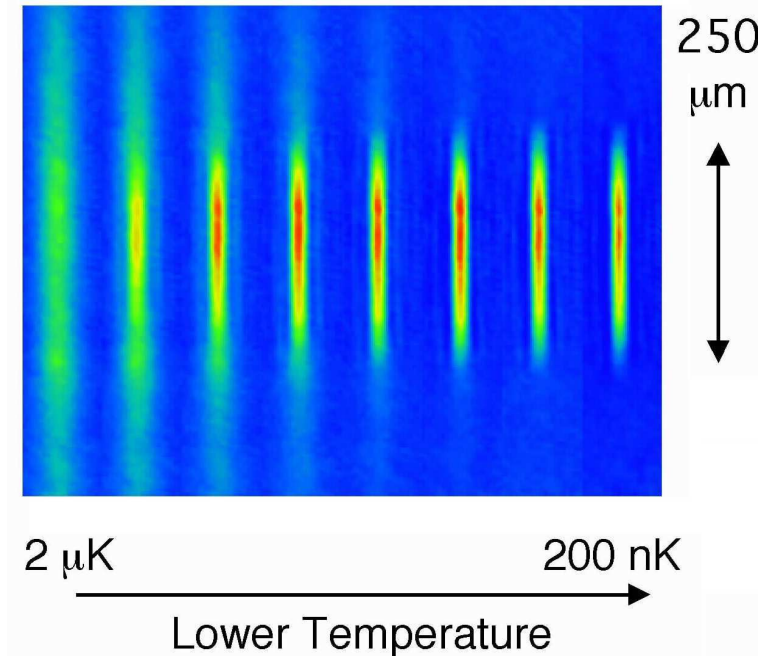
Figure 4.1: "Direct observation of the formation of a Bose-Einstein condensate using dispersive light scattering (phase contrast images). The intensity of the scattered light is a measure of the density of atoms (integrated along the line-of-sight). The left picture shows the cloud slightly above the BEC transition temperature. When the temperature was lowered, a dense core formed in the center of the trap - the Bose condensate. Further cooling increased the condensate fraction to close to 100% (right)." [72, 73]

The condensation transition of the weakly interacting Bose gas belongs to the $O(2)$ universality class and many of its properties like critical exponents are well known. At length scales larger than the thermal de-Broglie wavelength λ_{th} quantum fluctuations become unimportant and the Bose gas behaves universal on these scales [74, 75]. In this regime a description in terms of a classical ϕ^4-model is sufficient [76]. As a consequence of the extended universality the self-energy is universal for momenta $k < \lambda_{th}^{-1}$ and may be written in a scaling form independent of the interaction.

In the following we present a detailed investigation of the full momentum dependent zero-frequency self-energy at the critical point of BEC. We calculate the anomalous dimension and obtain the interaction induced shift of the critical temperature as a testing tool of our method. For the self-energy we observe at

a critical momentum scale k_c the crossover from anomalous scaling to the perturbative regime. Here the latter is characterized by the self-energy becoming negligible compared to the bare dispersion. Note that in $D < 4$ at finite temperatures a perturbative treatment of the self-energy is ultraviolet divergent. As long as $D > 3$ these divergences can be cured by using the de-Broglie wavelength λ_{th} as an effective ultraviolet cutoff. However in the perturbative regime as defined above, in $D = 3$ additional logarithmic infrared divergences appear that can adequately be treated only by resummation techniques [76] - this approach however is uncontrolled in the anomalous scaling regime. Therefore a couple of renormalization group approaches have been used [77–79] although none addressed the problem of finding the momentum dependence for the self-energy. The derivation of the momentum dependent self-energy within a RG approach has only recently been reconsidered by other authors [80].

4.2   Functional RG for bosons

4.2.1   Setup

Effective classical field theory

We describe the bosons in terms of a complex bosonic field ϕ. The non-interacting part of the action is then given by

$$S_0 = \int_{\mathbf{K}} \phi^*(\mathbf{K}) \left(-i\omega_n + \epsilon_{\mathbf{k}} - \mu + \Sigma(i0, 0) \right) \phi(\mathbf{K}) \tag{4.1}$$

with a simple quadratic dispersion

$$\epsilon_{\mathbf{k}} = \frac{\hbar^2 \mathbf{k^2}}{2m}. \tag{4.2}$$

and Matsubara frequencies $\omega_n = 2\pi n T$. We observe that for finite temperatures the Greensfunction

$$G(\mathbf{K}) = \frac{1}{i\omega_n - \epsilon_{\mathbf{k}} + \mu - \Sigma(i0, 0)} \tag{4.3}$$

if effectively cut off at non-zero frequencies and momenta smaller than the inverse thermal de-Broglie wavelength

$$k \approx \Lambda_0 := \frac{2\pi}{\lambda_{th}} \tag{4.4}$$

with $\lambda_{th} = \frac{1}{\hbar} \sqrt{\frac{mT}{2\pi}}$. This is the reason why it is sufficient just to consider a classical ϕ^4-theory with a complex $O(2)$ field. We therefore introduce this Λ_0 as an ultraviolet cutoff into our theory and consider the zero frequency part only.

For simplicity from now on we drop the frequencies from our notation and get at the critical point ($\mu = \Sigma(0)$)

$$S_0 = T \int_{\mathbf{k}} \phi^*(\mathbf{k})\phi(\mathbf{k})\epsilon_{\mathbf{k}}. \tag{4.5}$$

The interaction is introduced as

$$
\begin{aligned}
S_I \;=\;& T \int_{\mathbf{k}} \phi^*(\mathbf{k})\left(\Sigma_{\Lambda_0} - \Sigma(0)\right)\phi(\mathbf{k}) \\
&+ \frac{T^3}{4} \int_{\mathbf{k'_1}} \int_{\mathbf{k'_2}} \int_{\mathbf{k_2}} \int_{\mathbf{k_1}} \delta_{\mathbf{k'_1}+\mathbf{k'_2}=\mathbf{k_2}+\mathbf{k_1}} \, \Gamma^{(4)}_{\Lambda_0}(\mathbf{k'_1}, \mathbf{k'_2}, \mathbf{k_2}, \mathbf{k_1})\phi^*(\mathbf{k'_1})\phi^*(\mathbf{k'_2})\phi(\mathbf{k_2})\phi(\mathbf{k_1}).
\end{aligned}
\tag{4.6}
$$

We start from a local (momentum independent) interaction which is related to the s-wave scattering length a as

$$g := \Gamma^{(4)}_{\Lambda_0}(\mathbf{k'_1}, \mathbf{k'_2}, \mathbf{k_2}, \mathbf{k_1}) = \frac{8\pi\hbar^2 a}{m} =: 16\pi\rho_0 a. \tag{4.7}$$

Rescaled picture

We rescale as usual all momenta and vertices. Here we use

$$\mathbf{q} \;=\; \frac{\mathbf{k}}{\Lambda} \tag{4.8}$$

$$\tilde{\Gamma}^{(2n)}(\{\mathbf{q}\}) \;=\; (K_D T)^{n-1}\, \Lambda^{D(n-1)-2n} \left(\frac{Z_\tau}{\rho_0}\right)^n \Gamma^{(2n)}(\{\mathbf{k}\}) \tag{4.9}$$

$$\tilde{G}(\mathbf{q}) \;=\; \frac{\Theta(1 < |\mathbf{q}| < e^\tau)}{Z_\tau \mathbf{q}^2 + \tilde{\Gamma}^{(2)}(\mathbf{q})} = \frac{\Theta(1 < |\mathbf{q}| < e^\tau)}{R_\tau(\mathbf{q}^2)} \tag{4.10}$$

$$\dot{\tilde{G}}(\mathbf{q}) \;=\; \frac{\delta(|\mathbf{q}| - 1)}{Z_\tau \mathbf{q}^2 + \tilde{\Gamma}^{(2)}(\mathbf{q})} = \frac{\delta(|\mathbf{q}| - 1)}{R_\tau(\mathbf{q}^2)} \tag{4.11}$$

$$\int_{\mathbf{q}} \;=\; \int \frac{d\mathbf{q}}{\Omega_D} \tag{4.12}$$

here we have (overloading the definition for Ω) introduced the surface area of the D-dimensional unit sphere $\Omega_D = \frac{2\pi^{D/2}}{\Gamma(D/2)}$ and defined $K_D = \frac{\Omega_D}{(2\pi)^D}$. The wavefunction renormalization is defined by

$$Z_\tau = 1 - \partial_{\mathbf{q}^2}\tilde{\Gamma}^{(2)}(\mathbf{q})|_{\mathbf{q}=\mathbf{0}} \ . \tag{4.13}$$

We write the flow equations for the vertices as

$$\partial_\tau \tilde{\Gamma}^{(2n)}(\{\mathbf{q}\}) \;=\; \left(2n - D(n-1) - n\eta_\tau - \mathbf{q}_i \cdot \partial_{\mathbf{q}_i}\right) \tilde{\Gamma}^{(2n)}(\{\mathbf{q}\}) + \dot{\tilde{\Gamma}}^{(2n)}(\{\mathbf{q}\}) \ , \tag{4.14}$$

where the anomalous dimension is obtained as

$$\eta_\tau = -\partial_\tau Z_\tau = \partial_{\mathbf{q}^2} \dot{\tilde{\Gamma}}^{(2)}(\mathbf{q})|_{\mathbf{q}=\mathbf{0}} \ . \tag{4.15}$$

The flow equation for the 2-point vertex is governed by

$$\dot{\tilde{\Gamma}}_\tau^{(2)}(\mathbf{q}) = \int_{\mathbf{q}'} \dot{\tilde{G}}_\tau(\mathbf{q}') \tilde{\Gamma}^{(4)}(\mathbf{q}, \mathbf{q}', \mathbf{q}', \mathbf{q}) \ . \tag{4.16}$$

Note that due to the rotational symmetry of the model the 2-point function will depend on the modulus of $q = |\mathbf{q}|$ only as $\tilde{\Gamma}^{(2)}(\mathbf{q}) \to \tilde{\Gamma}^{(2)}(q)$. For the 4-point vertex we get

$$\dot{\tilde{\Gamma}}_\tau^{(4)}(\mathbf{q}_1', \mathbf{q}_2', \mathbf{q}_2, \mathbf{q}_1) = \int_{\mathbf{q}} \dot{\tilde{G}}_\tau(\mathbf{q}) \tilde{\Gamma}^{(6)}(\mathbf{q}_1', \mathbf{q}_2', \mathbf{q}, \mathbf{q}, \mathbf{q}_2, \mathbf{q}_1) \tag{4.17}$$

$$- \int_{\mathbf{q}} \left(\dot{\tilde{G}}(\mathbf{q}) \tilde{G}(\mathbf{q}') \tilde{\Gamma}^{(4)}(\mathbf{q}_1', \mathbf{q}_2', \mathbf{q}', \mathbf{q}) \tilde{\Gamma}^{(4)}(\mathbf{q}, \mathbf{q}', \mathbf{q}_2, \mathbf{q}_1) \right)_{\mathbf{q}'=\mathbf{q}_1+\mathbf{q}_2-\mathbf{q}}$$

$$- \int_{\mathbf{q}} \left(\left[\dot{\tilde{G}}(\mathbf{q}) \tilde{G}(\mathbf{q}') + \tilde{G}(\mathbf{q}) \dot{\tilde{G}}(\mathbf{q}') \right] \tilde{\Gamma}^{(4)}(\mathbf{q}_1', \mathbf{q}', \mathbf{q}, \mathbf{q}_1) \tilde{\Gamma}^{(4)}(\mathbf{q}_2', \mathbf{q}, \mathbf{q}', \mathbf{q}_2) \right)_{\mathbf{q}'=\mathbf{q}_1-\mathbf{q}_1'+\mathbf{q}}$$

$$- \int_{\mathbf{q}} \left(\left[\dot{\tilde{G}}(\mathbf{q}) \tilde{G}(\mathbf{q}') + \tilde{G}(\mathbf{q}) \dot{\tilde{G}}(\mathbf{q}') \right] \tilde{\Gamma}^{(4)}(\mathbf{q}_2', \mathbf{q}', \mathbf{q}, \mathbf{q}_1) \tilde{\Gamma}^{(4)}(\mathbf{q}_1', \mathbf{q}, \mathbf{q}', \mathbf{q}_2) \right)_{\mathbf{q}'=\mathbf{q}_1-\mathbf{q}_2'+\mathbf{q}},$$

and have graphically depicted it in figure 4.2.
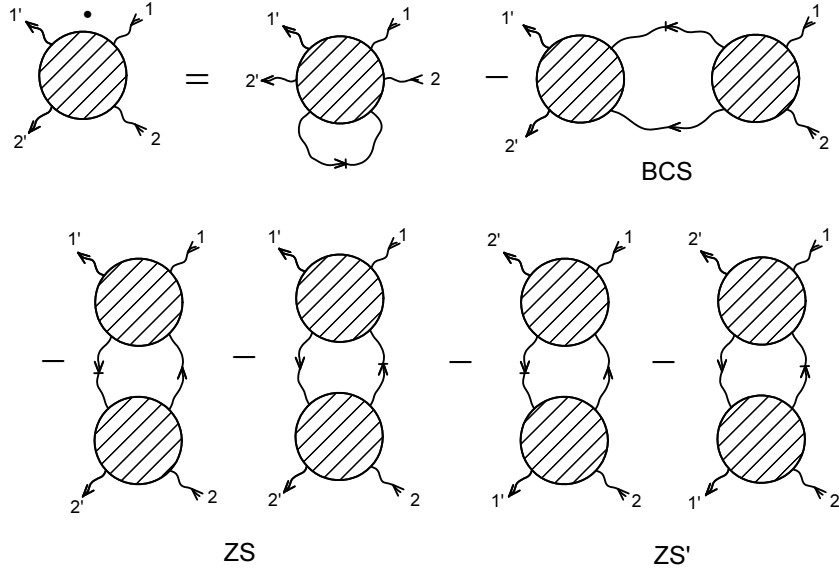
Figure 4.2: Flow of the 4-point vertex as described in (4.17). We denote different contributions generated by the 4-point vertices because of their diagrammatic structure as BCS, ZS and ZS'.

The flow equations for the 6-point and 8-point vertices will considered later on.

Classification according to relevance

As usual we can classify the couplings with regard to their behaviour under the RG as relevant, marginal or irrelevant. Because of their special importance for the flow of the RG we point out the relevant and marginal ones and obtain their flow equations in $D = 4 - \epsilon > 3$. The case $D = 3$ needs special consideration as there will be three additional marginal terms.

First there is the momentum independent part of the 2-point vertex $\tilde{r}$ with scaling dimension $[\tilde{r}] = 2$

$$\tilde{r}_\tau = \tilde{\Gamma}^{(2)}(0) . \tag{4.18}$$

As all other parts of the 2-point vertex are irrelevant we approximate for the Greensfunction

$$R_\tau(\mathbf{q}^2) = \mathbf{q}^2 + \tilde{r}_\tau . \tag{4.19}$$

The vertex $\tilde{r}$ then follows the flow equation

$$\partial_\tau \tilde{r}_\tau = (2 - \eta_\tau)\tilde{r}_\tau + \dot{\tilde{r}}_\tau = (2 - \eta_\tau)\tilde{r}_\tau + \frac{\dot{\tilde{g}}_\tau}{1 + \tilde{r}_\tau} , \tag{4.20}$$

On the right hand side of (4.20) we have introduced $\tilde{g}_\tau$, the relevant part of the 4-point vertex

$$\tilde{g}_\tau = \tilde{\Gamma}^{(4)}(0,0,0,0) . \tag{4.21}$$

with scaling dimension $[\tilde{g}] = 4 - D = \epsilon$. The flow equation for this vertex is

$$\partial_\tau \tilde{g}_\tau = (4 - D - 2\eta_\tau)\tilde{g}_\tau + \dot{\tilde{g}}_\tau = (4 - D - 2\eta_\tau)\tilde{g}_\tau - \frac{5}{2}\frac{\tilde{g}_\tau^2}{(1 + \tilde{r}_\tau)^2} . \tag{4.22}$$

The last vertex to close the set of flow equations is the marginal wavefunction renormalization Z_τ with

$$\partial_\tau Z_\tau = -\eta_\tau Z_\tau . \tag{4.23}$$

The anomalous dimension may be obtained from the latter using (4.15) as

$$\eta_\tau = \frac{1}{R_\tau(1)}\partial_{\mathbf{q}^2}\langle\tilde{\Gamma}^{(4)}(\mathbf{q}, \mathbf{q}', \mathbf{q}', \mathbf{q})\rangle_{\mathbf{q}'}|_{\mathbf{q}^2=0} \tag{4.24}$$

with

$$\langle A(\mathbf{q}')\rangle_{\mathbf{q}'} = \int_{\mathbf{q}'} \delta(|q'| = 1)A(\mathbf{q}') . \tag{4.25}$$

In $D = 3$ the two parts of the 4-point vertex which are linear in the momentum and the momentum independent part of the 6-point vertex are marginal as well. However we ignore them here and postpone an inclusion to a later section.

4.2.2 Solving the flow for relevant and marginal vertices

We note from (4.24) that within the present approximation we may neglect the anomalous dimension

$$\eta_\tau = 0 \ . \tag{4.26}$$

To reach the fixed point of BEC we have to fine tune the initial value $\tilde{r}_0$, see chapter 5. As long as we consider weak coupling $\tilde{g}_0 \ll 1$ only we derive from (4.20) that $\tilde{r}_\tau \ll 1$ as well. We then can then use it as a parameter for expansion and neglect it in leading order. The flow equation for $\tilde{g}$ decouples

$$\partial_\tau \tilde{g}_\tau = \epsilon \tilde{g}_\tau - \frac{5}{2} \tilde{g}_\tau^2 \tag{4.27}$$

and is simply solvable

$$\tilde{g}_\tau = \frac{\tilde{g}^*}{1 + e^{\epsilon(\tau_c - \tau)}} \ , \tag{4.28}$$

with the fixed point value

$$\tilde{g}^* = \frac{2}{5}\epsilon \ . \tag{4.29}$$
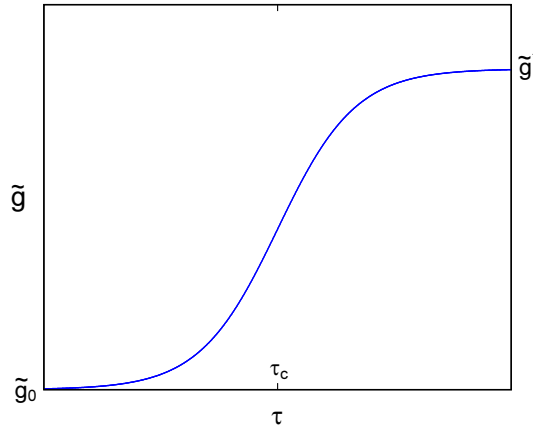
Figure 4.3: Principle flow of the 4-point vertex $\tilde{g}$.

The critical flow parameter τ_c where the effective interaction suddenly approaches its fixed point value is determined as

$$\tau_c = \frac{1}{\epsilon} \ln \left(\frac{\tilde{g}^* - \tilde{g}_0}{\tilde{g}_0} \right) \approx \frac{1}{\epsilon} \ln \left(\frac{\tilde{g}^*}{\tilde{g}_0} \right) \ . \tag{4.30}$$

Here the last line holds for $\tilde{g}_0 \ll \tilde{g}^*$ which will be the definition of weak coupling within this work. Note that the flow of $\tilde{g}_\tau$ looks like a Fermi-function with the step at τ_c. This scale actually has a physical significance and we will later on

relate it to the crossover from the anomalous scaling regime to the perturbative regime.

With the solution for $\tilde{g}$ at hand we can calculate with (5.23) the initial value $\tilde{r}_0$ from the requirement to flow into a fixed point as

$$
\tilde{r}_0 \;=\; -\frac{\epsilon}{5} + \frac{2\epsilon}{5} \int_0^\infty d\tau \, \frac{e^{-2\tau}}{1 + e^{\epsilon(\tau - \tau_c)}} \tag{4.31}
$$

$$
\;=\; -\tilde{g}_0 + O\left(\tilde{g}_0^2 \ln(\tilde{g}_0)\right), \qquad D = 3 \,. \tag{4.32}
$$

Using (5.20) we otain $\tilde{r}_\tau$ for general τ as

$$
\tilde{r}_\tau \;=\; -\frac{\epsilon}{5} + \frac{2\epsilon}{5} \int_\tau^\infty d\tau' \, \frac{e^{-2(\tau' - \tau)}}{1 + e^{\epsilon(\tau' - \tau_c)}} \tag{4.33}
$$

$$
\;\approx\; -\frac{2}{5} \frac{1}{1 + e^{\epsilon(\tau_c - \tau)}} \qquad D = 3 \,. \tag{4.34}
$$

We note that indeed $\tilde{r}_\tau \ll 1$ so that it is self-consistent to neglect $\tilde{r}$ in the flow equations as we have done above.

4.2.3 Improving the flow equations: hybrid approach

We now apply an iterative procedure by using the results derived above as input on the generating side of the flow equations. By this we are able to obtain the momentum dependence of the vertices. This is the hybrid approach as described in section 3.1.1. We exclusively consider the case $D = 3$ from now on.

4-point vertex

We begin with the flow of the 4-point vertex. Here we introduce the generalized susceptibilities

$$
\dot{\tilde{\chi}}_\tau(\mathbf{q}) \;=\; 2 \int_{\mathbf{q}'} \dot{\tilde{G}}(\mathbf{q}') \tilde{G}(\mathbf{q}' + \mathbf{q})
$$

$$
\;=\; \frac{\Theta(q_+ - q_-)}{(1 + \tilde{r}_\tau) 2|\mathbf{q}|} \ln\left(\frac{1 + \tilde{r}_\tau + \mathbf{q}^2 + 2|\mathbf{q}|q_+}{1 + \tilde{r}_\tau + \mathbf{q}^2 + 2|\mathbf{q}|q_-}\right) \,, \tag{4.35}
$$

with $q_+ = \min\{1, \frac{e^{2\tau} - 1 - \mathbf{q}^2}{2|\mathbf{q}|}\}$ and $q_- = \max\{-1, -\frac{|\mathbf{q}|}{2}\}$. For $\mathbf{q} < \min\{2, e^\tau - 1\}$ we get

$$
\dot{\chi}_\tau(\mathbf{q}) = \frac{1}{(1 + \tilde{r}_\tau) 2|\mathbf{q}|} \ln\left(\frac{(1 + |\mathbf{q}|)^2 + \tilde{r}_\tau}{1 + \tilde{r}_\tau}\right) \,. \tag{4.36}
$$

For later use we note that for small momenta we may expand as

$$
\dot{\chi}_\tau(\mathbf{q}) \;=\; \frac{1}{(1 + \tilde{r}_\tau)^2} - \frac{1 - \tilde{r}_\tau}{2(1 + \tilde{r}_\tau)^3} |\mathbf{q}| + O(|\mathbf{q}|^2)
$$

$$
\;=:\; \dot{\chi}_\tau(0) + \dot{\chi}'_\tau(0)|\mathbf{q}| + O(|\mathbf{q}|^2) \,. \tag{4.37}
$$

For large momenta $1 \ll |\mathbf{q}| \ll e^\tau$ the first term of an asymptotic expansion reads

$$\dot{\chi}_\tau(\mathbf{q}) = \frac{2}{(1 + \tilde{r}_\tau)\mathbf{q}^2} \; . \tag{4.38}$$

We define subtracted (non-relevant) susceptibilities as

$$\dot{\chi}_\tau^{nr}(\mathbf{q}) = \dot{\chi}_\tau(\mathbf{q}) - \dot{\chi}_\tau(0) \tag{4.39}$$

and write within this approximation the flow equation for the 4-point vertex (4.17) as

$$
\begin{aligned}
\dot{\tilde{\Gamma}}_\tau^{(4)}(\mathbf{q}_1', \mathbf{q}_2', \mathbf{q}_2, \mathbf{q}_1) &= \dot{\tilde{\Gamma}}_\tau^{(4)}(0,0,0,0) + \dot{\tilde{\Gamma}}_\tau^{(4\ nr)}(\mathbf{q}_1', \mathbf{q}_2', \mathbf{q}_2, \mathbf{q}_1) \\
&= -\frac{5}{2}\frac{\tilde{g}_\tau^2}{(1+\tilde{r}_\tau)^2} \\
&\quad -\frac{\tilde{g}_\tau^2}{2}\left\{\dot{\chi}_\tau^{nr}(\mathbf{q}_1 + \mathbf{q}_2) + \dot{\chi}_\tau^{nr}(\mathbf{q}_1 - \mathbf{q}_{1'}) + \dot{\chi}_\tau^{nr}(\mathbf{q}_1 - \mathbf{q}_{2'})\right\} \; .
\end{aligned}
\tag{4.40}
$$

The 4-point vertex can be decomposed in the same manner as

$$\tilde{\Gamma}_\tau^{(4)}(\mathbf{q}_1', \mathbf{q}_2', \mathbf{q}_2, \mathbf{q}_1) = \tilde{\Gamma}_\tau^{(4)}(0,0,0,0) + \tilde{\Gamma}_\tau^{(4\ nr)}(\mathbf{q}_1', \mathbf{q}_2', \mathbf{q}_2, \mathbf{q}_1) \; . \tag{4.41}$$

We write the solution to the flow equation for latter part (we already know how to solve the first one) as

$$\tilde{\Gamma}_\tau^{(4)\ nr}(\mathbf{q}_1', \mathbf{q}_2', \mathbf{q}_2, \mathbf{q}_1) = \int_0^\tau d\tau'\, e^{\tau(1-2\bar{\eta}_\tau)-\tau'(1-2\bar{\eta}_{\tau'})}\dot{\tilde{\Gamma}}_{\tau'}^{(4)\ nr}(\{e^{\tau'-\tau}\mathbf{q}\}) \tag{4.42}$$

with (5.21)

$$\bar{\eta}_\tau(\mathbf{q}) = \frac{1}{\tau}\int_0^\tau d\tau'\, \eta_\tau(\mathbf{q}) \; . \tag{4.43}$$

Anomalous dimension

Using (4.42) and (4.24) we can greatly improve our estimate for the anomalous dimension

$$\eta_\tau = -\frac{1}{4}\frac{1}{1+\tilde{r}_\tau}\int_0^\tau d\tau'\, e^{-2\int_{\tau-\tau'}^\tau d\tau''_\tau \eta_{\tau''}}\tilde{g}_{\tau-\tau'}^2(2\partial_z + e^{-\tau'}\partial_z^2)\dot{\tilde{\chi}}_{\tau-\tau'}(z)|_{z=e^{-\tau'}} \; . \tag{4.44}$$

The vertices $\tilde{r}_\tau$ and $\tilde{g}_\tau$ approximately follow a step function dependent on $\tau - \tau_c$ and we find the same behaviour for η_τ from the equation above. If we are only interested in the fixed point value for η we can derive the relation

$$\eta^* = \frac{\tilde{g}^{*2}}{4}\int_0^1 dz\, z^{2\eta^*}\frac{(1+z)^2 - \tilde{r}^*}{(1+\tilde{r}^*)^2(1+2z+z^2+\tilde{r}^*)^2 z} \; . \tag{4.45}$$

Fixed point

We are now able to improve our previously obtained fixed point values for the couplings $\tilde{r}$, $\tilde{g}$ and η. Using (4.20) and (4.22) we can write the fixed point vales as functions of η^* as

$$\tilde{r}^* = -\frac{2}{3}\frac{1 - 2\eta^*}{4 - 3\eta^*} \, , \tag{4.46}$$

$$\tilde{g}^* = \frac{10}{9}\frac{(1 - 2\eta^*)(2 - \eta^*)^2}{(4 - 3\eta^*)^2} \, . \tag{4.47}$$

Substituting these values into (4.45) and solving it numerically results (up to three digits) in

$$\tilde{r}^* = -0.143 \qquad \tilde{g}^* = 0.232 \qquad \eta^* = 0.104 \, . \tag{4.48}$$

This should be compared to the best available value for the anomalous dimension $\eta = 0.038$ [42, 81, 82]. Although our estimate for η is almost three times as large as this generally accepted value it is of the right order of magnitude. Compared to a self-consistent two-loop calculation [74, 76] which yielded $\eta = 0.5$ we consider our result as quite satisfactory. In a later section we shall actually improve our approximation and estimate η in the range $\eta \in [0.026, 0.070]$.

4.3 Momentum dependence of the self-energy

With an implicit solution for the momentum dependent part of $\Gamma^{(4)}$ by virtue of (4.42) at hand we now turn toward the self-energy. Actually it is more convenient to introduce a scaling form of the 2-point vertex as

$$\sigma_\tau(x) = e^{-2(\tau - \tau_c)}Z_\tau^{-1}\tilde{\Gamma}^{(2)}(xe^{\tau - \tau_c}) \, . \tag{4.49}$$

The limit $\tau \to \infty$ is well defined

$$\sigma(x) = lim_{\tau \to \infty}\sigma_\tau(x) = \frac{1}{\rho_0 k_c^2}\left(\Sigma(k_c x) - \Sigma(0)\right) \, . \tag{4.50}$$

Here we introduce the crossover scale $k_c = \Lambda_0 e^{-\tau_c} \approx \Lambda_0 \frac{\tilde{g}_0}{\tilde{g}^*}$. Momenta much smaller than this scale will lead to the scaling regime whereas momenta much larger to the perturbative regime. In the same way as we solved the flow equation for the 4-point vertex we can solve for the 2-point vertex

$$\tilde{\Gamma}_\tau^{(2)}(q) = \tilde{r}_0 e^{\tau(2 - \bar{\eta}_\tau)} + e^{\tau(2 - \bar{\eta}_\tau)}\int_0^\tau d\tau' \, e^{-\tau(2 - \bar{\eta}_{\tau'})}\dot{\tilde{\Gamma}}_{\tau'}^{(2)}(qe^{\tau' - \tau}) \, . \tag{4.51}$$

As we have fine-tuned $\tilde{r}$ to flow into a fixed point this momentum independent contribution from $\sigma(x)$ vanishes. Separating the 2-point vertex into momentum-dependent and momentum-independent parts as we have done for the 4-point vertex $\tilde{\Gamma}_\tau^{(2,nr)}(q) = \tilde{\Gamma}_\tau^{(2)}(q) - \tilde{\Gamma}_\tau^{(2)}(0)$ we are then left with

$$\sigma(x) = e^{2\tau_c} \int_0^\infty d\tau \, e^{-\tau(2-\bar{\eta}_\tau)} \dot{\tilde{\Gamma}}_\tau^{(2,nr)}(xe^{\tau-\tau_c}) \, . \qquad (4.52)$$

To evaluate the scaling function we substitute on the right-hand side our expression for the 4-point vertex

$$\begin{aligned}
\dot{\tilde{\Gamma}}_\tau^{(2,nr)}(q) &= -\frac{3}{2} \frac{e^{\tau(1-2\bar{\eta}_\tau)}}{1+\tilde{r}_\tau} \int_0^\tau d\tau' \, e^{-\tau'(1-2\bar{\eta}_{\tau'})} \tilde{g}_{\tau'}^2 \\
&\quad \times \left\langle \dot{\tilde{\chi}}_{\tau'}(|\mathbf{q}+\hat{e}|e^{\tau'-\tau}) - \dot{\tilde{\chi}}_{\tau'}(e^{\tau'-\tau}) \right\rangle_{\hat{e}}
\end{aligned} \qquad (4.53)$$

with the unit vector $\hat{e}$. We now approximate the right hand side of this equation by using (4.28) and substituting for η its fixed point value. Putting all together results in

$$\sigma(x) = \frac{3\tilde{g}^{*2}}{2} x^{2-\eta^*} \int_{xx_c}^\infty dy \, \frac{1}{y} \frac{1}{(x+y)^{2-2\eta^*}} F(x,y,x_c,\eta^*) \, , \qquad (4.54)$$

with

$$F(x,y,x_c,\eta^*) = \int_0^1 dz \, \left(x+\frac{y}{z}\right)^{-\eta^*} \frac{\left\langle \dot{\chi}_{\ln(\frac{y}{xx_c})}(z) - \dot{\chi}_{\ln(\frac{y}{xx_c})}(|y\hat{e}'+z\hat{e}|) \right\rangle_{\hat{e}}}{1+\tilde{r}_{\ln(\frac{y}{xx_c z})}} \, , \quad (4.55)$$

$x_c = e^{-\tau_c} \approx \frac{g_0}{g^*}$ and the unit vectors $\hat{e}, \hat{e}'$ ($\hat{e}'$ points into an arbitrary direction). The approximation of the bosons as a classical field is only justified for $|\mathbf{k}| \ll \Lambda_0$ (see section 4.2). Therefore we have to restrict ourselves to the region $0 \leq x \ll x_c^{-1}$. It is then in leading order correct to replace $xx_c \to 0$ in the lower limit of integration (which is well defined) in (4.54) to finally obtain

$$\sigma(x) = \frac{3\tilde{g}^{*2}}{2} x^{2-\eta^*} \int_0^\infty dy \, \frac{1}{y} \frac{1}{(x+y)^{2-2\eta^*}} F(x,y,x_c,\eta^*) \, . \qquad (4.56)$$

We approximate $\dot{\tilde{\chi}} := \lim_{\tau\to\infty} \chi_\tau$ in F which can be justified by noting that for $x \ll x_c^{-1}$ we get $q_+ = 1$ in (4.35) - which is the only explicitly τ-dependent part of $\dot{\tilde{\chi}}$.

Scaling regime

We define the scaling regime as the region $x \ll 1$. The integral in (4.53) is dominated by the region $\tau > \tau' > \tau_c$ due to the nearly step like course of $\tilde{g}$.

Because $\tilde{r}$ is nearly a step function as well we may set $\tilde{r}_\tau \approx \tilde{r}^*$. To calculate the leading order expression we now set $x = 0$ in the integrand of $\sigma(x)$ and get

$$
\begin{aligned}
\sigma(x) &= \frac{3\tilde{g}^{*2}}{2} x^{2-\eta^*} \int_0^\infty dy\, y^{-3+2\eta^*} F(0, y, x_c, \eta^*) \\
&= \frac{3\tilde{g}^{*2}}{2(1+\tilde{r}^*)} x^{2-\eta^*} \int_0^\infty dy\, y^{-3+\eta^*} \int_0^1 dz\, z^{\eta^*} \langle \dot{\chi}(z) - \dot{\chi}(|y\hat{e}' + z\hat{e}|) \rangle_{\hat{e}} \\
&=: A_3\, x^{2-\eta^*} .
\end{aligned}
\tag{4.57}
$$

By a numerical treatment using the fixed point values (4.48) we calculate

$$
A_3 = 1.17 ,
\tag{4.58}
$$

which should be compared to the best available result from a Monte-Carlo treatment [75] which yields $A_3 = 1.04$. Later on we shall improve our value to $A_3 = 1 + \frac{11}{6}\eta^*$. If we use the generally accepted value $\eta^* = 0.038$ our procedure gives $A_3 = 1.07$.

Perturbative regime

The perturbative regime is defined by $1 \ll x \ll x_c^{-1}$. Here we expect $\sigma(x) \propto x^0$ with eventually logarithmic corrections. In (4.56) only the region $y \gg 1$ can lead to such logarithmic terms. We observe that the dominating region is $\tau \approx \tau_c$ and we therefore use $\tilde{r}_\tau \approx \tilde{r}_0 \approx 0$ (in $\dot{\chi}$ as well). We also neglect the anomalous dimension $\eta \approx 0$ and approximate

$$
F(x, y \gg 1, 0, 0) = \int_0^1 dz\, \dot{\chi}(z) + O(y^{-2}) \approx \frac{\pi^2}{12} .
\tag{4.59}
$$

Therefore in leading order the scaling function looks like

$$
\sigma(x) = B_3 \ln(x) + B_3' ,
\tag{4.60}
$$

with

$$
B_3 = \frac{3\pi^2}{24} \tilde{g}^{*2} \approx 1.23 \tilde{g}^{*2} .
\tag{4.61}
$$

To obtain the coefficient B_3' we have to take into account the full y-dependence of F. Evaluating the resulting integrals numerically yields

$$
B_3' \approx 0.03 .
\tag{4.62}
$$
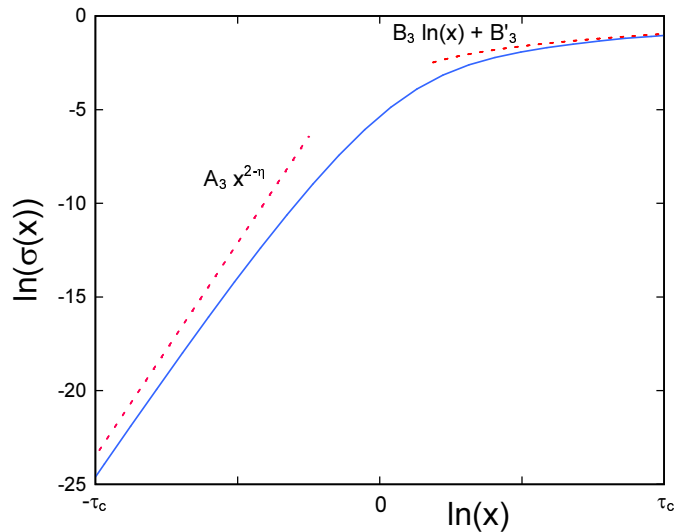
Figure 4.4: Numerical calculation of the scaling function $\sigma(x)$ in the limit of vanishing interactions. Included are the asymptotic forms as predicted by (4.57) and (4.60).

4.4   The shift of the critical temperature

In the past there has been some discussion about the leading order correction of the transition temperature of BEC due to interactions, for a recent review see [83]. Presently it is generally accepted that this correction is linear in the scattering length a. Measurements at a ^{4}He-Vycor system actually confirm this linear relationship [84].

As it has been shown by [76] to calculate the leading order shift of the critical temperature due to interactions it is sufficient just to consider the zero-frequency self-energy (which is implicitly included in the full Greensfunction $G(k)$) as

$$\frac{\Delta T_c}{T_{c,0}} = \frac{2T_c}{3n} \int_{\mathbf{k}} \left(G(k) - G_0(k) \right) \ . \tag{4.63}$$

This shift is proportional to the crossover scale k_c with the constant of proportionality depending on the momentum dependence of the self-energy close to k_c. Therefore evaluating the shift with our scaling function $\sigma(x)$ can be seen as a testing ground for our approach. If it compares well with other reliable results we conclude that we have come close to the correct momentum dependence of the self-energy.

As we will transform back to physical variables we note that

$$\tilde{g}_0 = \frac{16an^{1/3}}{\pi \zeta^{1/3}(3/2)} \approx an^{1/3} \ , \tag{4.64}$$

with the density n. Expressing the Greensfunctions with our scaling function we get the result

$$
\begin{aligned}
\frac{\Delta T_c}{T_{c,0}} &= an^{1/3}\,\frac{3.7748}{\tilde{g}^*}\int_0^{x_c^{-1}}dx\,\frac{\sigma(x)}{x^2+\sigma(x)} \\
&=:\ an^{1/3}\,\frac{3.7748}{\tilde{g}^*}\int_0^{\infty}dx\,h(x) \\
&=:\ c_1 an^{1/3}\ .
\end{aligned}
\tag{4.65}
$$

Here we have used that the integrand falls for large x rapidly enough so that we may replace in leading order the upper bound of integration by ∞. We now evaluate the integral over $h(x)$ to calculate the coefficient c_1 which unfortunately can be done only numerically. Using (4.56) for the scaling function and (4.48) for the fixed point values this yields

$$
c_1 = 1.23\ .
\tag{4.66}
$$

This numerical value is actually quite good when compared with the most accurate results available $c_1 = 1.30 \pm 0.02$ [85] and $c_1 = 1.29 \pm 0.05$ [86]. Results obtained by variational perturbation theory are similar $c_1 = 1.23 \pm 0.12$ [87], $c_1 = 1.27 \pm 0.11$ [88]. More values for c_1 are summarized in [89]. Note that the measurement of [84] yielded $c_1 = 4.66$ which is far off the values above. However as pointed out in [86] this difference might actually be traced back to uncertainties of the precise value for a in the experiment.

We conclude that our simple approach enables us to obtain the momentum dependence of the self-energy over the complete interval $k \in [0, \approx \Lambda_0]$. Our numerical estimate for the coefficient c_1 compares well to the best available results. We therefore regard our expression for the scaling function as a reliable approximation to the correct momentum dependent self-energy.

4.5   Including all marginal terms

The approximation we have used above to evaluate the flow of the vertices can formally be justified only in $D > 3$. Only in this case we have consistently included all relevant and marginal parameters. As already mentioned, in $D = 3$ there are three additional vertices that become marginal and therefore have to be considered in our treatment - marginal vertices are possible sources of logarithmic corrections. It is noteworthy that despite this inconsistency our approach above yields some quite good results. To proof that this accuracy is not merely an accidental feature we repeat our treatment now with all relevant and marginal vertices. We repeat our calculations in the spirit of the expansion in relevance, see section 3.1. Our goal is to investigate how our fixed-point values for the couplings

change compared to (4.48). Additionally we will reconsider a re-evaluation of the scaling function including only marginal terms and show that this approach actually fails to obtain the complete momentum dependence of the self-energy.

4.5.1　Flow of vertices

To start with we decompose the 4-point vertex in the spirit of (4.41) as

$$
\begin{aligned}
\tilde{\Gamma}_\tau^{(4)}(\mathbf{q}_1', \mathbf{q}_2', \mathbf{q}_2, \mathbf{q}_1) &= \tilde{g}_\tau + \tilde{a}_\tau \left(|\mathbf{q}_1 - \mathbf{q}_1'| + |\mathbf{q}_1 - \mathbf{q}_2|\right) + \tilde{b}_\tau |\mathbf{q}_1 + \mathbf{q}_2| \\
&\quad + \tilde{\Gamma}_\tau^{(4\,i)}(\mathbf{q}_1', \mathbf{q}_2', \mathbf{q}_2, \mathbf{q}_1) ,
\end{aligned} \tag{4.67}
$$

with the superscript " i " meaning *irrelevant*. The irrelevant part of the 4-point vertex contains terms which are at least quadratic in the momenta. Besides the two marginal vertices $\tilde{a}_\tau$ and $\tilde{b}_\tau$ there is the momentum independent part $\tilde{v}_\tau$ of the 6-point vertex which is marginal too

$$
\tilde{v}_\tau = \tilde{\Gamma}^{(6)}(0,0,0,0,0,0) . \tag{4.68}
$$

Note that initially all three marginal vertices vanish $\tilde{a}_0 = \tilde{b}_0 = \tilde{v}_0 = 0$.

6-point vertex

The full flow equation for the 6-point vertex is depicted in figure 4.5 and the corresponding expression may be found in the appendix (A.3). Inserting our
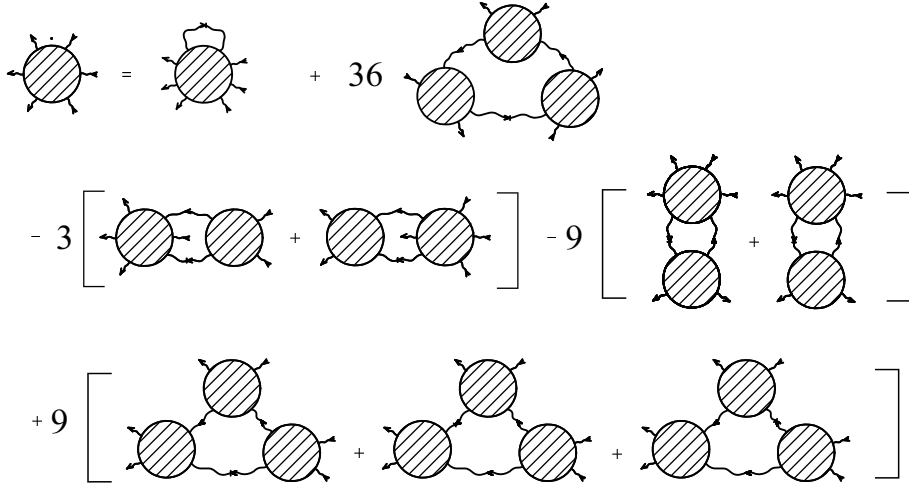

Figure 4.5: Flow for the 6-point vertex as described by Eq. (A.3).

approximations (4.67), (4.68) and (4.19) we receive

$$
\begin{aligned}
\partial_\tau \tilde{v}_\tau &= -3\eta_\tau \tilde{v}_\tau - \frac{3\tilde{v}_\tau(4\tilde{g}_\tau + 5\tilde{a}_\tau + 3\tilde{b}_\tau)}{(1+\tilde{r})^2} \\
&+ \frac{(\tilde{g}_\tau + \tilde{a}_\tau + \tilde{b}_\tau)}{(1+\tilde{r}_\tau)^3}\left[12(\tilde{g}_\tau + \tilde{a}_\tau + \tilde{b}_\tau)^2 + 9(\tilde{g}_\tau + 2\tilde{a}_\tau)^2\right].
\end{aligned} \qquad (4.69)
$$

4-point vertex

In the same way we evaluate the flow of the 4-point vertex. Here we decompose the flow (4.17) into three parts and denote these part with the superscripts BCS, ZS and ZS' because of the structure of these terms, see figure 4.2.

$$
\begin{aligned}
\dot{\tilde{\Gamma}}_\tau^{(4,\mathrm{BCS})}(\mathbf{q}_1', \mathbf{q}_2'; \mathbf{q}_2, \mathbf{q}_1) &\approx \\
&-\frac{1}{2}\left[\tilde{g}_\tau + \tilde{b}_\tau|\mathbf{q}_1 + \mathbf{q}_2|\right]^2 \dot{\tilde{\chi}}_\tau(|\mathbf{q}_1 + \mathbf{q}_2|) \\
&-\tilde{a}_\tau\left[\tilde{g}_\tau + \tilde{b}_\tau|\mathbf{q}_1 + \mathbf{q}_2|\right] \\
&\quad \times \frac{1}{1+\tilde{r}_\tau}\left\langle \frac{\Theta(1 < |\mathbf{q}_1 + \mathbf{q}_2 - \hat{\mathbf{q}}| < e^\tau)}{|\mathbf{q}_1 + \mathbf{q}_2 - \hat{\mathbf{q}}|^2 + r_\tau} \right. \\
&\quad \times [|\hat{\mathbf{q}} - \mathbf{q}_1'| + |\hat{\mathbf{q}} - \mathbf{q}_2'| + |\hat{\mathbf{q}} - \mathbf{q}_2| + |\hat{\mathbf{q}} - \mathbf{q}_1|]\Big\rangle_{\hat{\mathbf{q}}} \\
&\quad -\frac{\tilde{a}_\tau^2}{1+\tilde{r}_\tau}\left\langle \frac{\Theta(1 < |\mathbf{q}_1 + \mathbf{q}_2 - \hat{\mathbf{q}}| < e^\tau)}{|\mathbf{q}_1 + \mathbf{q}_2 - \hat{\mathbf{q}}|^2 + r_\tau)} \right. \\
&\quad \times (|\hat{\mathbf{q}}' - \mathbf{q}_1'| + |\hat{\mathbf{q}}' - \mathbf{q}_2'|)(|\hat{\mathbf{q}} - \mathbf{q}_2| + |\hat{\mathbf{q}} - \mathbf{q}_1|)\Big\rangle_{\hat{\mathbf{q}}},
\end{aligned} \qquad (4.70)
$$

and

$$
\begin{aligned}
\dot{\tilde{\Gamma}}_\tau^{(4,\mathrm{ZS})}(\mathbf{q}_1', \mathbf{q}_2'; \mathbf{q}_2, \mathbf{q}_1) &\approx \\
&- [\tilde{g}_\tau + \tilde{a}_\tau|\mathbf{q}_1 - \mathbf{q}_1'|]^2 \dot{\tilde{\chi}}_\tau(|\mathbf{q}_1 - \mathbf{q}_1'|) \\
&-(\tilde{a}_\tau + \tilde{b}_\tau)\left[\tilde{g}_\tau + \tilde{a}_\tau|\mathbf{q}_1 - \mathbf{q}_1'|\right] \\
&\quad \times \frac{1}{1+\tilde{r}_\tau}\left\langle \frac{\Theta(1 < |\mathbf{q}_1 - \mathbf{q}_1' + \hat{\mathbf{q}}| < e^\tau)}{|\mathbf{q}_1 - \mathbf{q}_1' + \hat{\mathbf{q}}|^2 + \tilde{r}_\tau} \right. \\
&\quad \times [|\hat{\mathbf{q}} - \mathbf{q}_1'| + |\hat{\mathbf{q}} + \mathbf{q}_2'| + |\hat{\mathbf{q}} - \mathbf{q}_2| + |\hat{\mathbf{q}} + \mathbf{q}_1|]\Big\rangle_{\hat{\mathbf{q}}} \\
&\quad -(\tilde{a}_\tau^2 + \tilde{b}_\tau^2)\frac{1}{1+\tilde{r}_\tau}\left\langle \frac{\Theta(1 < |\mathbf{q}_1 - \mathbf{q}_1' + \hat{\mathbf{q}}| < e^\tau)}{|\mathbf{q}_1 - \mathbf{q}_1' + \hat{\mathbf{q}}|^2 + \tilde{r}_\tau} \right. \\
&\quad \times [|\hat{\mathbf{q}} - \mathbf{q}_1'||\hat{\mathbf{q}} - \mathbf{q}_2| + |\hat{\mathbf{q}} + \mathbf{q}_1||\hat{\mathbf{q}} + \mathbf{q}_2'|]\Big\rangle_{\hat{\mathbf{q}}} \\
&\quad -2\tilde{a}_\tau\tilde{b}_\tau\frac{1}{1+r_\tau}\left\langle \frac{\Theta(1 < |\mathbf{q}_1 - \mathbf{q}_1' + \hat{\mathbf{q}}| < e^\tau)}{|\mathbf{q}_1 - \mathbf{q}_1' + \hat{\mathbf{q}}|^2 + r_\tau} \right. \\
&\quad \times [|\hat{\mathbf{q}} - \mathbf{q}_1'||\hat{\mathbf{q}} + \mathbf{q}_2'| + |\hat{\mathbf{q}} + \mathbf{q}_1||\hat{\mathbf{q}} - \mathbf{q}_2|]\Big\rangle_{\hat{\mathbf{q}}}.
\end{aligned} \qquad (4.71)
$$

The contribution from ZS' may be obtained by replacing $\mathbf{q}_1' \leftrightarrow \mathbf{q}_2'$ in the equation above.

Separating the contributions for the different vertices $\tilde{g}, \tilde{a}$ and $\tilde{b}$ we obtain for the flow of the relevant part of the 4-point vertex

$$
\begin{aligned}
\partial_\tau \tilde{g}_\tau &= (1 - 2\eta_\tau)\tilde{g}_\tau - \frac{5}{2}\frac{\tilde{g}_\tau^2}{(1+\tilde{r})^2} + \frac{\tilde{v}_\tau}{1+\tilde{r}_\tau} \\
&\quad - \frac{\tilde{g}_\tau(6\tilde{a}_\tau + 4\tilde{b}_\tau) + 2(2\tilde{a}_\tau^2 + \tilde{b}_\tau^2 + 2\tilde{a}_\tau\tilde{b}_\tau)}{(1+\tilde{r})^2} \ .
\end{aligned} \tag{4.72}
$$

The marginal parts are governed by

$$
\begin{aligned}
\partial_\tau \tilde{a}_\tau &= -2\eta_\tau \tilde{a}_\tau - \beta_1 \tilde{g}_\tau^2 - (2\beta_0 + 2\beta_1 + \beta_2)\tilde{g}_\tau \tilde{a}_\tau \\
&\quad - (2\beta_1 + \beta_2)\tilde{g}_\tau \tilde{b}_\tau - (2\beta_0 + \beta_1 + \beta_2)\tilde{a}_\tau^2 \\
&\quad - (\beta_1 + \beta_2)\tilde{b}_\tau^2 - 2(\beta_0 + \beta_1 + \beta_2)\tilde{a}_\tau \tilde{b}_\tau \\
&\quad - \frac{v_\tau}{1+\tilde{r}_\tau}\{2\beta_1\tilde{g}_\tau + (2\beta_0 + 2\beta_1 + \beta_2)\,\tilde{a}_\tau \\
&\hspace{7cm} + (2\beta_1 + \beta_2)\,\tilde{b}_\tau\} \ ,
\end{aligned} \tag{4.73}
$$

$$
\begin{aligned}
\partial_\tau \tilde{b}_\tau &= -2\eta_\tau \tilde{b}_\tau - \frac{\beta_1}{2}\tilde{g}_\tau^2 - (2\beta_1 + \beta_2)\tilde{g}_\tau \tilde{a}_\tau \\
&\quad - \beta_0 \tilde{g}_\tau \tilde{b}_\tau - 2(\beta_1 + \beta_2)\tilde{a}_\tau^2 - 2\beta_0 \tilde{a}_\tau \tilde{b}_\tau \\
&\quad - \frac{\tilde{v}_\tau}{1+\tilde{r}_\tau}\{\beta_1\tilde{g}_\tau + (2\beta_1 + \beta_2)\,\tilde{a}_\tau + \beta_0\tilde{b}_\tau\} \ .
\end{aligned} \tag{4.74}
$$

Here we have defined

$$
\beta_0 = \frac{1}{(1+\tilde{r}_\tau)^2} \ , \tag{4.75}
$$

$$
\beta_1 = \frac{r_\tau - 1}{2(1+\tilde{r}_\tau)^3} \ , \tag{4.76}
$$

$$
\beta_2 = \frac{1}{2(1+\tilde{r}_\tau)^2} \ , \tag{4.77}
$$

$$
\beta_3 = \frac{1}{3(1+\tilde{r}_\tau)} \ . \tag{4.78}
$$

2-point vertex

The relevant part of the 2-point vertex flows as

$$
\partial_\tau \tilde{r}_\tau = (2 - \eta_\tau)\tilde{r}_\tau + \frac{\tilde{g}_\tau + \tilde{a}_\tau + \tilde{b}_\tau}{1+\tilde{r}_\tau} \ . \tag{4.79}
$$

Anomalous dimension

The leading order expression for η within this scheme is simply obtained from the marginal parts of the 4-point vertex as

$$\eta_\tau = \beta_3(\tilde{a}_\tau + \tilde{b}_\tau) \ . \tag{4.80}$$

Improved fixed point values

We now obtain the values for the couplings at the fixed-point by setting the left-hand sides of the flow equations above equal to zero. Using (4.80) for the anomalous dimension yields

$$\begin{aligned}
\tilde{r}^* &\approx -0.227 \ , \quad \tilde{g}^* \approx 0.178 \ , \quad \tilde{a}^* \approx 0.083 \ , \\
\tilde{b}^* &\approx 0.077 \ , \quad \tilde{v}^* \approx 0.255 \ , \quad \eta^* \approx 0.069 \ .
\end{aligned} \tag{4.81}$$

Note that our value for η has greatly improved compared to our first approximation (4.48) with reference to the best result $\eta = 0.038$. Numerically solving the flow equations for the couplings results in similar Fermi-function like behaviour over τ as we have observed in our first approximation.

4.5.2 The scaling function with only marginal terms

One might be tempted to calculate the scaling function $\sigma(x)$ by considering relevant and marginal terms only on the generating side of the flow equation. As we will show this approach is justified only in the scaling regime $x \ll 1$, here however it yields a quite good approximation for the coefficient A_3 (4.58). For larger x on the other hand the behaviour of $\sigma(x)$ is wrongly predicted and results in a shift of $T_c \propto a\ln(a)$.

To see this we need the flow equation for the marginal part of the 2-point vertex generated just by the marginal part of $\tilde{\Gamma}^{(4)}$

$$\begin{aligned}
\dot{\tilde{\Gamma}}_\tau^{(2,m)}(\mathbf{q}) &= \frac{\tilde{a}_\tau + \tilde{b}_\tau}{1 + \tilde{r}_\tau} \left(\langle |\mathbf{q} + \mathbf{q}'| \rangle_{\mathbf{q}'} - 1 \right) \\
&= \frac{\tilde{a}_\tau + \tilde{b}_\tau}{1 + \tilde{r}_\tau} \begin{cases} \frac{\mathbf{q}^2}{3} & |\mathbf{q}| < 1 \\ \frac{3\mathbf{q}^2 - 3|\mathbf{q}| + 1}{3|\mathbf{q}|} & |\mathbf{q}| > 1 \ . \end{cases}
\end{aligned} \tag{4.82}$$

Scaling regime

To obtain the scaling function $\sigma(x)$ from this flow equation we note the expression for η within this approximation (4.80) and write

$$\begin{aligned}
\sigma(x) &= x_c^{-2} \int_0^\infty d\tau \, e^{-\tau(2-\bar{\eta}_\tau)} \, \eta_\tau \, \frac{|1 + xx_c e^\tau|^3 - |1 - xx_c e^\tau|^3 - 6xx_c e^\tau}{2xx_c e^\tau} \\
&= x^2 \left(3 \int_0^1 dy \, e^{\tau\bar{\eta}_\tau|_{\tau=-\ln(xx_c y)}} (1-y)^2 - 1 \right) \ ,
\end{aligned} \tag{4.83}$$

where we have performed one partial integration. To evaluate this integral in the scaling regime $x \ll 1$ we use the fact that it is dominated by the region $y < x^{-1}$ where we may set $\eta_\tau \approx \eta^*$

$$\sigma(x) = \frac{6x^{2-\eta^*}}{(1-\eta^*)(1-2\eta^*)(1-3\eta^*)} - x^2. \tag{4.84}$$

From this equation we obtain the coefficient A_3 as

$$A_3 = \frac{6}{(1-\eta^*)(1-2\eta^*)(1-3\eta^*)} \approx 1 + \frac{11}{6}\eta^* . \tag{4.85}$$

Substituting our first fixed point value (4.48) for η results in $A_3 \approx 1.22$ which is in relative good agreement with the value $A_3 = 1.17$ (4.58) which we obtained within the same approximation. Interpreting the equation above as a generally approximately valid functional relationship between A_3 and η we may use the best available value $\eta = 0.038$ to obtain $A_3 = 1.07$ which compares quite satisfactory with the results from a recent Monte-Carlo simulation [75].

Shift of T_c

To evaluate (4.83) at general x we approximate the anomalous dimension as a step function

$$\eta_\tau \approx \eta^* \Theta(\tau - \tau_c) \tag{4.86}$$

to receive the expression

$$\begin{aligned}
\sigma(x) &= x^2 \left(3 \int_0^1 dy \, (xy)^{-\eta^* \Theta(xy<1)} (1-y)^2 - 1 \right) \\
&\propto \frac{\eta^* x}{1-\eta^*} \qquad x \gg 1 .
\end{aligned} \tag{4.87}$$

Calculating the interaction induced shift of the critical temperature via (4.65) we note that for large x the integral there behaves as $\propto x^{-1}$. Therefore it is prohibited to replace the upper bound of integration by ∞, instead we have to integrate up to x_c^{-1}. The leading order result then looks like

$$\frac{\Delta T_c}{T_{c,0}} \propto a \ln(a) . \tag{4.88}$$

This relationship is however incorrect and we conclude that it is essential to include all irrelevant terms into the scaling function $\sigma(x)$ to obtain the correct shift of temperature. We therefore deduce that in the calculation of [79] the neglect of these irrelevant terms is responsible for the wrongly predicted $a \ln(a)$ behaviour.

4.6 Including the contributions from irrelevant vertices

In this section we will investigate a different scheme compared to the expansion in relevance to improve our results. The idea is that we can express irrelevant vertices in terms of the relevant and marginal ones [9, 18]. As we know from our previous treatment $\tilde{g}$ and all marginal parameters $(\tilde{g}, \tilde{a}, \tilde{b}, \tilde{v})$ will stay small under the RG and we therefore propose to expand all flow equations to some power of these couplings. In the following we will consider all terms up to and including $(\tilde{g}, \tilde{a}, \tilde{b}, \tilde{v})^2$. There are no second order contributions to the flow equations from vertices $\tilde{\Gamma}^{\geq 10}$ so we will truncate the hierarchy at $\tilde{\Gamma}^8$ - nevertheless we are insured that our calculations will be quite tedious. We perform no expansion in $\tilde{r}$ but keep all powers.

The difference to our expansion in relevance of the last section is that we now consider the additional flow generated by the irrelevant parts of the 6-point vertex and the momentum independent part of the 8-point vertex.

8-point vertex

The 8-point vertex is irrelevant and we just consider the parts that are maximal of order $O\left((\tilde{g}, \tilde{a}, \tilde{b}, \tilde{v})^2\right)$. Up to this order the flow equation is graphically depicted in figure 4.6 and the corresponding expression may be found in the appendix (A.4).
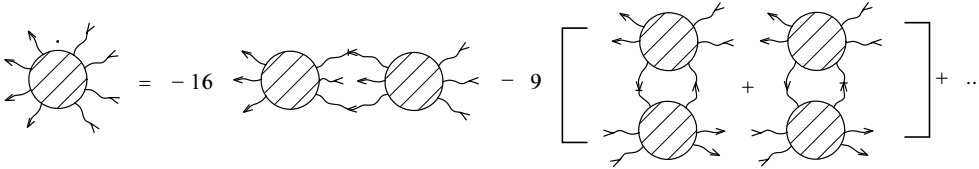
Figure 4.6: Flow of the 8-point vertex up to quadratic order in non-irrelevant couplings as described by (A.4).

Here we just have substituted $\tilde{v}$ for the complete 6-point vertex

$$
\begin{aligned}
\dot{\tilde{\Gamma}}_\tau^{(8)}(\mathbf{q}_1', \ldots, \mathbf{q}_4', \mathbf{q}_4, \ldots, \mathbf{q}_1) \;=\; \\
-2v_\tau^2 \Big\{ 16\, \mathcal{S}_{(1,2,3),4} \mathcal{S}_{(1',2',3'),4'}\, \dot{\tilde{\chi}}_\tau(\mathbf{q}_1' + \mathbf{q}_2' + \mathbf{q}_3' - \mathbf{q}_4) \\
+18\, \mathcal{S}_{(1,2),(3,4)} \mathcal{S}_{(1',2'),(3',4')}\, \dot{\tilde{\chi}}_\tau(\mathbf{q}_1 + \mathbf{q}_2 - \mathbf{q}_1' - \mathbf{q}_2') \Big\} \\
+O\left((\tilde{g}, \tilde{a}, \tilde{b}, \tilde{v})^3\right).
\end{aligned}
\tag{4.89}
$$

Note that the flow for the 8-point vertex can be solved as (neglecting η)

$$\tilde{\Gamma}_\tau^{(8)}(\mathbf{q}_1', \ldots, \mathbf{q}_4', \mathbf{q}_4, \ldots, \mathbf{q}_1) = \int_0^\tau d\tau' \; e^{-\tau'}$$

$$\cdot \dot{\tilde{\Gamma}}_{\tau-\tau'}^{(8)}(e^{-\tau'}\mathbf{q}_1', \ldots, e^{-\tau'}\mathbf{q}_4', e^{-\tau'}\mathbf{q}_4, \ldots, e^{-\tau'}\mathbf{q}_1) \; . \qquad (4.90)$$

6-point vertex

Because the 8-point vertex is proportional $\tilde{v}^2$ the flow equation for the momentum independent 6-point vertex acquires an additional term compared to (4.69). On the other hand as we neglect all cubic contributions it loses one term and finally reads

$$\partial_\tau \tilde{v}_\tau = -3\eta_\tau \tilde{v}_\tau - \frac{3\tilde{v}_\tau(4\tilde{g}_\tau + 5\tilde{a}_\tau + 3\tilde{b}_\tau)}{(1 + \tilde{r}_\tau)^2}$$

$$- \frac{2}{1 + \tilde{r}_\tau} \int_0^\tau d\tau' \; e^{-\tau'} \tilde{v}_{\tau-\tau'}^2 [16\dot{\tilde{\chi}}_{\tau-\tau'}(0) + 18\dot{\tilde{\chi}}_{\tau-\tau'}(e^{-\tau'})] \; . \qquad (4.91)$$

We note that obviously $\tilde{v}_\tau = 0$ for all τ within this approximation.

We turn toward the flow equation of the irrelevant part of the 6-point vertex and solve it at flow parameter τ. Hereby we neglect η again and as the integrand is exponentially damped we take all vertices that appear on the right-hand side of the corresponding flow equation at τ as well. We will only require the angular average over this vertex

$$\langle \tilde{\Gamma}_\tau^{(6i)}(\mathbf{q}_1', \mathbf{q}_2', \hat{\mathbf{q}}; \hat{\mathbf{q}}, \mathbf{q}_2, \mathbf{q}_1) \rangle_{\hat{\mathbf{q}}} \approx -\tilde{v}_\tau \int_0^1 \frac{d\lambda}{\lambda} \Big\{ 6\tilde{g}_\tau(\dot{\tilde{\chi}}_\tau(\lambda) - \beta_0) \qquad (4.92)$$

$$+ \tilde{a}_\tau \left(4\dot{\tilde{\chi}}_\tau(\lambda)(1 + \lambda) + 4\dot{\Phi}_\tau(\lambda) - 8\beta_0 + [\dot{\varphi}_\tau(\lambda) - \dot{\varphi}_\tau(0)] \right)$$

$$+ \tilde{b}_\tau \left(2\dot{\tilde{\chi}}_\tau(\lambda)(1 + \lambda) + 2\dot{\Phi}_\tau(\lambda) - 4\beta_0 + [\dot{\varphi}_\tau(\lambda) - \dot{\varphi}_\tau(0)] \right)$$

$$+ \lambda|\mathbf{q}_1 + \mathbf{q}_2| \left(\beta_1\tilde{g}_\tau + (2\beta_1 + \beta_2)\tilde{a}_\tau + \beta_0\tilde{b}_\tau \right)$$

$$+ \lambda\left(|\mathbf{q}_1 - \mathbf{q}_1'| + |\mathbf{q}_1 - \mathbf{q}_2'|\right) \left(2\beta_1\tilde{g}_\tau + (2\beta_0 + 2\beta_1 + \beta_2)\tilde{a}_\tau + (2\beta_1 + \beta_2)\tilde{b}_\tau \right) \Big\} \; .$$

with

$$\dot{\Phi}_\tau(\lambda) = \frac{2}{1 + \tilde{r}_\tau} \left\langle \tilde{G}_\tau(\hat{\mathbf{q}} + \hat{\mathbf{q}}'\lambda) \, |\hat{\mathbf{q}} + \hat{\mathbf{q}}'\lambda| \right\rangle_{\hat{\mathbf{q}}}$$

$$= \frac{\lambda + \sqrt{-\tilde{r}_\tau} \, \text{arctanh}\left[\frac{\lambda\sqrt{-\tilde{r}_\tau}}{1 + \tilde{r}_\tau + \lambda}\right]}{\lambda(1 + \tilde{r}_\tau)} \; , \qquad (4.93)$$

$$\dot{\varphi}_\tau(\lambda) = \frac{1}{(1 + \tilde{r}_\tau)^2} \left\langle |\hat{\mathbf{q}} + \hat{\mathbf{q}}'\lambda| \right\rangle_{\hat{\mathbf{q}}}$$

$$= \frac{3 + \lambda^2}{3(1 + \tilde{r}_\tau)^2} \; . \qquad (4.94)$$

4-point vertex

The flow equation of the 4-point vertex acquires an additional term due to the irrelevant 6-point vertex. We therefore obtain for $\tilde{g}$ the following result

$$
\begin{aligned}
\partial_\tau \tilde{g}_\tau \;=\;& (1 - 2\eta_\tau)\tilde{g}_\tau - \frac{5}{2}\beta_0 \tilde{g}_\tau^2 - \beta_0 \tilde{g}_\tau (6\tilde{a}_\tau + 4\tilde{b}_\tau) \\
& -2\beta_0(2\tilde{a}_\tau^2 + \tilde{b}_\tau^2 + 2\tilde{a}_\tau \tilde{b}_\tau) + \frac{v_\tau}{1 + r_\tau} - \frac{v_\tau}{1 + r_\tau}\int_0^1 \frac{d\lambda}{\lambda} \\
& \times \Big\{ 6\tilde{g}_\tau(\dot{\tilde{\chi}}_\tau(\lambda) - \beta_0) + \tilde{a}_\tau \Big(4\dot{\tilde{\chi}}_\tau(\lambda)(1 + \lambda) + 4\dot{\Phi}_\tau(\lambda) \\
& -8\beta_0 + [\dot{\varphi}_\tau(\lambda) - \dot{\varphi}_\tau(0)]\Big) + \tilde{b}_\tau\Big(2\dot{\tilde{\chi}}_\tau(\lambda)(1 + \lambda) \\
& +2\dot{\Phi}_\tau(\lambda) - 4\beta_0 + [\dot{\varphi}_\tau(\lambda) - \dot{\varphi}_\tau(0)]\Big)\Big\} \,. \qquad (4.95)
\end{aligned}
$$

There are no modifications to the flow equations for the marginal parts of the 4-point vertex within our approximation and we simply can use (4.73) and (4.74).

To calculate the flow of the 2-point vertex we need the irrelevant contributions to the 4-point vertex. Using (4.70) and (4.71) these are

$$
\begin{aligned}
\langle \tilde{\Gamma}_\tau^{(4\mathrm{i})}(0, \hat{\mathbf{q}}, \hat{\mathbf{q}}, 0)\rangle_{\hat{\mathbf{q}}} \;\approx\;& \int \frac{d\lambda}{\lambda^2} \Big\langle \dot{\Gamma}_{\tau,\mathrm{quad}}^{(4,\mathrm{BCS})}(0, \lambda\hat{\mathbf{q}}; \lambda\hat{\mathbf{q}}, 0) \\
& + \dot{\Gamma}_{\tau,\mathrm{quad}}^{(4,\mathrm{ZS})}(0, \lambda\hat{\mathbf{q}}; \lambda\hat{\mathbf{q}}, 0) + \dot{\Gamma}_{\tau,\mathrm{quad}}^{(4,\mathrm{ZS}')}(0, \lambda\hat{\mathbf{q}}; \lambda\hat{\mathbf{q}}, 0)\Big\rangle_{\hat{\mathbf{q}}} \,, \qquad (4.96)
\end{aligned}
$$

here the subscript "quad" means that we consider terms quadratic in λ only. We have neglected the explicit contribution from $\tilde{\Gamma}^{(6)}$ - note that there are implicit contributions from this vertex to the flow of $\tilde{g}, \tilde{a}$ and $\tilde{b}$.

2-point vertex

We arrive at the flow equation for the 2-point vertex which we write as

$$
\partial_\tau \tilde{r}_l \;=\; (2 - \eta_\tau)\tilde{r}_\tau + \frac{\tilde{g}_\tau + \tilde{a}_\tau + \tilde{b}_\tau}{1 + \tilde{r}_\tau} + \frac{1}{1 + \tilde{r}_\tau}\langle \tilde{\Gamma}_\tau^{(4\mathrm{i})}(0, \hat{\mathbf{q}}; \hat{\mathbf{q}}, 0)\rangle_{\hat{\mathbf{q}}} \qquad (4.97)
$$

with the last term on the right-hand side defined in (4.96).

Anomalous dimension

We use the same expression (4.80) as before

$$
\eta_\tau = \beta_3(\tilde{a}_\tau + \tilde{b}_\tau) \,. \qquad (4.98)
$$

Fixed point values

Again by setting the left-hand sides of the flow equations above equal to zero we now obtain the fixed point values for the couplings as

$$
\begin{aligned}
&\tilde{r}^* \approx -0.0996 \ , && \tilde{g}^* \approx 0.122 \ , && \tilde{a}^* \approx 0.0371 \ , \\
&\tilde{b}^* \approx 0.0339 \ , && \tilde{v}^* \approx 0 \ , && \eta^* \approx 0.0263 \ .
\end{aligned}
\tag{4.99}
$$

We observe that within this approximation we have improved our estimate for the anomalous dimension in terms of both relative and absolute error compared to $\eta = 0.038$. Note however that the 6-point vertex vanishes as we have neglected all terms cubic in the couplings $(\tilde{g}, \tilde{a}, \tilde{b}, \tilde{v})$. Including the term we have neglected in (4.91) but already obtained in (4.69) changes the fixed point to

$$
\begin{aligned}
&\tilde{r}^* \approx -0.134 \ , && \tilde{g}^* \approx 0.127 \ , && \tilde{a}^* \approx 0.0693 \ , \\
&\tilde{b}^* \approx 0.0639 \ , && \tilde{v}^* \approx 0.0917 \ , && \eta^* \approx 0.0513 \ .
\end{aligned}
\tag{4.100}
$$

With this approximation we are even closer to the exact value for η and observe that our estimates for the anomalous dimension somehow oscillate around the true value. However we do not achieve a fast convergence and we assume that this can be attributed to the sharp cutoff we have used. As discussed this form of cutoff generally seems to lead to a slow convergence when used with a momentum scale expansion, see section 3.1.

Calculating η including irrelevant terms

So far we have calculated the anomalous dimension by only considering the marginal contributions from the 4-point vertex. Including the irrelevant parts we write the anomalous dimension at the fixed point $(\tau \to \infty)$ as

$$
\eta^* = \frac{1}{1 + \tilde{r}^*} \int_0^1 d\lambda \, \lambda^{-2+2\eta^*} \partial_{\mathbf{q}^2} \left\langle \tilde{\Gamma}^{(4)}_\infty(\lambda\mathbf{q}, \lambda\mathbf{q}', \lambda\mathbf{q}', \lambda\mathbf{q}) \right\rangle_{\mathbf{q}'} \Big|_{\mathbf{q}^2=0} \ .
\tag{4.101}
$$

We present the tedious calculations to evaluate this integral in the appendix A.2. This equation generally results in quite small values for η. Including just quadratic terms of relevant and marginal couplings we get $\eta^* = 0.0127$, and when including the cubic terms for the flow of $\tilde{v}$ we even receive $\eta^* = 0.00797$. We note that including the irrelevant terms makes our estimate for η worse. A possible source of this behaviour is that we have neglected terms in the flow for $\tilde{g}, \tilde{a}$ and $\tilde{b}$ that we have now included in our calculation for η as above. One feels that we should use the same approximations for the flow equations of $\tilde{g}, \tilde{a}, \tilde{b}$ and η to be consistent. This is however just what we have done before by using (4.80) - with far better results for η.

4.7   Summary

In this chapter we investigate weakly interacting bosons at the critical point of Bose-Einstein condensation. As the critical temperature is finite it is sufficient to describe the system in terms of a classical ϕ^4-theory. We classify the vertices of the problem according to their relevance under the RG and solve the flow equations for the relevant and marginal ones. As a next step we take these vertices as an input to our flow equations to derive the momentum dependent self-energy of the bosons. We are able to cover the full interval from the scaling regime at small momentum up to the perturbative regime at large momentum. As a test of our result we calculate the interaction induced shift of the critical temperature and observe that it compares quite well with the best available results obtained by other means. Finally we extend our approach to include even irrelevant vertices and investigate the fixed point values of various couplings. Hereby we are able to improve our estimates at the fixed point. However the results are converging quite slowly and we assume that this behaviour can be attributed to the sharp cutoff we have used. In principle we could also apply our improved flow equations to re-calculate the shift of the critical temperature.

Chapter 5

The Fermi surface

We tackle the question of calculating the true Fermi surface for a general system of interacting fermions. Without the need to perform any approximations we derive a self-consistency equation relating the shape of the Fermi surface to the effective interaction vertex along the complete trajectory of the RG. This exact equation follows from the requirement that the system flows into a fixed point and the need of fine-tuning the relevant part of the fermionic 2-point vertex to achieve this. We point out that the Fermi surface therefore has to be viewed as a fixed point manifold of the RG. We discuss some possible applications and approximations. The work presented below has been published [90] in a modified form.

5.1 Introduction

At an earlier point (2.48) we have defined the Fermi surface S_F as the set of momenta satisfying

$$\epsilon_{\mathbf{k}} = \mu - \Sigma(i0, \mathbf{k}) \ . \tag{5.1}$$

Here $\epsilon_{\mathbf{k}}$ is the bare energy dispersion, μ the chemical potential and Σ the self-energy of the interacting system. We referred to this true Fermi surface when we defined a local coordinate system (2.50) to set up the renormalization group and further used it for the rescaling of momenta and vertices. Now clearly we have no knowledge of this true Fermi surface a-priori. Rather we would like to obtain it from the renormalization group treatment by some kind of self-consistency equation [19].

Even for weak interactions a perturbative calculation will generally produce unphysical singularities has as been pointed out by [91]. The origin of these singularities can be understood as follows [92]. Let us write the interacting Hamiltonian as

$$H(g) = H_0 + gH_I \ , \tag{5.2}$$

with the free part H_0. Adiabatically switching on the interaction g transforms the groundstate of the non-interacting system to a new state

$$|0(g = 0)\rangle \rightarrow |0'(g)\rangle \,, \tag{5.3}$$

which has the same Fermi surface S_{0F} as the non-interacting state. Generally this state is different from the true groundstate at g

$$|0'(g)\rangle \neq |0(g)\rangle \,, \tag{5.4}$$

but an excited state of $H(g)$. Moreover the state $|0'(g)\rangle$ will generally be unstable. We therefore can only define it unambiguously as long as the adiabatical switching on of the interaction is much faster than its lifetime. Only if the true Fermi surface is close to the bare one we can expect this approach to be meaningful.

Technically the singularities arise within the perturbative expansion as it involves Feynman diagrams containing the bare Greensfunction $G_0(\mathbf{K})$. This Greensfunction however has its pole at the bare Fermi surface rather than the true one. To cure these problems we add and subtract the true self-energy as a counter term

$$H_0 \quad \rightarrow \quad H_0' = H_0 + \sum_{\mathbf{k}} \Sigma(\mathbf{k}_F(\mathbf{k})) c_{\mathbf{k}}^+ c_{\mathbf{k}} \,, \tag{5.5}$$

$$H_I \quad \rightarrow \quad H_I' = H_I - \sum_{\mathbf{k}} \Sigma(\mathbf{k}_F(\mathbf{k})) c_{\mathbf{k}}^+ c_{\mathbf{k}} \,, \tag{5.6}$$

with the Fermi operators c^+, c and $\mathbf{k}_F$ as defined by (5.1). By the inclusion of the counter-term the Greensfunction G_0' of the newly defined bare Hamiltonian H_0' has its pole correctly at the true Fermi surface S_F. The usual approach is now to calculate the self-energy perturbatively in H_I' and to require it to vanish on the true Fermi surface $\mathbf{k}_F \in S_F$. The resulting integral equations for $\Sigma(\mathbf{k}_F)$ are generally quite cumbersome and one has to solve them numerically [93].

In the following we will show how do derive a self-consistency equation for the shape of the Fermi surface within a renormalization group approach. Our method is inherently non-perturbative and we like to stress Andersons observation [94] of the importance to obtain the true Fermi surface in a non-perturbative way, especially in the context of finding the correct low energy effective action of strongly correlated electrons in two dimensions. Later on we will actually apply this method to tackle the question of finding the Fermi surface for an one-dimensional, chapter 6 and a (quasi) two-dimensional system, chapter 7.

5.2   The Fermi surface as a fixed point manifold

We investigate a system of interacting fermions in arbitrary dimensions D. For simplicity we assume these fermions to be spinless but a generalization is straight

forward. The non-interacting part of the action is

$$S_0 = \int_{\mathbf{K}} \psi_{\mathbf{K}}^+ \left(-i\omega_n + \xi(\mathbf{k})\right) \psi_{\mathbf{K}} \ , \tag{5.7}$$

with the subtracted bare energy dispersion $\xi(\mathbf{k}) = \epsilon_{\mathbf{k}} - \epsilon_{\mathbf{k}_F}$. Here we have included a counter term to expand around the true Fermi surface [38] as laid out in the introduction to this chapter. After subtracting the same counter-term from the irreducible 2-point vertex the latter reads

$$\Gamma_\Lambda^{(2)}(\mathbf{K}) = \Sigma_\Lambda(\mathbf{K}) - \Sigma(i0, \mathbf{k}_F) \ . \tag{5.8}$$

To define a scale Ω we perform a coordinate transformation of the momenta as laid out in (2.50) and rescale them as discussed in section 2.6.2 by using (2.67)

$$q_\parallel = \frac{|v_F| k_\parallel}{\Lambda} \ , \quad \mathbf{q}_\perp = \frac{\mathbf{k}_\perp}{\Lambda_0} \ , \quad \epsilon_n = \frac{\omega_n}{\Lambda} \ . \tag{5.9}$$

The integration is defined as in (2.71). To obtain invariance of the Gaussian part of the action we have to use

$$\psi(\mathbf{K}) = \tilde{\psi}(\mathbf{Q}) \sqrt{\frac{Z}{\nu_0 \Lambda^3}} \ , \tag{5.10}$$

and write the rescaled vertices as

$$\tilde{\Gamma}_\tau^{(2n)}(\{\mathbf{Q}\}) = \nu_0^{n-1} \Lambda^{n-2} \left[Z_\tau(\mathbf{q}_{\perp 1}) \ldots Z_\tau(\mathbf{q}_{\perp 2n})\right]^{\frac{1}{2}} \Gamma_\Lambda^{(2n)}(\{\mathbf{K}\}) \ . \tag{5.11}$$

The rescaled Greensfunctions are generally given by

$$\tilde{G}(\mathbf{Q}) = \frac{\theta(1 < |q_\parallel| < e^\tau)}{Z_\tau(\mathbf{q}_\perp)(i\epsilon - \tilde{\xi}(\mathbf{q})) - \tilde{\Gamma}_\tau^{(2)}(\mathbf{Q})} \ , \tag{5.12}$$

$$\dot{\tilde{G}}(\mathbf{Q}) = \frac{\delta(|q_\parallel| - 1)}{Z_\tau(\mathbf{q}_\perp)(i\epsilon - \tilde{\xi}(\mathbf{q})) - \tilde{\Gamma}_\tau^{(2)}(\mathbf{Q})} \ , \tag{5.13}$$

with the rescaled dispersion $\tilde{\xi}(\mathbf{q}) = \frac{\epsilon_{\mathbf{k}} - \epsilon_{\mathbf{k}_F}}{\Lambda}$.

The flow equation for the 2-point vertex then can easily be derived from (2.39) and reads

$$\partial_\tau \tilde{\Gamma}_\tau^{(2)}(\mathbf{Q}) = (1 - \eta_\tau(\mathbf{q}_\perp) - \mathbf{Q} \cdot \partial_{\mathbf{Q}}) \tilde{\Gamma}_\tau^{(2)}(\mathbf{Q}) + \int_{\mathbf{Q}'} \dot{\tilde{G}}_\tau(\mathbf{Q}') \tilde{\Gamma}_\tau^{(4)}(\mathbf{Q}, \mathbf{Q}'; \mathbf{Q}', \mathbf{Q}) \ . \tag{5.14}$$

Focusing just on the relevant part

$$\tilde{r}_\tau(\mathbf{q}_\perp) = \tilde{\Gamma}_\tau^{(2)}(\mathbf{Q}_0) \ , \quad \mathbf{Q}_0 = (i\epsilon = 0, q_\parallel = 0, \mathbf{q}_\perp) \ , \tag{5.15}$$
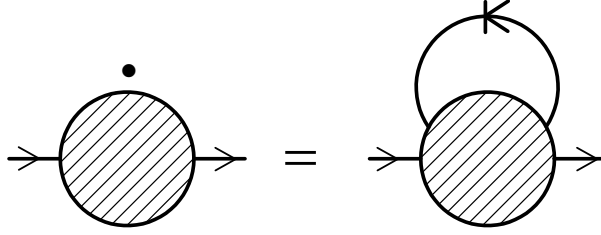
Figure 5.1: Graphical representation of the flow equation for the fermionic 2-point vertex as described by (5.14).

we write the corresponding flow equation as

$$\partial_\tau \tilde{r}_\tau(\mathbf{q}_\perp) = (1 - \eta_\tau(\mathbf{q}_\perp))\, \tilde{r}_\tau(\mathbf{q}_\perp) + \dot{\tilde{r}}_\tau(\mathbf{q}_\perp)\,, \qquad (5.16)$$

with

$$\dot{\tilde{r}}_\tau(\mathbf{q}_\perp) = \int_{\mathbf{Q}'} \dot{\tilde{G}}_\tau(\mathbf{Q}')\tilde{\Gamma}^{(4)}_\tau(\mathbf{Q}_0, \mathbf{Q}'; \mathbf{Q}', \mathbf{Q}_0)\,. \qquad (5.17)$$

The flow equations for the 4-point and 6-point vertex are not of interest here and can be found in [20, 38].

The vertices $\tilde{r}_\tau(\mathbf{q}_\perp)$ are relevant with full scaling-dimension $[\tilde{r}_\tau(\mathbf{q}_\perp)] = 1 - \eta(\mathbf{q}_\perp)$ as long as $\eta < 1$. Suppose for the time that we have somehow determined the bare couplings $\tilde{r}_0(\mathbf{q}_\perp)$ such that they flow into a fixed point $\tilde{r}^*(\mathbf{q}_\perp) := \lim_{\tau \to \infty} \tilde{r}_\tau(\mathbf{q}_\perp)$. Then we actually have found the Fermi surface of the interacting system [38] and can express its shape in terms of these bare couplings as

$$\mathbf{k}_F(\mathbf{k}_\perp) = \mathbf{k}_{F0}(\mathbf{k}_\perp) + \frac{\mathbf{v}_F(\mathbf{q}_\perp)}{|\mathbf{v}_F(\mathbf{q}_\perp)|}\tilde{r}_0(\mathbf{q}_\perp)\Lambda_0 \qquad (5.18)$$

for a system with linear dispersion.

Note that the true Fermi surface has to be viewed as a fixed point manifold, the notion of a flowing Fermi surface is not adequate within this context. We can try to define such a flowing (fermi) surface $S_{F\tau}$ (for linear dispersion) by

$$\mathbf{k}_{F\tau}(\mathbf{k}_\perp) = \mathbf{k}_F(\mathbf{k}_\perp) - \frac{\mathbf{v}_F(\mathbf{q}_\perp)}{|\mathbf{v}_F(\mathbf{q}_\perp)|}\frac{\tilde{r}_\tau(\mathbf{q}_\perp)\Lambda_\tau}{|\tilde{\mathbf{v}}_{F\tau}(\mathbf{q}_\perp)|}\,, \qquad (5.19)$$

with the renormalized Fermi velocities $\tilde{\mathbf{v}}_{F\tau}(\mathbf{q}_\perp)$, $\tilde{\mathbf{v}}_{F0}(\mathbf{q}_\perp) = 1$ as defined in (3.2). However the physical interpretation of this flowing surface is unclear, as it lies outside the allowed momentum space: the fermions at cutoff parameter τ never propagate on $S_{F\tau}$. This situation changes if we use a bosonized interaction as laid out in section 2.5 and consider an interaction cutoff instead of the bandwidth cutoff. In this case each value of $\Lambda_{B\tau}$ defines an unique theory with a specific form of interaction. Here we can study the deformation of the Fermi surface as we gradually switch on the entire interaction, i.e. lower the infrared cutoff of the momentum transferred by the interaction.

Self-consistency equation

To reach our goal of deriving a self-consistency equation for the Fermi surface we need a scheme of how to calculate the bare couplings $\tilde{r}_0(\mathbf{q}_\perp)$. Let us therefore take a closer look at the flow equation (5.16). We note that we actually can solve it

$$\tilde{r}_\tau(\mathbf{q}_\perp) = e^{\tau(1-\bar{\eta}_\tau(\mathbf{q}_\perp))} \left(\tilde{r}_0(\mathbf{q}_\perp) + \int_0^\tau d\tau' \, e^{-\tau'(1-\bar{\eta}_{\tau'}(\mathbf{q}_\perp))} \dot{\tilde{r}}_{\tau'}(\mathbf{q}_\perp) \right) . \qquad (5.20)$$

Here for convenience we have defined

$$\bar{\eta}_\tau(\mathbf{q}_\perp) = \frac{1}{\tau} \int_0^\tau d\tau' \, \eta_\tau(\mathbf{q}_\perp) , \qquad (5.21)$$

i.e. we can write the anomalous wavefunction renormalization Z as

$$Z_\tau(\mathbf{q}_\perp) = e^{-\tau\bar{\eta}_\tau(\mathbf{q}_\perp)} . \qquad (5.22)$$

Note that hereby we have exploited reparametrization invariance and set $Z_0 = 1$. Under the premise that the anomalous dimensions are small enough $\eta < 1$ we can only reach a finite limit in (5.20) for $\tau \to \infty$ if we choose

$$\begin{aligned}
\tilde{r}_0(\mathbf{q}_\perp) &= -\int_0^\infty d\tau \, e^{-\tau(1-\bar{\eta}_\tau(\mathbf{q}_\perp))} \dot{\tilde{r}}_\tau(\mathbf{q}_\perp) \\
&= -\int_0^\infty d\tau \, e^{-\tau(1-\bar{\eta}_\tau(\mathbf{q}_\perp))} \int_{\mathbf{Q}'} \dot{\tilde{G}}_\tau(\mathbf{Q}') \tilde{\Gamma}_\tau^{(4)}(\mathbf{Q}_0, \mathbf{Q}'; \mathbf{Q}', \mathbf{Q}_0) , \qquad (5.23)
\end{aligned}$$

which is the self-consistency equation we were looking for.

Equation (5.23) relates the bare vertices $\tilde{r}_0(\mathbf{q}_\perp)$, i.e. the shape of the Fermi surface (5.18), to the full momentum dependent vertices $\tilde{\Gamma}^{(2)}$ and $\tilde{\Gamma}^{(4)}$ along the entire trajectory of the renormalization group flow. Note that both of these vertices implicitly depend on all $\{\tilde{r}_0(\mathbf{q}_\perp)\}$ and it doesn't look to promising to actually perform any computation. However for (5.18) to make sense we require that $|\tilde{r}_0(\mathbf{q}_\perp)| < |\mathbf{v}_F(\mathbf{q}_\perp)|$ as it describes the shift of the true Fermi surface relative to the bare one in units of the ultraviolet cutoff Λ_0. Actually in most cases we can assume that this shift is indeed much smaller than Λ_0. Assuming that a similar relation holds at any τ such that $\frac{|\tilde{r}_\tau(\mathbf{q}_\perp)|}{|\mathbf{v}_F(\mathbf{q}_\perp)|} \ll 1$ makes $\tilde{r}_0(\mathbf{q}_\perp)$ a suitable parameter for expansion - in leading order we shall simply neglect it on the right-hand side of (5.23).

Note that if $\eta(\mathbf{q}_\perp) > 1$ for any set of momenta $\{\mathbf{q}_\perp\}$ the vertices $\tilde{r}_0(\mathbf{q}_\perp)$ for this set are finite even without the need to fine-tune their bare values. In this case we can not properly define a Fermi surface for this set as the momentum distribution function of the fermions becomes smooth. However properties of the system that depend on the shape of the Fermi surface are then protected against the *unnatural* [48] fine-tuning of bare quantities. Especially in the context of cuprate-superconductivity it is assumed that the Fermi surface is partly truncated in this way [27, 30].

Unrescaled picture

We can switch back to the picture with unrescaled momenta and vertices. Therefore we note that

$$\tilde{r}_0 = \frac{Z_0}{\Lambda_0}\Gamma^{(2)}_{\Lambda_0}(i0,\mathbf{k}_F) = \frac{Z_0}{\Lambda_0}\left(\Sigma_{\Lambda_0}(i0,\mathbf{k}_F) - \Sigma(i0,\mathbf{k}_F)\Sigma_{\Lambda_0}(i0,\mathbf{k}_F)\right). \qquad (5.24)$$

If we choose the bare self-energy to vanish and make use of the reparametrization invariance setting $Z_0 = 1$ we obtain from (5.23) after some rearrangements the equivalent equation for the self-energy of the interacting system

$$\Sigma(i0,\mathbf{k}_F) = \int_{\mathbf{K}'} \frac{\Theta(\Lambda_0 - \Lambda(\mathbf{K}'))}{i\omega' - \epsilon_{\mathbf{k}'} + \mu - \Sigma_{\Lambda(\mathbf{K}')}(\mathbf{K}')}\Gamma^{(4)}_{\Lambda(\mathbf{K}')}(\mathbf{K}_0,\mathbf{K}';\mathbf{K}',\mathbf{K}_0). \qquad (5.25)$$

Here we have introduced the scale $\Lambda(\mathbf{K}) = |\epsilon_{\mathbf{K}} - \epsilon_F|$ and defined the projected momentum $\mathbf{K}_0$ equivalent to (5.15). It is important to note that the vertices on the right-hand side are evaluated at a scale which depends on the distance to the true Fermi surface. We like to stress that in deriving (5.23) and (5.25) no approximations have been made - both equations are exact.

   We can actually reverse the direction of our derivation and show that (5.25) implies (5.23). To do so we that note that as long as the self-energy is properly defined by (5.25) the 2-point vertex has to vanish on the Fermi surface as $\Lambda \to 0$

$$\Gamma^{(2)}_{\Lambda\to 0}(i0,\mathbf{k}_F) \propto \Lambda^{\geq 1} \qquad (5.26)$$

Here the exponent of Λ has to be ≥ 1 because the flowing Fermi surface defined by $\mu - \Sigma_\Lambda$ has to stay within the bounds set by Λ around the true Fermi surface for the procedure of scaling toward the Fermi surface [38] to be properly defined. We conclude that $\tilde{r}_\tau = \frac{Z_\tau}{\Lambda}\Gamma^{(2)}$ then flows into a fixed point and that for $\tau = 0$ its value given by (5.23).

   We may derive from (5.25) the well known Hartree-Fock self-consistency equation. Here we neglect all frequency dependencies and project the momenta onto the true Fermi surface by $\mathbf{k} \to \mathbf{k}_\perp$, i.e. we use the projection $\mathbf{K} \to \mathbf{K}_0$. Evaluating the integral in (5.25) is then simple and we note that we only require the value of the self-energy on the true Fermi surface. This amounts to setting $\Lambda(\mathbf{K}) = 0$ for the self-energy: we only need its fixed point value. Assuming that the leading corrections to the self-energy stem from the bulk of the system we neglect the renormalization of the 4-point vertex and set here $\Lambda(\mathbf{K}) \approx \Lambda_0$. Skipping the ultraviolet cutoff we finally arrive at

$$\Sigma(i0,\mathbf{k}_F) = \int_{\mathbf{k}'} \Gamma^{(4)}_{\Lambda_0}(\mathbf{K}_0,\mathbf{K}_0';\mathbf{K}_0',\mathbf{K}_0)\,\Theta\left(\mu - \epsilon_{\mathbf{k}}' - \Sigma(i0,\mathbf{k}_F')\right). \qquad (5.27)$$

Using (5.25) as a starting point we can systematically derive corrections to the Hartree-Fock approximation.

5.3   Application: the compressibility

In the formalism we have used above we are working with a constant chemical potential rather than with a fixed density. As it has been pointed out by [92, 95, 96] such an approach is more suitable to calculate the Fermi surface self-consistently. If however we prefer to work at a specific density we have to obtain the true Fermi surface as a function of the chemical potential first. We can then relate the density of particles to the volume in momentum space enclosed by this Fermi surface [97] as

$$n = \int_{\mathbf{k}} \Theta(|\mathbf{k}_F(\mathbf{k}_\perp)| - |\mathbf{k}|) \ , \tag{5.28}$$

and tune the chemical potential such as to reach the desired density.

Differentiating (5.28) with respect to the chemical potential enables us to obtain the compressibility

$$n^2 \chi_n \;\; = \;\; \partial_\mu n \ . \tag{5.29}$$

As an example let us consider a simple model of spinless fermions in one dimension with interactions $g_2 = g_4 =: g$. Moreover we take the dispersion to be linear $\xi(k_\parallel) = v k_\parallel$. To calculate a bulk property like the density we have to postulate a low momentum bandwidth cutoff conveniently placed at $\mathbf{k} = 0$. As we like to include systems with a finite anomalous dimension we switch to the rescaled picture. The lower bandwidth cutoff then translates into an additional Θ-function we have to multiply the Greensfunction with

$$\tilde{G}_\tau(\mathbf{Q}) \to \tilde{G}_\tau(\mathbf{Q}) \, \Theta\left(e^\tau > -q_\parallel \frac{\Lambda_0}{k_F}\right) . \tag{5.30}$$

We substitute the 4-point vertex by its marginal part

$$\tilde{g}_\tau = \tilde{\Gamma}_\tau^{(4)}(\{\mathbf{Q}_0\}) \ , \tag{5.31}$$

and assume that we may neglect the anomalous dimensions $\eta \approx 0$. Using (5.23) we can calculate the bare vertex $\tilde{r}_0$ as

$$\begin{aligned}
\tilde{r}_0 \;\; &= \;\; -\int_0^\infty d\tau \, e^{-\tau(1-\eta)} \tilde{g}_\tau \int_{\mathbf{Q}} \dot{\tilde{G}}(\mathbf{Q}) \\
&\approx \;\; -\tilde{g}_0 \int_{\ln(\Lambda_0/k_F)}^\infty d\tau \, e^{-\tau} \\
&= \;\; -\tilde{g}_0 \frac{k_F}{\Lambda_0} \ .
\end{aligned} \tag{5.32}$$

We now apply (5.18) to obtain the self-consistency equation

$$k_F = k_{F0} - g k_F \ . \tag{5.33}$$

The compressibility (5.29) is then simply evaluated as

$$n^2 \chi_n = \frac{\nu_0}{1 + \tilde{g}_0} \ ,$$

(5.34)

which actually is the correct result. Note the relative simplicity by which we derived this equation - usually we have to perform some infinite summation of bubble diagrams to obtain the same result.

Chapter 6

Confinement in two coupled Luttinger liquids

In this chapter we study the deformation of the Fermi surface of two coupled spinless metallic chains. Here the band structure consists of two bands and the Fermi surface is in the simplest case a set of just four points. We introduce the notion of a confinement transition to describe the situation where the energy difference between these two bands vanishes as an effect of interactions. Using the formalism developed in the chapters before we study the effect of different interactions and determine that one which is responsible for a tendency toward confinement. We then bosonize this relevant interaction by a Hubbard-Stratonovich transformation and study the problem at strong coupling looking for a confinement transition. The results of this chapter have been published in [98, 99].

6.1   Introduction

In a system of interacting electrons we generally have to assume that the topology and shape of the Fermi surface depend on the interaction. This effect is especially marked for strong interactions where the system might undergo a quantum phase transition. Examples are the Pomeranchuk instability [100] with a symmetry reduction of the Fermi surface due to strong forward scattering and the Lifshitz transition [101] which involves a change of topology.

As long as there are no changes in the topology of a two-dimensional Fermi surface we can generally express the interaction induced change of its shape in terms of local changes of its curvature. There are two possible extreme cases of curvature: an infinite curvature corresponding to a sharp edge on one hand and zero curvature corresponding to a local flattening of the Fermi surface on the other. We are especially interested in the latter case which we term a *confinement transition*. This confinement may be complete if for example in a two-dimensional system the Fermi surface consists of two disconnected exactly flat sheets. The

Fermi surface might be only partially confined when the curvature vanishes just on some finite section. Note that a confined Fermi surface has a greater symmetry than the bare one.

As it has been argued by Clarke et al. [33–35] a system of metallic chains coupled by sufficiently small interchain hopping $t_\perp$ should undergo such a confinement transition. Strictly speaking the confinement arises due to decoherence of interchain single particle hopping. It is therefore the coherence that is confined within the chains and not necessarily the electrons themselves. The authors above pointed out that the anomalous anisotropy properties along the c-axis of cuprate superconductors can be understood in terms of such a confined coherence and that intrachain non-Fermi liquid behaviour is a necessary prerequisite. During the last decade there has been some considerable interest [102–108] to prove or disprove this scenario and present common understanding is that the proposal of Clarke et al. is not appropriate. However especially in the next chapter we shall open the discussion again by presenting a treatment within our novel functional renormalization group approach which actually confirms the emergence of confinement.

On the other hand a partial confinement might arise for a closed two-dimensional Fermi surface such that only certain sectors are exactly flat with a possible breakdown of the Fermi-liquid description here [25, 27–32]. For the two-dimensional Hubbard model close to half filling there is evidence [109] for an interaction induced tendency toward confinement. However so far there is no proof that this model develops exactly flat sectors.

The full problem of determining the Fermi surface of a two-dimensional system is quite complicated. To determine the relevant mechanism of a confinement transition it is convenient to consider a much simpler problem first. The simplest toy model to study confinement is to consider a system of two coupled spinless metallic chains [110–116]. Here the Fermi surface consists of just four points defined by the Fermi momenta of the so called anti-bonding and bonding bands. Without interactions the energy distance between these two bands is determined by twice the interchain hopping amplitude $t_\perp$. Including interactions this hopping amplitude might get renormalized to a $t_\perp^*$ and we would observe a confinement transition if $t_\perp^* = 0$. To study this problem we like to apply the self-consistent formalism for the Fermi surface we have developed in chapter 5. Our primary goal is to calculate the interaction induced shift of the Fermi surface and to investigate a possible confinement transition.

From the work of Fabrizio [113] we know that for a finite parameter space the system is a stable Luttinger liquid with gapless excitations. It is known however that sufficiently strong pair tunnelling can lead to a destabilization of this phase [102, 117]. We assume that the fixed point structure remains qualitatively correct even when investigating strong coupling as we shall do in sec. 6.4. In this work will we only consider bare parameters such as to reach this fixed point.

6.2   The model

To set up our model we linearise the energy dispersion around the true Fermi surface as

$$\epsilon_\sigma(k) - \epsilon_{F,\sigma} = v_\sigma(k - k_{F,\sigma}) \ , \tag{6.1}$$

with the band index $\sigma = \pm 1$ to denote the bands B/A, the Fermi momenta $k_{F,\sigma}$ and the Fermi energies $\epsilon_{F,\sigma} = \mu - \sigma t_\perp$. The non-interacting part of the action is
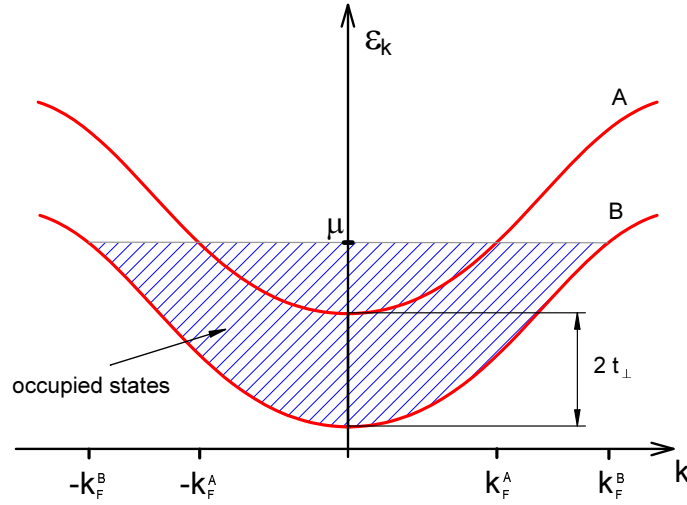

Figure 6.1: Energy dispersion of two coupled metallic chains. A and B denote the anti-bonding and bonding band and μ the chemical potential. The Fermi surface is defined by the four Fermi momenta $\pm k_F^A, \pm k_F^B$. The bands are separated by twice the interchain hopping $t_\perp$.

$$S_0 = -\sum_\sigma \int_K \bar{\psi}_{\sigma,K}(i\omega - \epsilon_\sigma(k) + \epsilon_{F,\sigma})\psi_{\sigma,K} \ , \tag{6.2}$$

and the interacting part

$$
\begin{aligned}
S_I \ = \ & \sum_\sigma \int_K \Gamma_\sigma^{(2)}(K)\bar{\psi}_{\sigma,K}\psi_{\sigma,K} \\
& + \frac{1}{4} \sum_{\{\sigma_i\},\{\alpha_i\}} \int_{\{K_i\}} (2\pi^2)\delta(\alpha_1 K_1 + \alpha_2 K_2 - \alpha_{1'} K_{1'} + \alpha_{2'} K_{2'}) \cdot \\
& \cdot \Gamma^{(4)}\left(\{\sigma_i\}, \{\alpha_i\}, \{K_i\}\right) \bar{\psi}_{\sigma_{1'},\alpha_{1'},K_{1'}} \bar{\psi}_{\sigma_{2'},\alpha_{2'},K_{2'}} \psi_{\sigma_2,\alpha_2,K_2} \psi_{\sigma_1,\alpha_1,K_1} \ .
\end{aligned} \tag{6.3}
$$

Here we have decomposed the interaction dependent on the directions ($\alpha = \text{R/L}$) and bands ($\sigma = \text{A/B}$) of the scattered electrons as in figure 6.2.

$$\Gamma^{(4)}\big(\sigma_{1'},\sigma_{2},\sigma_{2},\sigma_{1}\,;\,\alpha_{1'},\alpha_{2'},\alpha_{2},\alpha_{1}\big) \quad = $$

Figure 6.2: Notation of the 4-point vertex dependent on band and direction.

It is convenient to label the 4-point vertex for different sectors differently and we define (suppressing frequencies and momenta)

$$
\begin{aligned}
g_A &= \Gamma^{(4)}(AAAA, RLLR) & \text{intraband A forward,} & \qquad (6.4)\\
g_B &= \Gamma^{(4)}(BBBB, RLLR) & \text{intraband B forward ,} &\\
g_f &= \Gamma^{(4)}(ABBA, RLLR) & \text{interband forward,} &\\
g_t &= \Gamma^{(4)}(BBAA, RLLR) & \text{interband pair tunnelling ,} &\\
g_b &= \Gamma^{(4)}(BABA, RLLR) & \text{interband backward .} &
\end{aligned}
$$

A pictorial description of these couplings is presented in figure 6.3.
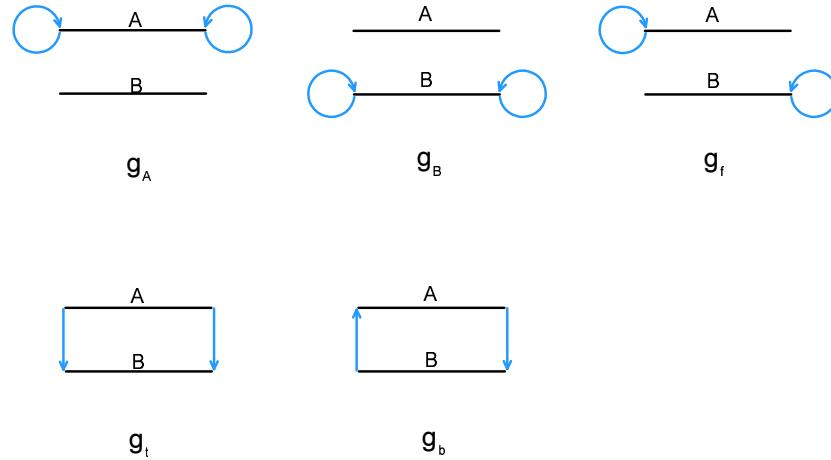
Figure 6.3: Pictorial description of the various couplings defined in (6.4)

Here we have chosen not to consider chiral terms, involving fermions moving in the same direction, and umklapp scattering. The first just renormalize the Fermi velocities and the latter is only important at certain band fillings. All other sectors of the 4-point vertex are related to the couplings above by an exchange of external legs. Note that the interaction g_b in general does not conserve momentum on the Fermi surface. As it has already been noticed by Fabrizio [113] but not

quantitatively investigated it is this interaction that is responsible to drive the system toward confinement.

6.3   Fermionic picture

We start our treatment with a purely fermionic description of the system. To classify the vertices according to their relevance we rescale momenta and vertices. Only the 2-point vertex and the 4-point vertices contain relevant or marginal terms and we consider the corresponding flow equations. All other vertices are irrelevant and we neglect them in the spirit of an expansion in relevance, see sec. 3.1. After an evaluation of the flow of the couplings in 1-loop we proceed to obtain self-consistently the shift of the Fermi surface.

6.3.1   Rescaling and classification according to relevance

We rescale the momenta and vertices as

$$\epsilon \;=\; \frac{\omega}{\Lambda_\tau} \,, \tag{6.5}$$

$$q_\sigma \;=\; \frac{|k| - k_{F,\sigma}}{\Lambda_\tau} \,, \tag{6.6}$$

$$\int_K \;=\; \int \frac{d\omega}{2\pi}\frac{dk}{2\pi} \;=\; \Lambda_\tau^2\,\nu_0 \int \frac{d\epsilon}{2\pi}dq \;=\; \Lambda_\tau^2\nu_0 \int_Q \,, \tag{6.7}$$

$$\psi_{\sigma,K} \;=\; \sqrt{\frac{Z_{\sigma,\tau}}{\Lambda^3\nu_0}}\,\tilde{\psi}_{\sigma,Q} \,, \tag{6.8}$$

$$\tilde{\Gamma}_\tau^{(2n)}(\{Q_i\}) \;=\; \nu_0^{n-1}\Lambda^{n-2}\left(Z_{\sigma_{1'}\tau}\cdot\ldots\cdot Z_{\sigma_1\tau}\right)^{\frac{1}{2}}\Gamma_\tau^{(2n)}(\{K_i\}) \,. \tag{6.9}$$

Here we have introduced ν_0 which is defined as

$$\nu_0 = \frac{1}{2\pi} \,. \tag{6.10}$$

The rescaled Greensfunctions are written as

$$\tilde{G}_{\sigma,\tau}(Q) \;=\; \frac{\Theta(1 < |q| < e^\tau)}{Z_{\sigma,\tau}(i\epsilon - v_\sigma q) - \tilde{\Gamma}_{\sigma,\tau}^{(2)}(Q)} \,, \tag{6.11}$$

$$\dot{\tilde{G}}_{\sigma,\tau}(Q) \;=\; \frac{\delta(|q| - 1)}{Z_{\sigma,\tau}(i\epsilon - v_\sigma q) - \tilde{\Gamma}_{\sigma,\tau}^{(2)}(Q)} \,. \tag{6.12}$$

The only relevant coupling is the frequency/momentum independent part of the 2-point vertex

$$\tilde{r}_\sigma = \tilde{\Gamma}^{(2)}(i0,0) \,. \tag{6.13}$$

There are two marginal couplings associated with the 2-point vertex namely the wavefunction renormalization and the renormalized Fermi velocity

$$Z_{\sigma,\tau} = 1 + \partial_{i\epsilon} \tilde{\Gamma}^{(2)}_{\sigma,\tau}(Q)|_{Q=0} , \tag{6.14}$$

$$\tilde{v}_{\sigma,\tau} = v_\sigma Z_{\sigma,\tau} - \partial_q \tilde{\Gamma}^{(2)}_{\sigma,\tau}(Q)|_{Q=0} , \tag{6.15}$$

which allow us to write the Greensfunctions up to relevant and marginal terms as

$$\tilde{G}_{\sigma,\tau}(Q) = \frac{\Theta(1 < |q| < e^\tau)}{i\epsilon - \tilde{v}_{\sigma,\tau}q - \tilde{r}_{\sigma,\tau}} , \tag{6.16}$$

$$\dot{\tilde{G}}_{\sigma,\tau}(Q) = \frac{\delta(|q|-1)}{i\epsilon - \tilde{v}_{\sigma,\tau}q - \tilde{r}_{\sigma,\tau}} . \tag{6.17}$$

The anomalous dimensions are as usual defined by

$$\eta_{\sigma,\tau} = -\partial_\tau \ln(Z_{\sigma,\tau}) . \tag{6.18}$$

The frequency/momentum independent parts of the 4-point vertex are marginal as well and we denote these as $\tilde{g}$ in the same spirit as in (6.4) where the lack of the frequency/momentum argument means that we consider both to be zero, i.e the scattered fermions propagate on the Fermi surface.

6.3.2 Flow of vertices

2-point vertex

The 2-point vertex flows as

$$\partial_\tau \tilde{\Gamma}^{(2)}_{\sigma,\tau}(Q) = (1 - \eta_{\sigma,\tau} - Q \cdot \partial_Q) \tilde{\Gamma}^{(2)}_{\sigma,\tau}(Q) + \dot{\tilde{\Gamma}}^{(2)}_{\sigma,\tau}(Q) \tag{6.19}$$

with

$$\dot{\tilde{\Gamma}}^{(2)}_{\sigma,\tau}(Q) = \sum_{\sigma'} \int_{Q'} \dot{\tilde{G}}_{\sigma',\tau}(Q') \tilde{\Gamma}^{(4)}_\tau \left(\{\sigma,\sigma',\sigma',\sigma\}, \{Q,Q',Q',Q\}\right) . \tag{6.20}$$

4-point vertices

The general expression for the flow equation of the 4-point vertices is

$$\partial_\tau \tilde{\Gamma}^{(4)}_\tau(\{\sigma_i\}, \{Q_i\}) = \sum_i \left(-\frac{\eta_{\sigma_i,\tau}}{2} - Q_i \cdot \partial_{Q_i} \right) \tilde{\Gamma}^{(4)}_\tau(\{\sigma_i\}, \{Q_i\})$$

$$+ \dot{\tilde{\Gamma}}^{(4)}_\tau(\{\sigma_i\}, \{Q_i\}) . \tag{6.21}$$

To evaluate $\dot{\tilde{\Gamma}}^{(4)}$ [20, 21, 38] we introduce the general susceptibilities $\dot{\tilde{\chi}}$. Neglecting $\tilde{r}$ which we assume to be small and dropping for simplicity the tilde over the renormalized Fermi velocities results in

$$
\dot{\tilde{\chi}}_{\sigma\sigma'}(Q) = \Theta(e^\tau - 1 > |q|) \left(\frac{1}{v_\sigma + v_{\sigma'} + s_q(v_{\sigma'}q + i\epsilon)} \right.
$$
$$
\left. + \frac{1}{v_\sigma + v_{\sigma'} + s_q(v_\sigma q - i\epsilon)} \right) , \qquad (6.22)
$$

where $s_x = \text{sign}(x)$. We are now able to write the inhomogeneity on the right-hand side of the flow equation as

$$
\dot{\tilde{g}}_\sigma(\{Q_i\}) = \tilde{g}_\sigma^2 \{ \dot{\tilde{\chi}}_{\sigma\sigma}(Q_1 - Q_2') - \dot{\tilde{\chi}}_{\sigma\sigma}(Q_1 + Q_2) \} \qquad (6.23)
$$
$$
- \tilde{g}_t^2 \, \dot{\tilde{\chi}}_{\bar{\sigma}\bar{\sigma}}(Q_1 + Q_2) + \tilde{g}_b^2 \, \dot{\tilde{\chi}}_{\bar{\sigma}\bar{\sigma}}(Q_1 - Q_2' + 2\sigma\tilde{\Delta}_\tau) ,
$$

$$
\dot{\tilde{g}}_f(\{Q_i\}) = \tilde{g}_f^2 \{ \dot{\tilde{\chi}}_{AB}(Q_1 - Q_2') - \dot{\tilde{\chi}}_{AB}(Q_1 + Q_2) \} \qquad (6.24)
$$
$$
+ \tilde{g}_t^2 \, \dot{\tilde{\chi}}_{BA}(Q_1 - Q_2') - \tilde{g}_b^2 \, \dot{\tilde{\chi}}_{BA}(Q_1 + Q_2 - 2\tilde{\Delta}_\tau)) ,
$$

$$
\dot{\tilde{g}}_t(\{Q_i\}) = \tilde{g}_f\tilde{g}_t \{ \dot{\tilde{\chi}}_{AB}(Q_1 - Q_2') + \dot{\tilde{\chi}}_{BA}(Q_1 - Q_2') \} \qquad (6.25)
$$
$$
- \tilde{g}_A^2 \, \dot{\tilde{\chi}}_{AA}(Q_1 + Q_2) - \tilde{g}_B^2 \, \dot{\tilde{\chi}}_{BB}(Q_1 + Q_2) ,
$$

$$
\dot{\tilde{g}}_b(\{Q_i\}) = -\tilde{g}_f\tilde{g}_b \{ \dot{\tilde{\chi}}_{AB}(Q_1 + Q_2) + \dot{\tilde{\chi}}_{BA}(Q_1 + Q_2) \} \qquad (6.26)
$$
$$
+ \tilde{g}_A\tilde{g}_b \, \dot{\tilde{\chi}}_{AA}(Q_1 - Q_2') + \tilde{g}_B\tilde{g}_b \, \dot{\tilde{\chi}}_{BB}(Q_1 - Q_2') .
$$

Here we have introduced $\bar{\sigma} = -\sigma$ and

$$
\tilde{\Delta}_\tau = \frac{\Delta}{\Lambda_\tau} = \frac{k_{F,B} - k_{F,A}}{\Lambda_\tau} > 0 . \qquad (6.27)
$$

As a shorthand we write $Q + \tilde{\Delta} := (i\epsilon, q + \tilde{\Delta})$. Note that on the (generating) right-hand sides we have only considered non-irrelevant terms.

6.3.3　1-loop calculation

We start with a simple 1-loop calculation of the frequency/momentum independent vertices.

4-point vertices

At zero momentum the susceptibilities are

$$
\dot{\tilde{\chi}}_{\sigma\sigma'}(0) = \frac{2}{v_\sigma + v_{\sigma'}} , \qquad (6.28)
$$

and in order $O(\tilde{g}^2)$ we receive the following flow equations (η is of order $O(\tilde{g}^2)$ and therefore does not contribute to these equations within leading order)

$$\partial_\tau \tilde{g}_A = -\frac{1}{v_B}\tilde{g}_t^2 + \beta_{BB,\tau}\tilde{g}_b^2 , \qquad (6.29)$$

$$\partial_\tau \tilde{g}_B = -\frac{1}{v_A}\tilde{g}_t^2 + \beta_{AA,\tau}\tilde{g}_b^2 , \qquad (6.30)$$

$$\partial_\tau \tilde{g}_f = \frac{2}{v_A + v_B}\tilde{g}_t^2 - \beta_{AB,\tau}\tilde{g}_b^2 , \qquad (6.31)$$

$$\partial_\tau \tilde{g}_t = -\tilde{g}_0\tilde{g}_t , \qquad (6.32)$$

$$\partial_\tau \tilde{g}_b = \tilde{g}_0\tilde{g}_b , \qquad (6.33)$$

$$\partial_\tau \tilde{g}_0 = -\tilde{\nu}_0\tilde{g}_t^2 + \beta_{0,\tau}\tilde{g}_b^2 , \qquad (6.34)$$

with

$$\tilde{g}_0 = \frac{1}{v_A}\tilde{g}_A + \frac{1}{v_B}\tilde{g}_B - \frac{4}{v_A + v_B}\tilde{g}_f , \qquad (6.35)$$

$$\beta_{\sigma\sigma',\tau} = \frac{\Theta(e^\tau - 1 - 2|\tilde{\Delta}_\tau|)}{v_\sigma + v_{\sigma'} + 2v_\sigma|\tilde{\Delta}_\tau|} + \frac{\Theta(e^\tau - 1 - 2|\tilde{\Delta}_\tau|)}{v_\sigma + v_{\sigma'} + 2v_{\sigma'}|\tilde{\Delta}_\tau|} , \qquad (6.36)$$

$$\beta_{0,\tau} = \frac{\beta_{AA,\tau}}{v_B} + \frac{\beta_{BB,\tau}}{v_A} + \frac{4\beta_{AB,\tau}}{v_A + v_B} , \qquad (6.37)$$

$$\tilde{\nu}_0 = \frac{2}{v_A v_B} + \frac{8}{(v_A + v_B)^2} . \qquad (6.38)$$

Up to this order the flow equations coincide with those derived by Fabrizio [113] who studied the flow up to 2-loop quite extensively. Note that the vertices $\tilde{g}_t$ and $\tilde{g}_b$ only couple to the forward scattering amplitudes via the combination $\tilde{g}_0$ and the three flow equations (6.32), (6.33) and (6.34) form a closed set.

The flow for $\tau \to \infty$ in the de-confined phase

The de-confined phase is characterized by a non vanishing magnetization. Consequently $\tilde{\Delta}_\tau \to \infty$ for $\tau \to \infty$ and the functions β vanish. The flow equations decouple further and we obtain

$$\partial_\tau \tilde{g}_0 = -\tilde{\nu}_0\tilde{g}_t^2 , \qquad (6.39)$$

$$\partial_\tau \tilde{g}_t = -\tilde{g}_0\tilde{g}_t , \qquad (6.40)$$

$$\partial_\tau \tilde{g}_b = \tilde{g}_0\tilde{g}_b , \qquad (6.41)$$

which is also generally valid if $\tilde{g}_b = 0$. The combination $\tilde{g}_0^2 - \tilde{g}_t^2$ is a constant under the RG and we receive the following infinite set of fixed points

$$\tilde{g}_t^* = 0 \quad \wedge \quad \tilde{g}_b^* = 0 . \qquad (6.42)$$
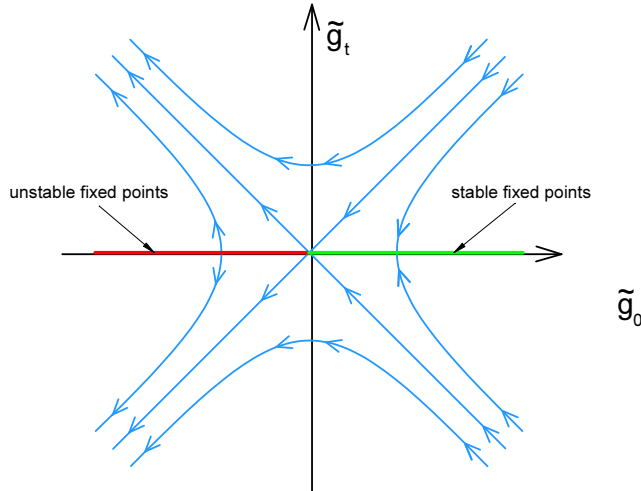
Figure 6.4: Flow for $\tilde{g}_0$ and $\tilde{g}_t$. Here we do not consider $\tilde{g}_b$ for the stability analysis.

For $\tilde{g}_0^* > 0$ these fixed points are stable with respect to $\tilde{g}_t$, i.e. the latter is an irrelevant perturbation. However our analysis only includes the leading order in $\tilde{g}$ and therefore is only applicable to weak coupling. From the work of Fabrizio [113] follows that this fixed point structure is correct even for finite $\tilde{g}_0$ and that $\tilde{g}_b$ flows into a fixed point as well even if it is nonzero initially.

For $\tilde{g}_0^* < 0$ the fixed points are unstable with respect to $\tilde{g}_t$ - the system flows toward strong coupling.

2-point vertex - shift of Fermi surface

Within a 1-loop calculation we only consider the frequency/momentum independent vertices. Therefore here we do observe neither a renormalization of the Fermi velocities nor an anomalous dimension. Using our results of section 5 we fine-tune $\tilde{r}_\sigma$ to reach a fixed point

$$\tilde{r}_{\sigma,0} = - \int_0^\infty d\tau \, e^{-\tau} \, \dot{\tilde{r}}_{\sigma,\tau} \, , \tag{6.43}$$

with

$$\dot{\tilde{r}}_{\sigma,\tau} = \tilde{g}_{\sigma,\tau} + \tilde{g}_{f,\tau} \, . \tag{6.44}$$

Assuming that the couplings $\tilde{g}$ remain small under the RG (as we have stated above we just consider bare couplings such as to flow into a fixed point) we then obtain for the interaction induced shift of the Fermi surface

$$\tilde{\Delta}_0 - \tilde{\Delta}_0^{(0)} \quad = \quad \frac{\tilde{r}_{B,0}}{v_B} - \frac{\tilde{r}_{A,0}}{v_A}$$

$$
\begin{aligned}
= \ &\frac{\tilde{g}_{A,0}}{v_A} - \frac{\tilde{g}_{B,0}}{v_B} - \tilde{g}_{f,0}\frac{v_A - v_B}{v_A v_B} - \tilde{g}_{t,0}^2\frac{2}{v_A v_B}\frac{v_A - v_B}{v_A + v_B} \\
&+ \tilde{g}_{b,0}^2\frac{2(v_A - v_B)}{v_A v_B(v_A + v_B)}\Big\{1 - 2\tilde{\Delta}_0 \\
&+ \frac{v_A}{v_A + v_B}\tilde{\Delta}_0 \ln\left(\frac{2v_A\tilde{\Delta}_0}{v_A + v_B - 2v_B\tilde{\Delta}_0}\right) \\
&+ \frac{v_B}{v_A + v_B}\tilde{\Delta}_0 \ln\left(\frac{2v_B\tilde{\Delta}_0}{v_A + v_B - 2v_A\tilde{\Delta}_0}\right)\Big\} \ ,
\end{aligned}
\tag{6.45}
$$

with the bare difference of the Fermi momenta $\tilde{\Delta}_0^{(0)} = \frac{k_{F0,B} - k_{F0,A}}{\Lambda_0}$ of the non-interacting system.

However we have to note that the equation above is only consistent up to order $O(\tilde{g}^1)$ as we have neglected irrelevant parts of the 4-point vertices which are of order $O(\tilde{g}^2)$. To cure this deficiancy we therefore have to repeat the calculation taking into account these irrelevant parts of the 4-point vertices - this is basically the hybrid approach we described in section 3.1 and applied in section 4 in the context of weakly interacting bosons. For the same reasons we believe that the results for the shift of the Fermi surface derived by [112] are inconsistent.

6.3.4 The 2-point vertex in 2-loop

4-point vertices

As we have done before we decompose the 4-point vertices into marginal (frequency/momentum independent) and irrelevant parts as

$$
\tilde{g}(Q) = \tilde{g} + \tilde{g}^{(i)}(Q) \ .
\tag{6.46}
$$

Writing the flow equation for $\tilde{g}(Q)$ as $\partial_\tau \tilde{g}_\tau(Q) = X_\tau\dot{\tilde{\chi}}(\tilde{Q})_{\tilde{Q}=\tilde{Q}(\{Q\})}$ we obtain for the irrelevant part

$$
\begin{aligned}
\tilde{g}_\tau^{(i)}(Q) \ = \ &\int_0^\tau d\tau' \, X_{\tau-\tau'}\left(\dot{\tilde{\chi}}_{\sigma\sigma',\tau}(\tilde{Q}e^{-\tau'}) - \dot{\tilde{\chi}}_{\sigma\sigma',\tau}(0)\right) \\
= \ &\frac{X_\tau\Theta(e^\tau - 1 - |\tilde{q}|)}{v_\sigma + v_{\sigma'}} \\
&\times \ln\left(\frac{(v_\sigma + v_{\sigma'})e^\tau - v_\sigma|\tilde{q}| + s_{\tilde{q}}i\tilde{\epsilon}}{v_\sigma + v_{\sigma'} + v_{\sigma'}|\tilde{q}| + s_{\tilde{q}}i\tilde{\epsilon}}\frac{(v_\sigma + v_{\sigma'})e^\tau - v_{\sigma'}|\tilde{q}| + s_{\tilde{q}}i\tilde{\epsilon}}{v_\sigma + v_{\sigma'} + v_\sigma|\tilde{q}| + s_{\tilde{q}}i\tilde{\epsilon}}\right) \\
&- \frac{X_\tau\tau}{v_\sigma + v_{\sigma'}} \\
=: \ &X_\tau\left(\tilde{\chi}_{\sigma\sigma',\tau}(\tilde{Q}) - \tilde{\chi}_{\sigma\sigma',\tau}(0)\right) \ .
\end{aligned}
\tag{6.47}
$$

Here we have used that the difference $\dot{\tilde{\chi}}(\tilde{Q}e^{-\tau'}) - \dot{\tilde{\chi}}(0)$ vanishes exponentially for large τ' and approximated $X_{\tau-\tau'} \approx X_\tau$. Using this approximation we can

now calculate the 4-point vertices consistently up to order $O(\tilde{g}^2)$. However we shall not study all of these vertices further but consider just the parts we need to obtain the flow of the 2-point vertices.

2-point vertices

To calculate the flow of the 2-point vertices we require the following integral

$$
\sum_{q''=\pm 1} \int_{\epsilon''} \frac{\tilde{\chi}_{\sigma\sigma'}(\epsilon + m\epsilon'', q + nq'')}{i\epsilon'' - v_{\sigma''}q''} \;=\; \frac{\Theta(e^\tau - 2)}{v_\sigma + v_{\sigma'}} s_{\alpha_q} \tag{6.48}
$$
$$
\times \left\{ \delta_{m,n} \ln\left(\frac{(v_\sigma + v_{\sigma'})e^\tau + v_{\sigma''} - v_\sigma + v_\sigma q - i\epsilon}{(v_\sigma + v_{\sigma'})e^\tau + v_{\sigma''} - v_\sigma - v_\sigma q + i\epsilon} \frac{v_\sigma + 2v_{\sigma'} + v_{\sigma''} + v_{\sigma'}q + i\epsilon}{v_\sigma + 2v_{\sigma'} + v_{\sigma''} - v_{\sigma'}q - i\epsilon} \right) \right.
$$
$$
\left. \delta_{m,-n} \ln\left(\frac{(v_\sigma + v_{\sigma'})e^\tau + v_{\sigma''} - v_{\sigma'} + v_{\sigma'}q + i\epsilon}{(v_\sigma + v_{\sigma'})e^\tau + v_{\sigma''} - v_{\sigma'} - v_{\sigma'}q - i\epsilon} \frac{v_{\sigma'} + 2v_\sigma + v_{\sigma''} + v_\sigma q - i\epsilon}{v_{\sigma'} + 2v_\sigma + v_{\sigma''} - v_\sigma q + i\epsilon} \right) \right\},
$$

which is valid for $|q| < 1$. Here $m, n = \pm 1$.

Vanishing inter-band backward scattering: $\tilde{g}_b = 0$

The coupling $\tilde{g}_b$ is the one leading to confinement but makes the treatment more tedious. As the flow of the 2-point vertices depends additively on this coupling we can neglect it for a first analysis and consider it later on. We obtain for $|q| < 1$

$$
\dot{\tilde{\Gamma}}^{(2)}_{A\tau}(Q) \;=\; \tilde{g}_{A0} + \tilde{g}_{f0} - \tilde{g}_{A\tau}^2 \frac{\Theta(e^\tau > 2)}{v_A} \ln\left(\frac{2v_A e^\tau - v_A q - i\epsilon}{2v_A e^\tau + v_A q + i\epsilon} \frac{4v_A - v_A q + i\epsilon}{4v_A + v_A q - i\epsilon} \right) \tag{6.49}
$$
$$
- \tilde{g}_{f\tau}^2 \frac{2\Theta(e^\tau > 2)}{v_A + v_B} \ln\left(\frac{(v_A + v_B)e^\tau - v_B q - i\epsilon}{(v_A + v_B)e^\tau + v_B q + i\epsilon} \frac{2(v_A + v_B) - v_A q + i\epsilon}{2(v_A + v_B) + v_A q - i\epsilon} \right)
$$
$$
- \tilde{g}_{t\tau}^2 \frac{\Theta(e^\tau > 2)}{2v_B} \ln\left(\frac{2v_B e^\tau - v_B q - i\epsilon}{2v_B e^\tau + v_B q + i\epsilon} \frac{4v_B - v_B q + i\epsilon}{4v_B + v_B q - i\epsilon} \right)
$$
$$
- \tilde{g}_{t\tau}^2 \frac{\Theta(e^\tau > 2)}{v_A + v_B} \ln\left(\frac{(v_A + v_B)e^\tau + v_B - v_A - v_A q - i\epsilon}{(v_A + v_B)e^\tau + v_B - v_A + v_A q + i\epsilon} \frac{v_A + 3v_B - v_B q + i\epsilon}{v_A + 3v_B + v_B q - i\epsilon} \right)
$$
$$
\;=\; +\tilde{g}_{A0} + \tilde{g}_{f0} + q\Theta(e^\tau > 2)\left\{ \tilde{g}_{A\tau}^2 \frac{2e^{-\tau} + 1}{2v_A} + 2\tilde{g}_{f\tau}^2 \frac{2v_B e^{-\tau} + v_A}{(v_A + v_B)^2} \right.
$$
$$
\left. + \tilde{g}_{t\tau}^2 \left(\frac{2e^{-\tau} + 1}{4v_B} + \frac{2v_A}{(v_A + v_B)^2 e^\tau + v_B^2 - v_A^2} + \frac{2v_B}{(v_A + v_B)(v_A + 3v_B)} \right) \right\}
$$
$$
+ i\epsilon\Theta(e^\tau > 2)\left\{ \tilde{g}_{A\tau}^2 \frac{2e^{-\tau} - 1}{2v_A^2} + 2\tilde{g}_{f\tau}^2 \frac{2e^{-\tau} - 1}{(v_A + v_B)^2} \right.
$$
$$
\left. + \tilde{g}_{t\tau}^2 \left(\frac{2e^{-\tau} - 1}{4v_B^2} + \frac{2}{(v_A + v_B)^2 e^\tau + v_B^2 - v_A^2} - \frac{2}{(v_A + v_B)(v_A + 3v_B)} \right) \right\},
$$

where for the last equality we have performed an expansion in (ϵ, q) up to linear order. The flow for $\tilde{\Gamma}^{(2)}_{B,\tau}(Q)$ may simply be obtained by exchanging the indices $A \leftrightarrow B$.

From the equation above we can calculate the anomalous dimension

$$
\begin{aligned}
\eta_{A\tau} &= -\partial_{i\epsilon} \dot{\tilde{\Gamma}}^{(2)}_{A\tau}|_{q,\epsilon=0} \\
&= -\Theta(e^\tau > 2)\left\{ \tilde{g}^2_{A\tau} \frac{2e^{-\tau}-1}{2v^2_A} + 2\tilde{g}^2_{f\tau} \frac{2e^{-\tau}-1}{(v_A+v_B)^2} \right. \\
&\left. \quad + \tilde{g}^2_{t\tau}\left(\frac{2e^{-\tau}-1}{4v^2_B} + \frac{2}{(v_A+v_B)^2 e^\tau + v^2_B - v^2_A} - \frac{2}{(v_A+v_B)(v_A+3v_B)} \right) \right\},
\end{aligned}
\tag{6.50}
$$

and the flow for the renormalized Fermi velocity

$$
\begin{aligned}
\partial_\tau v_{A\tau} &= -\eta_{A\tau} v_{A\tau} + \partial_q \dot{\tilde{\Gamma}}^{(2)}_{A\tau}|_{q,\epsilon=0} \\
&= \Theta(e^\tau > 2)\left\{ \tilde{g}^2_{A\tau} \frac{2e^{-\tau}}{v_A} + \tilde{g}^2_{f\tau} \frac{4e^{-\tau}}{v_A+v_B} + \tilde{g}^2_{t\tau}\left(\frac{e^{-\tau}}{2} \frac{v_a+v_B}{v^2_B} \right. \right. \\
&\left. \left. \quad + \frac{1}{4} \frac{v_A - v_B}{v^2_B} + \frac{4v_A}{(v_A+v_B)^2 e^\tau + v^2_B - v^2_A} + \frac{2}{v_A+3v_B} \frac{v_B - v_A}{v_A+v_B} \right) \right\}.
\end{aligned}
\tag{6.51}
$$

To obtain the shift of the Fermi surface up to $\tilde{g}^2$ we neglect the anomalous dimension as it does not contribute to that order. We observe that with the quadratic terms cancelling each other there actually is only a linear contribution

$$
\tilde{\Delta}_0 - \tilde{\Delta}^{(0)}_0 = \frac{\tilde{g}_{A,0}}{v_A} - \frac{\tilde{g}_{B,0}}{v_B} - \tilde{g}_{f,0} \frac{v_A - v_B}{v_A v_B} .
\tag{6.52}
$$

This is just the ordinary Hartree-Fock shift and we denote it by $\tilde{\Delta}_{HF}$.

In the case that the Fermi velocities $v_A = v_B =: v$ and the couplings $\tilde{g}_A = \tilde{g}_B =: \tilde{g}_\rho$ are equal the equations above simplify considerably and we obtain

$$
\tilde{\Delta}_{HF} = \tilde{\Delta}^{(0)}_0 ,
\tag{6.53}
$$

$$
\eta_\tau = \Theta(e^\tau > 2) \frac{1 - 2e^{-\tau}}{2v^2}(\tilde{g}^2_{\rho\tau} + \tilde{g}^2_{f\tau} + \tilde{g}^2_{t\tau}) ,
\tag{6.54}
$$

$$
\partial_\tau v_\tau = \Theta(e^\tau > 2) \frac{2e^{-\tau}}{v}(\tilde{g}^2_{\rho\tau} + \tilde{g}^2_{f\tau} + \tilde{g}^2_{t\tau}) .
\tag{6.55}
$$

Finite inter-band backward scattering $\tilde{g}_b \neq 0$

To study the effect of this coupling for simplicity we only consider the case $v_A = v_B = v$. In the flow equations for the 4-point vertices there appear terms involving $\dot{\tilde{\chi}}(\tilde{\epsilon}, \tilde{q} + 2\tilde{\Delta}_0 e^\tau)$. To solve these flow equations in the same manner as before we define

$$
\dot{\tilde{\chi}}_\tau(\epsilon, q, y) = \dot{\tilde{\chi}}_\tau(\epsilon, q + ye^\tau) ,
\tag{6.56}
$$

and
$$\tilde{\chi}_\tau(\epsilon, q, y) = \int_0^\tau d\tau' \, \dot{\tilde{\chi}}_{\tau-\tau'}(\epsilon e^{-\tau'}, q e^{-\tau'} + y) \; . \tag{6.57}$$

We can re-use (6.48) with the redefined $\tilde{\chi}$ to evaluate the flow for the 2-point vertex. Here we shall only consider the shift of the Fermi surface and skip a study of the anomalous dimension and the renormalized Fermi velocity. At vanishing frequency/momentum we get

$$\sum_{q=\pm 1} \int_\epsilon \frac{\tilde{\chi}_{\sigma\sigma',\tau}(m\epsilon, nq, y)}{i\epsilon - vq} =$$
$$-\frac{\sum_q s_q \Theta(e^\tau - 1 > |nq + ye^\tau|)}{2v} \ln\left(\frac{2e^\tau + 1 - |nq + ye^\tau|}{3 + |nq + ye^\tau|}\right) \; . \tag{6.58}$$

We integrate over $\int_0^\infty d\tau \, e^{-\tau}$ and expand for small y to yield in leading order

$$\int_0^\infty d\tau \, e^{-\tau} \sum_{q=\pm 1} \int_\epsilon \frac{\tilde{\chi}_{\sigma\sigma',\tau}(m\epsilon, nq, y)}{i\epsilon - vq} = -\frac{n\Theta(1-|y|)}{4v} y \ln(|y|) \; . \tag{6.59}$$

Now we have all equations together to evaluate the shift of the Fermi surface. We obtain (dropping the subscript 0 of $\tilde{\Delta}$) the self-consistency equation

$$\tilde{\Delta} = \tilde{\Delta}_{HF} + \frac{2\tilde{g}_{b,0}^2 \tilde{\Delta}}{v^2} \ln(|\tilde{\Delta}|) \, \Theta(\tilde{\Delta} < 1/2) \; , \tag{6.60}$$

which is the central result of this section. Defining $\tilde{g}^2 = \frac{2\tilde{g}_{b,0}^2}{v^2}$ we can solve this equation in terms of the LambertW (LW)-function [118] as

$$\tilde{\Delta} = \frac{\tilde{\Delta}_{HF}}{-\tilde{g}^2 LW\left(-1, -\frac{\tilde{\Delta}_{HF} e^{-1/\tilde{g}^2}}{\tilde{g}^2}\right)} \; , \tag{6.61}$$

and have plotted the result in figure 6.5. Note that an alternative way to write the self-consistency equation (6.60) is

$$\tilde{\Delta} = \frac{\tilde{\Delta}_{HF}}{1 - \frac{\tilde{g}_{b,0}^2}{v^2} \ln(\tilde{\Delta}^2)} \; . \tag{6.62}$$

We observe that for strong coupling the denominator grows large and reduces the difference between the Fermi momenta. This reduction actually enhances the interaction by virtue of the logarithmic term if the true difference is small enough. We observe a clear tendency toward confinement, i.e. an initial difference between the Fermi momenta is strongly suppressed as the interaction becomes stronger.

Note that our approach enables us to obtain a self-consistency equation for the shape of the Fermi surface. However within our expansion up to $\tilde{g}^2$ we cannot expect to describe the strong interacting case properly. Consequently the observation of a confinement transition is beyond the scope of this approximation. To extent our analysis even to strong coupling we shall show in the next section how this can be achieved by a suitable bosonization of the interaction.
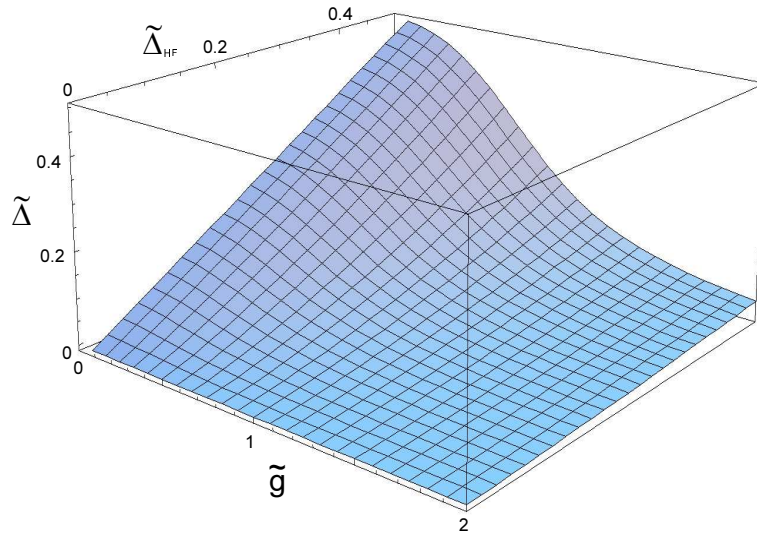
Figure 6.5: Plot of equation (6.61). The tendency toward confinement as the interaction strength increases is clearly visible.

6.4 Bosonized interaction

We repeat our study of the previous section by bosonizing the interaction by means of a Hubbard-Stratonovich transformation as laid out in section 2.5. As we have identified the interaction described by the coupling $\tilde{g}_b$ as the dominant process for confinement we will focus on just this interaction. After deriving the flow equation for the rescaled vertices we calculate the shift of the Fermi surface in different approximations.

6.4.1 Setup of the RG

The model with a bosonized interaction

It is convenient to rewrite the action in pseudo-spin language as

$$S = \int_K \bar{\psi}_{\sigma,K}(-i\omega + \epsilon_k - \mu)\psi_{\sigma,K} - \mathbf{H} \cdot \mathbf{S} + S_I \,, \tag{6.63}$$

where here and in the following we make use of the scalar product (2.6) in favor of a compact notation. The index σ labels the two bands and we use a linear dispersion

$$\epsilon_k = v|k| \,, \tag{6.64}$$

where for simplicity we take the Fermi velocities of both bands to be equal. We have introduced the spin densities

$$\mathbf{S}(K) = \frac{1}{2}\boldsymbol{\tau}_{\sigma\sigma'} \int_{K'} \psi^+_{K'\sigma}\psi_{K'+K\sigma'} \,, \tag{6.65}$$

using the Pauli matrices $\boldsymbol{\tau}_{\sigma\sigma'}$. We assume that the magnetic field points into the z-direction $\mathbf{H} = H\mathbf{e}_z$ ($H > 0$) and it induces at vanishing interaction a magnetization

$$k_{0\uparrow} - k_{0\downarrow} = \Delta_0 = \frac{H}{v} \ , \tag{6.66}$$

with the bare Fermi momenta $k_{0\sigma}$. The interaction $\tilde{g}_b$ translates into a ferromagnetic xy-interaction. We decompose it into two parts with definite chirality, here nch stands for the coupling of fermions with opposite chirality and ch for fermions with the same chirality and we term these two as non-chiral/chiral interactions

$$
\begin{aligned}
S_I &= -2f_{ch}(\mathbf{S}_x{\cdot}\mathbf{S}_x + \mathbf{S}_y{\cdot}\mathbf{S}_y)_{ch} - 2f_{nch}(\mathbf{S}_x{\cdot}\mathbf{S}_x + \mathbf{S}_y{\cdot}\mathbf{S}_y)_{nch} \qquad (6.67)\\
&= -2\rho_{\alpha,\uparrow\downarrow} \cdot \mathbf{f}_{\alpha\alpha'} \cdot \rho_{\alpha',\downarrow\uparrow} \ ,
\end{aligned}
$$

where α, α' run over R, L denoting right- and left-movers. The interaction constants are taken to be non-negative $f_{ch}, f_{nch} > 0$. The interaction matrix contains the elements

$$
\begin{aligned}
f_{RR} &= f_{LL} = f_{ch} \ , \qquad (6.68)\\
f_{RL} &= f_{LR} = f_{nch} \ .
\end{aligned}
$$

Additionally we have introduced the densities

$$\rho_{\alpha,\sigma\sigma'}(K) = \int_{K'} \psi^+_{\alpha,\sigma,K'}\psi_{\alpha,\sigma',K'+K} \ , \tag{6.69}$$

and observe that S_i can be written as a square in these densities. As announced we bosonize it via a Hubbard-Stratonovich transformation in the zero sound channel. The description of the interaction is now in terms of the complex bosonic field Φ. We write the generating functional for the 1-PI vertex functions as

$$
\begin{aligned}
\Gamma &= \int_K \bar{\psi}_{\sigma,K}\psi_{\sigma,K}\left(-i\omega + vk + \Gamma^{(2)}_\sigma(K)\right) + \Phi^*_\kappa \cdot F^{-1}_{\kappa\lambda} \cdot \Phi_\lambda \\
&\quad + i\gamma\left(\Phi^*_\kappa \cdot \rho_{\kappa,\uparrow\downarrow} + \Phi_\kappa \cdot \rho_{\kappa,\downarrow\uparrow}\right) \ , \qquad (6.70)
\end{aligned}
$$

where the indices κ, λ run over left- and right-movers. Here F denotes the Greens-function for the bosonic field and γ is the frequency/momentum independent part of the 3-point vertex coupling fermions to bosons $\gamma = \Gamma^{(2,1)}(\{0\})$. The initial values for the vertices are

$$\Gamma^{(2)}_\sigma(K) = -\sigma\frac{v\Delta_0}{2} \ , \tag{6.71}$$

$$\mathbf{F}^{-1} = \frac{1}{2(f_{ch}^2 - f_{nch}^2)}\begin{bmatrix} f_{ch} & -f_{nch} \\ -f_{nch} & f_{ch} \end{bmatrix} \ , \tag{6.72}$$

$$\gamma = 1 \ . \tag{6.73}$$

Interaction cutoff

So far we have have not fixed the cutoff scheme for the RG. We will use an interaction cutoff (see section 2.5.2) which we formally introduce by substituting for the bosonic Greensfunction

$$\mathbf{F} \to \mathbf{F}\,\Theta(\Lambda < |k| < \Lambda_0)\,, \tag{6.74}$$

where we assume that the ultraviolet cutoff is smaller than the Fermi momenta $\Lambda_0 < \min(k_\uparrow, k_\downarrow)$. This kind of cutoff is associated with some non-trivial initial conditions for purely bosonic n-point vertices [39, 41] as symmetrized closed fermionic loops with n external bosonic legs. Within this work we shall truncate the flow beyond the 3-point vertex γ and the only initial condition we have to consider is for the bosonic 2-point function, i.e. the Greensfunction. We write it as

$$\mathbf{F}^{-1}(K) = \mathbf{F}_0^{-1} + \mathbf{\Pi}(K)\,, \tag{6.75}$$

with $\mathbf{F}_0$ given by (6.72). The polarization $\mathbf{\Pi}$ is then defined as

$$
\begin{aligned}
\Pi_{RR}(K) &= \int_{K'} G_{R\uparrow}(K')G_{R\downarrow}(K'+K) \tag{6.76} \\
&= \frac{1}{2\pi}\frac{\Delta_0 + k}{i\omega - v(\Delta_0 + k)}\,, \\
\Pi_{LL}(K) &= \int_{K'} G_{L\uparrow}(K')G_{L\downarrow}(K'+K) \tag{6.77} \\
&= \frac{1}{2\pi}\frac{\Delta_0 - k}{i\omega - v(\Delta_0 - k)}\,, \\
\Pi_{RL}(K) &= \Pi_{LR}(K) = 0\,. \tag{6.78}
\end{aligned}
$$

Focusing just on right-moving bosons we obtain for the bosonic Greensfunction

$$F_{RR}(K) = 2\pi\tilde{f}_{ch}\frac{(i\omega - v\Delta_0 - vk)\left(i\omega - (v\Delta_0 - vk)(1 - \tilde{f}_{ch} + \frac{\tilde{f}_{nch}^2}{\tilde{f}_{ch}})\right)}{(i\omega - \omega_+)(i\omega - \omega_-)}\,, \tag{6.79}$$

with

$$\omega_\pm = v\Delta_0(1 - \tilde{f}_{ch}) \pm v\sqrt{k^2\left((1 - \tilde{f}_{ch})^2 - \tilde{f}_{nch}^2\right) + \tilde{f}_{nch}^2\Delta_0^2}\,, \tag{6.80}$$

where we have introduced the rescaled interactions $\tilde{f} = \frac{f}{\pi v}$. Note that the bosons propagate with a gap which vanishes as $\tilde{f}_{ch} + \tilde{f}_{nch} = 1$. As these bosons induce a spin flip of the fermions we eventually expect a quantum phase transition to a confined state at this point.

Rescaling

To classify the vertices according to their relevance we rescale momenta and vertices as we have done before.

$$\Lambda_\tau = \Lambda_0 e^{-\tau} , \tag{6.81}$$

$$\omega = \epsilon\Lambda_\tau , \tag{6.82}$$

$$k - k_\sigma = \frac{q\Lambda_\tau}{v} , \tag{6.83}$$

$$\Gamma^{(2)}_{\Lambda,\sigma}(K) = Z^{-1}_{\tau,\sigma}\Lambda_\tau\tilde{\Gamma}^{(2)}_{\tau,\sigma}(Q) , \tag{6.84}$$

$$\Gamma^{(2,1)}(\{K\}) = Z^{-1/2}_{\tau,\uparrow}Z^{-1/2}_{\tau,\downarrow}\tilde{\Gamma}^{(2,1)}(\{Q\}) , \tag{6.85}$$

$$F(K) = \frac{1}{v}\tilde{F}(Q) . \tag{6.86}$$

As mentioned in section 5 we generally view the Fermi surface as a fixed point manifold of the RG. However in the case of an interaction cutoff it is perfectly sensible to define a flowing Fermi momentum $k_{\tau,\sigma}$ via

$$\tilde{r}_{\tau,\sigma} = \frac{k_\sigma - k_{\tau,\sigma}}{\Lambda_\tau} , \tag{6.87}$$

with the true Fermi momentum k_σ and the frequency/momentum independent part of the fermionic 2-point vertex $\tilde{r}_\sigma = \tilde{\Gamma}^{(2)}(i0,0)$. We then introduce the following notations for the magnetization

$$\Delta(\tau) = k_{\tau,\uparrow} - k_{\tau,\downarrow} , \tag{6.88}$$

$$\tilde{\Delta}_\tau(\tau') = \frac{\Delta(\tau')}{\Lambda_\tau} , \tag{6.89}$$

$$\tilde{\Delta}^*_\tau = \tilde{\Delta}_\tau(\tau' \to \infty) . \tag{6.90}$$

Expanding the fermionic 2-point function as

$$\tilde{\Gamma}^{(2)}_{\tau,\sigma} = \tilde{r}_{\tau,\sigma} + i\epsilon(Z_{\tau,\sigma} - 1) - q(Z_{\tau,\sigma} - \tilde{v}_{\tau,\sigma}) , \tag{6.91}$$

we may write the fermionic Greensfunction as

$$\tilde{G}_{\tau,\sigma}(Q) = \frac{1}{i\epsilon - \tilde{v}_{\tau,\sigma}\tilde{q} - \tilde{r}_{\tau,\sigma}} . \tag{6.92}$$

Note that in the interaction cutoff scheme this Greensfunction is independent of any cutoff.

Classification according to relevance

There is one relevant coupling namely $\tilde{r}$. Additionally there are three marginal couplings which are the wavefunction renormalization Z, the renormalized Fermi velocities $\tilde{v}$ and the frequency/momentum independent part of the 3-point vertex $\tilde{\gamma} = \tilde{\Gamma}^{(2,1)}(\{0\})$. There is one more marginal coupling - the frequency/momentum independent part of a fermionic 4-point vertex $\tilde{g} = \tilde{\Gamma}^{(4)}(\{0\})$. However this vertex vanishes at $\tau = 0$ as we have absorbed the interaction into the field Φ and it doesn't couple to the flow of the fermionic 2-point vertex. As our primary goal is to calculate the interaction induced renormalization of the magnetization which is obtained from the flow of this 2-point vertex we shall neglect $\tilde{g}$. We do not decompose the bosonic Greensfunction into vertices with definite relevance but shall apply the adiabatic approximation developed in section 3.2 instead. All other vertices are irrelevant and we do not consider them here.

Flow equations

Lets turn toward the flow equations. The exact equation in the interaction cutoff scheme [41] for the fermionic 2-point function is

$$\partial_\tau \tilde{\Gamma}^{(2,0)}_{\tau,\sigma}(Q,\alpha) \;\;=\;\; (1 - \eta_{\tau,\sigma} - Q \cdot \partial_Q)\tilde{\Gamma}^{(2,0)}_{\tau,\sigma}(Q,\alpha) + \dot{\tilde{\Gamma}}^{(2,0)}_{\tau,\sigma}(Q,\alpha) \;, \quad (6.93)$$

with chirality index $\alpha = R, L$ and

$$
\begin{aligned}
\dot{\tilde{\Gamma}}^{(2,0)}_{\tau,\sigma}(Q,\alpha) \;\;=\;\; & \sum_{\alpha'} \int_{Q'} \dot{\tilde{F}}_{\tau,\alpha'\alpha'}(Q')\tilde{\Gamma}^{(2,2)}_{\tau,\sigma\sigma}(Q,\alpha;Q',\alpha';Q',\alpha',Q,\alpha) \qquad\qquad (6.94)\\
& + \sum_{\alpha'} \int_{Q'} \Big\{ \dot{\tilde{F}}_{\tau,\alpha'\alpha'}(Q')\tilde{\Gamma}^{(2,1)}_{\tau,\sigma\bar{\sigma}}(Q,\alpha;-\sigma Q',\alpha';Q+\sigma Q',\alpha)\cdot\\
& \qquad\cdot \tilde{G}_{\tau,\bar{\sigma}}(Q + \sigma Q' + \sigma \tilde{\Delta}^*,\alpha)\tilde{\Gamma}^{(2,1)}_{\tau,\bar{\sigma}\sigma}(Q+\sigma Q',\alpha;\sigma Q',\alpha';Q,\alpha) \Big\}\;,
\end{aligned}
$$

here the momentum dependence of the vertices is for $\tilde{\Gamma}^{(2,1)}$ (outgoing fermionic; incoming bosonic; incoming ermionic) and for $\tilde{\Gamma}^{(2,2)}$ (outgoing fermionic; outgoing bosonic; incoming bosonic; incoming fermionic). This equation is graphically represented in figure 6.6. Note that the vertex $\tilde{\Gamma}^{(2,2)}$ is irrelevant and we neglect it.

As we are only interested in relevant and marginal couplings we can write the corresponding flow equations as

$$
\begin{aligned}
\partial_\tau \tilde{r}_{\tau,\sigma} \;\;&=\;\; (1 - \eta_{\tau,\sigma})\tilde{r}_{\tau,\sigma} + \dot{\tilde{r}}_{\tau,\sigma} \qquad\qquad\qquad\qquad\qquad (6.95)\\
&=\;\; (1 - \eta_{\tau,\sigma})\tilde{r}_{\tau,\sigma} - \tilde{\gamma}^2_\tau \int_Q \dot{\tilde{F}}_{RR}(\sigma i\epsilon, q)\tilde{G}_{\bar{\sigma}}(i\epsilon, \sigma(q + \tilde{\Delta}^*_\tau))\;,\\
\eta_{\tau,\sigma} \;\;&=\;\; -\partial_{i\epsilon}\dot{\tilde{\Gamma}}^{(2)}_{\tau,\sigma}(Q)|_{Q=0} \qquad\qquad\qquad\qquad\qquad (6.96)
\end{aligned}
$$
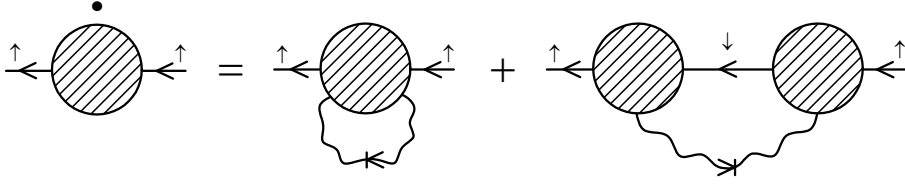
Figure 6.6: Graphical representation of the flow of the fermionic 2-point vertex for $\sigma = \uparrow$ as described in (6.94).

$$
\begin{aligned}
&= -\tilde{\gamma}_\tau^2 \int_Q \dot{\tilde{F}}_{RR}(\sigma i\epsilon, q) \tilde{G}_{\bar{\sigma}}^2(i\epsilon, \sigma(q + \tilde{\Delta}_\tau^*)) \; , \\
\partial_\tau \tilde{v}_{\tau,\sigma} &= -\eta_{\tau,\sigma}\tilde{v}_{\tau,\sigma} + \partial_q \dot{\tilde{\Gamma}}_{\tau,\sigma}^{(2)}(Q)|_{Q=0} \\
&= 0 \; .
\end{aligned}
\tag{6.97}
$$

We observe that the Fermi velocities do not renormalize and are therefore determined by their bare values $\tilde{v} = 1$. The anomalous dimensions are in leading order actually equal and we shall use $\eta_{\tau,\uparrow} \approx \eta_{\tau,\downarrow} =: \eta_\tau$.

We can usually assume that $|\tilde{r}| \ll 1$ and therefore use it as a paramater for expansion in the flow equations. For (6.95) in leading order this amounts to

$$
\partial_\tau \tilde{r}_{\tau,\sigma} = \tilde{r}_{\tau,\sigma} - \tilde{\gamma}_\tau^2 \int_Q \dot{\tilde{F}}_{RR}(\sigma i\epsilon, q) \tilde{G}_{\bar{\sigma}}'(i\epsilon, \sigma(q + \tilde{\Delta}_\tau(\tau))) + O(\tilde{r}^2) \; ,
\tag{6.98}
$$

where we now approximate the Greensfunction as

$$
\tilde{G}(Q) \approx \tilde{G}'(Q) = \frac{1}{i\epsilon - q} \; .
\tag{6.99}
$$

We note that therefore in leading order one can in $\tilde{r}$ neglect the anomalous dimension and use the flowing rescaled magnetization $\tilde{\Delta}_\tau(\tau)$ instead of $\tilde{\Delta}_\tau^*$. We shall apply this expansion in powers of $\tilde{r}$ from now on.

We turn toward the flow equation for the 3-point vertex [41] describing scattering of fermions by absorption/emission of a spin-flip boson

$$
\begin{aligned}
\partial_\tau \tilde{\Gamma}_{\tau,\sigma}^{2,1}(\{Q\}, \{\alpha\}) =& \\
&\left(-\frac{\eta_{\tau,\uparrow} + \eta_{\tau,\downarrow}}{2} - Q_i \cdot \partial_{Q_i}\right) \tilde{\Gamma}_{\tau,\sigma}^{2,1}(\{Q\}, \{\alpha\}) + \dot{\tilde{\Gamma}}_{\tau,\sigma}^{2,1}(\{Q\}, \{\alpha\}) \; ,
\end{aligned}
\tag{6.100}
$$

with the inhomogeneity as depicted in figure 6.7. Note that all vertices of the inhomogeneous term are irrelevant and consequently within our approximation $\dot{\tilde{\Gamma}}_{\tau,\sigma}^{2,1}(\{Q\}, \{\alpha\}) = 0$.

The flow for the marginal 3-point vertex is then simply determined by the anomalous dimensions as

$$
\begin{aligned}
\partial_\tau \tilde{\gamma}_\tau &= -\frac{\eta_{\tau,\uparrow} + \eta_{\tau,\downarrow}}{2} \tilde{\gamma}_\tau \\
&\approx -\eta_\tau \tilde{\gamma}_\tau \; ,
\end{aligned}
\tag{6.101}
$$
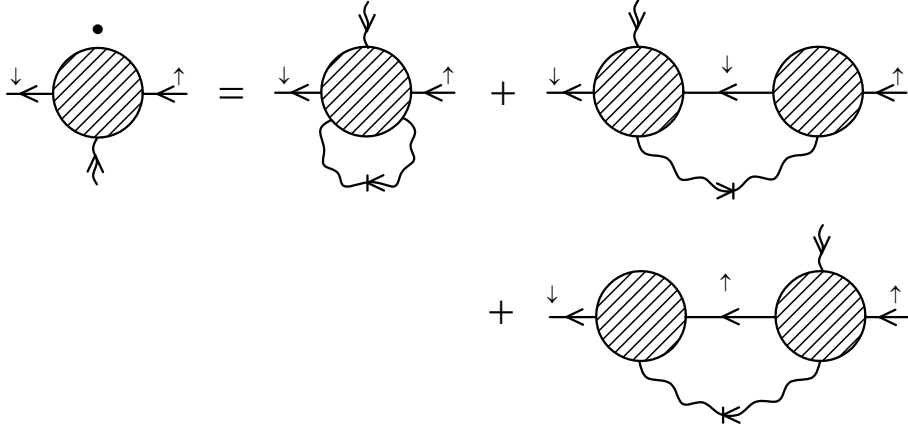
Figure 6.7: Graphical representation for the flow of the 3-point vertex.

which is easy to solve as

$$\tilde{\gamma}_\tau = e^{-\int_0^\tau d\tau'\, \eta_{\tau'}} =: e^{-\tau\bar{\eta}_\tau} \ . \tag{6.102}$$

We observe that if the fixed point anomalous dimension is finite the 3-point vertex vanishes for $\tau \to \infty$.

The last vertex we have to investigate is the flow of the bosonic polarization, i.e. the renormalization of the bosonic Greensfunction. This equation is simply [41]

$$\partial_\tau \tilde{\Pi}_{\tau,\alpha\alpha'}(\{Q_i\}, \{\alpha_i\}) = -Q_i \cdot \partial_{Q_i} \tilde{\Pi}_{\tau,\alpha\alpha'}(\{Q_i\}, \{\alpha_i\}) + \dot{\tilde{\Pi}}_{\tau,\alpha\alpha'}(\{Q_i\}, \{\alpha_i\}) \ , \tag{6.103}$$

with the inhomogeneity

$$\dot{\tilde{\Pi}}_{\tau,\alpha\alpha'}(\{Q_i\}, \{\alpha_i\}) \;=\; \int_{Q'} \dot{\tilde{F}}_{\tau,\alpha''\alpha''}(Q')\tilde{\Gamma}_\tau^{(0,4)}(Q, \alpha; Q', \alpha''; Q', \alpha''; Q, \alpha') \ , \tag{6.104}$$

which is graphically represented in figure 6.8.

As the bosonic 4-point vertex is irrelevant the polarization within our approximation doesn't flow. This is the point where the adiabatic approximation we derived in section 3.2 comes into consideration. With its help we approximate the polarization as

$$\begin{aligned}
\tilde{\Pi}_{\tau,\alpha\alpha'}(Q) &= \delta_{\alpha\alpha'}\tilde{\gamma}_\tau^2 \int_{Q'} \tilde{G}'_{\tau,\uparrow,\alpha}(Q')\tilde{G}'_{\tau,\downarrow,\alpha}(Q' + Q + \alpha\tilde{\Delta}_\tau(\tau)) \\
&= \delta_{\alpha\alpha'}\frac{\tilde{\gamma}^2}{2\pi}\frac{\tilde{\Delta}_\tau(\tau) + \alpha q}{i\omega - (\tilde{\Delta}_\tau(\tau) + \alpha q)} \ .
\end{aligned} \tag{6.105}$$
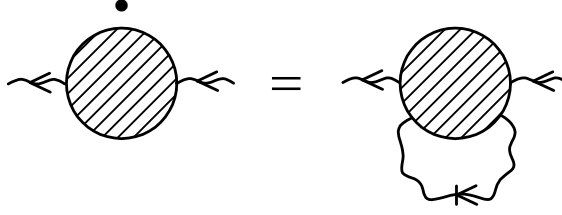
Figure 6.8: Graphical representation for the flow of the bosonic polarization as described in (6.104).

The bosonic Greensfunction within this adiabatic approximation is then written as (suppressing the Θ-function of the interaction cutoff)

$$\tilde{F}_{\tau,RR}(Q) = \frac{2\pi \tilde{f}_{\tau,ch}}{\tilde{\gamma}_\tau^2} \frac{\left(i\epsilon - \tilde{\Delta}_\tau(\tau) - q\right)\left(i\epsilon - (\tilde{\Delta}_\tau(\tau) - q)(1 - \tilde{f}_{\tau,ch} + \frac{\tilde{f}_{\tau,nch}^2}{\tilde{f}_{\tau,ch}})\right)}{(i\epsilon - \epsilon_+)(i\epsilon - \epsilon_-)} \, , \quad (6.106)$$

with the frequencies

$$\epsilon_\pm = \tilde{\Delta}_\tau(\tau)(1 - \tilde{f}_{\tau,ch}) \pm \sqrt{q^2\left((1 - \tilde{f}_{\tau,ch})^2 - \tilde{f}_{\tau,nch}^2\right) + \tilde{f}_{\tau,nch}^2 \tilde{\Delta}_\tau(\tau)^2} \, , \quad (6.107)$$

and the effective interaction

$$\tilde{f}_{\tau,ch} = \tilde{\gamma}_\tau^2 \tilde{f}_{ch} \qquad\qquad \tilde{f}_{\tau,nch} = \tilde{\gamma}_\tau^2 \tilde{f}_{nch} \, . \quad (6.108)$$

We now have considered all flow equations for the interesting vertices at hand and begin with our analysis of the interaction induced shift of the Fermi surface.

6.4.2   The Fermi surface

From the results of section 5 we know that we have to fine-tune the bare 2-point vertex $\tilde{r}_{0,\sigma}$ to flow into a fixed point. Together with (6.95) and the approximation (6.98) this bare value is obtained as

$$\begin{aligned}
\tilde{r}_{0,\sigma} &= \int_0^\infty d\tau \, e^{-\tau} \tilde{\gamma}_\tau^2 \int_Q \dot{\tilde{F}}_{\tau,RR}(Q) \tilde{G}'(\sigma Q + \sigma \tilde{\Delta}_\tau(\tau)) \\
&= \tilde{\Delta}_0^* \int_{\tilde{\Delta}_0^*}^\infty dx \, \frac{\tilde{\gamma}_x}{x^2} \int_Q \dot{\tilde{F}}_{x,RR}(Q) \tilde{G}'_{x,\sigma}(Q + \sigma x y_x) \\
&=: \tilde{\Delta}_0^* \int_{\tilde{\Delta}_0^*}^\infty dx \, I_\sigma(x, y_x) \, , \quad (6.109)
\end{aligned}$$

where we have used $x = \tilde{\Delta}_0^* e^\tau$ and write all dependencies on τ as dependencies on x. Additionally we have defined $y_x = \frac{\tilde{\Delta}_\tau(\tau)}{\tilde{\Delta}_\tau^*}$. For the shift of the magnetization

this means

$$
\begin{aligned}
\tilde{\Delta}_0^* - \tilde{\Delta}_0(0) &= \tilde{r}_{0,\uparrow} - \tilde{r}_{0,\downarrow} \\
&= \sum_\sigma \sigma \tilde{\Delta}_0^* \int_{\tilde{\Delta}_0^*}^\infty dx\, I_\sigma(x, y_x) \\
&=: \tilde{\Delta}_0^* \int_{\tilde{\Delta}_0^*}^\infty dx\, I(x, y_x) \, ,
\end{aligned}
\tag{6.110}
$$

with

$$
I(x, y_x) =
\begin{cases}
-\dfrac{1}{x^2} \dfrac{2\tilde{f}_{x,nch}^2\, x y_x}{\sqrt{\left((1-\tilde{f}_{x,ch})^2 - \tilde{f}_{x,nch}^2\right) + \tilde{f}_{x,nch}^2 x^2 y_x^2}} & x < 1 \\[4ex]
\dfrac{2\tilde{f}_{x,ch}}{x^2} & x > 1 \, .
\end{cases}
\tag{6.111}
$$

The integral over x seems to be dominated by small x. To observe a confinement transition we need the right-hand side of (6.110) to be finite for $\tilde{\Delta}_0^* \to 0$. This can only achieved if for small x the integrand diverges at least as $I(x, y_y) \propto x^{-2}$. Clearly this asymptotic behaviour depends on the flow of the effective interactions as well as on the flow of the magnetization itself.

Note that alternatively we can write a flow equation for the magnetization itself as

$$
\partial_\tau \tilde{\Delta}_\tau(\tau) = \tilde{\Delta}_\tau(\tau) - (\dot{\tilde{r}}_{\tau,\uparrow} - \dot{\tilde{r}}_{\tau,\downarrow}) \, ,
\tag{6.112}
$$

which we shall use later on.

6.4.3   Self-consistent 1-loop calculation

We start with evaluating the true magnetization in the simplest nontrivial way, which is a self consistent 1-loop approximation. To evaluate the integral of (6.110) we assume the fermions to be on their true Fermi surface right away, i.e. we set $\tilde{\Delta}_\tau(\tau) \to \tilde{\Delta}_\tau^*$. This amounts to setting $y_x = 1$. Additionally we neglect the flow of the 3-point vertex, i.e. $\tilde{f}_{\tau,ch} = \tilde{f}_{ch}$ and $\tilde{f}_{\tau,nch} = \tilde{f}_{nch}$.

Chiral and non-chiral interactions

For $\tilde{f}_{ch} + \tilde{f}_{nch} \to 1$ the function $I(x, y_x)$ shows the desired behaviour to reach a confinement transition. In fact we obtain the self-consistency equation

$$
\tilde{\Delta}_0^* - \tilde{\Delta}_0(0) = 2\tilde{f}_{ch}\tilde{\Delta}_0^* + \frac{2\tilde{\Delta}_0^* \tilde{f}_{nch}^2}{\sqrt{(1 - \tilde{f}_{ch})^2 - \tilde{f}_{nch}^2}} \cdot
\tag{6.113}
$$

$$
\cdot \ln \left\{ \frac{\tilde{\Delta}_0^* \left(\sqrt{(1 - \tilde{f}_{ch})^2 - \tilde{f}_{nch}^2} + 1 - \tilde{f}_{ch} \right)}{\sqrt{\left((1 - \tilde{f}_{ch})^2 - \tilde{f}_{nch}^2\right) + \tilde{f}_{nch}^2 \tilde{\Delta}_0^{*2}} + \sqrt{(1 - \tilde{f}_{ch})^2 - \tilde{f}_{nch}^2}} \right\}
$$

$$= \begin{cases} 2\tilde{f}_{ch}\tilde{\Delta}_0^* + 2\tilde{f}_{nch}^2\tilde{\Delta}_0^* \ln(\tilde{\Delta}_0^*) + O(\tilde{f}^3) & \tilde{f}_{ch}, \tilde{f}_{nch} \to 0 \\ 2\tilde{f}_{ch}\tilde{\Delta}_0^* + \dfrac{2\tilde{\Delta}_0^*\tilde{f}_{nch}^2}{\sqrt{(1-\tilde{f}_{ch})^2-\tilde{f}_{nch}^2}} \ln\left(\dfrac{\tilde{\Delta}_0^*\left(\sqrt{(1-\tilde{f}_{ch})^2-\tilde{f}_{nch}^2}+1-\tilde{f}_{ch}\right)}{2\sqrt{(1-\tilde{f}_{ch})^2-\tilde{f}_{nch}^2}}\right) & \tilde{\Delta}_0^* \to 0 \ . \end{cases}$$

We observe that there are two competing interactions. Looking at the first term of the right-hand side the chiral part of the interaction tends to increase the difference between the Fermi surfaces leading to de-confinement. The non chiral part does the opposite, i.e. it drives the system toward confinement. This tendency toward confinement however is enhanced or reduced by a finite chiral interaction.

In general we can solve for $\tilde{\Delta}_0^*$ only numerically and we have plotted the corresponding solution in figure 6.9. However as $\tilde{f}_{ch} + \tilde{f}_{nch} \to 1$ we can solve
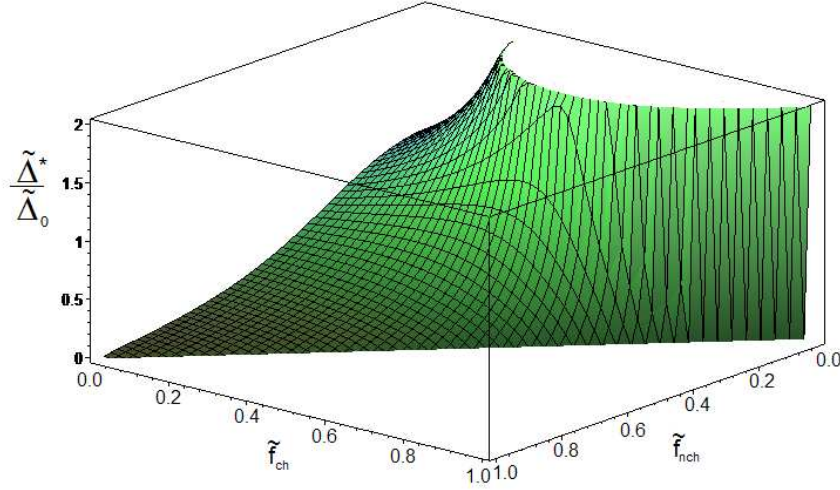

Figure 6.9: Numerical solution for the true magnetization for $\tilde{f}_{ch} + \tilde{f}_{nch} < 1$ at $\tilde{\Delta}_0(0) = 0.1$ in 1-loop. For large $\tilde{f}_{ch}$ and small $\tilde{f}_{nch}$ there is an instability toward ferromagnetism in the z-direction.

(6.113) approximately and obtain that the magnetization vanishes as

$$\tilde{\Delta}_0^* = \tilde{\Delta}_0(0)\frac{\sqrt{(1-\tilde{f}_{ch})^2-\tilde{f}_{nch}^2}}{2\tilde{f}_{nch}^2 \ln\left(\frac{4\tilde{f}_{nch}^2}{\tilde{\Delta}_0(0)(1-\tilde{f}_{ch})}\right)} \ . \tag{6.114}$$

Note that this solution is only well defined if the logarithm is positive. Consequently we expect a confinement transition if the initial magnetization is not too large. At the critical interaction strength the excitation energy of the spin flip bosons goes to zero for all momenta and we expect a nonzero average of the occupation number of those bosons. In turn any difference of the Fermi momenta is destroyed by spin flips.

Non-chiral interaction

As an additional result of this section we observe that the interaction coupling fermions of opposite chirality $\tilde{f}_{nch}$ is responsible for the tendency toward confinement. Therefore from now on we set $\tilde{f}_{ch} = 0$ and $\tilde{f} := \tilde{f}_{nch}$ for all further investigation. Now the bosonic Greensfunction coupling to fermionic right-movers $\tilde{F}_{RR}$ reads

$$\tilde{F}_{\tau,RR}(Q) = \frac{2\pi \tilde{f}_\tau^2 (i\epsilon - \tilde{\Delta}_\tau(\tau) - q)(q - \tilde{\Delta}_\tau(\tau))}{\tilde{\gamma}_\tau^2 (i\epsilon - \epsilon_+)(i\epsilon - \epsilon_-)} \ \Theta(1 < |q| < e^\tau) \,, \qquad (6.115)$$

with the poles at

$$\epsilon_\pm = \tilde{\Delta}_\tau(\tau) \pm \sqrt{q^2(1 - \tilde{f}_\tau^2) + \tilde{f}_\tau^2 \tilde{\Delta}_\tau^2(\tau)} \,. \qquad (6.116)$$

At $\tilde{f} = 1$ the bosons now become gapless as well as dispersion-free and we expect
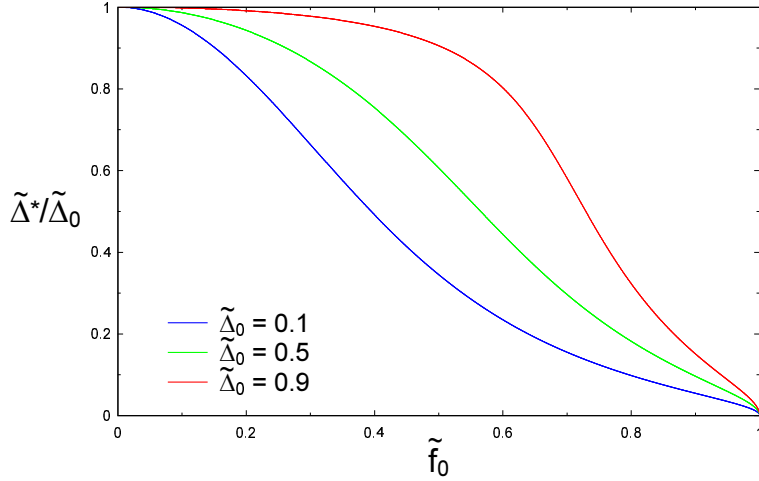

Figure 6.10: Numerical solution for the true magnetization with respect to $\tilde{f}_0$ for different values of the initial magnetization in 1-loop.

a confinement transition. Repeating the 1-loop calculation for the magnetization we obtain

$$\tilde{\Delta}_0^* - \tilde{\Delta}_0(0) = \frac{2\tilde{f}^2 \tilde{\Delta}_0^*}{\sqrt{1 - \tilde{f}^2}} \ln\left\{ \frac{|\tilde{\Delta}_0^*|(1 + \sqrt{1 - \tilde{f}^2})}{\sqrt{1 - \tilde{f}^2 + \tilde{f}^2 \tilde{\Delta}_0^{*2}} + \sqrt{1 - \tilde{f}^2}} \right\}. \qquad (6.117)$$

For general $\tilde{f}$ the true magnetization can be obtained only numerically, see figure 6.10. We clearly observe a confinement transition as $\tilde{f}_0 \to 1$.

We conclude that our simple 1-loop calculation predicts a confinement transition at strong coupling $\tilde{f}_0 \to 1$, i.e. the renormalized interchain hopping amplitude vanishes $t_\perp^* = 0$. Extrapolating our results to $\tilde{f} > 1$ suggests the emergence

of ferromagnetic long-range order in the xy-plane. However we know that there
is no long range order in this kind of one-dimensional systems and conclude that
fluctuations beyond 1-loop must be important. To take these fluctuations into
account we have to improve our approximation by including the renormalization
of the effective interaction.

6.4.4   Including the renormalized interaction

In this section we include the renormalization of the effective interaction. It is
convenient to consider the flow equation for the rescaled magnetization (6.112).
We obtain the following system of coupled flow equations

$$\partial_\tau \tilde{\Delta}_\tau(\tau) = \tilde{\Delta}_\tau(\tau) \left(1 - \frac{2\tilde{f}_\tau^2\, \Theta(\tilde{\Delta}_\tau(\tau) < 1)}{\sqrt{1 - \tilde{f}_\tau^2 + \tilde{f}_\tau^2 \tilde{\Delta}_\tau(\tau)}} \right) , \qquad (6.118)$$

$$\partial_\tau \tilde{f}_\tau = -2\eta_\tau \tilde{f}_\tau , \qquad (6.119)$$

where the anomalous dimension is determined by

$$\eta_\tau = \Theta(\tilde{\Delta}_\tau(\tau) < 1) \, \frac{1 - \sqrt{1 - \tilde{f}_\tau^2 + \tilde{f}_\tau^2 \tilde{\Delta}_\tau^2}}{\sqrt{1 - \tilde{f}_\tau^2 + \tilde{f}_\tau^2 \tilde{\Delta}_\tau^2} \left(1 - \tilde{\Delta}_\tau^2 \right)} \; . \qquad (6.120)$$

Lets take a look at the flow in the $\tilde{f} - \tilde{\Delta}$ plane as depicted in figure 6.11(a).
We observe that the effective interaction always flows to weak coupling driven
by an initially large anomalous dimension. As the effective interaction decreases
the second term on the right-hand side of (6.118) becomes smaller than one and
consequently the rescaled magnetization flows toward infinity, see figure 6.11(b).
Note that $\tilde{r}$ is numerically much smaller than one as we have assumed in our
approximations and it approaches its fixed point value non-monotonously.

We conclude that the confinement transition we observed in the 1-loop analysis
is an artifact of the approximation. Indeed the plot of the fixed point magne-
tization as a function of the bare interaction in figure 6.11(c) and the relation
between the fixed point magnetization and the bare magnetization at $\tilde{f}_0 = 1$ in
figure 6.11(d) confirm this observation. The interchain backscattering strongly
reduces the magnetization but never enough to reach a confined phase.

The absence of confinement is related to the renormalization of the effective
interaction away from strong coupling. As in this section we have just focused
on the interchain backscattering we missed the possibility of a stabilization of
this coupling under the RG through other processes. As we will show in the
next section we actually can keep $\tilde{\gamma}_\tau$ at strong coupling by including umklapp
scattering transversal to the two chains.
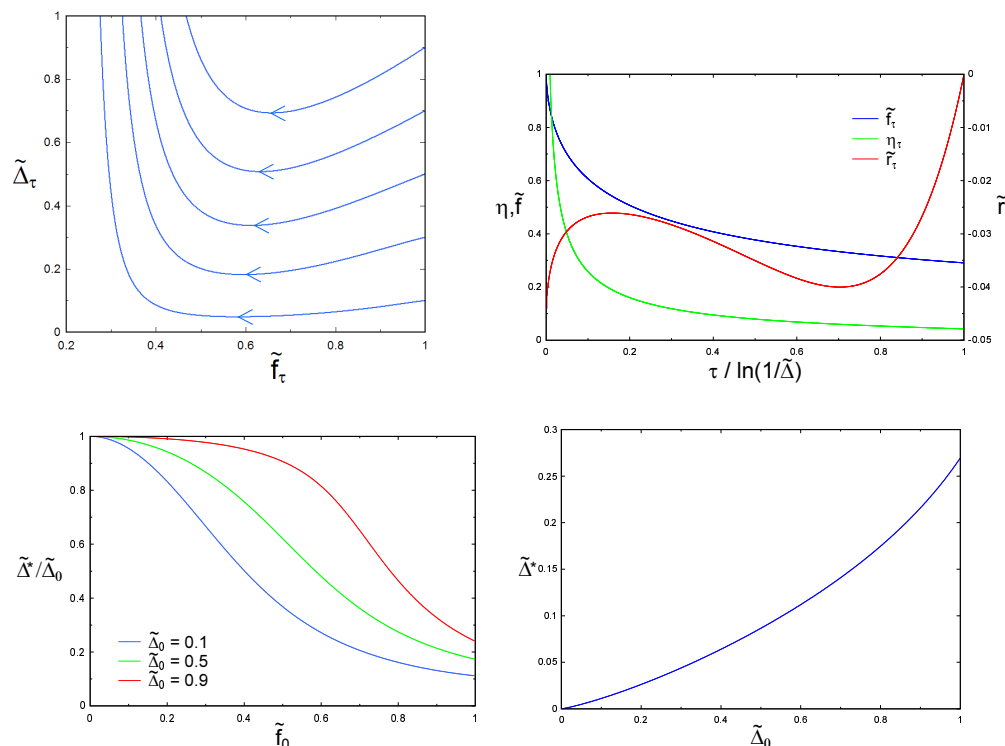
Figure 6.11: From top left to bottom right: (a) flow of the couplings $\tilde{\Delta}$ and $\tilde{f}$ as described by the equations (6.118) and (6.119); (b) the flow for $\tilde{r}_\uparrow$, $\tilde{f}$ and η for $\tilde{\Delta}_0(0) = 0.1$ and $\tilde{f}_0 = 1$ as function of the flow parameter τ; (c) true magnetization $\tilde{\Delta}^*$ as function of the initial interaction strength for various $\tilde{\Delta}_0(0)$; (d) true magnetization $\tilde{\Delta}^*$ for $\tilde{f}_0 = 1$ as function of the bare distance $\tilde{\Delta}_0(0)$.

6.4.5   The inclusion of umklapp scattering

We now include umklapp scattering (pair tunneling) transversal to the two chains as well as a density-density interaction. As we will show the first of these processes stabilizes the interband backscattering indeed and we obtain a confinement transition at $\tilde{f}_c < 1$. We just focus on the region close to this transition where all interesting flow equations can be expanded in powers of the rescaled magnetization. Actually this case bears many similarities with a system consisting of an infinite number of coupled chains which we will investigate with more detail in the next chapter.

Setup of the RG

We perform a change of our notation and write the action as

$$S = \int_K \bar{\psi}_K \psi_K (-i\omega + v|k_x| - v|k_f(k_y)|) + \frac{f}{2} \boldsymbol{\rho}_\alpha \cdot \boldsymbol{\rho}_{\bar{\alpha}} , \qquad (6.121)$$

with the chirality indices $\alpha = R, L$ and $\bar{R} = L, \bar{L} = R$. The integration over momenta is defined as

$$\int_K = \int \frac{d\omega}{2\pi} \int \frac{dk_x}{2\pi} \frac{1}{2} \sum_{k_y = 0, \pi} , \qquad (6.122)$$

where k_x denotes momenta parallel to the chains and k_y perpendicular momenta.

To allow umklapp scattering we assume that the k_y momentum is only conserved modulo 2π and takes the values $0, \pi$. Therefore there are three distinct interaction processes taking place. First there is the momentum conserving interband backward scattering and secondly there is the interband umklapp scattering. The third interaction is the density-density interaction. After performing a Hubbard-Stratonovich transformation we obtain in the interaction cutoff scheme neglecting irrelevant couplings

$$\Gamma = \int_K \bar{\psi}_K \psi_K (-i\omega + v|k_x| - v|k_f(k_y)|) + \frac{1}{2} \boldsymbol{\phi}_\alpha \cdot \mathbf{F}_{\alpha\beta}^{-1} \cdot \boldsymbol{\phi}_\beta + \gamma \phi_\alpha \cdot \rho_\alpha , \quad (6.123)$$

where the interaction is now mediated by a real valued bosonic field. The bosonic Greensfunction is given by

$$\mathbf{F}_{\alpha\beta}^{-1}(K) = \frac{\boldsymbol{\delta}_{\alpha\bar{\beta}}}{f} + \delta_{\alpha\beta} \boldsymbol{\Pi}_\alpha(K) , \qquad (6.124)$$

and the polarization

$$
\begin{aligned}
\Pi_\alpha(K) &= \int_{K'} \gamma(k_y, k_y')\gamma(-k_y, k_y' + k_y) G_\alpha(K') G_\alpha(K' + K) \qquad (6.125) \\
&= \frac{1}{2} \sum_{k_y' = 0, \pi} \frac{\gamma(k_y, k_y')\gamma(-k_y, k_y' + k_y)}{2\pi} \frac{\alpha k + \Delta_0(k_y', k_y)}{i\omega - v(\alpha k + \Delta_0(k_y', k_y))} ,
\end{aligned}
$$

where in $\gamma(k_1, k_2)$ the argument k_1 means the incoming bosonic y-momentum and k_2 the incoming fermionic y-momentum. Here we have additionally defined

$$\Delta(k_1, k_2) = k_f(k_1) - k_f(k_1 + k_2) . \qquad (6.126)$$

By symmetry there are actually only two distinct couplings

$$
\begin{aligned}
\gamma(\pi) &:= \gamma(\pi, 0) = \gamma(\pi, \pi) , \qquad (6.127) \\
\gamma(0) &:= \gamma(0, 0) = \gamma(0, \pi) , \qquad (6.128)
\end{aligned}
$$

so that

$$
\begin{aligned}
\Pi_\alpha(K) &= \frac{\gamma^2(k_y)}{4\pi} \sum_{k_y' = 0, \pi} \frac{\alpha k + \Delta_0(k'y, k_y)}{i\omega - v(\alpha k + \Delta_0(k_y', k_y))} \qquad (6.129) \\
&= \begin{cases} \frac{\gamma^2(0)}{2\pi} \frac{\alpha k}{i\omega - v\alpha k} & k_y = 0 \\ \frac{\gamma^2(\pi)}{4\pi} \left(\frac{\alpha k + \Delta}{i\omega - v(\alpha k + \Delta)} + \frac{\alpha k - \Delta}{i\omega - v(\alpha k - \Delta)} \right) & k_y = \pi , \end{cases} \qquad (6.130)
\end{aligned}
$$

with $\Delta = k_f(0) - k_f(\pi)$.

We are especially interested in the bosonic Greensfunction coupling right movers to right movers

$$F_{RR} = -\frac{f^2 \Pi_L}{1 - f^2 \Pi_R \Pi_L} \,, \tag{6.131}$$

and setting for simplicity from now on $v = 1$ we obtain for zero bosonic momentum (i.e. the density-density interaction)

$$F_{RR}(k_y = 0) = \frac{2\pi \tilde{f}_0^2 k(i\omega - k)}{\gamma^2(0)(i\omega - \omega_1)(i\omega + \omega_1)} \Theta(\Lambda < |k_x| < \Lambda_0) \,, \tag{6.132}$$

with

$$\omega_1 = k\sqrt{1 - \tilde{f}_0^2} \,, \tag{6.133}$$

and the effective interaction

$$\tilde{f}_k = \frac{\gamma^2(k)f}{\pi v} \,. \tag{6.134}$$

At momentum π (interband backward/umklapp scattering) the bosonic Greensfunction reads

$$F_{RR}(k_y = \pi) = \frac{2\pi \tilde{f}_\pi^2 (i\omega - k + \Delta)(i\omega - k - \Delta)(i\omega k + k^2 - \Delta^2)}{\gamma^2(\pi)(\omega^2 - \omega_+^2)(\omega^2 - \omega_-^2)} \cdot$$
$$\cdot \Theta(\Lambda < |k_x| < \Lambda_0) \,, \tag{6.135}$$

with

$$\omega_\pm^2 = -\Delta^2 - k^2 \frac{2 - \tilde{f}_\pi^2}{2} \pm \frac{1}{2}\sqrt{4\tilde{f}_\pi^2 \Delta^4 + k^2(16\Delta^2 - 12\tilde{f}_\pi^2 \Delta^2 + k^2 \tilde{f}_\pi^4)} \,. \tag{6.136}$$

Rescaling

We rescale frequencies, momenta parallel to the chains and vertices as in the last section. However we do not rescale the momenta in y-direction, i.e. momenta perpendicular to the chains. There are now two marginal 3-point vertices $\tilde{\gamma}(0)$ and $\tilde{\gamma}(\pi)$ we have to consider.

Flow of the fermionic 2-point vertex

The flow of the relevant part of the fermionic 2-point vertex at perpendicular momentum q_y acquires an additional term due to the density-density interaction, see figure 6.12. Note that this term does not contribute to the flow of the magnetization but just to the anomalous dimension. We write the flow equation
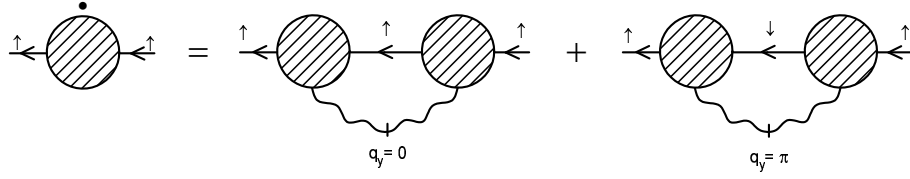
Figure 6.12: Flow of the fermionic 2-point vertex generated by marginal vertices.

as

$$
\begin{aligned}
\partial_\tau \tilde{r}_\tau(q_y) &= (1 - \eta_{q_y})\tilde{r}_\tau(q_y) - \int_{Q'} \dot{\tilde{F}}_{RR}(Q')\tilde{\gamma}_\tau^2(q_y')\tilde{G}(Q' + \tilde{\Delta}^*(q_y, q_y')) \\
&= \tilde{r}_\tau(q_y) - \int_{Q'} \dot{\tilde{F}}_{RR}(Q')\tilde{\gamma}_\tau^2(q_y')\tilde{G}'(Q' + \tilde{\Delta}_\tau(q_y, q_y')) + O(\tilde{r}_\tau^2(q_y)) ,
\end{aligned}
$$
(6.137)

with the flowing difference of Fermi momenta $\tilde{\Delta}_\tau(q_y, q_y') = \frac{k_{F,\tau}(q_y) - k_{F,\tau}(q_y + q_y')}{\Lambda_\tau}$.

As we are just interested in the difference between both Fermi momenta we consider the flow of the rescaled magnetization instead

$$
\begin{aligned}
\partial_\tau \tilde{\Delta}_\tau(\tau) &= \tilde{\Delta}_\tau(\tau) - \int_{Q'} \dot{\tilde{F}}_{RR}(Q')\tilde{\gamma}_\tau^2(q_y') \Big(\tilde{G}'(Q' + \tilde{\Delta}_\tau(0, q_y')) \\
&\qquad\qquad\qquad\qquad\qquad - \tilde{G}'(Q' + \tilde{\Delta}_\tau(\pi, q_y'))\Big) \\
&= \tilde{\Delta}_\tau(\tau)\left(1 - \frac{1 - \sqrt{1 - \tilde{f}_\pi^2}}{\sqrt{1 - \tilde{f}_\pi^2}}\right) \qquad \tilde{\Delta}_\tau \to 0 .
\end{aligned}
$$
(6.138)

To reach a confined phase we require that the term in brackets on the right-hand side is always smaller than one. This constraint defines a lower critical effective interaction strength of

$$
\tilde{f}_{c,\pi} = \frac{\sqrt{3}}{2} \approx 0.866 .
$$
(6.139)

The anomalous dimension for the fermions with y-momentum q_y is obtained as

$$
\begin{aligned}
\eta_{\tau,q_y} &= -\partial_{i\epsilon}\dot{\tilde{\Gamma}}_\tau^{(2)}(\epsilon, q_x, q_y)|_{\epsilon, q_x = 0} \\
&= -\int_{Q'} \dot{\tilde{F}}_{\tau,RR}(Q')\tilde{\gamma}_\tau^2(q_y')\tilde{G}_\tau'^2(Q' + \tilde{\Delta}_\tau(q_y, q_y')) \\
&= \begin{cases} \dfrac{1 - \sqrt{1 - \tilde{f}_{\tau,0}^2}}{2\sqrt{1 - \tilde{f}_{\tau,0}^2}} + \dfrac{1 - \sqrt{1 - \tilde{f}_{\tau,\pi}^2}}{2\sqrt{1 - \tilde{f}_{\tau,\pi}^2}} & \tilde{\Delta}_\tau \to 0 \\[4mm] \dfrac{1 - \sqrt{1 - \tilde{f}_{\tau,0}^2}}{2\sqrt{1 - \tilde{f}_{\tau,0}^2}} & \tilde{\Delta}_\tau \to \infty . \end{cases}
\end{aligned}
$$
(6.140)

We can actually show that the anomalous dimensions for both bands are equal

$$\eta := \eta_0 = \eta_\pi . \tag{6.141}$$

Flow of the 3-point vertices

To determine if the system flows toward a confinement transition for an effective interaction larger than $\tilde{f}_c$ we have to investigate the modified flow of the 3-point vertices $\tilde{\gamma}(q_y)$. The vertex $\tilde{\gamma}(\pi)$ acquires two additional terms, figure 6.13, where one is due to the density-density interaction and the other due to the umklapp scattering. The first one is actually compensated for by the additional term for the anomalous dimension, the latter is partly (depending on $\tilde{\Delta}_\tau$) compensating the flow generated by the rest of the anomalous dimension which destroyed confinement in the model without umklapp scattering.
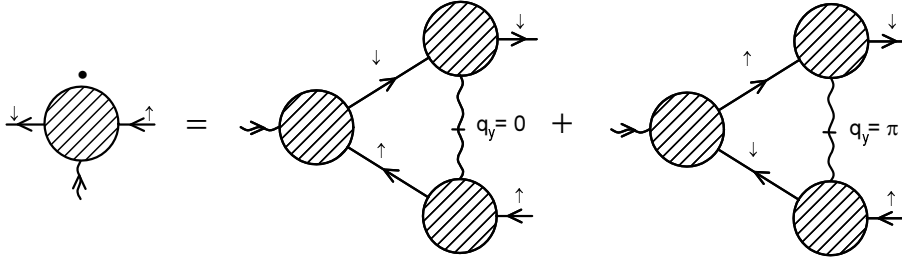

Figure 6.13: Flow of the 3-point vertex generated by marginal couplings.

We write the flow for $\tilde{\gamma}$ as

$$
\begin{aligned}
\partial_\tau \tilde{\gamma}_\tau(q_y) &= -\eta_{q_y} \tilde{\gamma}_\tau(q_y) \\
&\quad -\tilde{\gamma}_\tau(q_y) \int \dot{\tilde{F}}_{RR}(Q') \tilde{\gamma}_\tau^2(q_y') \tilde{G}'(Q' + \tilde{\Delta}_\tau(0, q_y')) \tilde{G}'(Q' + \tilde{\Delta}_\tau(q_y, q_y')) \\
&= \frac{\tilde{\gamma}_\tau(q_y)}{2} \int \dot{\tilde{F}}_{RR}(Q') \tilde{\gamma}_\tau^2(q_y') \left\{ \tilde{G}'(Q' + \tilde{\Delta}_\tau(0, q_y')) - \tilde{G}'(Q' + \tilde{\Delta}_\tau(q_y, q_y')) \right\}^2.
\end{aligned}
\tag{6.142}
$$

At zero perpendicular momentum the flow for $\tilde{\gamma}$ obviously vanishes and we obtain

$$\tilde{\gamma}_\tau(0) = 1 . \tag{6.143}$$

Consequently the effective interaction at zero y-momentum exchange does not renormalize

$$\tilde{f}_{\tau,0} = \tilde{f}_0 . \tag{6.144}$$

As $\tilde{\Delta}(q_y, 0) = 0$ the flow equation at momentum transfer π reads

$$
\begin{aligned}
\partial_\tau \tilde{\gamma}_\tau(\pi) &= \tilde{\gamma}_\tau^3(\pi) \int \delta_{q_y',\pi} \dot{\tilde{F}}_{RR}(Q') \tilde{G}'^2(Q' + \tilde{\Delta}_\tau) \\
&= -\tilde{\gamma}_\tau(\pi) \frac{\tilde{f}_{\tau,\pi}^2 \tilde{\Delta}_\tau^2}{\sqrt{1 - \tilde{f}_{\tau,\pi}^2} \left(1 + \sqrt{1 - \tilde{f}_{\tau,\pi}^2} \right)^3} ,
\end{aligned}
\tag{6.145}
$$

and we obtain for the flow of the effective interaction

$$\partial_\tau \tilde{f}_{\tau,\pi} = -\frac{2\tilde{f}_{\tau,\pi}^3 \tilde{\Delta}_\tau^2}{\sqrt{1 - \tilde{f}_{\tau,\pi}^2} \left(1 + \sqrt{1 - \tilde{f}_{\tau,\pi}^2}\right)^3} \ . \tag{6.146}$$

Compared with equation (6.101) where we excluded umklapp scattering we here observe that the flow of the effective interaction is proportional to the square of the rescaled magnetization. At confinement this rescaled magnetization is supposed to flow toward zero and we expect that the effective interaction gets only weakly renormalized stabilizing the confined phase in turn. To investigate whether this picture is correct we plot the flow of couplings in the $\tilde{\Delta}$-$\tilde{f}_\pi$ plane, see figure 6.14. We notice that there is indeed a small region where the system flows into a confined phase. Note that apart from a minimum critical interaction strength there is an upper bound on the interchain hopping amplitude (expressed through $\tilde{\Delta}_0$) for which confinement is realized. This is in agreement with the results of [33–35].
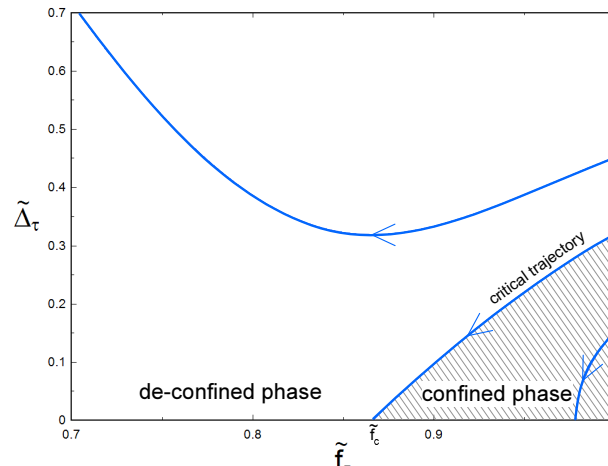
Figure 6.14: Flow of the couplings as described in (6.138) and (6.146). Note the finite region in the lower right corner where the system flows into a confined phase.

6.5 Summary

In this chapter we successfully apply our self-consistency equation (5.23) to the problem of finding the true Fermi surface in a system of two coupled metallic chains. We introduce the notion of a confinement transition to describe the situation where the Fermi momenta of these chains coincide due to the influence

of interactions. A weak coupling analysis confirms our expectation that the process termed as non-chiral interband backscattering is the one driving the system toward confinement. To investigate the system at strong coupling we just consider this interaction as an one channel problem and bosonize it by means of a Hubbard-Stratonovich transformation. We observe that although interband backscattering is the relevant process to reach confinement it is destabilized by fluctuations and a confinement transition is not observed even at strong coupling. Actually the inclusion of interband umklapp scattering (pair tunneling) leads to a stabilization and there is a finite region in parameter space where the system is flowing toward confinement.

Chapter 7

Confinement in a two-dimensional system

In this chapter we investigate a two-dimensional system of infinitely many coupled metallic chains where the Fermi surface consists of two disconnected sheets. We derive the equations to self-consistently determine the shape of the Fermi surface. After a perturbative treatment we consider the flow of all relevant and marginal vertices. For a harmonically distorted Fermi surface we show that sufficiently strong interactions lead to a confinement transition. The results of this chapter have been published in [119].

7.1 Introduction

We now extent our analysis of the last chapter to the physically more relevant system of an infinite array of coupled metallic chains. For simplicity again we focus on spinless fermions. This system possesses an open Fermi surface which is periodic in the direction transversal to the chains and has one mirror symmetric branch each for right- and left movers in the parallel direction, see figure 7.1. The width of the Brillouin zone in transverse direction is $\Lambda_\perp = \frac{\pi}{a_\perp}$ where $a_\perp$ is the corresponding lattice spacing in this direction.

As discussed in the introduction to chapter 6 this model is deemed relevant to explain the anomalous properties of High-T_c superconductors transversal to the copperoxide planes [33–35]. Here within these planes the electronic state is believed to be a non-Fermi liquid. The idea of Clarke et al. is that these non-Fermi liquid properties could be retained even when these planes are coupled by a weak interplane hopping $t_\perp$. This could be achieved if the coherence of this transversal single particle hopping is completely destroyed by interactions.

We decompose momenta around the true Fermi surface $\mathbf{k}_F(k_\perp)$ as

$$\mathbf{k} = \alpha \left(k_\| + |\mathbf{k}_F(k_\perp)| \right) \mathbf{e}_x + k_\perp \mathbf{e}_y \qquad (7.1)$$
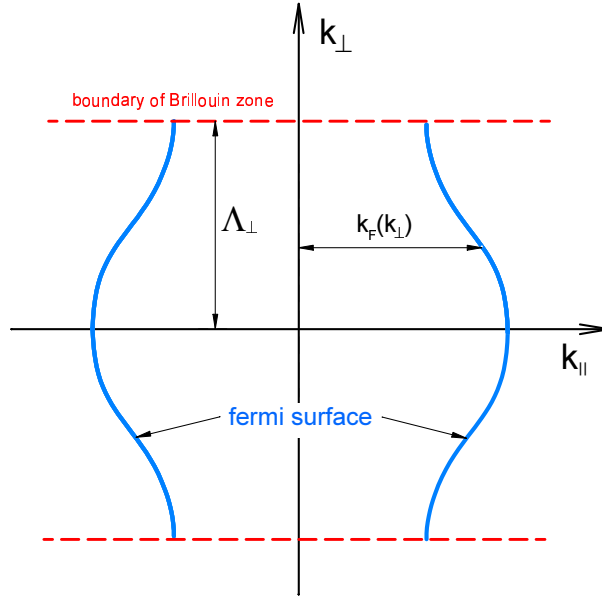
Figure 7.1: Fermi surface of an infinite array of coupled metallic chains.

where $k_\parallel$ denotes the momentum parallel to the chains and $k_\perp$ the one perpendicular to the chains. The index α refers to the chirality and distinguishes between right- and left-movers.

7.2   The model

Effective low-energy action

We start with a low-energy effective model with repulsive density-density interactions and a linearised dispersion to write the action as

$$S \;=\; \sum_\alpha \int_{\mathbf{K}} (-i\omega + v k_\parallel - \mu(k_\perp)) \bar\psi_{\mathbf{K},\alpha} \psi_{\mathbf{K},\alpha} + \frac{1}{2} \sum_{\alpha,\alpha'} \bar\rho_\alpha \cdot \mathbf{f}_{\alpha,\alpha'} \cdot \rho_{\alpha'} \;, \quad (7.2)$$

where we have made use of the scalar product (2.6) and introduced the chiral densities

$$\rho_\alpha(\bar{\mathbf{K}}) = \int_{\mathbf{K}} \bar\psi_{\mathbf{K},\alpha} \psi_{\mathbf{K}+\bar{\mathbf{K}},\alpha} \;. \quad (7.3)$$

The momentum integration has to understood such that the momenta $k_\parallel$ are restricted to the half plane defined by α and we use the normalization

$$\int_{\mathbf{K}} = \int \frac{d\omega}{2\pi} \int_{-\Lambda_\perp}^{\Lambda_\perp} \frac{dk_\perp}{2\pi} \int \frac{dk_\parallel}{2\pi} \;. \quad (7.4)$$

In the same manner as in (6.68) we label the elements of the interaction matrix as

$$
\begin{aligned}
f_{RR} &= f_{LL} = f_{ch} \,, & (7.5) \\
f_{RL} &= f_{LR} = f_{nch} \,, & (7.6)
\end{aligned}
$$

where for repulsive interactions $f_{\alpha\alpha'} > 0$. We have graphically depicted the chiral and non-chiral interactions in figure 7.2.
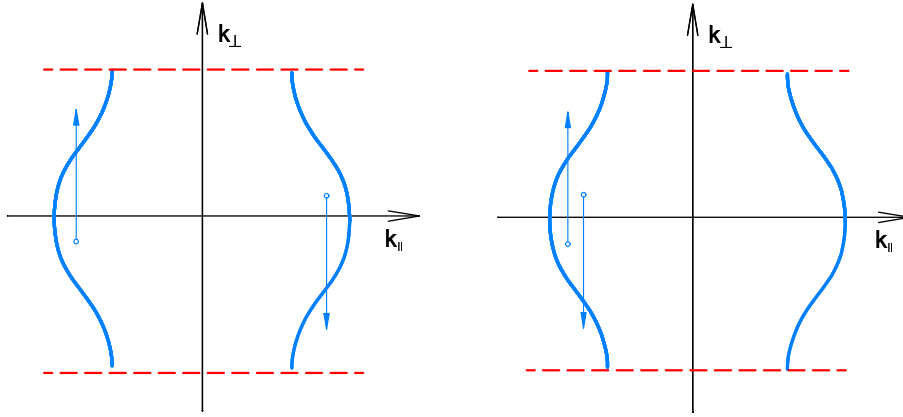

Figure 7.2: Examples for non-chiral scattering (left picture) and chiral scattering (right picture).

We shall work with an interaction cutoff again and we assume that the momentum transferred by the interaction in direction parallel to the chains is restricted by an ultraviolet cutoff $\Lambda_\parallel$ with $\Lambda_\parallel < \min(\{k_F\})$ such that the interaction cannot transfer momentum between the two Fermi surface sheets. In a more realistic model of course we would have to relax this restriction. In the direction perpendicular to the chains the momentum transfer is restricted by $\bar{\Lambda}_\perp = \lambda \Lambda_\perp$ with $0 < \lambda \leq 1$, it therefore might be of the order of the Brillouin zone such that umklapp scattering in this direction is possible.

Bosonized interaction

To bosonize the interaction we perform a Hubbard-Stratonovich transformation as we have done before. The interaction is now mediated by the real valued bosonic fields ϕ. We obtain

$$
\begin{aligned}
S &= \sum_\alpha \int_{\mathbf{K}} (-i\omega + vk_\parallel - \mu(k_\perp)) \bar{\psi}_{\mathbf{K},\alpha} \psi_{\mathbf{K},\alpha} + \frac{1}{2} \sum_{\alpha,\alpha'} \phi_\alpha \cdot \mathbf{F}^{-1}_{\alpha\alpha'} \cdot \phi_{\alpha'} \\
&\quad + i\gamma \sum_\alpha \phi_\alpha \cdot \rho_\alpha \,. & (7.7)
\end{aligned}
$$

Note that we have pulled out a factor i and consequently the initial value for the
3-point vertex is $\gamma = 1$. For the bosonic Greensfunction we obtain the non-trivial
initial conditions (2.60)

$$\mathbf{F}^{-1}(\bar{\mathbf{K}}) = \mathbf{f}^{-1} + \mathbf{\Pi}(\bar{\mathbf{K}}) \,, \tag{7.8}$$

where the polarizations are calculated from

$$
\begin{aligned}
\Pi_{\alpha\alpha'}(\bar{\mathbf{K}}) &= \delta_{\alpha\alpha'}\gamma^2 \int_{\mathbf{K}} G_\alpha(\mathbf{K}) G_\alpha(\mathbf{K} + \bar{\mathbf{K}}) \\
&= \delta_{\alpha\alpha'} \frac{\gamma^2}{2\pi} \int_{k_\perp} \frac{\alpha\bar{k}_\parallel + \Delta_0(k_\perp, \bar{k}_\perp)}{i\bar{\omega} - v(\alpha\bar{k}_\parallel + \Delta_0(k_\perp, \bar{k}_\perp))} \,.
\end{aligned} \tag{7.9}
$$

Here Δ_0 denotes the difference between bare Fermi momenta as

$$\Delta_0(k_\perp, \bar{k}_\perp) = k_{F,0}(k_\perp) - k_{F,0}(k_\perp + \bar{k}_\perp) \,, \tag{7.10}$$

with $k_{F,0}$ the Fermi momenta of the non-interacting system.

7.3   Rescaling and flow equations

Rescaling of momenta

We will perform the RG such as to successively eliminate interaction processes
with momentum exchange parallel to the chains in the range $\Lambda_{\parallel,\tau} < |k_\parallel| < \Lambda_{\parallel,0}$.
Therefore we define rescaled momenta as

$$
\begin{aligned}
\Lambda_{\tau,\parallel} &= \Lambda_\parallel e^{-\tau} \,, & \tag{7.11}\\
\omega &= \epsilon\Lambda_{\tau,\parallel} \,, & \tag{7.12}\\
k_\parallel &= \frac{q_\parallel \Lambda_{\tau,\parallel}}{v} \,, & \tag{7.13}\\
k_\perp &= q_\perp \Lambda_\perp \,. & \tag{7.14}
\end{aligned}
$$

Note that we have rescaled momenta perpendicular to the chains just to make
them dimensionless. The rescaled measure of integration is

$$\int_{\mathbf{Q}} = \int_\epsilon \int_{q_\perp} \int_{q_\parallel} = \int \frac{d\epsilon}{2\pi} \int_{-\pi}^{\pi} \frac{dq_\perp}{2\pi} \int \frac{dq_\parallel}{2\pi} \,. \tag{7.15}$$

Rescaling of vertices

The rescaling for fields and vertices is straightforward

$$\tilde{\psi}_{\mathbf{Q},\alpha} = \psi_{\mathbf{K},\alpha} \sqrt{\frac{\Lambda_{\tau,\parallel}^3 \Lambda_\perp}{v Z_{\tau,q_\perp}}}, \tag{7.16}$$

$$\tilde{\phi}_{\mathbf{Q},\alpha} = \phi_{\mathbf{Q},\alpha} \frac{\Lambda_{\tau,\parallel}\Lambda_\perp}{v} , \tag{7.17}$$

$$\tilde{\Gamma}_\tau^{(2n,m)}(\{\mathbf{Q}\}) = \Lambda_{\tau,\parallel}^{n+m-2}\Lambda_\perp^{n-1}v^{1-n}\left(\prod_i Z_{\tau,q_{i,\perp}}\right)\Gamma_{\Lambda_{\tau,\parallel}}^{(2n,m)}(\{\mathbf{K}\}) , \tag{7.18}$$

where $2n$ labels the number of fermionic lines and m the number of bosonic lines.

Classification according to relevance

As before we will only consider vertices which are relevant or marginal under the RG to perform an expansion in relevance. From (7.18) we infer that we only have to retain vertices with $n + m \leq 2$. As the momenta perpendicular to the chains do not contribute to the scaling dimensions we obtain infinite sets of relevant and marginal vertices parametrized by these perpendicular momenta. Despite this dependence on transversal momentum we obtain the same vertices as in the last chapter and denote them equivalently. The fermionic 2-point vertex is expanded as

$$\tilde{\Gamma}_\tau^{(2)}(\mathbf{Q}) = \tilde{r}_{\tau,q_\perp} + i\epsilon(Z_{\tau,q_\perp} - 1) - q_\parallel(Z_{\tau,q_\perp} - \tilde{v}_{\tau,q_\perp}) , \tag{7.19}$$

and as the Fermi velocities do not get renormalized (7.26) we write the fermionic Greensfunction as

$$\tilde{G}_\tau(\mathbf{Q}) = \frac{1}{i\epsilon - q_\parallel - \tilde{r}_{\tau,q_\perp}} . \tag{7.20}$$

The 3-point vertex describing the coupling between fermions and bosons is marginal. It does depend on the transversal momentum of the scattered fermions and the transversal momentum transferred by the bosons. We write it as $\tilde{\gamma}_\tau(\bar{q}_\perp, q_\perp)$ where the first momentum denotes the incoming bosonic momentum and the last the momentum of the incoming fermion.

As before we do not expand the bosonic Greensfunction in relevance and as its flow is generated by irrelevant vertices only (which we neglect) we use the adiabatic approximation, section 3.2. Suppressing the Θ-function describing the interaction cutoff we write its diagonal elements as

$$\tilde{F}_{\tau,\alpha\alpha}(\bar{\mathbf{Q}}) = \tag{7.21}$$

$$\frac{2\pi\tilde{f}_{ch} + (2\pi)^2(\tilde{f}_{ch}^2 - \tilde{f}_{nch}^2)\tilde{\Pi}_{\tau,\bar{\alpha}}(\bar{\mathbf{Q}})}{1 + 2\pi\tilde{f}_{ch}\left(\tilde{\Pi}_{\tau,R}(\bar{\mathbf{Q}}) + \tilde{\Pi}_{\tau,L}(\bar{\mathbf{Q}})\right) + (2\pi)^2(\tilde{f}_{ch}^2 - \tilde{f}_{nch}^2)\tilde{\Pi}_{\tau,R}(\bar{\mathbf{Q}})\tilde{\Pi}_{\tau,L}(\bar{\mathbf{Q}})} ,$$

with the polarization

$$\tilde{\Pi}_{\tau,\alpha}(\bar{\mathbf{Q}}) = \frac{1}{2\pi}\int_{\mathbf{Q}}\tilde{\gamma}_\tau^2(\bar{q}_\perp, q_\perp)\tilde{G}(\mathbf{Q})\tilde{G}(\mathbf{Q} + \bar{\mathbf{Q}} + \tilde{\Delta}_\tau^*(q_\perp, \bar{q}_\perp)) . \tag{7.22}$$

Here we have exploited time reversal symmetry to write the product of 3-point vertices as a square. The rescaled interactions are defined as

$$\tilde{f}_{ch/nch} = \frac{\Lambda_\perp f_{ch/nch}}{2\pi v} . \tag{7.23}$$

The last marginal vertex is a fermionic 4-point vertex. However as in the last chapter it does not couple to the fermionic 2-point function and vanishes initially. We neglect it assuming that its contributions to the flow are small.

Flow equations

As described for (6.98) we shall expand all flow equations in powers of $\tilde{r}$ and consequently use the truncated fermionic Greensfunction

$$\tilde{G}'(\mathbf{Q}) = \frac{1}{i\epsilon - q_\parallel} \,, \tag{7.24}$$

instead of (7.20) and substitute $\tilde{\Delta}_\tau^*$ by the flowing difference of Fermi momenta $\tilde{\Delta}_\tau$.

The flow equations of section 6.4.5 can easily be generalized to the present model. We obtain the same vanishing of the flow for the renormalized Fermi velocities. The equations for $\tilde{r}$, $\tilde{v}$ and η are

$$\partial_\tau \tilde{r}_{\tau,q_\perp} = \tilde{r}_{\tau,q_\perp} - \int_{\bar{\mathbf{Q}}} \dot{\tilde{F}}_{\tau,RR}(\bar{\mathbf{Q}}) \, \tilde{\gamma}_\tau^2(\bar{q}_\perp, q_\perp) \, \tilde{G}'(\bar{\mathbf{Q}} + \tilde{\Delta}_\tau(q_\perp, \bar{q}_\perp)) \,, \tag{7.25}$$

$$\partial_\tau \tilde{v}_{\tau,q_\perp} = 0 \,, \tag{7.26}$$

$$\eta_{\tau,q_\perp} = -\int_{\bar{\mathbf{Q}}} \dot{\tilde{F}}_{\tau,RR}(\bar{\mathbf{Q}}) \, \tilde{\gamma}_\tau^2(\bar{q}_\perp, q_\perp) \, \tilde{G}'^2(\bar{\mathbf{Q}} + \tilde{\Delta}_\tau(q_\perp, \bar{q}_\perp)) \,. \tag{7.27}$$

For the 3-point vertex we receive

$$
\begin{aligned}
\partial\tau \tilde{\gamma}_\tau(\bar{q}_\perp, q_\perp) &= -\frac{1}{2}\tilde{\gamma}_\tau(\bar{q}_\perp, q_\perp)(\eta_{\tau,q_\perp} + \eta_{\tau,q_\perp + \bar{q}_\perp}) + \dot{\tilde{\gamma}}_\tau(\bar{q}_\perp, q_\perp) \\
&= -\int_{\bar{\mathbf{Q}}'} \dot{\tilde{F}}_{\tau,RR}(\bar{\mathbf{Q}}') \Big\{ \tilde{G}'(\bar{\mathbf{Q}}' + \tilde{\Delta}_\tau(q_\perp, \bar{q}'_\perp)) \tilde{G}'(\bar{\mathbf{Q}}' + \tilde{\Delta}_\tau(q_\perp + \bar{q}_\perp, \bar{q}'_\perp)) \cdot \\
&\qquad \cdot \tilde{\gamma}(\bar{q}_\perp, q_\perp + \bar{q}'_\perp)\tilde{\gamma}(\bar{q}'_\perp, q_\perp)\tilde{\gamma}(\bar{q}'_\perp, \bar{q}_\perp + q_\perp) \\
&\qquad - \frac{1}{2}\tilde{G}'^2(\bar{\mathbf{Q}}' + \tilde{\Delta}_\tau(q_\perp, \bar{q}'_\perp)) \, \tilde{\gamma}(\bar{q}_\perp, q_\perp)\tilde{\gamma}^2(\bar{q}'_\perp, q_\perp) \\
&\qquad - \frac{1}{2}\tilde{G}'^2(\bar{\mathbf{Q}}' + \tilde{\Delta}_\tau(q_\perp + \bar{q}_\perp, \bar{q}'_\perp)) \, \tilde{\gamma}(\bar{q}_\perp, q_\perp)\tilde{\gamma}^2(\bar{q}'_\perp, \bar{q}_\perp + q_\perp) \Big\} \,.
\end{aligned}
\tag{7.28}
$$

For an arbitrary Fermi surface it is unfortunately impossible to find a closed expression for the polarization (7.22). In general we can solve the equations only numerically. However for weak coupling the flow equations can be expanded in powers of the interactions $\tilde{f}$ to obtain a self-consistent perturbative result. On the other hand at strong coupling in the confined phase $\tilde{\Delta}$ is a suitable parameter for expansion.

7.4 Perturbative treatment

We start with a perturbative treatment up to second order in the interaction $\tilde{f}$. Further on we neglect the flow of the couplings and set $\tilde{\gamma}(\bar{q}_\perp, q_\perp) = 1$ and $\tilde{\Delta}_\tau = \tilde{\Delta}_\tau^*$. With (5.23) and (7.25) we obtain

$$
\begin{aligned}
r_{0,q_\perp} &= \tilde{f}_{ch} \int_{\bar{q}_\perp} (1 - \Delta_0^*(q_\perp, \bar{q}_\perp)) \\
&\quad + \frac{\tilde{f}_{ch}^2 + \tilde{f}_{nch}^2}{2} \int_{\bar{q}_\perp} \int_{q'_\perp} (\Delta_0^*(q_\perp, \bar{q}_\perp) - \Delta_0^*(q'_\perp, \bar{q}_\perp)) \\
&\quad + \tilde{f}_{nch}^2 \int_{\bar{q}_\perp} \int_{q'_\perp} Y\left(\Delta_0^*(q_\perp, \bar{q}_\perp), \Delta_0^*(q'_\perp, \bar{q}_\perp)\right).
\end{aligned}
\tag{7.29}
$$

Note that $\tilde{\Delta}_0^*(q_\perp, \bar{q}_\perp) = \frac{k_F(q_\perp) - k_F(q_\perp + \bar{q}_\perp)}{\Lambda_{0,\parallel}}$ and we have introduced the function

$$
Y(x, y) = \frac{x + y}{4} \ln\left(\frac{(x + y)^2}{4 - (x - y)^2}\right).
\tag{7.30}
$$

Defining the interaction induced shift of the Fermi surface as $\delta\tilde{k}_F(q_\perp) = \tilde{k}_F(q_\perp) - \tilde{k}_{F,0}(q_\perp) = \frac{k_F(q_\perp) - k_{F,0}(q_\perp)}{\Lambda_{0,\parallel}}$ we obtain the self-consistency equation at constant density

$$
\begin{aligned}
\delta\tilde{k}_F(q_\perp) &= \left(-\tilde{f}_{ch} + \frac{\tilde{f}_{ch}^2 + \tilde{f}_{nch}^2}{2}\right) \int_{\bar{q}_\perp} \tilde{\Delta}_0^*(q_\perp, \bar{q}_\perp) \\
&\quad + \tilde{f}_{nch}^2 \int_{\bar{q}_\perp} \int_{q'_\perp} Y\left(\Delta_0^*(q_\perp, \bar{q}_\perp), \Delta_0^*(q'_\perp, \bar{q}_\perp)\right).
\end{aligned}
\tag{7.31}
$$

Generally this non-linear equation can only be solved numerically. However we note that the dominant term for weak warping $|\tilde{\Delta}_0^*| \ll 1$ of the Fermi surface stems from the logarithmic contribution of Y. Let us become specific and use a bare Fermi surface of the harmonic form

$$
\tilde{k}_{F,0}(q_\perp) = \langle \tilde{k}_{F,0} \rangle + \tilde{A}_0 \cos(q_\perp).
\tag{7.32}
$$

The renormalized Fermi surface at constant density can be expanded in a fourier series as

$$
\tilde{k}_F(q_\perp) = \langle \tilde{k}_{F,0} \rangle + \tilde{A}^* \cos(q_\perp) + \ldots
\tag{7.33}
$$

where the dots indicate higher harmonics corresponding to longer range hopping. These higher harmonics are in most cases negligible and here we will just consider the first non-trivial term. We may write the renormalized amplitude as

$$
\tilde{A}^* = 2 \int_{q_\perp} \cos(q_\perp) \tilde{k}_F(q_\perp).
\tag{7.34}
$$

Expanding in (7.31) for small $\tilde{A}$ yields

$$\tilde{A}^* = \frac{\tilde{A}_0}{1 + R(\tilde{A}^*)} \qquad (7.35)$$

with

$$R(\tilde{A}^*) = C_\lambda \left\{ \frac{\tilde{f}_{nch}}{2} - \frac{\tilde{f}_{nch}^2}{4} + \frac{\tilde{f}_{ch}^2}{2} \left(|\ln(\tilde{A}^*)| - I_\lambda \right) \right\} . \qquad (7.36)$$

Remember that λ defines the momentum cutoff in transverse direction which leads to an effective normalization factor

$$C_\lambda = \lambda - \frac{\sin(\pi\lambda)}{\pi} . \qquad (7.37)$$

The function I_λ is determined by

$$
\begin{aligned}
I_\lambda &= 1 + \ln(2) + 4 \int_{\bar{q}_\perp} \int_{q_\perp} \sin\left(\frac{\bar{q}_\perp}{2}\right) \cos\left(\frac{q_\perp}{2}\right) \sin\left(\frac{q_\perp + \bar{q}_\perp}{2}\right) \cdot \\
&\quad \cdot \ln\left(\left| \sin\left(\frac{\bar{q}_\perp}{2}\right) \cos\left(\frac{q_\perp}{2}\right) \sin\left(\frac{q_\perp + \bar{q}_\perp}{2}\right) \right| \right) ,
\end{aligned} \qquad (7.38)
$$

and is of the order of unity.

For sufficiently small $\tilde{A}^*$ the logarithmic term in (7.36) dominates and leads to a flattening of the Fermi surface. As in the last chapter a repulsive chiral interaction suppresses the tendency toward confinement. Therefore from now on we only consider a non-chiral interaction and have plotted the solution to the self-consistency equation in figure 7.3. Note that our perturbative approach does not predict a confinement transition. However within this approximation we can not expect to describe the situation at strong coupling properly.
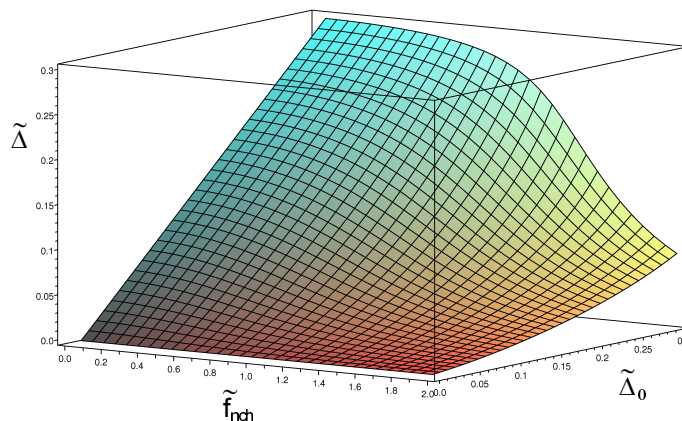

Figure 7.3: Numerical solution of (7.35) for $\tilde{f}_{ch} = 0$.

For non-harmonic Fermi surfaces we have to rely on numerical computations. Despite an overall renormalization of the amplitude one can observe a small

suppression of higher harmonics relative to the lowest harmonic. In figure 7.4 we have plotted the true Fermi surface of an initially rectangular Fermi surface. Note that initially flat parts of the Fermi surface get renormalized to be weakly curved.
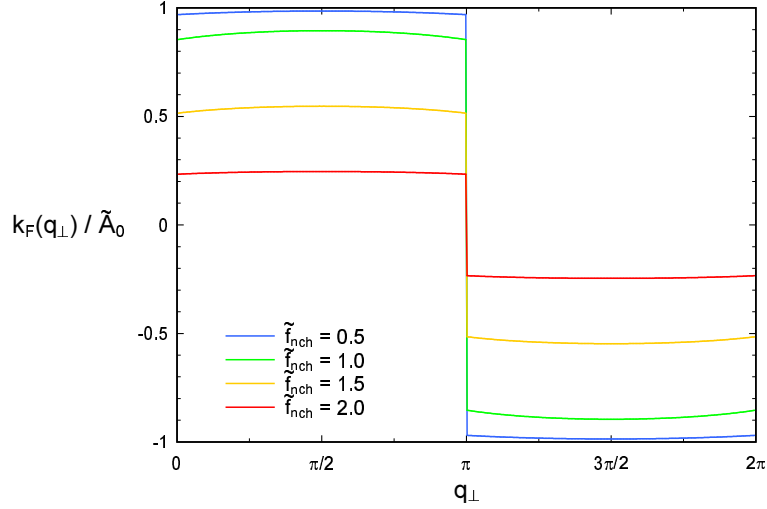

Figure 7.4: Numerical solution of (7.35) for an initially rectangular Fermi surface and vanishing chiral scattering $\tilde{f}_{ch} = 0$.

7.5　Self-consistent 1-loop approximation

The perturbative treatment of the last section is clearly not suitable to consider strong coupling. We therefore need a sensible extrapolation to large $\tilde{f}$ without becoming too complicated. We follow the approach laid out in the last chapter and perform a self-consistent 1-loop treatment. Within this approximation we neglect the anomalous dimension, i.e. $Z_\tau = 1$, vertex corrections, i.e. $\tilde{\gamma}_\tau = 1$ and self-energy correction, i.e. $\tilde{\Delta}_\tau = \tilde{\Delta}_\tau^*$.

Considering a harmonic Fermi surface (7.32) we actually may evaluate the polarization for $\lambda = 1$ as

$$
\begin{aligned}
2\pi\tilde{\Pi}_{\tau,\alpha}(\bar{\mathbf{Q}}) &= \frac{i\bar{\epsilon}}{i\bar{\epsilon} - \alpha\bar{q}_\parallel} \sum_{n=0}^{\infty} (x_\alpha)^n \int_{q_\perp} \sin^n(q_\perp) - 1 \qquad (7.39) \\
&= \frac{i\bar{\epsilon}(1 - \sqrt{1 - x_\alpha^2}) + \alpha\bar{q}_\parallel\sqrt{1 - x_\alpha^2}}{(i\bar{\epsilon} - \alpha\bar{q}_\parallel)\sqrt{1 - x_\alpha^2}} \ ,
\end{aligned}
$$

with

$$
x_\alpha = \frac{2\tilde{A}_\tau^* \sin(\bar{q}_\perp/2)}{i\bar{\epsilon} - \alpha\bar{q}_\parallel} \ , \qquad (7.40)
$$

and $\tilde{A}_\tau^* = \frac{\tilde{A}^*}{\Lambda_{\tau,\parallel}}$. With the help of this equations we can write the bosonic Greens-function with the correct poles up to order $\tilde{A}_\tau^*$ as

$$\tilde{F}_{\tau,RR}(\bar{\mathbf{Q}}) = -\frac{2\pi \tilde{f}_{nch}^2 \, \bar{q}_\parallel (i\bar{\epsilon} - \bar{q}_\parallel)^3}{(i\bar{\epsilon} - \tilde{\epsilon}_+^{(1)})(i\bar{\epsilon} - \tilde{\epsilon}_-^{(1)})(i\bar{\epsilon} - \tilde{\epsilon}_+^{(2)})(i\bar{\epsilon} - \tilde{\epsilon}_-^{(2)})} \; , \qquad (7.41)$$

using

$$\tilde{\epsilon}_\pm^{(1)} = \pm \bar{q}_\parallel \sqrt{1 - \tilde{f}^2}, \qquad (7.42)$$

$$\tilde{\epsilon}_\pm^{(2)} = \bar{q}_\parallel \pm i \frac{2\tilde{A}_\tau^* \sin(\bar{q}_\perp)}{\sqrt{2}} \; . \qquad (7.43)$$

Evaluating the flow for $\tilde{r}$ we observe that in leading order in $\tilde{A}_\tau^*$ we may actually neglect the amplitude in (7.43). Consequently it is then sufficient to evaluate $\tilde{F}$ for a completely flat Fermi surface

$$\tilde{F}_{\tau,RR}(\bar{\mathbf{Q}}) = \frac{2\pi \tilde{f}_{nch}^2 \, \bar{q}_\parallel (i\bar{\epsilon} - \bar{q}_\parallel)}{\bar{\epsilon}^2 + (1 - \tilde{f}_{nch}^2)\bar{q}_\parallel^2} \; . \qquad (7.44)$$

Performing the relevant computations we receive in leading order in $\tilde{A}^*$ and for general transverse momentum cutoff λ

$$\delta \tilde{k}_F(q_\perp) = \frac{1 - \sqrt{1 - \tilde{f}_{nch}^2}}{\sqrt{1 - \tilde{f}_{nch}^2}} \int_{\bar{q}_\perp} \tilde{\Delta}_0^*(q_\perp, \bar{q}_\perp) \ln(|\tilde{\Delta}_0^*(q_\perp, \bar{q}_\perp)|) \qquad (7.45)$$

or

$$R(\tilde{A}^*) = C_\lambda \frac{1 - \sqrt{1 - \tilde{f}_{nch}^2}}{\sqrt{1 - \tilde{f}_{nch}^2}} |\ln(\tilde{A}^*)| \; . \qquad (7.46)$$

We observe that the right-hand side of these equations diverges for $\tilde{f}_{nch} \to 1$ even for finite $\tilde{A}^*$. This implies that the system undergoes a confinement transition at strong coupling. Note the similarities to our investigation of two coupled chains in the last chapter. There we obtained an equivalent result and predicted a confinement transition in 1-loop, however including vertex renormalizations the persistence of confinement was crucially dependent on transverse umklapp processes stabilizing the 3-point vertex. To decide if the two-dimensional system truly approaches confinement we therefore have to perform a self-consistent 2-loop calculation investigating the renormalization of the 3-point vertex as well.

7.6   Inclusion of vertex renormalization

So far we have set $\tilde{\gamma} = \tilde{\gamma}_0 = 1$. However during renormalization according to (7.28) the marginal 3-point vertex will become momentum dependent. Additionally so far we have neglected the anomalous dimension $\eta(q_\perp)$ which carries a

transverse momentum dependence as well. To simplify calculations from now on we will set $\lambda = 1$ and $\tilde{f} =: \tilde{f}_{nch}$ (neglecting chiral processes).

7.6.1 3-point vertex

Flow equation

Lead by a numerical study we observe that the 3-point vertex $\tilde{\gamma}_\tau(\bar{q}_\perp, q_\perp)$ does only depend weakly on the fermionic momentum $q_\perp$ see figure 7.5. Therefore we define

$$\tilde{\gamma}_\tau(\bar{q}_\perp) = \int_{q_\perp} \tilde{\gamma}_\tau(\bar{q}_\perp, q_\perp) \,, \tag{7.47}$$

and introduce the effective interaction

$$\tilde{f}_\tau(\bar{q}_\perp) = \tilde{f} \tilde{\gamma}_\tau^2(\bar{q}_\perp) \,. \tag{7.48}$$

We may then simplify (7.28) and write the flow equation as

$$\partial\tau \tilde{\gamma}_\tau(\bar{q}_\perp) = -\frac{\tilde{\gamma}_\tau(\bar{q}_\perp)}{2} \int_{q_\perp} \int_{\bar{\mathbf{Q}}'} \dot{F}(\bar{\mathbf{Q}}') \tilde{\gamma}_\tau^2(\bar{q}'_\perp) \left(\tilde{G}'(\bar{\mathbf{Q}}' + \tilde{\Delta}_\tau(q_\perp, \bar{q}'_\perp)) \right.$$
$$\left. - \tilde{G}'(\bar{\mathbf{Q}}' + \tilde{\Delta}_\tau(q_\perp + \bar{q}_\perp, \bar{q}'_\perp)) \right)^2. \tag{7.49}$$

Note that the vertex at zero transversal momentum exchange $\bar{q}_\perp = 0$ does not get renormalized. Actually at intermediate scales we observe a dependence on fermionic momenta. As $\tilde{\Delta} \approx \frac{1}{2}$ (resp. $\tilde{A} \approx \frac{1}{2}$) the interaction cutoff becomes comparable to the warping of the Fermi surface. At this point the 3-point vertex becomes strongly renormalized and the dependence on fermionic momenta is smoothed out again, see figure 7.5.

Approximations

Unfortunately we are unable to perform the integral of the simplified flow equation (7.49) exactly because the full bosonic Greensfunction is quite complicated. However we can derive simple approximations for weak coupling and for strong coupling in the confined phase. In the regime of weak coupling we expand up to $O(\tilde{f}^2)$ to get

$$\int_{\bar{\mathbf{Q}}} \dot{F}(\bar{\mathbf{Q}}) \tilde{G}'(\bar{\mathbf{Q}} + \tilde{\Delta}_1) \tilde{G}'(\bar{\mathbf{Q}} + \tilde{\Delta}_2) = -\tilde{f}^2 \int_{\bar{q}_\perp} \int_{q_\perp} \tilde{\gamma}_\tau^2(\bar{q}_\perp, q_\perp) \Big\{$$

$$\frac{(1 - \tilde{\Delta}_0)\Theta(1 + \tilde{\Delta}_2)}{(2 + \tilde{\Delta}_2 - \tilde{\Delta}_0)(\tilde{\Delta}_2 - \tilde{\Delta}_1)} + \frac{(1 + \tilde{\Delta}_0)\Theta(\tilde{\Delta}_2 - 1)}{(2 - \tilde{\Delta}_2 + \tilde{\Delta}_0)(\tilde{\Delta}_2 - \tilde{\Delta}_1)}$$

$$+ \frac{(1 - \tilde{\Delta}_0)\Theta(1 + \tilde{\Delta}_1)}{(2 + \tilde{\Delta}_1 - \tilde{\Delta}_0)(\tilde{\Delta}_1 - \tilde{\Delta}_2)} + \frac{(1 + \tilde{\Delta}_0)\Theta(\tilde{\Delta}_1 - 1)}{(2 - \tilde{\Delta}_1 + \tilde{\Delta}_0)(\tilde{\Delta}_1 - \tilde{\Delta}_2)}$$

$$- \frac{(1 + \tilde{\Delta}_0)\Theta(1 + \tilde{\Delta}_0)}{(2 - \tilde{\Delta}_2 + \tilde{\Delta}_0)(2 - \tilde{\Delta}_1 + \tilde{\Delta}_0)} - \frac{(\tilde{\Delta}_0 - 1)\Theta(\tilde{\Delta}_0 - 1)}{(2 + \tilde{\Delta}_2 - \tilde{\Delta}_0)(2 + \tilde{\Delta}_1 - \tilde{\Delta}_0)} \Big\}. \tag{7.50}$$

On the other hand in the confined phase $\tilde{\Delta} \to 0$ and we can expand the integral in powers of the Fermi surface difference up to $O(\tilde{\Delta}^2)$ as

$$\int_{\bar{\mathbf{Q}}} \dot{F}(\bar{\mathbf{Q}})\tilde{\gamma}^2(\bar{q}_\perp)G(\bar{\mathbf{Q}}+\tilde{\Delta}_1)G(\bar{\mathbf{Q}}+\tilde{\Delta}_2) \;\; = \tag{7.51}$$

$$-\int_{\bar{q}_\perp} \frac{\tilde{f}_\tau^2(\bar{q}_\perp)}{\sqrt{1-\tilde{f}_\tau^2(\bar{q}_\perp)}\left(1+\sqrt{1-\tilde{f}_\tau^2(\bar{q}_\perp)}\right)} - \int_{\bar{q}_\perp} \frac{\tilde{f}^2(\bar{q}_\perp)\left(\tilde{\Delta}_1^2+\tilde{\Delta}_2^2+\tilde{\Delta}_1\tilde{\Delta}_2\right)}{\sqrt{1-\tilde{f}_\tau^2(\bar{q}_\perp)}\left(1+\sqrt{1-\tilde{f}_\tau^2(\bar{q}_\perp)}\right)^3} \cdot$$

Confined phase

In the confined phase the expansion (7.51) is appropriate. Here we receive

$$\partial\tau\tilde{\gamma}(\bar{q}_\perp) \;\; = \;\; -\tilde{\gamma}_\tau(\bar{q}_\perp)\int_{\bar{q}'_\perp} \frac{\tilde{f}_\tau^2(\bar{q}'_\perp)\int_{q'_\perp}\left(\tilde{\Delta}_\tau(q'_\perp,\bar{q}'_\perp)-\tilde{\Delta}_\tau(\bar{q}_\perp+q'_\perp,\bar{q}'_\perp)\right)^2}{2\sqrt{1-\tilde{f}_\tau^2(\bar{q}'_\perp)}\left(1+\sqrt{1-\tilde{f}_\tau^2(\bar{q}'_\perp)}\right)^3}. \tag{7.52}$$

For a harmonic Fermi surface $k_F(q_\perp) = \tilde{A}_\tau \cos(q_\perp)$ we can evaluate the integral over $q'_\perp$ and obtain

$$\int_{q'_\perp}\left(\tilde{\Delta}_\tau(q'_\perp,\bar{q}'_\perp)-\tilde{\Delta}_\tau(\bar{q}_\perp+q'_\perp,\bar{q}'_\perp)\right)^2 = 8\tilde{A}_\tau^2\sin^2\left(\frac{\bar{q}_\perp}{2}\right)\sin^2\left(\frac{\bar{q}'_\perp}{2}\right). \tag{7.53}$$

Note that this expression is maximal for $\bar{q}_\perp = \pi$, $\bar{q}'_\perp = \pi$. Assuming that $\tilde{\gamma}(\bar{q}_\perp)$ varies only weakly with $\bar{q}_\perp$ which actually is the case at confinement we may write for the effective interaction

$$\partial\tau\tilde{f}_\tau(\bar{q}_\perp) \;\; = \;\; -\frac{4\tilde{A}_\tau^2\sin^2\left(\frac{\bar{q}_\perp}{2}\right)\tilde{f}(\bar{q}_\perp)\tilde{f}_\tau^2(\pi)}{\sqrt{1-\tilde{f}_\tau^2(\pi)}\left(1+\sqrt{1-\tilde{f}_\tau^2(\pi)}\right)^3}. \tag{7.54}$$

Numerical study

We perform a numerical evaluation of the vertex $\tilde{\gamma}_\tau(\bar{q}_\perp, q_\perp)$ using a perturbative expansion as introduced in (7.50). Starting point is a harmonic Fermi surface at small warping $\tilde{A}_0 = 0.001$ and interaction strength $\tilde{f} = 0.4$. We follow the evolution of this vertex as τ increases and have plotted the relevant results in figure 7.5.

We continue with a numerical evaluation of the vertex $\tilde{\gamma}_\tau(\bar{q}_\perp)$ for a harmonic Fermi surface at various coupling strengths. To evaluate the flow of $\tilde{A}_\tau$ we use (7.58). The results are plotted in figure 7.6. Note the qualitative difference in the dependence on the transverse momentum in the de-confined phase and the confined phase. In the former $\tilde{\gamma}^*(\bar{q}_\perp)$ follows a nearly box like shape whereas in the latter there is a smooth $\propto \sin^2(\bar{q}_\perp)$ dependence. Computations have been
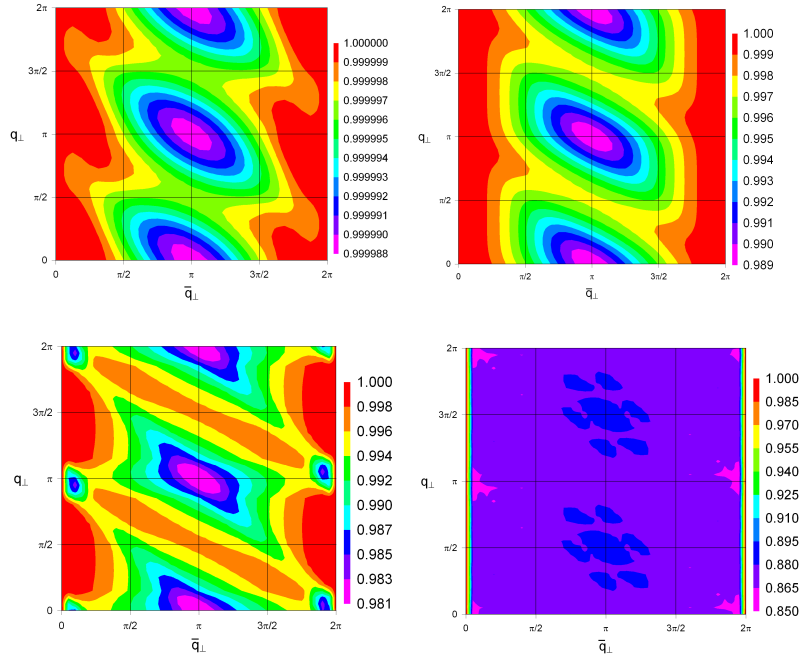
Figure 7.5: Evolution of the 3-point vertex $\tilde{\gamma}(\bar{q}_\perp, q_\perp)$ for bare interaction $\tilde{f} = 0.4$ and a harmonic Fermi surface with amplitude $\tilde{A}_0 = 0.001$. From top left to bottom right: $\tau = \frac{1}{2}\tau_c$, $\tau = \tau_c$, $\tau = \tau_c + 0.1$ and $\tau = 3\tau_c$. Here the critical flow parameter is determined from the condition that the warping of the Fermi surface is comparable to the cutoff $\tilde{A}_{\tau_c} = 1/2$.
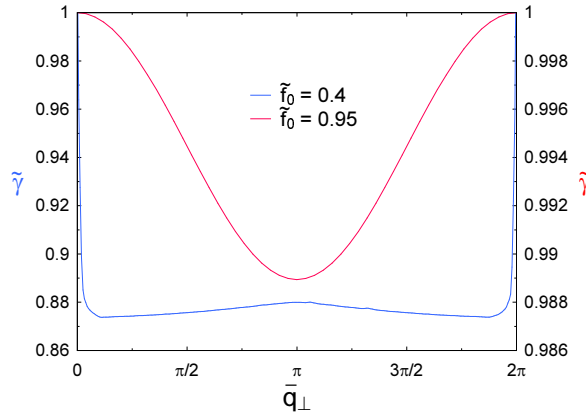

Figure 7.6: Momentum dependent 3-point vertex $\tilde{\gamma}(\bar{q}_\perp)$ for a harmonic Fermi surface at bare amplitude $\tilde{A}_0 = 0.1$. At $\tilde{f}_0 = 0.4$ the system is in a de-confined phase and the shape of $\tilde{\gamma}(\bar{q}_\perp)$ is nearly box-like. At $\tilde{f}_0 = 0.95$ the system is confined and we observe a smooth momentum dependence.

performed for a system of 100 coupled chains, comparison with the results for different system sizes suggest that the finiteness of the simulated system is the dominant factor contributing to the smoothing of the box-like shape at $\tilde{f}_0 = 0.4$.

7.6.2 Anomalous dimension

Turning toward the fermionic anomalous dimension (7.27) we receive in the confined phase at small warping $\tilde{\Delta}_\tau$

$$
\begin{aligned}
\eta_{\tau,q_\perp} &= \int_{\bar{q}'_\perp} \frac{1 - \sqrt{1 - \tilde{f}_\tau^2(\bar{q}'_\perp)}}{\sqrt{1 - \tilde{f}_\tau^2(\bar{q}'_\perp)}} \frac{\tilde{\gamma}^2(\bar{q}'_\perp, q_\perp)}{\langle \tilde{\gamma}^2(\bar{q}'_\perp) \rangle} + O(\tilde{\Delta}_\tau^2) \\
&\rightarrow \int_{\bar{q}'_\perp} \frac{1 - \sqrt{1 - \tilde{f}^{*2}(\bar{q}'_\perp)}}{\sqrt{1 - \tilde{f}^{*2}(\bar{q}'_\perp)}} \qquad \tau \rightarrow \infty \; .
\end{aligned}
\tag{7.55}
$$

As the 3-point vertex looses its dependency on the fermionic momentum $q_\perp$ for $\tau \rightarrow \infty$ so does the anomalous dimension. Note that in the confined phase the anomalous dimension is finite and as we shall see even larger than one. In that case we can no longer properly define a Fermi surface.

From a numerical study we observe that as long as the interaction cutoff is larger than the warping of the renormalized Fermi surface determined by $t_\perp$ the anomalous dimension is approximately determined by the value for small $\tilde{\Delta}$, Eq. (7.55), with a small cusp as cutoff and warping become comparable. As the cutoff gets smaller $\tilde{\Delta}_\tau \gg 1$ the anomalous dimension is exponentially approaching zero which can be directly inferred from (7.50). Consequently here the system always is a Fermi-liquid. Note however that as at intermediate scales the anomalous dimension if finite at these scales the system approximately resembles a non-Fermi liquid.

7.6.3 2-point vertex

In general we have to solve (7.25) numerically. For small $\tilde{\Delta}$ we can use the expansion (7.51) to obtain in leading order

$$
\partial_\tau \tilde{k}_{F,\tau}(q_\perp) = \tilde{k}_{F,\tau}(q_\perp) - \int_{\bar{q}_\perp} \frac{1 - \sqrt{1 - \tilde{f}_\tau^2(\bar{q}_\perp)}}{\sqrt{1 - \tilde{f}_\tau^2(\bar{q}_\perp)}} \frac{\tilde{\gamma}^2(\bar{q}_\perp, q_\perp)}{\tilde{\gamma}^2(\bar{q}_\perp)} \tilde{\Delta}_\tau(q_\perp, \bar{q}_\perp) \; . \tag{7.56}
$$

Here we have defined

$$
\tilde{k}_{F\tau}(q_\perp) = \frac{k_{F\tau}(q_\perp) - \int_{q'_\perp} k_{F\tau}(q'_\perp)}{\Lambda_\tau} \; , \tag{7.57}
$$

with the flowing Fermi surface $k_{F\tau}(q_\perp)$ at scale τ. For a harmonic Fermi surface we may approximate further and receive the flow equation for the rescaled amplitude

$$\partial_\tau \tilde{A}_\tau = \tilde{A}_\tau (1 - \eta_{\tau,\pi}) \ . \tag{7.58}$$

Actually lead by a numerical study, see figure 7.7, the flow for $\tilde{k}_{F,\tau}(q_\perp)$ is dominated by the region $\tilde{\Delta}_\tau < 1$, for larger $\tilde{\Delta}_\tau$ it is approximately $\partial_\tau \tilde{k}_{F,\tau}(q_\perp) \approx \tilde{k}_{F,\tau}(q_\perp)$. We therefore conclude that we can use (7.56) with a suitable truncation $\propto \Theta(|\tilde{\Delta}_\tau| < 1)$ of the second term even in the de-confined phase. Because of this
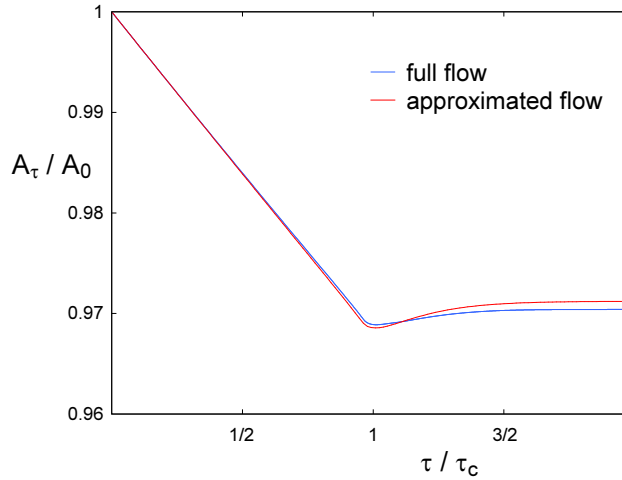

Figure 7.7: Renormalization of the amplitude of a harmonic Fermi surface with $\tilde{A}_0 = 0.001$ at $\tilde{f}_0 = 0.1$. Note that the flow stops approximately when the cutoff becomes comparable to the warping of the flowing Fermi surface at $\tilde{A}_{\tau_c} = 1/2$. The approximated flow is generated by the truncated (as described in the text) equation (7.56); the full flow is evaluated using (7.25).

behaviour the wavefunction renormalization (quasiparticle weight) will almost coincide with the renormalized warping of the Fermi surface $Z \approx A^*/A_0$, as plotted in figure 7.9 . Note that we now have proved our claim made at the end of section 3.2 that the flow equations are dominated by the region $|\tilde{\Delta}| < 1$ for the adiabatic approximation at least what the flow of the Fermi surface is concerned.

## 7.6.4	Phase diagram

For a harmonic Fermi surface near confinement it is sufficient to consider the two flow equations (7.58) and (7.54) at $\bar{q}_\perp = \pi$. We plot the flow in the $\tilde{A}_\tau$-$\tilde{f}_\tau(\pi)$ plane in figure 7.8 and observe that it is similar to the flow for two coupled chains with umklapp scattering, section 6.4.5. There is indeed a finite parameter space for which the system undergoes a confinement transition. The weakest interaction
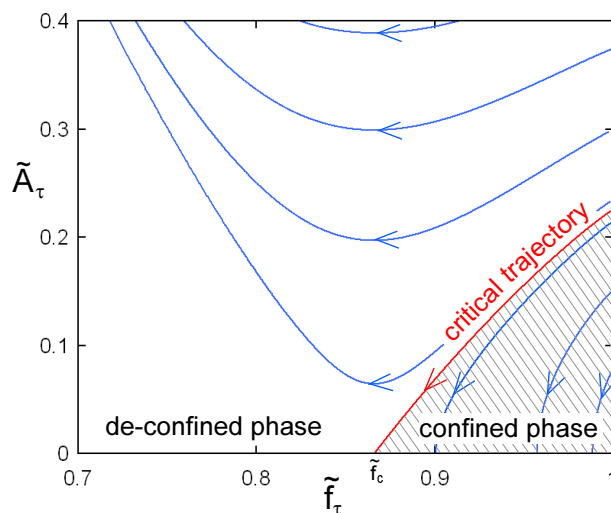
Figure 7.8: Flow diagram of equations (7.58) and (7.54) for $\tilde{A}_\tau$ and $\tilde{f}_\tau(\pi)$. Note the finite region where the system flows into a confined phase.

strength to observe this behaviour is $\tilde{f}_c = \frac{\sqrt{3}}{2} \approx 0.866$. Additionally there is an upper bound $\tilde{A}_c \approx 0.225$ on the bare warping of the Fermi surface (i.e. the interchain hopping amplitude) for which confinement is realized.

7.6.5   Numerics

We study the problem for a harmonic Fermi surface at general interaction strengths. We do not perform any approximations but study the full equations (7.25) and (7.28) by a numerical treatment. In figure 7.9 we have plotted the renormalized amplitude $\tilde{A}^*$ and the 3-point vertex $\tilde{\gamma}^*(\pi)$. Included in this plot are the results of a perturbative expansion using (7.50). Note that these perturbative results for the 3-point vertex are quite good even at intermediate interaction strengths. At strong interactions we observe a confinement transition as expected.

   As we performed our approximations close to confinement by expanding in powers of $\tilde{\Delta}_\tau$ we have always used the bosonic Greensfunction of a flat Fermi surface (7.44). In leading order this is justified, however we like to investigate how this approach compares to a full treatment using (7.39). Therefore we have solved (7.25) and (7.28) close to the confinement transition and calculated the critical interaction strength dependent on the bare amplitude, see figure 7.10. We observe that our approximation so far is quite good and there are only minor deviations for large bare amplitudes $\tilde{A}_0 \approx 0.2$.

   So far we have neglected the influence of higher harmonics in our calculations. One might speculate that a non-harmonic Fermi surface develops only partially flat sectors [25, 27–32]. This would lead to a truncation of the Fermi surface where only certain sectors are well defined while the Fermi surface breaks down in the
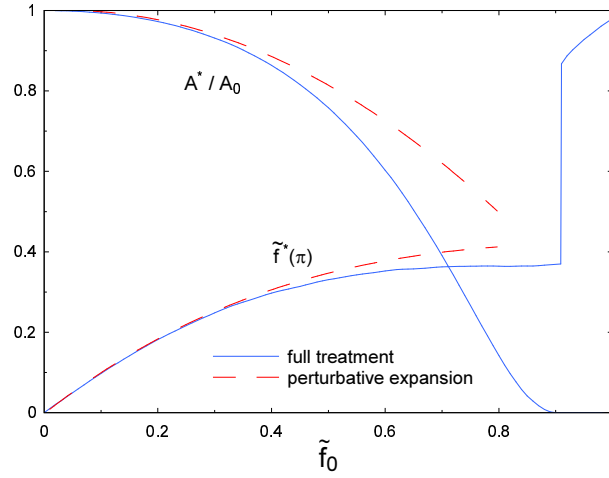
Figure 7.9: Numerical solution of (7.25) and (7.28) for a harmonic Fermi surface with bare amplitude $\tilde{A}_0 = 0.1$ at various interaction strengths. Additionally the results of a perturbative expansion (7.50) are included.
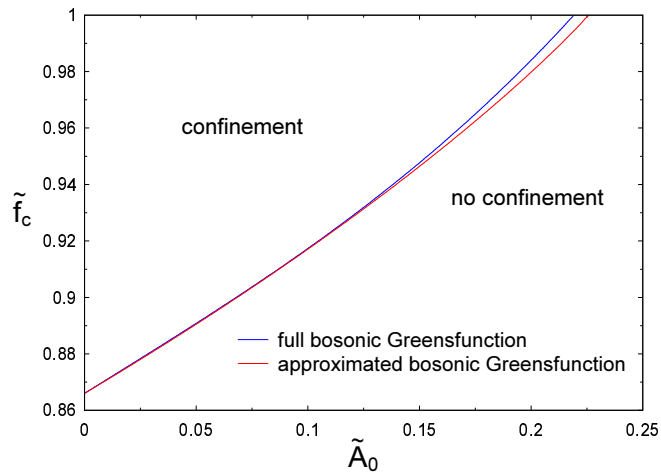
Figure 7.10: Comparison of the critical interaction strength between using the full bosonic Greensfunction (7.39) and the one for a flat Fermi surface (7.44).

confined regions. We have numerically studied various different bare shapes but never observed such a partial confinement. We argue that this behaviour might be a consequence of the topology of the Fermi surface. While in the problem at hand the Fermi surface is disconnected the situation could change for a nearly square shaped one which might get renormalized to consist of flat sectors at the faces of the square and regions of large curvature at the edges. There are some hints for this behaviour from [109].

7.7 Summary

In this chapter we consider the problem of finding the true Fermi surface for a two-dimensional system of infinitely many coupled metallic chains. The Fermi surface here consists of two disconnected weakly curved sheets. We are especially interested if at strong coupling the system undergoes a confinement transition where the sheets of the Fermi surface are completely flat. Considering a symmetric density-density interaction we study the deformation of the Fermi surface in different approximations. Starting with a perturbative treatment which indicates the tendency toward confinement we perform a 1-loop calculation which postulates a confinement transition at $\tilde{f}_c = 1$. As a next step we include vertex renormalizations and study the resulting flow equations in various limits. As the 3-point vertices at strong coupling are stabilized by interaction processes the system stays at strong coupling and indeed flows into a confined phase.

Earlier studies [102–108] revealed that on energy scales larger than the interchain hopping the system behaves as a quasi one-dimensional Luttinger liquid whereas on lower scales there is a crossover to a two-dimensional Fermi liquid. Within our formulation this crossover is reached when the interaction cutoff becomes comparable to the renormalized warping of the Fermi surface. At weak and intermediate coupling strengths we observe the same crossover as the anomalous dimension vanishes leaving the quasiparticle weight finite. The novel result of this work is that at strong coupling the Fermi surface becomes strongly renormalized such that the renormalized warping is always smaller than the interaction cutoff. Therefore the crossover regime is never reached and the system is stabilized at a non-Fermi liquid fixed point with an anomalous dimension larger than one.

We do not observe a partial confinement as observed for systems with a closed Fermi surface [25, 27–29, 31, 32] where only certain sectors of the Fermi surface remain well defined.

Chapter 8

Summary

The topic of this thesis is the functional renormalization group. There are a variety of different implementations of this procedure [10, 15, 17, 26, 120] however these approaches generally neglect the rescaling of fields and vertices as it has been advocated for by Wilson [6]. A formulation which explicitly takes these rescalings into account has been developed by [20, 21, 38] for interacting fermions and in a more general form by [39–41]. We follow these approaches with rescaled fields and vertices and discuss some approximations schemes. Thereafter in the main part of this thesis we apply these approximations to study different fields of condensed matter physics.

8.1   Approximations

Generally we reduce the problem into the determination of an infinite set of vertex functions (most conveniently one-particle irreducible) describing the scattering of particles. These vertex functions get renormalized away from their bare values governed by an infinite hierarchy of flow equations that couple different vertices with each other. We cannot expect to actually solve these equations in any closed form but have to apply a couple of approximations for simplification. The aim is to somehow separate relevant contributions from irrelevant ones and to neglect the latter in leading order. One possible scheme opens up if we rescale fields and vertices as described above. Here the term "relevance" is used in a quantitative way to describe the scaling behaviour of vertices close to a fixed point of the RG. We therefore propose to discard contributions that are irrelevant in the quantitative sense (maybe with some kind of expansion to successively take these into account as well). Doing so leaves us with only a handful of vertices whose flow equations we can at least treat numerically. As the "irrelevant" vertices lead to quantitative renormalizations of the couplings within this approach we can generally not hope for exact quantitative predictions of bulk properties. We are much more interested in a qualitative understanding of the important processes

that determine the physics instead. Properties that do not depend on the bulk of the system (like critical exponents) can be quantitatively evaluated as well.

One disadvantage of describing the system in terms of infinitely many vertices is that the majority of these vertices we have to evaluate are not of interest to us. In most cases we are just looking for the self-energy (2-point function) or the two-particle effective interaction (4-point function). However there might be contributions to the flow of these vertices that are generated by irrelevant vertices. We generally assume that we can express irrelevant vertices in terms of the relevant and marginal ones [9, 18]. Then in turn it should be possible to write the contributions of these irrelevant vertices to the flow of relevant and marginal ones in terms of relevant and marginal vertices as well. We show how this can be achieved by what we term the adiabatic approximation which we present for the Greensfunction of a bosonized interaction. This approximation allows us later on to calculate the true fermi surface of strongly interacting fermions in one and two dimensions in a self-consistent way. We argue that this adiabatic approximation might be useful in the context of other problems as well.

8.2   Weakly interacting bosons

After the discussion of these approximation schemes we consider weakly interacting bosons in $3 + \epsilon$ dimension at the critical point of Bose-Einstein condensation. As the transition takes place at a finite temperature T_c this temperature defines an effective ultraviolet cut-off. For the investigation of physical properties that depend on momenta smaller than this cut-off it is therefore sufficient to describe the system of interacting bosons by a classical field theory. In a first approximation we just consider relevant and marginal vertices and solve the flow equations in an iterative way. Our central topic here is the self-energy of the bosons and we are able to evaluate it with the full momentum dependence (4.56)

$$\sigma(x) \;\; = \;\; \frac{3\tilde{g}^{*2}}{2} x^{2-\eta^*} \int_0^\infty dy \, \frac{1}{y} \frac{1}{(x+y)^{2-2\eta^*}} F(x, y, x_c, \eta^*) \,.$$

For small momenta it approaches a scaling form and as the momentum is gradually increased we observe a crossover to the perturbative regime . Unfortunately there are no experimental data to compare our results with and we have to look for indirect validations. As a test for the reliability of our expression for the self-energy we investigate the interaction induced shift of the critical temperature which is related to the former along the complete momentum interval [76]. Our results compare quite satisfactory to the best available estimates for this shift.

Regarding the fixed point values of other vertices, especially the anomalous dimension, our approach predicts the correct order of magnitude however with a considerable error. As an improvement we include more vertices into our investigation and consider even irrelevant ones up to a certain magnitude. Here we

observe that our fixed point estimates indeed approach the best known results but this convergence is quite weak. We assume that this lack of fast convergence can be attributed to the sharp cutoff we use in our formulation of the renormalization group, and note that the momentum scale expansion of Morris [44, 46, 55] is plagued similarly. Therefore it might prove successful to improve these convergence properties by the application of different cutoff schemes like e.g. the Litim cutoff [43, 47]. However we do not pursue this topic further.

8.3   The Fermi surface of interacting fermions

We turn toward systems of interacting fermions. The formulation of the functional renormalization group implicitly requires knowledge of the true Fermi surface of the full interacting system. In general however we can just calculate it a-posteriori from the self-energy. We argue that the Fermi surface is a fixed point property of the system and consequently has to be regarded as a fixed point manifold in some self-consistent way. The requirement to flow into a fixed point can be translated into a fine-tuning of the frequency/momentum independent part $\tilde{r}_0$ of the rescaled 2-point function. We show how this bare value is related to the momentum dependent effective interaction along the complete trajectory of the RG (5.23)

$$\tilde{r}_0(\mathbf{q}_\perp) \;\; = \;\; -\int_0^\infty d\tau \, e^{-\tau(1-\bar{\eta}_\tau(\mathbf{q}_\perp))} \int_{\mathbf{Q}'} \dot{\tilde{G}}_\tau(\mathbf{Q}') \tilde{\Gamma}_\tau^{(4)}(\mathbf{Q}_0, \mathbf{Q}'; \mathbf{Q}', \mathbf{Q}_0) \; .$$

On the other hand $\tilde{r}_0$ expresses the difference between the bare and the true Fermi surface [38]. Putting both equations together results into an exact self-consistency equation for the Fermi surface. This self-consistency equation can be expressed in terms of un-rescaled vertices as well. In leading order then it reduces to the well known Hartree-Fock result for the self-energy.

We apply our self-consistency equation above to tackle the problem of finding the true Fermi surface of interacting fermions in low dimensions. The most simple non-trivial model with an inhomogeneous Fermi surface is a system of two coupled metallic chains. Here the band structure consists of two bands which on the bare level are separated by twice the interchain hopping amplitude. We only consider the case of a monotonic dispersion such that the Fermi surface is defined by a set of just four momenta. Starting with a purely fermionic treatment we evaluate the shift of the Fermi surface pertubatively. The process of interband backward scattering leads to a smoothing of the Fermi surface, termed confinement. Of special interest is if the confinement is complete such that the Fermi momenta of the two bands collapse into just one value. We propose the term *confinement transition* for this behaviour.

Actually we cannot expect to observe such a transition within a perturbative treatment. Therefore we bosonize the interband backward scattering by means of

a Hubbard-Stratonovich transformation and treat our system as a single channel problem. This bosonization together with the adiabatic approximation allows us to investigate the system even at strong coupling. We cannot exclude the possibility of inadvertently having neglected other non-perturbative strong coupling contributions by our specific scheme of truncation. Our results therefore have to be viewed as a sensible extrapolation of the weak coupling analysis to strong coupling. However guided by the appearance and implications of our results we assume that our approach covers all essential parts. Within a simple one-loop treatment our method predicts a confinement transition at strong coupling. However taken vertex renormalizations into account we observe that this confinement is destroyed by fluctuations beyond one-loop. Actually we observe how the confined phase can be stabilized by the inclusion of interband umklapp scattering (= pair tunnelling).

As we have gained some knowledge on how our simple toy model behaves we consider the physically more relevant case of a two-dimensional system of infinitely many coupled metallic chains. Here the Fermi surface consists of two disconnected weakly curved sheets. The observation of a confinement transition would mean that these sheets of the true Fermi surface are exactly flat. In the context of cuprate superconductivity there is a considerable interest in such a transition as it might open the possibility to explain the anomalous properties observed in terms of non Fermi liquid behaviour [33–36]. Bosonizing the interaction between the fermions which we take to be of the density-density type we are able to repeat the calculations we have performed for our toy model. Within a self-consistent 2-loop calculation indeed signs for a confinement transition at finite coupling strength emerge.

This transition is additionally reflected in the non-trivial dependence on transversal momentum of the 3-point vertex describing the scattering of fermions by the bosonized interaction. A confined Fermi surface always implies that the corresponding anomalous dimension become larger than one. In that case the notion of a Fermi surface actually breaks down as the momentum dependence of the fermion distribution function becomes smooth. It has been proposed

[25, 27, 30–32] that in high-T_c superconductors the confinement could only be partial such that only certain sectors of the Fermi surface become flat. We do not observe such a behaviour for our model and argue that this might be attributed to the topology of the Fermi surface - the bare Fermi surface for the superconductors is nearly square shaped whereas for our model it consists of two disconnected parts. We propose that it should be attempted to apply our method to a system
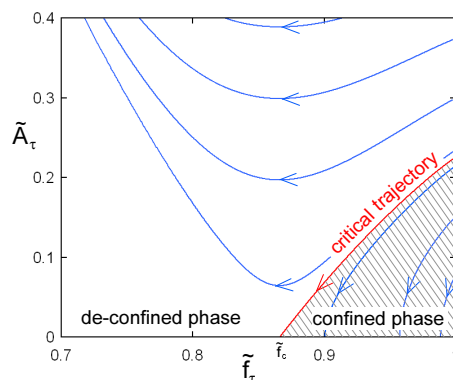
with such a nearly square shaped Fermi surface as it is realized within a two-dimensional Hubbard-model with suitable hopping amplitudes and filling factor. Here it should be most promising to divide the Fermi surface into four nearly flat patches to expand momenta around. We do not attempt this treatment here but leave it to future research.

Appendix A

Weakly interacting bosons

A.1 Flow equations for bosonic 6-point and 8-point vertices

To improve our calculations of the weakly interacting bose gas we need the flow equations for the 6-point and 8-point vertex. We use the symmetrizing operator $\mathcal{S}$ which is defined as

$$
\begin{aligned}
\mathcal{S}_{1,2,3} f(1,2,3) &= \frac{1}{6} \left[f(1,2,3) + f(2,3,1) + f(3,1,2) \right. \\
&\qquad \left. + f(3,2,1) + f(2,1,3) + f(1,3,2) \right] , \qquad \text{(A.1)} \\
\mathcal{S}_{1,(2,3)} f(1,2,3) &= \mathcal{S}_{(2,3),1} f(1,2,3) \\
&= \frac{1}{3} \left[f(1,2,3) + f(2,1,3) + f(3,2,1) \right] . \qquad \text{(A.2)}
\end{aligned}
$$

The generalization to more indices as we will need in a moment in straightforward. The flow equation of the six-point vertex has been derived by [18] as

$$
\begin{aligned}
\dot{\tilde{\Gamma}}_\tau^{(6)}(\mathbf{q}_1', \mathbf{q}_2', \mathbf{q}_3', \mathbf{q}_3, \mathbf{q}_2, \mathbf{q}_1) &= \int_{\mathbf{q}} \dot{\tilde{G}}_\tau(\mathbf{q}) \tilde{\Gamma}_\tau^{(8)}(\mathbf{q}_1', \mathbf{q}_2', \mathbf{q}_3', \mathbf{q}, \mathbf{q}, \mathbf{q}_3, \mathbf{q}_2, \mathbf{q}_1) \\
&\quad -3\int_{\mathbf{q}} \Big\{ \mathcal{S}_{3,(2,1)} \Big[\dot{\tilde{G}}_\tau(\mathbf{q}) \tilde{G}_\tau(\mathbf{q}') \tilde{\Gamma}_\tau^{(6)}(\mathbf{q}_1', \mathbf{q}_2', \mathbf{q}_3'; \mathbf{q}_3, \mathbf{q}', \mathbf{q}\tilde{\Gamma}_\tau^{(4)}(\mathbf{q}, \mathbf{q}'; \mathbf{q}_2, \mathbf{q}_1) \Big]_{\mathbf{q}'=\mathbf{q}_1+\mathbf{q}_2-\mathbf{q}} \\
&\quad + \mathcal{S}_{(1',2'),3'} \Big[\dot{\tilde{G}}_\tau(\mathbf{q}) \tilde{G}_\tau(\mathbf{q}') \tilde{\Gamma}_\tau^{(4)}(\mathbf{q}_1', \mathbf{q}_2'; \mathbf{q}', \mathbf{q}) \tilde{\Gamma}_\tau^{(6)}(\mathbf{q}, \mathbf{q}', \mathbf{q}_3'; \mathbf{q}_3, \mathbf{q}_2, \mathbf{q}_1) \Big]_{\mathbf{q}'=\mathbf{q}_1'+\mathbf{q}_2'-\mathbf{q}} \Big\} \\
&\quad -9 \int_{\mathbf{q}} \mathcal{S}_{(1',2'),3'} \mathcal{S}_{3,(2,1)} \Big[[\dot{\tilde{G}}_\tau(\mathbf{q}) \tilde{G}_\tau(\mathbf{q}') + \tilde{G}_\tau(\mathbf{q}) \dot{\tilde{G}}_\tau(\mathbf{q}')] \\
&\qquad\qquad \times \tilde{\Gamma}_\tau^{(4)}(\mathbf{q}_3', \mathbf{q}'; \mathbf{q}, \mathbf{q}_3) \tilde{\Gamma}_\tau^{(6)}(\mathbf{q}_1', \mathbf{q}_2', \mathbf{q}; \mathbf{q}', \mathbf{q}_2, \mathbf{q}_1) \Big]_{\mathbf{q}'=\mathbf{q}_3-\mathbf{q}_3'+\mathbf{q}} \\
&\quad +9 \int_{\mathbf{q}} \mathcal{S}_{(1',2'),3'} \mathcal{S}_{3,(2,1)} \Big[[\dot{\tilde{G}}_\tau(\mathbf{q}) \tilde{G}_\tau(\mathbf{q}') \tilde{G}_\tau(\mathbf{q}'') + \tilde{G}_\tau(\mathbf{q}) \dot{\tilde{G}}_\tau(\mathbf{q}') \tilde{G}_\tau(\mathbf{q}'') \\
&\qquad\qquad + \tilde{G}_\tau(\mathbf{q}) \tilde{G}_\tau(\mathbf{q}') \dot{\tilde{G}}_\tau(\mathbf{q}'')]
\end{aligned}
$$

117

$$\times\tilde{\Gamma}_\tau^{(4)}(\mathbf{q}_1', \mathbf{q}_2'; \mathbf{q}, \mathbf{q}')\tilde{\Gamma}_\tau^{(4)}(\mathbf{q}_3', \mathbf{q}'; \mathbf{q}'', \mathbf{q}_3)\tilde{\Gamma}_\tau^{(4)}(\mathbf{q}'', \mathbf{q}; \mathbf{q}_2, \mathbf{q}_1)\Big]_{\mathbf{q}'=\mathbf{q}_1'+\mathbf{q}_2'-\mathbf{q}}^{\mathbf{q}''=\mathbf{q}_1+\mathbf{q}_2-\mathbf{q}}$$

$$+36\int_{\mathbf{q}} \mathcal{S}_{1',2',3'}\mathcal{S}_{1,2,3}\Big[\dot{\tilde{G}}_\tau(\mathbf{q})\tilde{G}_\tau(\mathbf{q}')\tilde{G}_\tau(\mathbf{q}'')$$

$$\times\tilde{\Gamma}_\tau^{(4)}(\mathbf{q}_1', \mathbf{q}'; \mathbf{q}, \mathbf{q}_1)\tilde{\Gamma}_\tau^{(4)}(\mathbf{q}_2', \mathbf{q}''; \mathbf{q}', \mathbf{q}_2)\tilde{\Gamma}_\tau^{(4)}(\mathbf{q}_3', \mathbf{q}; \mathbf{q}'', \mathbf{q}_3)\Big]_{\mathbf{q}'=\mathbf{q}_1-\mathbf{q}_1'+\mathbf{q}}^{\mathbf{q}''=\mathbf{q}_3'-\mathbf{q}_3+\mathbf{q}}. \tag{A.3}$$

We will also need the following parts of the flow equation for the 8-point vertex generated by $\tilde{\Gamma}^{(6)}$,

$$\dot{\tilde{\Gamma}}_\tau^{(8)}(\mathbf{q}_1', \mathbf{q}_2', \mathbf{q}_3', \mathbf{q}_4'; \mathbf{q}_4, \mathbf{q}_3, \mathbf{q}_2, \mathbf{q}_1) =$$
$$-16\int_{\mathbf{q}} \mathcal{S}_{(1,2,3),4}\mathcal{S}_{(1',2',3'),4'}\Big[\dot{\tilde{G}}_\tau(\mathbf{q})\tilde{G}_\tau(\mathbf{q}')$$
$$\times\tilde{\Gamma}_\tau^{(6)}(\mathbf{q}_1', \mathbf{q}_2', \mathbf{q}_3'; \mathbf{q}_4, \mathbf{q}', \mathbf{q})\tilde{\Gamma}_\tau^{(6)}(\mathbf{q}, \mathbf{q}', \mathbf{q}_4'; \mathbf{q}_3, \mathbf{q}_2, \mathbf{q}_1)\Big]_{\mathbf{q}'=\mathbf{q}_1'+\mathbf{q}_2'+\mathbf{q}_3'-\mathbf{q}_4-\mathbf{q}}$$
$$-9\int_{\mathbf{q}} \mathcal{S}_{(1',2'),(3',4')}\mathcal{S}_{(1,2),(3,4)}\Big[[\dot{\tilde{G}}_\tau(\mathbf{q})\tilde{G}_\tau(\mathbf{q}') + \tilde{G}_\tau(\mathbf{q})\dot{\tilde{G}}_\tau(\mathbf{q}')]$$
$$\times\tilde{\Gamma}_\tau^{(6)}(\mathbf{q}_3', K_4', \mathbf{q}'; \mathbf{q}, \mathbf{q}_4, \mathbf{q}_3)\tilde{\Gamma}_\tau^{(6)}(\mathbf{q}_1', \mathbf{q}_2', \mathbf{q}; \mathbf{q}', \mathbf{q}_2, \mathbf{q}_1)\Big]_{\mathbf{q}'=\mathbf{q}_1'+\mathbf{q}_2'-\mathbf{q}_1-\mathbf{q}_2+\mathbf{q}}$$
$$+ \dots \tag{A.4}$$

A.2 The anomalous dimension including irrelevant terms

Here we present the necessary formulas to calculate the anomalous dimension including irrelevant contributions form the 6-point and 4-point vertex. We will need the following average over the 6-point vertex

$$\partial_{q^2}\left\langle\dot{\tilde{\Gamma}}_\tau^6(\lambda\mathbf{q}, \lambda\hat{\mathbf{q}}', \lambda'\hat{\mathbf{q}}''; \lambda'\hat{\mathbf{q}}'', \lambda\hat{\mathbf{q}}', \lambda\mathbf{q})\right\rangle_{\hat{\mathbf{q}}',\hat{\mathbf{q}}''}\Big|_{q^2=0} = \tag{A.5}$$
$$-\tilde{v}_\tau\Big\{3\tilde{g}_\tau\left[\dot{\tilde{\chi}}_\tau''(\lambda, \lambda) + \dot{\tilde{\chi}}_\tau''(\lambda, \lambda')\right]$$
$$+2(2\tilde{a}_\tau + \tilde{b}_\tau)[\dot{f}_\tau''(\lambda, \lambda) + \dot{f}_\tau''(\lambda, \lambda') + \dot{\alpha}_\tau(\lambda, \lambda')] + (\tilde{a}_\tau + \tilde{b}_\tau)\dot{\varphi}_\tau''(\lambda)\Big\},$$

with

$$\dot{f}_\tau''(\lambda, \lambda') = \frac{\partial}{\partial q^2}\left\langle\dot{f}_\tau(\lambda\mathbf{q}, \lambda'\hat{\mathbf{q}}')\right\rangle_{\hat{\mathbf{q}}'}\Big|_{q^2=0}$$
$$= \frac{-\lambda^2(1+\lambda')^2 + \lambda^2(3+2\lambda')\tilde{r}_\tau}{12\lambda'(1+\tilde{r}_\tau)\left[(1+\lambda')^2+\tilde{r}_\tau\right]^2}, \tag{A.6}$$
$$\dot{\varphi}_\tau''(\lambda) = \dot{\chi}_\tau(0)\frac{\partial}{\partial q^2}\left\langle|\hat{\mathbf{q}}' + \lambda\mathbf{q}|\right\rangle_{\hat{\mathbf{q}}'}\Big|_{q^2=0} = \frac{\lambda^2}{3(1+\tilde{r}_\tau)^2}, \tag{A.7}$$

$$
\begin{aligned}
\dot{\chi}''_\tau(\lambda, \lambda') &= \frac{2}{1 + \tilde{r}_\tau} \frac{\partial}{\partial q^2} \left\langle \tilde{G}_\tau \left(\lambda \mathbf{q} + \lambda' \hat{\mathbf{q}}'' + \hat{\mathbf{q}}'\right)\right\rangle_{\hat{\mathbf{q}}', \hat{\mathbf{q}}''}\Bigg|_{q^2 = 0} \\
&= \frac{\lambda^2[\tilde{r}_\tau - (1 + \lambda')^2]}{6(1 + \tilde{r}_\tau)\lambda'[(1 + \lambda')^2 + \tilde{r}_\tau]^2} \ , \qquad\qquad\qquad (A.8) \\
\dot{\alpha}_\tau(\lambda, \lambda') &= \frac{1}{1 + \tilde{r}_\tau} \frac{\partial}{\partial q^2} \left\langle \tilde{G}_\tau \left(\lambda \mathbf{q} + \lambda' \hat{\mathbf{q}}'' + \hat{\mathbf{q}}'\right) |\lambda \mathbf{q} + \lambda' \hat{\mathbf{q}}''|\right\rangle_{\hat{\mathbf{q}}', \hat{\mathbf{q}}''}\Bigg|_{q^2 = 0} \\
&= \frac{\lambda^2[(1 + \lambda')^2(2 + \lambda') + (2 + 3\lambda')\tilde{r}_\tau]}{12(1 + \tilde{r}_\tau)\lambda'[(1 + \lambda')^2 + \tilde{r}_\tau]} \qquad\qquad\qquad (A.9)
\end{aligned}
$$

and

$$
\begin{aligned}
\dot{f}_\tau(\mathbf{q}_1, \mathbf{q}_2) &= \frac{1}{1 + \tilde{r}_\tau} \left\langle \frac{\Theta(1 < |\mathbf{q}_1 + \mathbf{q}_2 - \hat{\mathbf{q}}| < e^\tau)}{|\mathbf{q}_1 + \mathbf{q}_2 - \hat{\mathbf{q}}|^2 + \tilde{r}_\tau}\right. \\
&\qquad \left. \times [|\hat{\mathbf{q}} - \mathbf{q}_1| + |\hat{\mathbf{q}} - \mathbf{q}_2|]\right\rangle_{\hat{\mathbf{q}}} \ , \qquad\qquad (A.10)
\end{aligned}
$$

$$
\begin{aligned}
\dot{g}_\tau(\mathbf{q}_1, \mathbf{q}_2) &= \frac{1}{1 + \tilde{r}_\tau} \left\langle \frac{\Theta(1 < |\mathbf{q}_1 + \mathbf{q}_2 - \hat{\mathbf{q}}| < e^\tau)}{|\mathbf{q}_1 + \mathbf{q}_2 - \hat{\mathbf{q}}|^2 + \tilde{r}_\tau}\right. \\
&\qquad \left. \times [|\hat{\mathbf{q}} - \mathbf{q}_1|^2 + |\hat{\mathbf{q}} - \mathbf{q}_2|^2]\right\rangle_{\hat{\mathbf{q}}} \ , \qquad\qquad (A.11)
\end{aligned}
$$

$$
\begin{aligned}
\dot{h}_\tau(\mathbf{q}_1, \mathbf{q}_2) &= \frac{2}{1 + \tilde{r}_\tau} \left\langle \frac{\Theta(1 < |\mathbf{q}_1 + \mathbf{q}_2 - \hat{\mathbf{q}}| < e^\tau)}{|\mathbf{q}_1 + \mathbf{q}_2 - \hat{\mathbf{q}}|^2 + \tilde{r}_\tau}\right. \\
&\qquad \left. \times |\hat{\mathbf{q}} - \mathbf{q}_1||\hat{\mathbf{q}} - \mathbf{q}_2|\right\rangle_{\hat{\mathbf{q}}}. \qquad\qquad\qquad (A.12)
\end{aligned}
$$

To obtain the contributions from the BCS, ZS and ZS' parts of the 4-point vertex we need

$$
\frac{\partial}{\partial q^2} \left\langle \dot{g}_\tau \left(\lambda \mathbf{q}, \lambda \hat{\mathbf{q}}'\right)\right\rangle_{\hat{\mathbf{q}}'}\Bigg|_{q^2 = 0} = \qquad\qquad\qquad\qquad\qquad (A.13)
$$

$$
\frac{-\lambda\left[\lambda(1+\lambda)^2(2+3\lambda) + (-4 + (-2+\lambda)\lambda)\tilde{r}_\tau + 2((1+\lambda)^2 + \tilde{r}_\tau)^2 \ln\left(\frac{1+\tilde{r}_\tau}{(1+\lambda)^2 + \tilde{r}_\tau}\right)\right]}{12(1 + \tilde{r}_\tau)\left[(1 + \lambda)^2 + \tilde{r}_\tau\right]^2}
$$

$$
\frac{\partial}{\partial q^2} \left\langle \dot{f}_\tau \left(\lambda \mathbf{q}, \lambda \hat{\mathbf{q}}'\right) |\lambda \mathbf{q} + \lambda \hat{\mathbf{q}}'|\right\rangle_{\hat{\mathbf{q}}'}\Bigg|_{q^2 = 0} =
$$

$$
\begin{aligned}
&\frac{\lambda\left[8(1+\tilde{r}_\tau) + \lambda\left[(3+\lambda)^2(3 + \lambda(2+\lambda)) + 2(10 + \lambda(6+\lambda))\tilde{r}_\tau + \tilde{r}_\tau^2\right]\right]}{24(1+\tilde{r}_\tau)\left[(1+\lambda)^2 + \tilde{r}_\tau\right]^2} \\
&+ \frac{2(1 - \lambda^2 + \tilde{r}_\tau)\left[(1+\lambda)^2 + \tilde{r}_\tau\right]^2 \operatorname{arctanh}\left(\frac{\lambda\sqrt{-\tilde{r}_\tau}}{1 + \lambda + \tilde{r}_\tau}\right)}{24(1+\tilde{r}_\tau)\left[(1+\lambda)^2 + \tilde{r}_\tau\right]^2 \sqrt{-\tilde{r}_\tau}} \\
&+ \frac{(1 + \lambda^2 + \tilde{r}_\tau)\left[(1+\lambda)^2 + \tilde{r}_\tau\right]^2 \sqrt{-\tilde{r}_\tau} \ln\left(\frac{1+\tilde{r}_\tau}{(1+\lambda)^2 + \tilde{r}_\tau}\right)}{24(1+\tilde{r}_\tau)\left[(1+\lambda)^2 + \tilde{r}_\tau\right]^2 \sqrt{-\tilde{r}_\tau}} , \qquad\qquad (A.14)
\end{aligned}
$$

$$\frac{\partial}{\partial q^2} \left\langle \dot{h}_\tau \left(\lambda \mathbf{q}, \lambda \hat{\mathbf{q}}' \right) \right\rangle_{\hat{\mathbf{q}}'} \Bigg|_{q^2=0} =$$

$$-\lambda \frac{\left[(\lambda - 1)(1+\lambda)^2 \left(\lambda + \lambda^2 + 2\tilde{r}_\tau \right) + \lambda \tilde{r}_\tau^2 \right] \sqrt{-\tilde{r}_\tau}}{6(1+\tilde{r}_\tau) \left[(1+\lambda)^2 + \tilde{r}_\tau \right]^2 \sqrt{-\tilde{r}_\tau}}$$

$$-\lambda \frac{(1 - \lambda^2 - \tilde{r}_\tau) \left[(1+\lambda)^2 + \tilde{r}_\tau \right]^2 \operatorname{arctanh}\left(\frac{\lambda \sqrt{-\tilde{r}_\tau}}{1+\lambda+\tilde{r}_\tau} \right)}{6(1+\tilde{r}_\tau) \left[(1+\lambda)^2 + \tilde{r}_\tau \right]^2 \sqrt{-\tilde{r}_\tau}}, \qquad \text{(A.15)}$$

$$\dot{\chi}_\tau(0) \frac{\partial}{\partial q^2} \left\langle |\hat{\mathbf{q}}'' + \lambda \mathbf{q}| \, |\hat{\mathbf{q}}'' + \lambda \hat{\mathbf{q}}'| \right\rangle_{\hat{\mathbf{q}}', \hat{\mathbf{q}}''} \Bigg|_{q^2=0} = \frac{\lambda^2 (3 + \lambda^2)}{9(1 + \tilde{r}_\tau)^2}, \qquad \text{(A.16)}$$

$$\frac{\partial}{\partial q^2} \left\langle \dot{\chi}_\tau(|\lambda \hat{\mathbf{q}}' + \lambda \mathbf{q}|) \, |\lambda \hat{\mathbf{q}}' + \lambda \mathbf{q}|^2 \right\rangle_{\hat{\mathbf{q}}'} \Bigg|_{q^2=0} = \qquad \text{(A.17)}$$

$$\frac{\lambda^2 (1+\lambda)^2 (4 + 3\lambda) + \lambda^2 (4 + 5\lambda) \tilde{r}_\tau + \lambda \left[(1+\lambda)^2 + \tilde{r}_\tau \right]^2 \ln\left(\frac{(1+\lambda)^2 + \tilde{r}_\tau}{1 + \tilde{r}_\tau} \right)}{6(1+\tilde{r}_\tau) \left[(1+\lambda)^2 + \tilde{r}_\tau \right]^2}.$$

Using the flow equations presented in section 4.6 we can now evaluate the anomalous dimension (4.101).

Bibliography

[1] E.C.G. STÜCKELBERG AND A. PETERMAN, *On the normalizations of the quantum theory constants*, Helv. Phys. Acta **26** (1953), 499.

[2] M. GELL-MANN AND F.E. LOW, *Quantum electrodynamics at small distances*, Phys. Rev. **95** (1954), 1300.

[3] L.P. KADANOFF, *Scaling laws for Ising models near T_c*, Physics **2** (1966), 263.

[4] L.P. KADANOFF, *Static phenomena near critical points: Theory and experiment*, Rev. Mod. Phys. **39** (1974), 395.

[5] K.G. WILSON, *Renormalization group and critical phenomena. I. Renormalization group and the Kadanoff scaling picture*, Phys. Rev. B **4** (1971), 3174.

[6] K.G. WILSON, *Renormalization group and critical phenomena. II. Phase-space cell analysis of critical behavior*, Phys. Rev. B **4** (1971), 3184.

[7] K.G. WILSON AND J.G. KOGUT, *The renormalization group and the ϵ expansion*, Phys. Rep. C **12** (1974), 75.

[8] F.J. WEGNER AND A. HOUGHTON, *Renormalization group equation for critical phenomena*, Phys. Rev. A **8** (1973), 401.

[9] J. POLCHINSKI, *Renormalization and effective lagrangians*, Nucl. Phys. B **231** (1984), 269.

[10] C. BAGNULS AND C. BERVILLIER, *Exact renormalization group equations. An introductory review.*, Phys. Rept. **348** (2002), 91.

[11] S.R. WHITE, *Density matrix formulation for quantum renormalization groups*, Phys. Rev. Lett. **69** (1992), 2863.

[12] S.R. WHITE, *Density-matrix algorithms for quantum renormalization groups*, Phys. Rev. B **48** (1993), 10345.

[13] C. DiCastro, G. Jona-Lasinio and L. Peliti, *Variational principles, renormalization group and Kadanoff's universality*, Annals of Physics **87** (1974), 327.

[14] J.F. Nicoll and T.S. Chang, *An exact one-particle-irreducible renormalization-group generator for critical phenomena*, Phys. Lett. A **62** (1977), 287.

[15] J.F. Nicoll, T.S. Chang and H.E. Stanley, *Exact and approximate differential renormalization-group generators*, Phys. Rev. A **13** (1976), 1251.

[16] C. Wetterich, *Exact evolution equation for the effective potential*, Phys. Lett. B **301** (1993), 90.

[17] T.R. Morris, *The exact renormalization group and approximate solutions*, Int. J. Mod. Phys. A **9** (1994), 2411.

[18] P. Kopietz, *Two-loop β-function from the exact renormalization group*, Nucl. Phys. B **595** (2001), 493.

[19] R. Shankar, *Renormalization-group approach to interacting fermions*, Rev. Mod. Phys. **66** (1994), 129.

[20] T. Busche, *Renormalization-group approach to the spectral function of the Tomonaga-Luttinger model*, PhD thesis, Universität Frankfurt, 2003.

[21] T. Busche, L. Bartosch and P. Kopietz, *Dynamic scaling in the vicinity of the Luttinger liquid fixed point*, J. Phys. Cond. Mat. **14** (2002), 8513.

[22] A.A. Katanin and A.P. Kampf, *Renormalization group analysis of magnetic and superconducting instabilities near van Hove band fillings*, Phys. Rev. B **68** (2003), 195101.

[23] B. Binz, D. Beariswyl and B. Doucot, *Wilson's renormalization group applied to 2D lattice electrons in the presence of van Hove singularities*, Eur. Phys. J. B **25** (2002), 69.

[24] C. Honerkamp, M. Salmhofer and T.M. Rice, *Flow to strong coupling in the two-dimensional Hubbard model*, Eur. Phys. J. B **27** (2002), 127.

[25] C. Honerkamp, M. Salmhofer, N. Furukawa and T.M. Rice, *Breakdown of the Landau-Fermi liquid in two dimensions due to umklapp scattering*, Phys. Rev. B **63** (2001), 35109.

[26] C.J. Halboth and W. Metzner, *Renormalization-group analysis of the two dimensional Hubbard model*, Phys. Rev. B **61** (2000), 7364.

[27] A. Ferraz, *Non-Fermi liquid in a truncated two-dimensional Fermi surface*, Phys. Rev. B **68** (2003), 75115.

[28] A. Luther, *Interacting electrons on a square Fermi surface*, Phys. Rev. B **50** (1994), 11446.

[29] A.T. Zheleznyak, V.M. Yakovenko and I.E. Dzyaloshinskii, *Parquet solution for a flat Fermi surface*, Phys. Rev. B **55** (1997), 3200.

[30] H. Freire, E. Correa and A. Ferraz, *"Luttinger" and insulating spin liquids in two dimensions*, cond-mat/0304347 (2003).

[31] H. Freire, E. Correa and A. Ferraz, *Field-theoretical renormalization group for a flat two-dimensional Fermi surface*, Phys. Rev. B **71** (2005), 165113.

[32] N. Furukawa, T.M. Rice, and M. Salmhofer, *Truncation of a two-dimensional Fermi surface due to quasiparticle gap formation at the saddle points* , Phys. Rev. Lett. **81** (1998), 3195.

[33] D.G. Clarke, S.P. Strong, *"Confined coherence" in strongly correlated, anisotropic metals*, Adv. Phys. **46** (1997), 454.

[34] D.G. Clarke, S.P. Strong and P.W. Anderson, *Incoherence of single particle hopping between Luttinger liquids*, Phys. Rev. Lett. **72** (1994), 3218.

[35] D.G. Clarke, S.P. Strong and P.W. Anderson, *Conductivity between Luttinger liquids in the confinement regime and c-axis conductivity in the cuprate superconductors*, Phys. Rev. Lett. **74** (1995), 4499.

[36] P.W. Anderson, *The resonating valence bond state in La_2CuO_4 and superconductivity*, Science **235** (1987), 1196.

[37] M.E. Fisher, *Renormalization group theory: Its basis and formulation in statistical physics*, Rev. Mod. Phys. **70** (1998), 653.

[38] P. Kopietz and T. Busche, *Exact renormalization group flow equations for nonrelativistic fermions: Scaling towards the Fermi surface*, Phys. Rev. B **64** (2001), 155101.

[39] F. Schütz, *Aspects of strong correleations in low dimensions*, PhD thesis, Universität Frankfurt, 2005.

[40] F. Schütz and P. Kopietz, *Functional renormalization group with vacuum expectation values and spontaneous symmetry breaking*, J. Phys. A **39** (2006), 8205.

[41] F. Schütz, L. Bartosch and P. Kopietz, *Collective fields in the functional renormalization group for fermions, Ward identities, and the exact solution of the Tomonaga-Luttinger model*, Phys. Rev. B **72** (2005), 35107.

[42] J. Zinn-Justin, *Quantum Field Theory and Critical Phenomena*, Clarendon Press, Oxford, 1989.

[43] D.F. Litim, *Optimized renormalization group flows*, Phys. Rev. D **64** (2001), 105007.

[44] T.R. Morris and J.F. Tighe, *Convergence of derivative expansions of the renormalization group*, J. High Energy Phys. **8** (1999), 7.

[45] T.R. Morris, *Derivative expansion of the exact renormalization group*, Phys. Lett. B **329** (1994), 241.

[46] T.R. Morris, *Properties of derivative expansion approximations to the renormalization group*, Int. J. Mod. Phys. B **12** (1998), 1343.

[47] A. Sinner, N. Hasselmann and P. Kopietz. in preparation.

[48] J. Polchinski, *Effective field theory and the Fermi surface*, in Recent Developments in Particle Theory, Proceedings of TASI 1992, (1992), 235.

[49] J. Hubbard, *Calculation of partition functions*, Phys. Rev. Lett. **3** (1959), 77.

[50] J.A. Hertz, *Quantum critical phenomena*, Phys. Rev. B **214** (1976), 1165.

[51] P. Kopietz, *Bosonization of interacting fermions in arbitrary dimensions*, Springer, Berlin, 1997.

[52] R.L. Stratonovich, *On a method of calculating quantum distribution functions*, Doklady Akad. Nauk S.S.S.R. **115** (1959), 1097. Sov. Phys. Doklady 2, 416 (1958).

[53] J. Solyom, *The Fermi gas model of one-dimensional conductors*, Adv. Phys. **28** (1979), 201.

[54] T.R. Morris, *The derivative expansion of the renormalization group*, Nucl. Phys. B **42** (1995), 811.

[55] T.R. MORRIS, *Momentum scale expansion of sharp cutoff flow equations*, Nucl. Phys. B **458** (1996), 477.

[56] J.F. NICOLL, T.S. CHANG AND H.E. STANLEY, *Approximate renormalization group based on the Wegner-Houghton differential generator*, Phys. Rev. Lett. **33** (1974), 540.

[57] N. HASSELMANN, S. LEDOWSKI AND P. KOPIETZ, *Critical behavior of weakly interacting bosons: A functional renormalization-group approach*, Phys. Rev. A **70** (2004), 63621.

[58] D.C. MATTIS AND E.L. LIEB, *Exact solution of a many-Fermion system and its associated Boson field*, J. Math. Phys. **6** (1965), 304.

[59] J.M. LUTTINGER, *An exactly soluble model of a many-Fermion system*, J. Math. Phys. **4** (1963), 1154.

[60] S. TOMONAGA, *Remarks on Bloch's method of sound waves applied to many-fermion problems*, Prog. Theor. Phys. **5** (1950), 544.

[61] S. LEDOWSKI, N. HASSELMANN AND P. KOPIETZ, *Self-energy and critical temperature of weakly interacting bosons*, Phys. Rev. A **69** (2004), 61601.

[62] S. N. BOSE, *Plancks Gesetz und Lichtquantenhypothese*, Z. Phys **26** (1924), 178.

[63] A. EINSTEIN, *Quantentheorie des einatomigen idealen Gases*, Sitzber. Preuss. Akad. Wiss. **2** (1924), 261.

[64] A. EINSTEIN, *Quantentheorie des einatomigen idealen Gases. Zweite Abhandlung*, Sitzber. Preuss. Akad. Wiss. **1** (1925), 3.

[65] J.F. ALLEN AND A.D. MISENER, *Flow of liquid helium II*, Nature **141** (1938), 75.

[66] P.L. KAPITZA, *Viscosity of liquid helium below the λ-Point*, Nature **141** (1938), 913.

[67] F. LONDON, *The λ-Phenomenon of liquid helium and the Bose-Einstein degeneracy*, Nature **141** (1938), 643.

[68] K.B. DAVIS, M.-O. MEWES, M.R. ANDREWS, N.J. VAN DRUTEN, D.S. DURFEE, D.M. KURN AND W. KETTERLE, *Bose-Einstein condensation in a gas of sodium atoms*, Phys. Rev. Lett. **75** (1995), 3969.

[69] M.H. Anderson, J.R. Ensher, M.R. Matthews, C.E. Wiemann and E.A. Cornell, *Observation of Bose-Einstein condensation in a dilute atomic vapor*, Science **269** (1995), 198.

[70] F. Dalfovo, S. Giorgini, L.P. Pitaevskii and S.Stringari, *Theory of Bose-Einstein condensation in trapped gases*, Rev. Mod. Phys. **71** (1999), 463.

[71] L. Pitaevskii and S. Stringari, *Bose-Einstein condensation*, Clarendon Press, Oxford, 2003.

[72] Modified and reproduced with permission of W. Ketterle.

[73] D.S. Durfee and W. Ketterle, *Experimental studies of Bose-Einstein condensation*, Optics Express **2** (1998), 299.

[74] G. Baym, J.-P. Blaizot, M. Holzmann, F. Laloë and D. Vautherin, *The transition temperature of the dilute interacting Bose gas*, Phys. Rev. Lett. **83** (1999), 1703.

[75] N. Prokof'ev, O. Ruebenacker and B. Svistunov, *Weakly interacting Bose gas in the vicinity of the critical point*, cond-mat/0401002 (2004).

[76] G. Baym, J.-P. Blaizot, M. Holzmann, F. Laloë and D. Vautherin, *Bose-Einstein transition in a dilute interacting gas*, Euro. Phys. J. B **24** (2001), 107.

[77] F. Pistolesi, C. Castellani, C. Di Castro and G.C. Strinati, *Renormalization group approach to the infrared behaviour of a zero-temperature Bose system*, Phys. Rev. B **69** (2004), 24513.

[78] J.O. Andersen and M. Strickland, *Application of renormalization-group techniques to a homogeneous Bose gas at finite temperature*, Phys. Rev. A **60** (1999), 1442.

[79] M. Bjilsma and H.T.C. Stoof, *Renormalization group theory of the three-dimensional dilute Bose gas*, Phys. Rev. A **54** (1996), 5085.

[80] J.-P. Blaizot, R.Mendez Galain and N. Wschebor, *Non-Perturbative Renormalization Group calculation of the transition temperature of the weakly interacting Bose gas*, Europhys. Lett. **72** (2005), 705.

[81] M. Hasenbusch and T. Török, *High-precision Monte Carlo study of the 3D xy-universality class*, J. Phys. A **32** (1999), 6361.

[82] R. Guida and J. Zinn-Justin, *Critical exponents of the N-vector model*, J. Phys. A **31** (1998), 8103.

[83] MASUDUL HAQUE, *Weakly non-ideal Bose gas: Comments on critical temperature calculations*, preprint cond-mat/0302076 (2003).

[84] J.D. REPPY, B.C. CROOKER, B. HEBRAL, A.D. CORWIN, J. HE AND G.M. ZASSENHAUS, *Density dependence of the transition temperature in a homogeneous Bose-Einstein condensate*, Phys. Rev. Lett. **84** (2000), 2060.

[85] P. ARNOLD AND G. MOORE, *BEC transition temperature of a dilute homogeneous imperfect Bose gas* , Phys. Rev. Lett. **87** (2001), 120401.

[86] V.A. KASHURNIKOV, N.V. PROKOF'EV AND B.V. SVISTUNOV, *Critical temperature shift in weakly interacting Bose gas*, Phys. Rev. Lett. **87** (2001), 120402.

[87] H. KLEINERT, *Five-loop critical temperature shift in weakly interacting homgeneous Bose-Einstein condensates*, Mod. Phys. Lett. B **17** (2003), 1011.

[88] B. KASTENING, *Bose-Einstein condensation temperature of homogeneous weakly interacting Bose gas in variational perturbation theory through six loops*, Phys. Rev. A **69** (2004), 43613.

[89] J.O. ANDERSEN, *Theory of the weakly interacting Bose gas*, Rev. Mod. Phys. **76** (2004), 599.

[90] S. LEDOWSKI AND P. KOPIETZ, *Exact integral equation for the renormalized Fermi surface*, J. Phys. Cond. Mat **15** (2003), 4779.

[91] W. KOHN AND J.M. LUTTINGER, *Ground state energy of a many-fermion system*, Phys. Rev. **118** (1960), 41.

[92] P. NOZIERES, *Theory of interacting Fermi systems*, Benjamin, New York, 1964.

[93] A. NEUMAYR AND W. METZNER, *Renormalized perturbation theory for Fermi systems: Fermi surface deformation and superconductivity in the two-dimensional Hubbard model*, Phys. Rev. B **67** (2002), 35112.

[94] P.W. ANDERSON, *Criterion for validity of many-body perturbation theory of the electron gas*, Phys. Rev. Lett. **71** (1993), 1220.

[95] A. FERRAZ, *Fermi surface renormalization in two spacial dimensions*, Europhys. Lett. **61** (2002), 228.

[96] J. GONZALEZ, F. GUINEA AND M.A.H. VOZMEDIANO, *Kinematics of electrons near a van Hove singularity*, Phys. Rev. Lett. **84** (2000), 4930.

[97] J.M. Luttinger, *Fermi surface and some simple equilibrium prperties of a system of interacting Fermions*, Phys. Rev. **119** (1960), 1153.

[98] S. Ledowski and P. Kopietz, *Fermi surface renormalization and confinement in two coupled metallic chains*, Phys. Rev. B **75** (2007), 45134.

[99] S. Ledowski, P. Kopietz and A. Ferraz, *Self-consistent Fermi surface renormalization in two coupled Luttinger liquids*, Phys. Rev. B **71** (2005), 235106.

[100] I.J. Pomeranchuk, *Stability of a Fermi liquid*, Zh. Eksp. Teor. Fiz. **35** (1958), 524. Sov. Phys. JETP **8**, 361 (1958).

[101] I.M. Lifshitz, *Anomalies of electron characteristics of a metal in the high pressure region*, Zh. Eksp. Teor. Fiz. **38** (1960), 1569. Sov. Phys. JETP **11**, 1130 (1960).

[102] D. Boies, C. Bourbonnais and A.-M.S. Tremblay, *One-particle and two-particle instability of coupled Luttinger liquids*, Phys. Rev. Lett. **74** (1995), 968.

[103] E. Arrigoni, *Interchain coherence of coupled Luttinger liquids at all orders in perturbation theory*, Phys. Rev. Lett. **80** (1998), 790.

[104] E. Arrigoni, *Crossover from Luttinger- to Fermi-liquid behavior in strongly anisotropic systems in large dimensions*, Phys. Rev. Lett. **83** (1999), 128.

[105] E. Arrigoni, *Crossover to Fermi-liquid behavior for weakly coupled Luttinger liquids in the anisotropic large-dimension limit*, Phys. Rev. B **61** (2000), 7909.

[106] P. Kopietz, V. Meden and K. Schönhammer, *Anomalous scaling and spin-charge separation in coupled chains*, Phys. Rev. Lett. **74** (1994), 2997.

[107] P. Kopietz, V. Meden, and K. Schönhammer, *Crossover between Luttinger and Fermi-liquid behavior in weakly coupled metallic chains*, Phys. Rev. B **56** (1997), 7232.

[108] X.G. Wen, *Metallic non-Fermi liquid fixed point in two and higher dimensions*, Phys. Rev. B **42** (1990), 6623.

[109] R. Roldan, M.P. Lopez-Sancho, F. Guinea and S.-W. Tsai, *Self-energy corrections to anisotropic Fermi surfaces*, cond-mat/0612368 (2006).

[110] F. KUSMARTSEV, A.LUTHER, A.A. NERSESYAN AND D. PARSONS, *Theory of a 2D Luttinger liquid*, Zh. Eksp. Teor. Fiz **55** (1992), 692. JETP Lett. **55**, 724 (1992).

[111] K. HAMACHER, C. GROS AND W. WENZEL, *Interaction-induced collapse of a section of the Fermi sea in the zigzag Hubbard ladder*, Phys. Rev. Lett. **88** (2002), 217203.

[112] K. LOUIS, J.V. ALVAREZ AND C. GROS, *Fermi surface renormalization in Hubbard ladders*, Phys. Rev. B **64** (2001), 113106.

[113] M. FABRIZIO, *Role of transverse hopping in a two-coupled-chains model*, Phys. Rev. B **48** (1993), 15838.

[114] S. DUSUEL AND B. DOUCOT, *Interaction-induced Fermi surface deformations in quasi-one-dimensional electronic systems*, Phys. Rev. B **67** (2003), 205111.

[115] U. LEDERMANN AND K. LE HUR, *Phases of the two-band model of spinless fermions in one dimension*, Phys. Rev. B **61** (2000), 2497.

[116] V.M. YAKOVENKO, *Once again about interchain hopping*, Zh. Eksp. Teor. Fiz. **56** (1992), 523. JETP Lett. **56**, 510 (1992).

[117] S.A. BRAZOVSKII AND V.M. YAKOVENKO, *On the theory of the organic superconducting materials*, Zh. Eksp. Teor. Fiz. **89** (1985), 2318. Sov. Phys JETP **62**, 1340 (1985).

[118] R.M. CORLESS, G.H. GONNET, D.E.G. HARE, D.J. JEFFRY AND D.E. KNUTH, *On The Lambert W function*, Adv. Comp. Maths. **5** (1996), 329.

[119] S. LEDOWSKI AND P. KOPIETZ, *Confined coherence in quasi one-dimensional metals*, cond-mat/0703540 (2007).

[120] M. SALMHOFER AND C. HONERKAMP, *Fermionic Renormalization Group Flows*, Prog. Theor. Phys. **105** (2001), 1.

Deutsche Zusammenfassung

Einleitung

Starke Korrelationen und nicht-perturbative Effekte in quantenmechanischen Viel-teilchensystemen führen zu einer Vielzahl interessanter physikalischer Phänomene und stellen nach wie vor eine Herausforderung an ihre theoretische Beschrei-bung dar. In einer Raumdimension sind einige Quantensysteme durch Boson-isierung oder Bethe-Ansatz lösbar. Allerdings sind diese Methoden im Allge-meinen für die Behandlung höher dimensionaler Systeme ungeeignet. Ebenso existiert keine zufriedenstellende Verallgemeinerung des Luttinger-Flüssigkeits Konzepts auf höhere Dimensionen. Auf der anderen Seite sind Landaus Fermi-Flüssigkeits Theorie, die elementare Anregungen eines normalen fermionischen Systems durch sogenannte Quasiteilchen beschreibt, und Meanfield Verfahren meist nur für Systeme in drei oder mehr Raumdimensionen adäquat. Die Meth-ode der Störungstheorie ist schon aufgrund ihrer Definition zur Beschreibung stark wechselwirkender Felder ungeeignet.

Viele prominente experimentelle Entdeckungen der letzten Jahre, wie bei-spielsweise die Hochtemperatur Supraleitung, wurden in stark wechselwirkenden (quasi) zweidimensionalen Systemen gemacht, wo keine der oben beschriebenen Methoden anwendbar ist. Während der zweiten Hälfte des letzten Jahrhun-derts wurde das mächtige Verfahren der Renormierungsgruppe (RG) entwick-elt, welches inhärent nicht-perturbativ ist und vielversprechend erscheint, das Verständnis starker Wechselwirkung voranzutreiben.

Ursprünglich wurde die Renormierunggruppen Theorie entwickelt um Diver-genzen, die in der quantenfeldtheoretischen Beschreibung von Elementarteilchen auftauchen, in eine Neudefinition der Wechselwirkungskonstanten zu absorbieren. Die bahnbrechenden Arbeiten von Kadanoff [3, 4] und Wilson [5–7] erkannten die Nuetzlichkeit der Renormierungsgruppe zur Lösung von Problemen der statis-tischen Physik und der kondensierten Materie. Es konnte nun unter anderem verstanden werden weshalb unterschiedlichste physikalische Systeme am kritis-chen Punkt in nur wenige sogenannte Universalitätsklassen fallen, mit jeweils identischen kritischen Exponenten innerhalb einer Klasse. Ebenso konnten das Auftreten oberer kritischer Dimensionen mit einem Übergang zum Meanfield Ver-halten sowie bestimmte Relationen zwischen den kritischen Exponenten zufrieden-stellend geklärt werden.

Vorangetrieben durch Weiterentwicklungen von [8, 9, 16, 17] ist die elegante Formulierung der funktionalen Renormalisierungsgruppe (fRG) für einteilchen-irreduzible Greensfunktionen entstanden, die mittlerweile erfolgreich auf eine Vielzahl unterschiedlicher Probleme angewandt wurde. In den letzten Jahren rückten fermionische Systeme in den Fokus und insbesondere das zweidimensio-

nale Hubbard Modell, welches für ein Verständnis der Hochtemperatur Supraleitung als relevant erachtet wird, wurde vielfach untersucht.

Diese Arbeit widmet sich Anwendungen der funktionalen Renormierungsgruppe auf wechselwirkende Fermi- und Bosegase. Nach einer allgemeinen Diskussion des grundlegenden Formalismus und einiger Näherungsmethoden werden unterschiedliche Quantensysteme untersucht. Zum einen werden schwach wechselwirkende Bosonen in $3 + \epsilon$ Dimensionen am kritischen Punkt der Bose-Einstein Kondensation betrachtet. Hier liegt der Schwerpunkt auf der Berechnung der impulsabhängigen Selbstenergie. Zum anderen wird ein Verfahren zur selbstkonsistenten Bestimmung der Fermifläche stark wechselwirkender Fermionen entwickelt und im folgenden auf ein- und zweidimensionale metallische Systeme angewandt.

Näherungsverfahren

Innerhalb einer Renormierungsgruppen Behandlung reduziert man gewöhnlich das Problem darauf die Menge unendlich viele Vertexfunktionen zu bestimmen. Diese Vertexfunktionen sind wiederum durch eine unendliche Hierarchie von Flussgleichungen miteinander gekoppelt und es ist bis auf wenige spezielle Ausnahmen immer aussichtslos diese exakt zu lösen. Es ist deshalb von großer Wichtigkeit geeignete Trunkierungs- und Näherungsverfahren zu entwickeln, um dennoch qualitativ korrekte Aussagen über das physikalische Verhalten dieser Systeme machen zu können. In der Nähe eines Fixpunktes stellt die Renormierungsgruppen Analyse durch eine Quantifizierung der Ausdrücke relevant und irrelevant anhand der unterschiedlichen Skalendimensionen der Vertexfunktionen solch eine Unterscheidung zur Verfügung. Es erscheint somit natürlich in einer ersten Näherung nur relevante und marginale Vertices zu betrachten, was zu einer geeigneten Trunkierung der Flussgleichungen führt. Auf diese Weise erzielte Resultate lassen sich dann sukzessive durch den Einschluss irrelevanter Vertices verbessern. Wir verwenden dieses Verfahren in allen folgenden Untersuchungen.

Das qualitative Verhalten eines physikalischen Systems wird durch die nicht-irrelevanten Vertices bestimmt. Nun kann davon ausgegangen werden, das sich alle irrelevanten Vertices durch relevante und marginale ausdrücken lassen [9, 18]. Damit sollte es auch möglich sein Anteile an den Flussgleichungen für relevante und marginale Vertices die durch irrelevante generiert werden wiederum durch die relevanten und marginalen Vertices auszudrücken, und damit prinzipiell ein exaktes geschlossenes System zu erhalten. Wie dieses erreicht werden kann zeigen wir mit der *adiabatischen Näherung*, die wir für den Fall einer bosonisierten Wechselwirkung für die bosonische Greensfunktion herleiten.

Bosonen am kritischen Punkt der Bose-Einstein Kondensation

Wir betrachten schwach wechselwirkende Bosonen in $3 + \epsilon$ Dimensionen am kritischen Punkt der Bose-Einstein Kondensation. Der Phasenübergang findet bei endlicher Temperatur T_c statt, welche einen effektiven Ultraviolett Impuls-Cutoff Λ definiert. Zur Untersuchung physikalischer Eigenschaften, die nur von Impulsen $k < \Lambda$ abhängen, ist es deshalb ausreichend das System durch ein klassisches (Frequenz unabhängiges) Feld zu beschreiben. In einer ersten Näherung betrachten wir ausschließlich relevante und marginale Vertices und lösen die entsprechenden Flußgleichungen auf iterative Weise. Wie bereits erwähnt liegt hier unser besonderes Augenmerk auf der Impulsabhängigkeit der Selbstenergie und es gelingt die Herleitung eines geschlossenen Ausdrucks für diese innerhalb unserer Näherung. Wir sind in der Lage das volle Impulsintervall vom sogenannten Scaling Regime bei kleinen Impulsen bis zum perturbativen Regime bei großen Impulsen zu beschreiben.

Aufgrund fehlender experimenteller Daten zur Selbstenergie verwenden wir ein indirektes Verfahren um unser Ergebnis zu verifizieren. Dazu berechnen wir die wechselwirkungsinduzierte Verschiebung ΔT_c der kritischen Temperatur, welche nach [76] mit der Selbstenergie verbunden ist. Der Vergleich mit den besten auf anderen Wegen gewonnenen Resultaten [85–88] bestätigt die Qualität unserer Rechnungen. Diskrepanzen zu den derzeit einzigen experimentellen Daten zu ΔT_c von [84] können durch Schwierigkeiten die Streulänge im Experiment zu bestimmen erklärt werden.

Weiterhin untersuchen wir die Güte unserer Näherungen durch den Vergleich der Fixpunktwerte der Vertices, insbesondere der anomalen Dimension η, zu den besten verfügbaren Resultaten anderer Methoden. Unserer Näherung liefert hier die korrekte Größenordnung, nichtsdestoweniger ist eine erhebliche Diskrepanz feststellbar. Wir weiten daher unsere Näherung aus, indem wir zusätzlich den Fluss irrelevanter Vertices mit berücksichtigen. Tatsächlich ist eine Verbesserung unserer Resultate zu beobachten. Allerdings ist diese Konvergenz nur sehr schwach ausgeprägt, und eine substantielle Verbesserung bedeutet daher einen erheblichen Aufwand. Wir vermuten dass dieses Konvergenzverhalten auf die Form des verwendeten scharfen Cutoffs zurückzuführen ist, wie es auch bei der von Morris [44, 46, 55] verwendeten *Momentum-Scale* Entwicklung zu beobachten ist. Deshalb halten wir es für erfolgversprechend unsere Rechnungen mit anderen Cutoff-Funktionen, wie beispielsweise dem Litim Cutoff [43, 47], zu wiederholen.

Die Fermifläche stark wechselwirkender Fermionen

Eine zentrale Fragestellung bei der Untersuchung fermionischer Systeme im Normalzustand ist die Form der Fermifläche. Eine Formulierung der funktionalen Renormierungsgruppe benötigt implizit Wissen über diese Form, welche gemeinhin nur a-posteriori aus der Selbstenergie bestimmt werden kann. Wir argumentieren dass es sich bei der Fermifläche um eine Fixpunkt Eigenschaft des Systems handelt und diese somit als Fixpunkt-Mannigfaltigkeit betrachtet werden muss. Die Notwendigkeit einen Fixpunkt unter der RG zu erreichen lässt sich in eine Feinjustierung des frequenz- und impulsunabhängigen Anteils $\tilde{r}_0$ der fermionischen 2-Punkt Vertex übersetzen. Wir zeigen, wie diese Feinjustierung vorgenommen werden kann, und wie sie mit der effektiven Wechselwirkung entlang der kompletten RG Trajektorie zusammenhängt

$$\tilde{r}_0(\mathbf{q}_\perp) \;\; = \;\; -\int_0^\infty d\tau \, e^{-\tau(1-\bar{\eta}_\tau(\mathbf{q}_\perp))} \int_{\mathbf{Q}'} \dot{\tilde{G}}_\tau(\mathbf{Q}')\tilde{\Gamma}_\tau^{(4)}(\mathbf{Q}_0, \mathbf{Q}'; \mathbf{Q}', \mathbf{Q}_0) \; .$$

Da $\tilde{r}_0$ weiterhin die Differenz zwischen nicht-wechselwirkender und wechselwirkender Fermifläche quantifiziert [38], ergibt sich eine exakte Selbstkonsistenz Gleichung für die Form der Fermifläche. In führender Ordnung erhält man beispielsweise aus dieser Gleichung die wohlbekannte Hartree-Fock Näherung.

Wir wenden nun unsere Selbstkonsistenz Gleichung an, um die Fermifläche wechselwirkender Fermionen in einer und zwei Dimensionen zu bestimmen. Um mit dem Formalismus vertraut zu werden beginnen wir mit dem einfachsten nicht-trivialen Problem einer inhomogenen Fermifläche, wie sie in einem System von zwei gekoppelten metallischen Ketten spinloser Fermionen realisiert wird. Die Bandstruktur besteht hier aus zwei Bändern, deren energetische Differenz durch die Hüpfamplitude $t_\perp$ zwischen den Ketten festgelegt wird. In einer perturbativen Rechnung mit einer Vielzahl unterschiedlicher Kopplungen zeigen wir, dass Rückwärtsstreuung zwischen den Bändern ("interband") zu einer Annäherung der Fermipunkte beider Bänder führt. Von speziellem Interesse ist für uns der Fall, das diese Fermiimpulse wechselwirkungsbedingt gleich sind, und bezeichnen dies als *Confinement* Phasenübergang.

Da innerhalb einer perturbativen Rechnung solch ein Phasenübergang nicht zu erwarten ist, suchen wir nach einer Möglichkeit unsere Analyse zu starker Wechselwirkung hin zu extrapolieren. Hierfür bosonisieren wir die interband Rückwärtsstreuung mit Hilfe einer Hubbard-Stratonovich Transformation und betrachten nur dieses Einkanal Problem. Zusätzlich kommt die *adiabatische Näherung* wie oben beschrieben zur Anwendung. Aufgrund der Art und Weise wie wir die Flußgleichungen trunkieren und nähern können wir nicht ausschließen, andere nicht-perturbative Effekte vernachlässigt zu haben. Insofern ist unser Verfahren nur als vernünftige Extrapolation zu starker Wechselwirkung zu be-

trachten. Motiviert durch Erscheinungsbild und Implikationen unserer Resultate vermuten wir jedoch, dass unser Ansatz alle wesentlichen Aspekte berücksichtigt. Eine Ein-Schleifen Rechnung sagt hier einen *Confinement* Phasenübergang bei starker Wechselwirkung voraus. Im nächsten Schritt schließen wir in einer Zwei-Schleifen Rechnung die Renormierung der effektiven Wechselwirkung mit ein und beobachten das das *Confinement* durch Fluktuation destabilisiert wird. Schließlich zeigen wir wie durch den Einschluss einer interband Umklapp Wechselwirkung (auch als Paartunneln bezeichnet) das *Confinement* wiederum stabilisiert werden kann.

Nachdem wir am oben dargestellten einfachen Modell den Formalismus studiert haben wenden wir uns dem physikalisch relevanten zweidimensionalen Fall unendlich vieler gekoppelter metallischer Ketten spinloser Fermionen zu. Die Fermifläche besteht in diesem Fall aus zwei nicht-verbundenen schwach gekrümmten Kurven, wobei das Ausmaß der initialen Krümmung durch die Hüpfamplitude $t_\perp$ zwischen den Ketten festgelegt wird. Ein *Confinement* Phasenübergang äußert sich hier dadurch, dass diese Kurven exakt flach werden. In diesem Fall erfolgt die Bewegung der Elektronen transversal zu den Ketten inkohärent und eine Beschreibung dieses Systems als Fermi-Flüssigkeit ist nicht mehr adäquat. Es wird vermutet dass sich bestimmte anomale Eigenschaften senkrecht zu den Kupferoxid Schichten in Hochtemperatur Supraleitern auf diese Weise erklären lassen [33–36]. Ausgehend von einer Dichte-Dichte Wechselwirkung bosonisieren wir diese wie zuvor mit Hilfe einer Hubbard-Stratonovich Transformation. Wir beginnen zunächst wieder mit einer perturbativen Rechnung, die wie zuvor jedoch nicht geeignet ist das Regime starker Kopplung zu beschreiben. Nachfolgend betrachten wir das System bei starker Wechselwirkung in Ein-Schleifen Rechnung und erhalten wiederum als Ergebnis eine *confined* Phase. Diese Phase bleibt auch in einer Zwei-Schleifen Rechnung stabil und wir schließen hieraus, dass tatsächlich ein *Confinement* Phasenübergang bei starker Kopplung stattfindet.

Dieser Phasenübergang wird zusätzlich in einer nichttrivialen Impulsabhängigkeit der effektiven Wechselwirkung und einem Verschwinden des Quasiteilchen Gewichts reflektiert. Es ist vorgeschlagen worden [25, 27, 30–32], dass in Hochtemperatur Supraleitern innerhalb der Kupferoxid Schichten das *Confinement* nur partiell sein könnte indem nur bestimmte Sektoren der Fermifläche flach werden. In unserem Modell beobachten wir ein solches Verhalten nicht und argumentieren, dass dies eine Konsequenz der Topologie der Fermifläche sein könnte, denn die Fermifläche innerhalb der Kupferoxid Schichten ist geschlossen und nahezu quadratisch, wohingegen sie bei unserem
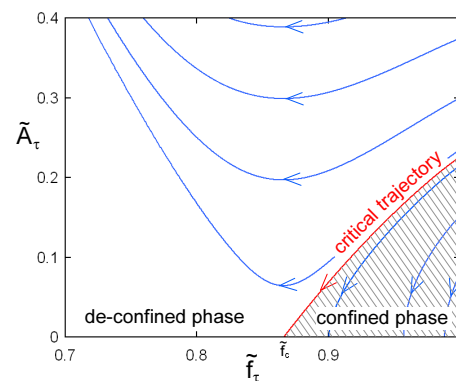
Modell offen ist. Wir schlagen jedoch vor diesen Fall einer geschlossenen fast quadratischen Fermifläche, wie er in einem zweidimensionalen Hubbard Modell mit geeigneter Kopplungskonstanten und Füllfaktor realisiert wird, mit der von uns vorgestellten Methode zu untersuchen.

Veröffentlichungen

1. HOLGER FRAHM AND SASCHA LEDOWSKI,
   Boundary states and edge singularities in the degenerate Hubbard chain,
   J. Phys. Cond. Mat. **10** (1998), 8829

2. SASCHA LEDOWSKI AND PETER KOPIETZ,
   Exact integral equation for the renormalized Fermi surface,
   J. Phys. Cond. Mat. **15** (2003), 4779

3. SASCHA LEDOWSKI, NILS HASSELMANN AND PETER KOPIETZ,
   Self-energy and critical temperature of weakly interacting bosons,
   Phys. Rev. A **69** (2004), 61601

4. NILS HASSELMANN, SASCHA LEDOWSKI AND PETER KOPIETZ,
   *Critical behavior of weakly interacting bosons: A functional
   renormalization-group approach*,
   Phys. Rev. A **70** (2004), 63621

5. SASCHA LEDOWSKI, PETER KOPIETZ AND ÁLVARO FERRAZ,
   *Self-consistent Fermi surface renormalization in two coupled Luttinger
   liquids*,
   Phys. Rev. B **71** (2005), 235106

6. SASCHA LEDOWSKI AND PETER KOPIETZ,
   *Fermi surface renormalization and confinement in two coupled metallic
   chains*,
   Phys. Rev. B **75** (2007), 45134

7. SASCHA LEDOWSKI AND PETER KOPIETZ,
   Confined coherence in quasi one-dimensional metals,
   Phys. Rev. B **76** (2007), 121403(R)

Lebenslauf

Angaben zur Person

Name:	Sascha Ledowski
Geburtstag:	3. Juni 1969
Geburtsort:	Langenhagen
Staatsangehörigkeit:	Deutsch

Beruflicher Werdegang

1988	Abitur am Kaiser-Wilhelm-Gymnasium, Hannover
1988-1989	Grundwehrdienst, Hannover
1989-1992	Ausbildung zum Piloten an der Verkehrsfliegerschule der Lufthansa, Bremen und Phoenix/USA
1992	1. Offizier auf Boeing 737, Deutsche Lufthansa AG, Frankfurt am Main
1992	Aufnahme des Diplomstudiengangs Physik, Universität Hannover
1994-1995	Auslandsstudium an der University of Oxford
1997	Diplomarbeit am Institut für Theoretische Physik, Hannover Thema: "Das SU(N) Hubbard Modell mit Randpotentialen" Betreuer: Prof. Dr. H. Frahm
1999	Diplom im Studiengang Physik, Universität Hannover
1998-2002	1. Offizier auf Airbus 320, Condor Berlin GmbH, Berlin
seit 2002	1. Offizier auf Airbus 320, Lufthansa AG, Frankfurt am Main
2002-2007	Doktorand am Institut für Theoretische Physik, Johann Wolfgang Goethe-Universität, Frankfurt am Main Betreuer: Prof. Dr. P. Kopietz

Danksagung

Das Doktorarbeit Schreiben hat nun ein Ende und es ist an der Zeit all jene zu würdigen, die mich auf meinem Weg hierher unterstützt und begleitet haben:

Vor fünf Jahren wandte ich mich auf der Suche nach einem geeigneten Thema für eine Dissertation in theoretischer Physik an Prof. Dr. Peter Kopietz. Aufgrund meines Berufes bin ich zeitlich recht eingeschränkt und abgesehen davon, dass ich keiner Bezahlung bedurfte hatte ich keine besonderen Anreize zu bieten, in die Arbeitsgruppe aufgenommen und mit einem interessanten Thema betraut zu werden. Genau letzteres geschah aber. Hierfür, sowie die stets hilfreiche und motivierende Betreuung in den folgenden Jahren möchte ich mich recht herzlich bedanken.

Bei Prof. Dr. Claudius Gros bedanke ich mich für die Bereitschaft die Begutachtung dieser Arbeit zu übernehmen.

Bei Herrn Prof. Dr. Holger Frahm möchte ich mich dafür bedanken, daß er, nachdem kurzfristig ein dritter Gutachter erforderlich wurde, diese Aufgabe übernommen hat.

An der Universität war ich die letzten Jahre nur sporadisch anzutreffen, da der Großteil dieser Arbeit zuhause und in diversen Hotelzimmern entstanden ist. Zwischen meinen Besuchen hatten nicht selten immer wieder personelle Veränderungen in der Arbeitsgruppe stattgefunden und der Kontakt zu meinen Kollegen dort ist leider eher locker geblieben. Trotzdem ergaben sich wenn ich vor Ort war immer wieder nette Gespräche und zusammen mit Dr. Nils Hasselmann sogar eine erfolgreiche Zusammenarbeit zum Thema wechselwirkender Bosonen, für die ich mich hier bedanken möchte.

Als ich vor gut fünfzehn Jahren überraschenderweise meinen Arbeitsplatz als Pilot verlor verfügte ich plötzlich über die nötige Zeit, mir den Wunsch Physik zu studieren, zu erfüllen. Zeit ist eine Sache, aber finanziert werden muss das dann auch noch. Ich bedanke mich bei meinen Eltern Barbara und Otto Ledowski insbesondere dafür dieses Problem gelöst zu haben.

Und schließlich zu Tanja, die das alles ertragen hat: Es ist mitunter schon nicht einfach das unstete Leben eines Piloten zu akzeptieren. Wenn dieser dann auch noch einen beträchtlichen Teil seiner Freizeit dazu nutzt über Probleme der theoretischen Physik zu sinnieren dann verlangt das schon eine signifikant große Portion guten Willens. In diesem Sinne: Danke !